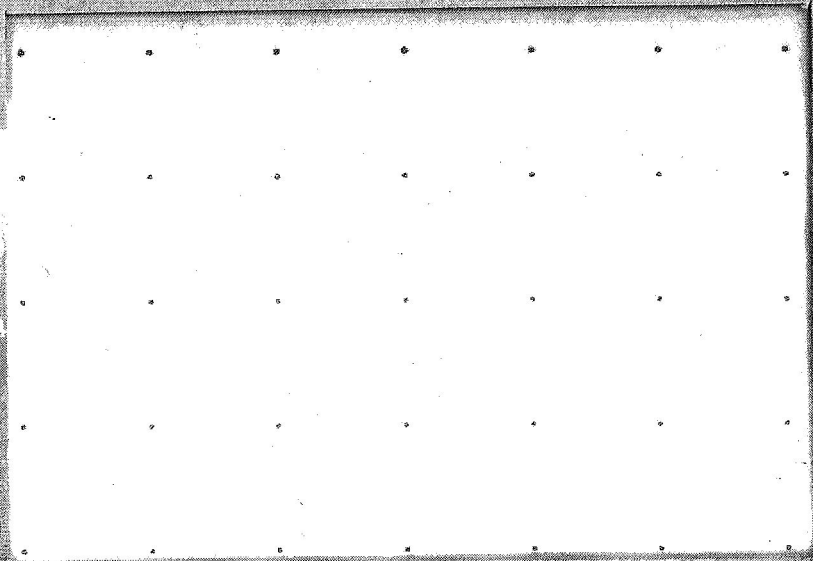
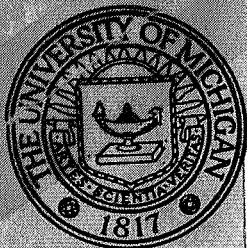


THE UNIVERSITY OF MICHIGAN RADIO ASTRONOMY OBSERVATORY

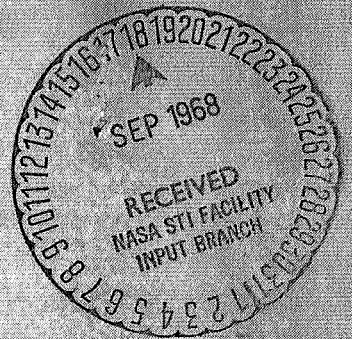


) _____
F) _____



FACILITY FORM 602

N 68 - 5564 1	_____
(ACCESSION NUMBER)	(THRU)
184	1
(PAGES)	(CODE)
CR-96630	30
(NASA CR OR TMX OR AD NUMBER)	(CATEGORY)



DEPARTMENT OF ASTRONOMY

THE UNIVERSITY OF MICHIGAN
RADIO ASTRONOMY OBSERVATORY

Report 68-6

MOTION OF A LUMPED-MASS MODEL
REPRESENTING A
KILOMETER WAVE ORBITING TELESCOPE

Daniel R. Hegg

Sponsored by National Aeronautics and Space Administration

Grant NGR-23-005-131

March 1968

Department of Astronomy

ABSTRACT

Scientific interest in radio astronomical observations at frequencies near 1 MHz have led to the consideration of large earth satellites as radio astronomy observatories. One such concept, a Kilometer Wave Orbiting Telescope (KWOT), consists of a system of four rigid bodies connected to a heavy reference satellite by flexible cables. The nominal configuration of the system is that of a 10-kilometer rhombic with a 10-kilometer cross-member extending across the rhombic along its minor diagonal. In operation, it is desired to spin the system about the reference satellite at 1 revolution per hour to maintain cable tension, and to precess the spin axis in stepwise increments of $1/2$ degree.

This report discusses a numerical analysis of the planar motion of a lumped-mass model representing the KWOT structure conducted to investigate the feasibility of the KWOT concept. The model consists of a system of particles with interconnecting nonlinear springs and an in-place tangential thrust capability. Specifically, the effects of small perturbations from a free-space condition of uniform rotation due to the gravitational gradient and to control thruster activation are investigated. Orbital constraints are assumed, with the reference satellite describing a circular orbit at synchronous altitude. In addition, a coordinated spin-up deployment method is studied. The effects of three-dimensional motion, structural damping or orbital eccentricity are not studied.

Results indicate that the amplitude of the structural oscillations excited by the deployment method are within the limits defining allowable structural distortion, and that a simple configuration control system can counteract small perturbations from a free-space equilibrium rotating condition for a lifetime in excess of one year.

TABLE OF CONTENTS

	<u>Page</u>
List of Appendices	iii
List of Tables	iv
List of Figures	v
Section I. PURPOSE	1
Section II. DESCRIPTION OF MODEL	3
Section III. COMPUTATIONAL CONSIDERATIONS	13
Section IV. INVESTIGATIONS PERFORMED	23
Section V. DISCUSSION OF RESULTS	27
Section VI. APPLICABILITY	40
References	42
Appendices	43
Tables	56
Figures	61

List of Appendices

	<u>Page</u>
A Glossary of Terms	43
B Elastic Potential Derivatives	47
C Incorporation of Artificial Damping	51

List of Tables

	<u>Page</u>
1 Configuration Specifications and Environmental Conditions	56
2 Configuration Solutions	57
3 Spectral Characteristics of Free Motion	58
4 Fuel Consumption Data	60

List of Figures

- 1 Continuous KWOT Structure
- 2 Lumped-mass Approximate Model of KWOT
- 3 Control System Position and Control Sectors
- 4 Control System Schematic Diagram
- 5 Free-space Equilibrium Configuration for a Quadrant
- 6 Plot II-B, m_4
- 7 Plot II-B, m_3
- 8 Plot II-B, m_2
- 9 Plot II-B, m_8
- 10 Plot II-B, m_9
- 11 Plot III-B, m_9
- 12 Plot IV-B, m_9
- 13 Plot II-D, m_9
- 14 Plot II-D, m_{16}
- 15 Plot II-D, m_8
- 16 Plot II-D, m_{15}
- 17 Plot II-D, m_7
- 18 Plot II-D, m_1
- 19 Plot II-D, m_{10}
- 20 Plot II-D, m_{14}
- 21 Plot II-D, m_{11}
- 22 Plot II-D, m_{13}
- 23 Plot II-D, m_4
- 24 Structure diagram, $t = 5400$ sec, Case D
- 25 Plot I-D, m_4
- 26 Plot III-D, m_9
- 27 Plot IV-D, m_9
- 28 Plot III-D, m_{16}
- 29 Plot IV-D, m_{16}
- 30 Plot II-E, m_9
- 31 Plot V-E, m_9

- 32 Plot VI-E, m_9
- 33 Plot II-E, m_{16}
- 34 Plot V-E, m_{16}
- 35 Plot VI-E, m_{16}
- 36 Plot II-E, m_8
- 37 Plot II-E, m_{15}
- 38 Plot II-E, m_7
- 39 Plot II-E, m_1
- 40 Plot II-E, m_{10}
- 41 Plot II-E, m_{14}
- 42 Plot II-E, m_{11}
- 43 Plot II-E, m_{13}
- 44 Plot II-E, m_4
- 45 Plot I-E, m_4
- 46 Plot III-E, m_9
- 47 Plot IV-E, m_9
- 48 Plot III-E, m_{16}
- 49 Plot IV-E, m_{16}
- 50 Plot I-F, m_4
- 51 Plot I-F, m_5
- 52 Plot I-F, m_6
- 53 Plot I-F, m_{10}
- 54 Plot I-F, m_{11}
- 55 Plot II-F, m_4
- 56 Plot II-F, m_5
- 57 Plot II-F, m_6
- 58 Plot II-F, m_7
- 59 Plot II-F, m_8
- 60 Plot II-F, m_9
- 61 Plot II-F, m_{15}
- 62 Plot II-F, m_{16}
- 63 Plot II-F, m_{10}
- 64 Plot II-F, m_{11}
- 65 Plot III-F, m_9
- 66 Plot IV-F, m_9

- 67 Plot III-F, m_{12}
- 68 Plot IV-F, m_{12}
- 69 Plot III-F, m_{16}
- 70 Plot IV-F, m_{16}
- 71 Plot I-G, m_4
- 72 Plot I-G, m_5
- 73 Plot I-G, m_6
- 74 Plot I-G, m_{10}
- 75 Plot I-G, m_{11}
- 76 Plot II-G, m_4
- 77 Plot II-G, m_5
- 78 Plot II-G, m_6
- 79 Plot II-G, m_7
- 80 Plot II-G, m_8
- 81 Plot II-G, m_9
- 82 Plot V-G, m_9
- 83 Plot VI-G, m_9
- 84 Plot II-G, m_{15}
- 85 Plot II-G, m_{16}
- 86 Plot V-G, m_{16}
- 87 Plot VI-G, m_{16}
- 88 Plot II-G, m_{10}
- 89 Plot II-G, m_{11}
- 90 Plot III-G, m_9
- 91 Plot IV-G, m_9
- 92 Plot III-G, m_{12}
- 93 Plot IV-G, m_{12}
- 94 Plot III-G, m_{16}
- 95 Plot IV-G, m_{16}
- 96 Plot I-H, m_4
- 97 Plot I-H, m_5
- 98 Plot I-H, m_6
- 99 Plot I-H, m_{10}
- 100 Plot I-H, m_{11}

- 101 Plot II-H, m₄
- 102 Plot II-H, m₅
- 103 Plot II-H, m₆
- 104 Plot II-H, m₇
- 105 Plot II-H, m₈
- 106 Plot II-H, m₉
- 107 Plot V-H, m₉
- 108 Plot VI-H, m₉
- 109 Plot II-H, m₁₅
- 110 Plot II-H, m₁₆
- 111 Plot V-H, m₁₆
- 112 Plot VI-H, m₁₆
- 113 Plot II-H, m₁₀
- 114 Plot II-H, m₁₁
- 115 Plot III-H, m₉
- 116 Plot IV-H, m₉
- 117 Plot III-H, m₁₂
- 118 Plot IV-H, m₁₂
- 119 Plot III-H, m₁₆
- 120 Plot IV-H, m₁₆
- 121 Plot I-J, m₄
- 122 Plot I-J, m₅
- 123 Plot I-J, m₆
- 124 Plot I-J, m₁₀
- 125 Plot I-J, m₁₁
- 126 Plot II-J, m₄
- 127 Plot II-J, m₅
- 128 Plot II-J, m₆
- 129 Plot II-J, m₇
- 130 Plot II-J, m₈
- 131 Plot II-J, m₉
- 132 Plot V-J, m₉
- 133 Plot VI-J, m₉
- 134 Plot II-J, m₁₅

- 135 Plot II-J, m_{16}
- 136 Plot V-J, m_{16}
- 137 Plot VI-J, m_{16}
- 138 Plot II-J, m_{10}
- 139 Plot II-J, m_{11}
- 140 Plot III-J, m_9
- 141 Plot IV-J, m_9
- 142 Plot III-J, m_{12}
- 143 Plot IV-J, m_{12}
- 144 Plot III-J, m_{16}
- 145 Plot IV-J, m_{16}
- 146 Plot III-L, m_9
- 147 Plot IV-L, m_9
- 148 Plot V-L, m_9
- 149 Plot VI-L, m_9
- 150 Plot III-L, m_{12}
- 151 Plot IV-L, m_{12}
- 152 Plot V-L, m_{12}
- 153 Plot VI-L, m_{12}
- 154 Plot III-L, m_{16}
- 155 Plot IV-L, m_{16}
- 156 Plot V-L, m_{16}
- 157 Plot VI-L, m_{16}
- 158 Plot I-M, m_4
- 159 Plot I-M, m_5
- 160 Plot I-M, m_6
- 161 Plot I-M, m_1
- 162 Plot I-M, m_8
- 163 Plot I-M, m_9
- 164 Plot I-M, m_2
- 165 Plot I-M, m_3
- 166 Plot II-M, m_4
- 167 Plot II-M, m_5
- 168 Plot II-M, m_6

- 169 Plot II-m, m_7
- 170 Plot II-M, m_8
- 171 Plot II-M, m_9
- 172 Plot II-M, m_2
- 173 Plot II-M, m_3
- 174 Plot III-M, m_9
- 175 Plot IV-M, m_9
- 176 Structure diagram, $t = 0$ sec, Case M
- 177 Structure diagram, $t = 300$ sec, Case M
- 178 Structure diagram, $t = 400$ sec, Case M
- 179 Structure diagram, $t = 500$ sec, Case M
- 180 Structure diagram, $t = 600$ sec, Case M
- 181 Structure diagram, $t = 700$ sec, Case M
- 182 Structure diagram, $t = 900$ sec, Case M
- 183 Structure diagram, $t = 1800$ sec, Case M

Section I: PURPOSE

Several previous investigations into the motion of cable-connected space structures have been reported by Haddock¹ and Crist.² The dynamical models used in all of these studies have the common characteristic that the motion of each model approximates the motion of a portion of the complete structure envisioned for the Kilometer Wave Orbiting Telescope (KWOT), whose main features are shown in Figure 1. In particular, these studies have concentrated heavily on dumbbell configurations which approximate the motion of the dipole leg.

The purpose of the present investigation is to study the motion of a model representing the entire structure to evaluate its feasibility for use as a radio astronomy observatory from the viewpoint of dynamics. Since major structural deformation degrades the electromagnetic characteristics of the antenna, some specifications are necessary to define the extent to which distortion can be permitted. From a dynamical standpoint, several important feasibility considerations are:

- (i) The type and extent of structural distortion which is produced by perturbing influences in the expected operating environment, and
 - (ii) The capability of an active control system to prevent the structural distortion from exceeding allowable limits for an extended period of time.
- These topics have been investigated in the present study.

The guideline used to define allowable distortion limits states that, to maintain acceptable antenna characteristics, no part of the structure should deviate more than a specified distance from its desired position during its motion in time, thus defining a "distortion circle" for each point of the structure. Since provision for active control devices on the actual structure is limited to thrusters on the small maneuvering subsatellite (SMS) units and the central observatory (CO), the distortion guideline also leads to the construction of two sectors related to the angular position of each SMS unit:

- (i) A "position sector" relative to the CO defined by the tangent rays to the distortion circle of that unit within which motion of the unit is acceptable, and

(ii) A "control sector" within which the control system for the unit remains quiescent.

In order to streamline the discussion, a complete glossary of terms has been compiled in Appendix A.

Section II: DESCRIPTION OF MODEL

The dynamical model selected to simulate the motion of the actual KWOT structure of Figure 1 is a lumped-mass approximation consisting of a set of 16 point masses with massless interconnecting springs, as shown in Figure 2. The equations which govern the motion of this model are derived under the following assumptions:

II-1. The point mass m_o , representing the mass of the CO, coincides with the center of mass of the model. This assumption is a valid approximation if the following inequality holds:

$$m_i/m_o \ll 1 \quad (2-1)$$

The total mass of the model is given by:

$$M = m_o + \sum_{i=1}^{16} m_i \quad (2-2)$$

II-2. The sole perturbing influence external to the model is the gravitational field of the earth.

II-3. The gravitational field of the earth is a pure inverse-square central force field.

II-4. The initial configuration of the model is such that all the point masses lie in a single plane containing the center of the earth, and the initial motion is such that the velocity vector of each mass lies in this plane.

II-5. The spring characteristic of the j th spring is a piecewise constant function of its instantaneous strain ϵ_{Ej} :

$$K_j = k_j u(\epsilon_{Ej}) \quad (j = 1 \dots 18) \quad (2-3)$$

where $u(t)$ is the unit step function:

$$u(t) = \begin{cases} 0 & (t < 0) \\ 1 & (t \geq 0) \end{cases}$$

This disallows the generation of compressive force in any spring.

II-6. Gravitational forces due to the mutual interaction of the point masses of the model are negligible compared to the spring forces.

II-7. A thruster for configuration control, installed on each model mass which represents an SMS unit, is capable of bi-directional thrust along a line lying in the plane of the initial configuration and normal to the line connecting m_0 and m_i .

As a consequence of assumptions II-2 through II-4, II-7 and Newton's second law of motion, the subsequent motion of the model is confined to the plane of its initial configuration. Thus, its configuration at any time is completely defined by 34 independent generalized coordinates, so that the system has 34 degrees of freedom. As described by Greenwood³, the equations of motion for this model may be readily obtained using Lagrange's equations in the form:

$$\frac{d}{dt} (\partial L / \partial \dot{q}) - \partial L / \partial q = Q \quad (2-4)$$

where

$$L(q, \dot{q}, t) = T(q, \dot{q}, t) - V(q, t) \quad (2-5)$$

is the Lagrangian of the system. The generalized coordinate vector used gives the system configuration in ordinary polar coordinates:

$$q = (r, \theta, l_1 \dots l_{16}, \phi_1 \dots \phi_{16}) \quad (2-6)$$

as indicated in Figure 2. If \underline{x}_i represents the position vector of the i th mass, m_i , relative to an inertial reference frame fixed at center of the earth, then

$$T(q, \dot{q}, t) = \sum_{i=0}^{16} m_i \|\dot{\underline{x}}_i\|^2 = \sum_{i=0}^{16} m_i \left\{ (\dot{r} \cos \theta - r\dot{\theta} \sin \theta + \dot{l}_i \cos \phi_i - l_i \dot{\phi}_i \sin \phi_i)^2 + (\dot{r} \sin \theta + r\dot{\theta} \cos \theta + \dot{l}_i \sin \phi_i + l_i \dot{\phi}_i \cos \phi_i)^2 \right\} \quad (2-7)$$

and

$$V(\underline{q}, t) = V_G(\underline{q}, t) + V_E(\underline{q}, t) \quad (2-8)$$

The gravitational potential is obtained from Newton's law of gravitation for the force \underline{f}_{G_i} on m_i due to the mass of the earth m_E :

$$\underline{f}_{G_i} = -\frac{G m_E m_i}{\|\underline{z}_i\|^3} \underline{z}_i = -\nabla V_{G_i}(\underline{q}, t) \quad (i = 0 \dots 16) \quad (2-9)$$

so that

$$V_G(\underline{q}, t) = -\sum_{i=0}^{16} \frac{\mu_E m_i}{\|\underline{z}_i\|} = -\sum_{i=0}^{16} \frac{\mu_E m_i}{\sqrt{\{r^2 + l_i^2 + 2r l_i \cos(\theta - \phi_i)\}}} \quad (2-10)$$

where

$$\mu_E = G m_E \quad (2-11)$$

The elastic potential $V_E(\underline{q}, t)$ is obtained from the law of linear elasticity for the force \underline{f}_{E_j} in an elastic spring:

$$\underline{f}_{E_j} = -K_j (s_j - s_{j_0}) \underline{e}_j = -\nabla V_{E_j}(\underline{q}, t) \quad (2-12)$$

so that

$$V_E(\underline{q}, t) = \frac{1}{2} \sum_{j=1}^{16} K_j (s_j - s_{j_0})^2 \quad (2-13)$$

The spring length s_j is expressed as a function of the generalized coordinates. If \underline{y}_j is the position vector of the j th mass, m_j , relative to a non-rotating reference frame attached to m_0 , then:

$$s_j = \left\{ \begin{array}{ll} ||y_{j+1} - y_j|| & (j=1\dots6) \\ ||y_j|| & (j=7) \\ ||y_j - y_{j-1}|| & (j=8,9,11\dots14) \\ ||y_j - y_{j-3}|| & (j=10) \\ ||y_{j-14} - y_{j-1}|| & (j=15) \\ ||y_{j-1} - y_{j-15}|| & (j=16) \\ ||y_{j-1} - y_{j-2}|| & (j=17) \\ ||y_{j-17}|| & (j=18) \end{array} \right\} \quad (2-14)$$

where, from the law of cosines:

$$||y_j - y_k|| = \sqrt{\{l_j^2 + l_k^2 - 2l_j l_k \cos(\varphi_j - \varphi_k)\}} \quad (2-15)$$

Combining equations (2-5) through (2-15), the Lagrangian of the system is obtained. The generalized forces are obtained from a computation of the virtual work of all forces not derivable from a potential function:

$$\delta W = \sum_{k=1}^{3n} F_k \delta x_k = \sum_{p=1}^n Q_p \delta q_p \quad (2-16)$$

The tangential forces produced by the control thrusters are the only such forces being considered, so that the components of the generalized force vector are given by:

$$Q_p = \left\{ \begin{array}{ll} T_p / l_p & (p = 4, 9, 12, 16) \\ 0 & \text{otherwise} \end{array} \right\} \quad (2-17)$$

By direct application of equation (2-4), the two equations for the motion of m_0 become:

$$\left(\ddot{r} - r\dot{\theta}^2 + \frac{\mu_E}{r} \right) + \sum_{i=1}^{16} \left(\frac{m_i}{m_0} \right) \left\{ \left(\ddot{r} - r\dot{\theta}^2 + \frac{\mu_E r}{[r^2 + l_i^2 + 2rl_i \cos(\theta - \varphi_i)]^{3/2}} \right) \right. \\ \left. + (l_i \ddot{\varphi}_i + 2\dot{l}_i \dot{\varphi}_i) \sin(\theta - \varphi_i) + (\ddot{l}_i - l_i \dot{\varphi}_i^2) \cos(\theta - \varphi_i) \right\} = 0 \quad (2-18)$$

$$(r\ddot{\theta} + 2\dot{r}\dot{\theta}) + \sum_{i=1}^{16} \left(\frac{m_i}{m_0} \right) \left\{ (r\ddot{\theta} + 2\dot{r}\dot{\theta}) + (\ddot{l}_i - l_i \dot{\varphi}_i^2) + \frac{\mu_E l_i}{[r^2 + l_i^2 + 2rl_i \cos(\theta - \varphi_i)]^{3/2}} \right\} \sin(\theta - \varphi_i) \\ + (l_i \ddot{\varphi}_i + 2\dot{l}_i \dot{\varphi}_i) \cos(\theta - \varphi_i) \left. \right\} = 0 \quad (2-19)$$

Similarly, the two equations for the motion of each mass m_i become:

$$\ddot{l}_i - l_i \dot{\varphi}_i^2 - (r\ddot{\theta} + 2\dot{r}\dot{\theta}) \sin(\theta - \varphi_i) + (\ddot{r} - r\dot{\theta}^2) \cos(\theta - \varphi_i) \\ + \frac{\mu_E [l_i + r \cos(\theta - \varphi_i)]}{[r^2 + l_i^2 + 2rl_i \cos(\theta - \varphi_i)]^{3/2}} + \left(\frac{1}{m_i} \right) \frac{\partial V_E}{\partial l_i} = 0 \quad (i=1 \dots 16) \quad (2-20)$$

$$l_i \ddot{\varphi}_i + 2\dot{l}_i \dot{\varphi}_i + \left(\ddot{r} - r\dot{\theta}^2 + \frac{\mu_E r}{[r^2 + l_i^2 + 2rl_i \cos(\theta - \varphi_i)]^{3/2}} \right) \sin(\theta - \varphi_i) \\ + (r\ddot{\theta} + 2\dot{r}\dot{\theta}) \cos(\theta - \varphi_i) + \left(\frac{1}{m_i l_i} \right) \left(\frac{\partial V_E}{\partial \varphi_i} - Q_i \right) = 0 \quad (i=1 \dots 16) \quad (2-21)$$

Equations (2-18) through (2-21) form a set of 34 coupled second order ordinary differential equations for the planar motion of the model of Figure 2. At this point, several additional assumptions are introduced for purposes of simplification:

II-8. The point mass m_0 is sufficiently large that, in addition to (2-1):

$$\left(\sum_{i=1}^{16} m_i \right) / m_0 \ll 1 \quad (2-22)$$

II-9. For all masses m_i , and for all $t \geq t_0$:

$$l_i / r \ll 1$$

When (2-22) is incorporated into equations (2-18) and (2-19), they reduce to the equations for a single point mass in a central force field:

$$\ddot{\mathbf{r}} - r\dot{\theta}^2 + \frac{\mu_E}{r^2} = 0 \quad (2-24)$$

$$r\ddot{\theta} + 2\dot{r}\dot{\theta} = 0 \quad (2-25)$$

Expanding the gravitational potential terms of (2-20) and (2-21) in Taylor series and making use of (2-23) through (2-25), equations (2-20) and (2-21) reduce to:

$$\ddot{l}_i - l_i \dot{\phi}_i^2 - \frac{\mu_E l_i}{2r^3} [1 + 3 \cos 2(\theta - \phi_i)] + \left(\frac{1}{m_i}\right) \frac{\partial V_E}{\partial l_i} = 0 \quad (i=1 \dots 16) \quad (2-26)$$

$$l_i \ddot{\phi}_i + 2\dot{l}_i \dot{\phi}_i - \frac{3\mu_E l_i}{2r^3} \sin 2(\theta - \phi_i) + \left(\frac{1}{m_i l_i}\right) \left(\frac{\partial V_E}{\partial \phi_i} - Q_i\right) = 0 \quad (i=1 \dots 16) \quad (2-27)$$

Since the derivatives $\frac{\partial V_E}{\partial l_i}$ and $\frac{\partial V_E}{\partial \phi_i}$ of the elastic potential are quite long expressions, their explicit forms are placed in Appendix B.

When assumptions II-1 through II-9 are justified, equations (2-24) through (2-27) describe the motion of the lumped-mass approximate model of Figure 2. It should be noted that no provision for damping is incorporated in the model, for reasons to be discussed at the end of section IV. The equations for a similar model incorporating linear viscous damping mechanisms in parallel with each spring are easily derived, however, as shown in Appendix C.

The purpose of the control thrusters on the peripheral masses of the model is to provide configuration control of the deformable structure. The thrusters are activated by a simple control law based upon the relative angular position and velocity of the peripheral masses only. One of these masses is chosen as a reference subsatellite. A measure of structural deformation is then defined by an angular position deviation:

$$\delta\varphi_i = \varphi_i - \varphi_R + \eta_i \pi \quad (i=i_1, i_2, i_3) \quad (2-28)$$

If $\varphi_R = \varphi_4$, then $i_1 = 9$, $i_2 = 12$, $i_3 = 16$, and

$$\eta_i = \begin{cases} \frac{1}{2} & (i=9) \\ 1 & (i=12) \\ -\frac{1}{2} & (i=16) \end{cases} \quad (2-29)$$

The control objective is to keep the deviation $\delta\varphi_i$ within a specified position sector P_i defined by:

$$|\delta\varphi_i| \leq \epsilon db_i \quad (2-30)$$

for each non-reference peripheral mass m_i . This is accomplished by activating the thruster for a mass m_i whenever the point $(\delta\varphi_i, \dot{\delta\varphi}_i)$ lies outside a certain control sector R_i in the $\delta\varphi_i - \dot{\delta\varphi}_i$ phase plane. Both the position sector and the control sector are shown in Figure 3 and are defined by the following expressions:

$$P_i = \left\{ (\delta\varphi_i, \dot{\delta\varphi}_i) \mid \delta\varphi_i^L \leq \delta\varphi_i \leq \delta\varphi_i^R, \text{ all } \delta\varphi_i^L \in \Gamma_{L_i}, \delta\varphi_i^R \in \Gamma_{R_i} \right\} \quad (2-31)$$

where

$$\Gamma_{L_i} = \left\{ (\delta\varphi_i, \dot{\delta\varphi}_i) \mid \delta\varphi_i = -\epsilon db_i \right\} \quad (2-32)$$

$$\Gamma_{R_i} = \left\{ (\delta\varphi_i, \dot{\delta\varphi}_i) \mid \delta\varphi_i = +\epsilon db_i \right\} \quad (2-33)$$

$$R_i = \left\{ (\delta\varphi_i, \dot{\delta\varphi}_i) \mid \delta\varphi_i^+ \leq \delta\varphi_i \leq \delta\varphi_i^-, \text{ all } \delta\varphi_i^+ \in \Gamma_{+i}, \delta\varphi_i^- \in \Gamma_{-i} \right\} \quad (2-34)$$

$$R_i^+ = \left\{ (\delta\varphi_i, \dot{\delta\varphi}_i) \mid \delta\varphi_i < \delta\varphi_i^+, \text{ all } \delta\varphi_i^+ \in \Gamma_{+i} \right\} \quad (2-35)$$

$$R_i^- = \left\{ (\delta\varphi_i, \dot{\delta\varphi}_i) \mid \delta\varphi_i > \delta\varphi_i^-, \text{ all } \delta\varphi_i^- \in \Gamma_{-i} \right\} \quad (2-36)$$

where

$$\Gamma_{+i} = \left\{ (\delta\varphi_i, \dot{\delta\varphi}_i) \mid \delta\varphi_i + \zeta_i \dot{\delta\varphi}_i = -\epsilon db_i \right\} \quad (2-37)$$

$$\Gamma_{-i} = \left\{ (\delta\varphi_i, \dot{\delta\varphi}_i) \mid \delta\varphi_i + \zeta_i \dot{\delta\varphi}_i = +\epsilon db_i \right\} \quad (2-38)$$

The position sector P_i is related to the distortion circle of m_i in the following way. Let δ_{M_i} be the radius of the circle centered at some desired position of m_i . Then the angle subtended at m_0 by a tangent to the circle and the line connecting m_0 to the desired position of m_i is given by:

$$\beta_i = \sin^{-1} \left\{ \frac{\delta_{M_i}}{l_i(t_0)} \right\} \quad (2-39)$$

For sufficiently small values of β_i :

$$\sin \beta_i = \sum_{n=1}^{\infty} (-1)^{n-1} \frac{\beta_i^{2n-1}}{(2n-1)!} \doteq \beta_i \quad (2-40)$$

so that (2-39) becomes:

$$\beta_i \doteq \frac{\delta_{M_i}}{l_i(t_0)} \quad (2-41)$$

By comparison with (2-30):

$$\beta_i \doteq \epsilon db_i \quad (2-42)$$

In order for m_i to remain within its distortion circle, the following equation must hold for all $t \geq t_0$:

$$\| y_i(t) - y_i(t_0) \| \leq \delta_{M_i} \quad (2-43)$$

For sufficiently small values of β_i , (2-43) may be approximated by:

$$0 \leq \sqrt{\left\{ \left[\delta_{1_i}(t) \right]^2 + \left[l_i(t) \delta\varphi_i(t) \right]^2 \right\}} \leq \delta_{M_i} \quad (2-44)$$

Since $\delta_{1_i}(t)$ for $i=1\dots 16$ and $\delta\varphi_i(t)$ for $i=9,12,16$ are obtained directly from the data reduction, as will be explained in Section IV, the following two special cases of (2-44) are most often referred to in the subsequent sections:

(i) m_i leaves its position sector $\rightarrow |\delta\varphi_i| > \epsilon db_i$

(ii) m_i leaves its distortion circle radially $\rightarrow |\delta_{1_i}| > \delta_{M_i}$

The control law for the i^{th} peripheral mass is now simply expressed as:

$$T_i(\delta\varphi_i, \dot{\delta\varphi}_i) = \left\{ \begin{array}{ll} +T_{m_i} & (\delta\varphi_i, \dot{\delta\varphi}_i) \in R_i^+ \\ 0 & (\delta\varphi_i, \dot{\delta\varphi}_i) \in R_i \\ -T_{m_i} & (\delta\varphi_i, \dot{\delta\varphi}_i) \in R_i^- \end{array} \right\} \quad (2-45)$$

or explicitly in terms of a switching function $\Delta_i(\delta\varphi_i, \dot{\delta\varphi}_i)$:

$$T_i(\delta\varphi_i, \dot{\delta\varphi}_i) = T_{m_i} \Delta_i(\delta\varphi_i, \dot{\delta\varphi}_i) \quad (2-46)$$

where

$$\Delta_i(\delta\varphi_i, \dot{\delta\varphi}_i) = -\text{dez} \left\{ \zeta_i(\delta\varphi_i + \zeta_i \dot{\delta\varphi}_i) / \epsilon db_i \right\} \quad (2-47)$$

and

$$\text{dez}(u) = \left. \begin{array}{l} -1 \\ 0 \\ +1 \end{array} \right\} \begin{array}{l} (u \leq -1) \\ (|u| < 1) \\ (u \geq +1) \end{array} \quad (2-48)$$

A schematic diagram showing a portion of the control system is shown in Figure 4, using m_4 as the reference subsatellite. The functions h_9, h_{12} and h_{16} represent all terms in the corresponding equations of motion exclusive of the control force terms. Only variables which appear explicitly in the equations are shown as arguments of each h_i , so that the coupling which is present between the equations is not fully illustrated in the figure.

Fuel consumption is easily calculated from the rate of mass decrease for each peripheral m_i :

$$\dot{m}_i = - \frac{|T_i|}{g_0 I_{sp}} = - \frac{T_{m_i}}{g_0 I_{sp}} = -b_i \quad (2-49)$$

The fuel $F_i(t)$ used by a given thruster in time t is given by:

$$F_i(t) = m_i(t) - m_i(t_0) = b_i \tau_{A_i}(t) \quad (2-50)$$

A current estimate of satellite lifetime, based on the fuel capacity F_{c_i} of each peripheral mass m_i , is then given by:

$$L_f(t) = \min \left\{ F_{c_i} / \left[F_i(t) / t \right] \right\} \quad (2-51)$$

$i=4,9,12,16$

Section III: COMPUTATIONAL CONSIDERATIONS

Equations (2-24) through (2-27), together with a set of initial conditions:

$$q(t_0) = q_0, \quad \dot{q}(t_0) = \dot{q}_0 \quad (3-1)$$

comprise an initial value problem for the motion of the lumped mass model of Figure 2. The algorithm chosen for solution of the equations was a fourth-order Runge-Kutta numerical integration procedure applicable to initial value problems for systems of second order equations, as shown by Collatz⁴. For the initial value problem in general form:

$$\ddot{x} = F(t, x, \dot{x}); \quad x(t_0) = x_0, \quad \dot{x}(t_0) = \dot{x}_0 \quad (3-2)$$

the Runge-Kutta algorithm is given by the two recursion formulae:

$$x_{n+1} = x_n + h\dot{x}_n + \frac{h^2}{6} (k_1 + k_2 + k_3) \quad (3-3)$$

$$\dot{x}_{n+1} = \dot{x}_n + \frac{h}{6} (k_1 + 2k_2 + 2k_3 + k_4) \quad (3-4)$$

The auxiliary functions k_i are given by:

$$k_1 = F(t_n, x_n, \dot{x}_n) \quad (3-5)$$

$$k_2 = F\left(t_n + \frac{h}{2}, x_n + \frac{h}{2}\dot{x}_n + \frac{h^2}{8}k_1, \dot{x}_n + \frac{h}{2}k_1\right) \quad (3-6)$$

$$k_3 = F\left(t_n + \frac{h}{2}, x_n + \frac{h}{2}\dot{x}_n + \frac{h^2}{8}k_1, \dot{x}_n + \frac{h}{2}k_2\right) \quad (3-7)$$

$$k_4 = F\left(t_n + h, x_n + h\dot{x}_n + \frac{h^2}{2}k_3, \dot{x}_n + hk_3\right) \quad (3-8)$$

In addition to their use in the recursion formulae, these auxiliary functions

can also be used to assist in determination of the proper integration step size h . If the ratio:

$$\frac{k_{2i} - k_{3i}}{k_{1i} - k_{2i}}$$

is larger than a few percent, a smaller step size should be used. A step size of $h = 1$ second was chosen with the aid of this guideline.

In order to obtain meaningful solutions for the motion of the model, a reasonable set of initial conditions must be chosen. Two sets of conditions immediately suggest themselves: a condition of dynamic equilibrium and a condition of rest. The first would be useful for an analysis of the effect of small disturbances from equilibrium, which pertains to stability of motion, while the second would be useful in studying the problem of deployment. Unfortunately, the equilibrium condition under the influence of the gravitational field cannot be determined without solving the initial value problem (3-2). However, a set of algebraic equations which describe a condition of uniform rotation in a free-space environment can be readily obtained, thus defining a configuration from which meaningful perturbation studies may be conducted.

Determination of such an equilibrium configuration is simplified by taking advantage of the structural symmetry. It is sufficient to solve the equilibrium problem for a quadrant, as shown in Figure 5. The following assumptions are made regarding the equilibrium problem:

III-1. The mass values m_i of the model are determined from the mass distribution of the continuous structure in some assumed rest configuration. For the quadrant of Figure 5, the equations are:

$$m_1 = \rho_D A_D \left(\frac{s_{160}}{2} + s_{180} \right) \quad (3-9)$$

$$m_2 = \rho_R A_R \left(\frac{s_{20}}{2} + \frac{s_{10}}{2} \right) \quad (3-10)$$

$$m_3 = \rho_R A_R \left(\frac{s_{30}}{2} + \frac{s_{20}}{2} \right) \quad (3-11)$$

$$m_4 = \rho_R A_R \left(\frac{s_{30}}{2} + \frac{s_{40}}{2} \right) + \frac{W_4}{g_0} \quad (3-12)$$

$$m_{15} = \rho_D A_D \left(\frac{s_{170}}{2} + \frac{s_{160}}{2} \right) \quad (3-13)$$

$$m_{16} = \rho_D A_D \left(\frac{s_{170}}{2} \right) + \frac{W_{16}}{g_0} \quad (3-14)$$

The physical properties of the continuous structure are assumed to be specified.

III-2. The spring characteristics k_j of the model are related to the physical properties of the continuous wire by the equations:

$$k_j = \frac{A_R E_R}{s_{j0}} \quad (j = 1 \dots 6, 10 \dots 15) \quad (3-15)$$

$$k_j = \frac{A_D E_D}{s_{j0}} \quad (j = 7 \dots 9, 16 \dots 18) \quad (3-16)$$

III-3. The equilibrium configuration is characterized as follows:

- a. The angular velocity, ω , is specified.
- b. The model radius, a , is specified.
- c. The rhombic half-angle, α , is specified.
- d. The distance between adjacent point masses on the rhombic is uniform.
- e. The distance between adjacent point masses of the dipole leg on and exterior to the rhombic is uniform.

Since the specifications of model size and spacing of the point masses are made in the equilibrium configuration, the rest configuration, which would be obtained by removing all energy from the system, is left unspecified, and is, in fact obtained as part of the solution for a particular equilibrium configuration. There are several advantages to this somewhat unconventional approach. First, in order to evaluate the electromagnetic characteristics of the actual KWOT structure in its operating environment, the specification of

geometric properties in the spinning configuration as given by III-3a through III-3c above is desirable. Secondly, the additional specifications III-3d and III-3e together with III-3a through III-3c reduce the number of algebraic equations that must be solved simultaneously to obtain the equilibrium configuration.

It is apparent from elementary principles that the rhombic legs of the model cannot remain straight, as shown in Figure 2, in a state of uniform rotation about m_0 , but must deform in a manner similar to that shown in Figure 5. The equations which define the equilibrium configuration are of four basic types: inertial, elastic, geometric and mass distribution.

The inertial equations may be obtained by writing the equations of motion for each point mass m_i of the quadrant of Figure 5.

$$\text{For } m_1: \quad \tau_{16} - \tau_{18} - 2\tau_1 \sin(\alpha - \theta_2) + m_1 s_{18} \omega^2 = 0 \quad (3-17)$$

$$\text{For } m_2: \quad \tau_3 \left(\frac{\tau_2}{\tau_3} \right) \left[\sin(\mu_2 - \psi_2) - \left(\frac{\tau_1}{\tau_2} \right) \sin \mu_2 \right] + m_2 l_2 \omega^2 = 0 \quad (3-18)$$

$$\left(\frac{\tau_1}{\tau_2} \right) - \cos \psi_2 - \tan \mu_2 \sin \psi_2 = 0 \quad (3-19)$$

$$\text{For } m_3: \quad \tau_3 \left[\sin \mu_3 - \left(\frac{\tau_2}{\tau_3} \right) \sin(\mu_3 + \psi_3) \right] + m_3 l_3 \omega^2 = 0 \quad (3-20)$$

$$\left(\frac{\tau_2}{\tau_3} \right) - \cos \psi_3 + \tan \mu_3 \sin \psi_3 = 0 \quad (3-21)$$

$$\text{For } m_4: \quad 2\tau_3 \cos(\alpha + \theta_3) - m_4 l_4 \omega^2 = 0 \quad (3-22)$$

$$\text{For } m_{15}: \quad \tau_{17} - \tau_{16} + m_{15} l_{15} \omega^2 = 0 \quad (3-23)$$

For m_{16} :

$$\tau_{17} - m_{16} l_{16} \omega^2 = 0 \quad (3-24)$$

The elastic equations are obtained from the law of linear elasticity, incorporating equations (3-15) and (3-16):

$$\tau_j = \frac{A_R E_R}{s_{j0}} (s_j - s_{j0}) \quad (j=1\dots3) \quad (3-25)$$

$$\tau_j = \frac{A_D E_D}{s_{j0}} (s_j - s_{j0}) \quad (j=16\dots18) \quad (3-26)$$

The geometric equations express: (i) the relations between the quantities of Figure 5 which appear in the equations of motion and the generalized coordinates, and (ii) the specifications of assumption III-3.

Transformation relations:

$$s_2^2 - l_2^2 - l_3^2 + 2l_2 l_3 \cos(\varphi_3 - \varphi_2) = 0 \quad (3-27)$$

$$l_3 \sin \varphi_3 + s_3 \cos(\alpha + \theta_3) - l_4 = 0 \quad (3-28)$$

$$l_3 \cos \varphi_3 - s_3 \sin(\alpha + \theta_3) = 0 \quad (3-29)$$

$$l_2 \sin \varphi_2 - s_1 \cos(\alpha - \theta_2) = 0 \quad (3-30)$$

$$l_2 \cos \varphi_2 - s_1 \sin(\alpha - \theta_2) - s_{18} = 0 \quad (3-31)$$

$$\mu_3 - \varphi_3 + (\alpha + \theta_3) = 0 \quad (3-32)$$

$$\mu_2 - \varphi_2 + (\alpha - \theta_2) = 0 \quad (3-33)$$

$$\psi_2 - \theta_2 + \tan^{-1} \left[\frac{s_3 \sin \theta_3 - s_1 \sin \theta_2}{\sqrt{(l_4^2 + s_{18}^2)} - s_3 \cos \theta_3 - s_1 \cos \theta_2} \right] = 0 \quad (3-34)$$

$$\psi_3 - \theta_3 - \tan^{-1} \left[\frac{s_3 \sin \theta_3 - s_1 \sin \theta_2}{\sqrt{(l_4^2 + s_{18}^2)} - s_3 \cos \theta_3 - s_1 \cos \theta_2} \right] = 0 \quad (3-35)$$

Simplifications:

$$l_4 = l_{16} = a \quad (3-36)$$

$$s_{18} = a \tan \alpha \quad (3-37)$$

$$s_1 = s_2 = s_3 = \sigma \quad (3-38)$$

$$s_{16} = s_{17} \quad (3-39)$$

$$s_{16} + s_{17} + s_{18} = l_{16} \quad (3-40)$$

$$s_{16} + s_{18} = l_{15} \quad (3-41)$$

The mass distribution equations are given in (3-9) through (3-14).

Equations (3-9) through (3-14) and (3-17) through (3-41) form a set of 38 independent equations for the 38 variables:

$$m_i \quad (i=1\dots 4, 15, 16)$$

$$s_i, s_{i0}, \tau_i \quad (i=1\dots 3, 16\dots 18)$$

$$\mu_i, \psi_i, \theta_i, \phi_i \quad (i=2,3)$$

$$l_i \quad (i=2\dots 4, 15, 16)$$

$$\sigma$$

By algebraic manipulation, these may be reduced to a set of two simultaneous equations for the rhombic bow angles θ_2 and θ_3 , which, in turn, are used to calculate the remaining variables from the other equations. The solution will be briefly outlined. The geometric transformation relations are rearranged to make θ_2 , θ_3 , s_1 and s_3 the independent variables. Combining (3-30), (3-31), and (3-37) yields:

$$l_2 = \sqrt{[s_1^2 - 2a s_1 \tan \alpha \sin (\alpha - \theta_2) + a^2 \tan^2 \alpha]} \quad (3-42)$$

$$\varphi_2 = \tan^{-1} \left[\frac{s_1 \cos (\alpha - \theta_2)}{a \tan \alpha - s_1 \sin (\alpha - \theta_2)} \right] \quad (3-43)$$

Combining (3-28), (3-29), and (3-36) yields:

$$l_3 = \sqrt{[s_3^2 - 2a s_3 \cos (\alpha + \theta_3) + a^2]} \quad (3-44)$$

$$\varphi_3 = \tan^{-1} \left[\frac{a - s_3 \cos (\alpha + \theta_3)}{s_3 \sin (\alpha + \theta_3)} \right] \quad (3-45)$$

Using (3-43) and (3-45), μ_2 and μ_3 can be expressed, from (3-32) and (3-33), in the form:

$$\mu_2 = \mu_2(\theta_2, \theta_3, s_1, s_3) ; \mu_3 = \mu_3(\theta_2, \theta_3, s_1, s_3) \quad (3-46)$$

Using (3-42) through (3-45), s_2 can be expressed, from (3-27), in the form:

$$s_2 = s_2(\theta_2, \theta_3, s_1, s_3) \quad (3-47)$$

The inertial equations are next reduced with the help of the geometric specifications. Combining (3-21) and (3-22) with (3-20), substituting values of l_2 , l_4 , μ_3 and ψ_3 from (3-44), (3-36), (3-46) and (3-35) and making use of (3-37) and (3-38) yields, after considerable manipulation:

$$\frac{m_3}{m_4} = \frac{\sin \theta_3 \sec \alpha - \left(\frac{\sigma}{a}\right) \sin (\theta_2 + \theta_3)}{2 \cos \epsilon_3 \left\{ \tan \alpha - \left(\frac{\sigma}{a}\right) [\sin \epsilon_2 + \tan \alpha \cos \epsilon_3] - \left(\frac{\sigma}{a}\right)^2 \sin (\theta_2 + \theta_3) \right\}} \quad (3-48)$$

where

$$\epsilon_2 = \alpha - \theta_2 \quad (3-49)$$

$$\epsilon_3 = \alpha + \theta_3 \quad (3-50)$$

Similar manipulations combining (3-19) through (3-22) with (3-18) yield:

$$\frac{m_2}{m_4} = \frac{\sin \theta_2 \sec \alpha - \left(\frac{\sigma}{a}\right) \sin (\theta_2 + \theta_3)}{2 \cot \epsilon_3 \cos \epsilon_2 \tan \alpha \left\{ \tan \alpha - \left(\frac{\sigma}{a}\right) [\sin \epsilon_2 + \tan \alpha \cos \epsilon_3] - \left(\frac{\sigma}{a}\right)^2 \sin (\theta_2 + \theta_3) \right\}} \quad (3-51)$$

Incorporating (3-38) into (3-47) results in a quadratic equation for $\left(\frac{\sigma}{a}\right)$:

$$\left[1 + 2 \cos (\theta_2 + \theta_3)\right] \left(\frac{\sigma}{a}\right)^2 - \left[(\cos \epsilon_2 + \cos \epsilon_3) + \tan \alpha (\sin \epsilon_2 + \sin \epsilon_3) \right] \left(\frac{\sigma}{a}\right) + \sec^2 \alpha = 0 \quad (3-52)$$

whose solution is real if the following condition holds:

$$\sin \theta_3 - \sin \theta_2 \leq 1 \quad (3-53)$$

Of the two solutions for $\frac{\sigma}{a}$, which are both real and positive if (3-53) is satisfied, the smaller root is easily seen to be the proper choice for this model. This root is given by:

$$\frac{\sigma}{a} = \left\{ \frac{[(\cos \epsilon_2 + \cos \epsilon_3) + \tan \alpha (\sin \epsilon_2 + \sin \epsilon_3)]}{[1 + 2 \cos (\theta_2 + \theta_3)]} \right\} \left\{ 1 - \sqrt{1 - \frac{\sec^2 \alpha [1 + 2 \cos (\theta_2 + \theta_3)]}{[(\cos \epsilon_2 + \cos \epsilon_3) + \tan \alpha (\sin \epsilon_2 + \sin \epsilon_3)]^2}} \right\} \quad (3-54)$$

Substitution of (3-54) into (3-48) and (3-51) yields two equations of the form:

$$\frac{m_3}{m_4} - g_3(\theta_2, \theta_3) = 0 \quad (3-55)$$

$$\frac{m_2}{m_4} - g_2(\theta_2, \theta_3) = 0 \quad (3-56)$$

To obtain the solution of (3-55) and (3-56) for θ_2 and θ_3 , an algorithm involving two nested iterations is employed, the second iteration process being carried to completion at each step of the first. Process A is an iteration on the values of m_i , while process B iterates on the values of θ_2 and θ_3 . A rest configuration for the model is assumed, which fixes the m_i values in accordance with equations (3-10) through (3-12). Equations (3-55) and (3-56) are then solved numerically using a multi-dimensional form of Newton's method, which applies to a system of algebraic equations of the form:

$$\underline{f}(\underline{x}) = \underline{0} \quad \underline{x} \in R^n, \underline{f} \in C^1(R^n, R^n) \quad (3-57)$$

The solution algorithm is given by the recursion relation:

$$\underline{x}^{(k+1)} = \underline{x}^{(k)} - \left(\frac{\partial \underline{f}}{\partial \underline{x}}\right)^{-1}_{\underline{x}^{(k)}} \underline{f}(\underline{x}^{(k)}) \quad (3-58)$$

and iteration continues until the criteria:

$$|f_i(\underline{x}^{(k)})| \leq \epsilon_{B_i} \quad (i=1\dots n) \quad (3-59)$$

are satisfied. This algorithm is known to converge quadratically toward the desired solution \underline{x}^* if the initial guess $\underline{x}^{(0)}$ is sufficiently close:

$$\|\underline{x}^{(0)} - \underline{x}^*\| < \epsilon_0 \quad (3-60)$$

The solution of the system (3-55), (3-56) by Newton's method should be expressed as:

$$\theta_2 = \theta_2(s_{20}^{(0)}, s_{30}^{(0)}, s_{40}^{(0)}) ; \theta_3 = \theta_3(s_{20}^{(0)}, s_{30}^{(0)}, s_{40}^{(0)}) \quad (3-61)$$

which shows the dependence upon the initial guess for the rest configuration. This completes process B. Using (3-60), it is then a simple exercise to compute the remaining variables which completely specify the equilibrium configuration. In particular, this includes the variables s_{i0} ($i=2,3,4$) as part of the rest configuration corresponding to the equilibrium configuration. This completes the first step of process A. In general, the solution $s_{i0}^{(k-1)}$ is used as a revised initial guess for step k of process A, which continues until the criteria:

$$|s_{i0}^{(k)} - s_{i0}^{(k-1)}| < \epsilon_A \quad (i=2,3,4) \quad (3-62)$$

is satisfied. Process A is then complete, yielding the correct equilibrium configuration together with the associated rest configuration corresponding to the assigned specifications.

Section IV: INVESTIGATIONS PERFORMED

With the aid of a Scientific Data Systems (SDS)-930 digital computer, performing double precision arithmetic, and a CALCOMP-565 automatic plotter, studies of the motion of the model of Figure 2 were made. A set of programs were written in FORTRAN II to accomplish, successively, the following tasks:

- IV-1. Using a set of configuration specifications,
- a. Compute the free-space equilibrium configuration meeting the specifications and the corresponding rest configuration using the nested iterations of section III.
 - b. Select the configuration to be used for problem initial conditions
- IV-2. Solve the initial value problem defined by (2-24) through (2-27) and (3-1) using the Runge-Kutta algorithm (3-3), (3-4) and record the results on magnetic tape.
- IV-3. Using the magnetic tape output records, perform data reduction by producing:
- a. Graphical displays of certain simple functions of the generalized coordinates and their derivatives, and
 - b. Diagrams of the model structure itself

The following functions were calculated specifically for graphical display: (i) Radial distance deviation, $\delta_{1i}(t)$ and (ii) Spin rate deviation, $\delta\dot{\phi}_i(t)$, defined by:

$$\delta_{1i}(t) = l_i(t) - l_{Ri} \quad (i=1\dots 16) \quad (4-1)$$

$$\delta\dot{\phi}_i(t) = \dot{\phi}_i(t) - \omega_R \quad (i=1\dots 16) \quad (4-2)$$

Six types of graphical display were produced:

- I. Radial distance deviation time history: δ_{1i} vs t , $t \in (0, t_f)$ ($i=1\dots 16$)
- II. Spin rate deviation time history: $\delta\dot{\phi}_i$ vs t , $t \in (0, t_f)$ ($i=1\dots 16$)

- III. Angular position deviation time history: $\delta\phi_i$ vs $t, t \in (0, t_f)$ ($i=9,12,16$)
- IV. Angular position deviation phase plane diagram: $\delta\phi_i$ vs $\delta\dot{\phi}_i, t \in (0, t_f)$
($i=9,12,16$)
- V. Control switching function time history: Δ_i vs $t, t \in (0, t_f)$ ($i=9,12,16$)
- VI. Control switching function time history: Δ_i vs $t, t \in (t_{si}, t_{si} + \tau_{ci})$
($i=9,12,16$)

Type VI plots are simply expanded scale views of the corresponding type V plots over a portion of the computational time interval: $(0, t_f)$.

The investigations performed using these programs may be classified in four categories: verification of equilibrium, small perturbations from equilibrium, large perturbations from equilibrium and deployment. Except for the fourth category, the model configuration at the instant of problem initiation was that corresponding to a free space equilibrium condition of uniform rotation. In all cases, however, the reference condition for computing the deviations of (4-1) and (4-2) was the equilibrium configuration. Each of the cases investigated is assigned a case identifying letter, given in parentheses after the case designation, to facilitate reference to them in the discussion of section V.

1. Verification of equilibrium. (A)

Unperturbed motion in a free space environment was computed.

2. Small perturbations from equilibrium.

a. Field perturbations

1. Gravitational field (B)

Motion perturbed only by the earth's gravitational field was computed.

b. Contact perturbations

Contact perturbations were induced by simulation of an unintentional activation of one of the SMS unit thrusters at problem initiation time. The perturbation thruster was subsequently deactivated when the mass m_i being perturbed attained a specified multiple of its initial angular velocity ω relative to m_0 . All contact perturbation studies were conducted under the simultaneous influence of the gravitational field.

1. Rhombic peripheral mass (m_4): 1.005ω (C)

- 2. Dipole leg peripheral mass (m_g): 1.005ω
 - (a) Free motion (D)
 - (b) Controlled motion: $\zeta = 60$ (E)
- 3. Rhombic peripheral mass: 1.01ω
 - (a) Free motion (F)
 - (b) Controlled motion
 - (i) $\zeta = 60$ (G)
 - (ii) $\zeta = 10$ (H)
 - (iii) $\zeta = 120$ (J)
- 3. Large perturbations from equilibrium.
 - a. Contact perturbations
 - 1. Rhombic peripheral mass: 1.01ω
 - (a) Free motion (K)
 - (b) Controlled motion: $\zeta = 60$ (L)
 - 4. Deployment (M)

A study of one method of deployment was made, starting from the rest configuration corresponding to free-space equilibrium. At problem initiation time, all peripheral mass thrusters were activated simultaneously providing a coordinated spin-up torque. When the reference mass, m_1 , reached the desired angular velocity ω relative to m_0 , all spin-up thrusters were deactivated. The resulting motion was observed under the simultaneous influence of the gravitational field.

All of the investigations were performed using a single set of configuration specifications and environmental conditions, which are listed in Table 1. These were chosen to approximate closely the expected physical characteristics of the actual KWOT structure and its operating environment. The terms "free motion" and "controlled motion" are to be interpreted in the following sense. Each of the perturbation studies considers motion of the system disturbed from the free space equilibrium configuration by certain combinations of field and contact perturbations. A study in which the motion of the system is allowed to evolve under the influences of the perturbations alone, regardless of the amplitudes of the resulting deviations as defined in section IV, is referred to as a study of "free motion". On the other hand, a study in which the motion of the system,

evolving under the influences of the perturbations, is further affected by activation of the configuration control system in order to limit the amplitudes of the angular position deviations, as described in section II, is referred to as a study of "controlled motion".

It is unfortunate that such a large number of restrictive assumptions were necessary. In particular, a similar model incorporating provisions for:

- (i) Three-dimensional motion
- (ii) Variable center-of-mass position, distinct from m_o .
- (iii) Linear damping

would give a better approximation to motion of the actual KWOT structure, without altering the mass distribution. The primary obstacle preventing study of any of these additional features was the word storage capacity of 8K for the computer used in the investigations.

Section V: DISCUSSION OF RESULTS

A. General

Before proceeding with a detailed discussion, the major results are summarized.

1. Free-motion generated by the gravitational field perturbation alone, as well as in combination with a small contact perturbation of a rhombic peripheral mass (1.005ω) appears to be neutrally stable with maximum amplitudes of radial and angular position deviations for each mass interior to the corresponding distortion circles.

2. Free motion generated by the combined influences of the gravitational field perturbation and a small contact perturbation of a dipole peripheral mass (1.005ω) appears to be unstable, with the dipole leg tending to deform in a vee shape with respect to the rhombic major axis.

3. Free motion generated by the combined influences of the gravitational field perturbation and a slightly larger contact perturbation of a rhombic peripheral mass (1.01ω) consists of neutrally stable oscillations which produce angular position deviations that lie outside the position sector for peripheral masses on the dipole leg.

4. The response to the gravitational field perturbation alone, as well as to the combined influences of the gravitational field perturbation and the coordinated deployment thrusting is characterized by radial symmetry in the sense that if $\varphi_i = \varphi_j + \pi$ in the initial configuration, the subsequent motion of m_i and m_j is identical.

5. The response to the combined effects of the gravitational field and tangential thrust perturbations is characterized by dividing the structure into two regions, whose common boundary passes through m_0 and is parallel to the direction of the thrust perturbation. If m_i and m_j are corresponding masses on opposite sides of this boundary (i.e. in mirror image positions) in the initial configuration, the subsequent motion of each is qualitatively similar with two exceptions: (i) A 180° -phase shift appears in the harmonics of order $k > 1$, and (ii) The amplitude of the harmonic components of order $k > 1$ is higher on the side of the perturbation.

6. A continuous-data control system sensing the error and error-rate in relative angular position is able to maintain the peripheral masses within their position sectors for all cases in which free motion exterior to the position sectors occurs. The extrapolated satellite lifetime based on SMS fuel capacity is satisfactory for small thrust perturbations (1.01ω) but not for large perturbations (1.05ω).

7. The control system is unstable for sufficiently small values of the error-rate constant, ζ .

8. Neither field nor contact perturbations generate a tendency for structural collapse because of the inability of the model interconnecting springs to support compressive loading.

9. A coordinated spin-up deployment method starting from a selected unstressed rest configuration can deliver the system into a steady state condition consisting of small amplitude free oscillations about a pre-selected free space equilibrium configuration, in the presence of the gravitational field, in which all masses remain within their respective distortion circles. No active control is required in the absence of further perturbing influences. During the thrusting period, the peripheral masses remain interior to their position sectors, while the rhombic line masses temporarily leave their distortion circles radially. As the heavier peripheral masses move toward their equilibrium positions, the amplitudes of radial oscillations for the line masses are reduced to values less than the radii of the distortion circles.

B. Specific

The results will now be discussed in more detail. Due to considerations of computation time and magnetic tape storage capacity, a uniform problem time, t_f , as listed in Table 1, was used for each case investigated. Consequently, certain motions which appear in the graphical output as non-periodic functions may in fact be periodic with a period $\tau > t_f$. The amplitude and period for those harmonic components of the response that are visible from the graphical displays for free motion are listed in Table 3. Superscripts enclosed in parentheses identify a particular frequency component.

Labeling of the figures displaying the results is simplified by using two identifying characters:

- (i) Plot identifier: a Roman numeral-letter pair that identifies:
 - (a) the type of graphical display (I...VI), defined on pages 23-24
 - (b) the conditions which generate the motion according to the case identifying letter (A...M), defined on pages 24-25
- (ii) Mass identifier: a subscripted letter that identifies the point mass of Figure 2 whose motion is displayed ($m_1 \dots m_{16}$)

1. Verification of equilibrium

The equilibrium configuration satisfying the specifications shown in Table 1 in a free-space environment, and the corresponding rest configuration are listed in Table 2 for the quadrant of Figure 5. With the system initially placed in this equilibrium configuration, the subsequent unperturbed motion showed no visible deviation in radial distance or spin rate for any m_i and consequently no deviation in angular position for any peripheral m_i when displayed on large scale plots. The scaling factors used for $\delta_{1_i}(t)$, $\delta_{\phi_i}^{\cdot}$, and δ_{ϕ_i} were identical to those used in Figures 6 through 12, namely 18.18 ft/in, 3.6375×10^{-6} rad/sec/in and 0.7275 deg/in, respectively.

2. Small perturbations from equilibrium

a. Field perturbations

- (1) Gravitational field (Figures 6-12)

The predominant effect of the gravitational field perturbation is a variation in the spin rate for the masses m_1 , since the radial distance deviations do not exceed 0.5% of the distortion circle radius, as given in Table 1, during periodic oscillations. Deviations in radial distance and spin rate are both symmetric with respect to m_0 :

$$\delta_{1i}(t) = \delta_{1j}(t) \quad (i=1\dots 6,8,9; j=7,10\dots 16) \quad (5-1)$$

$$\delta\dot{\phi}_i(t) = \delta\dot{\phi}_j(t) \quad (i=1\dots 6,8,9; j=7,10\dots 16) \quad (5-2)$$

Figure 6 shows the fundamental oscillation of the rhombic outer mass, $\delta\dot{\phi}_4$, while Figures 7 and 8 show two additional superposed harmonics in the motion of the rhombic line masses, $\delta\dot{\phi}_3$ and $\delta\dot{\phi}_2$, respectively. Figures 9 and 10, showing $\delta\dot{\phi}_8$ and $\delta\dot{\phi}_9$, indicate that:

$$\delta\dot{\phi}_9^{(1)}(t) \doteq -\delta\dot{\phi}_4(t) \quad (5-3)$$

and also show a superposed oscillation with the same frequency as $\delta\dot{\phi}_2^{(2)}(t)$ but of lower amplitude. The following empirical observations:

$$\delta\dot{\phi}_7(t) \doteq \delta\dot{\phi}_4(t) \quad (5-4)$$

$$\delta\dot{\phi}_i^{(k)}(t) = \delta\dot{\phi}_j^{(k)}(t) \quad (i=5,6; j=2,3; k=1,2) \quad (5-5)$$

$$\cancel{\delta\dot{\phi}_i^{(k)}}(t) = \cancel{\delta\dot{\phi}_j^{(k)}}(t) + \pi \quad (i=5,6; j=2,3; k=3) \quad (5-6)$$

allow the remaining spin rate deviations to be deduced from Figures 6 through 10. The deviations in angular position of the peripheral masses that result from these spin rate deviations remain interior to the position sectors. For these deviations:

$$\delta\phi_{1,2}(t) \equiv 0$$

and

$$\delta\varphi_9(t) = \delta\varphi_{16}(t) \quad (5-8)$$

where $\delta\varphi_9(t)$ is shown in Figure 11. The control sector corresponding to $\zeta = 60$ is drawn for reference on the phase plane diagram of Figure 12.

b. Contact perturbations

The duration of unbalanced thrust that produces each of the contact perturbations previously described is listed in Table 4.

(1) Rhombic peripheral mass: 1.005ω

(a) Free motion

The qualitative features of the free motion of the model under small tangential thrust perturbations of different magnitudes applied to a peripheral mass of the rhombic are similar in that the same frequency components appear in the resulting motion. The only difference lies in the amplitudes of the respective components. Thus, Figures 50 through 70, showing the motion for a 1.01ω perturbation, to be discussed later, are sufficient to show the qualitative behavior for the 1.005ω perturbation. The most significant result is that the radial and tangential motion excited by the 1.005ω rhombic perturbation occurs entirely within the distortion circle for each m_i , so that no control is required to maintain the configuration within allowable limits.

(2) Dipole peripheral mass: 1.005ω

(a) Free motion (Figures 13-29)

Motion under the influence of a tangential thrust perturbation of a peripheral mass on the dipole leg is significantly different. The primary effect is an increase in spin rate of the perturbed mass, as shown in Figure 13, accompanied by a decrease for the peripheral mass on the opposite end of the dipole leg, as shown in Figure 14. Both of these changes consist of a low frequency, low amplitude oscillation superposed on a monotonically divergent fundamental. Spin rate deviations for the other m_i are adequately represented by Figures 15-23, since motions of masses on the rhombic legs are connected by the following empirical relations:

$$\delta\dot{\varphi}_i^{(k)}(t) = \delta\dot{\varphi}_j^{(k)}(t) \quad (i=2,3,5,6; j=14,13,11,10; k=1,2) \quad (5-9)$$

$$\dot{\delta\phi}_i^{(k)}(t) = \dot{\delta\phi}_j^{(k)}(t) + \pi \quad (i=2,3,5,6; j=14,13,11,10; k=3) \quad (5-10)$$

$$\dot{\delta\phi}_4(t) = \dot{\delta\phi}_{12}(t) \quad (5-11)$$

Masses on or close to the dipole leg have a fundamental divergence with superposed harmonics in spin rate deviation, while those on the rhombic legs well away from the dipole legs (m_i : $i=3\dots5, 11\dots13$) show a tendency toward neutrally stable oscillations. Although the same frequency components are present for corresponding masses located along the same normal to the rhombic major axis, the amplitudes are higher for masses on the side of the perturbed mass. The result, shown in the full structure diagram of Figure 24, is major distortion of the dipole leg into a vee shape while the rhombic shifts in the direction of the perturbation. Although the radial distance deviations δ_{1i} for rhombic masses m_i undergo large changes, their relative magnitudes are such that major distortion of the rhombic shape does not occur. In view of the following empirical observations:

$$\delta_{1i}(t) \equiv 0 \quad (i=1,7\dots9,15,16) \quad (5-12)$$

$$\delta_{1i}(t) \doteq -\delta_{1j}(t) \quad (i=2\dots6; j=10\dots14) \quad (5-13)$$

the plot of δ_{14} in Figure 25 is sufficient to indicate the qualitative character of all the δ_{1i} . The angular deviations of the peripheral masses on the dipole leg and their corresponding phase plane trajectories leave the position sectors very rapidly, as shown in Figures 26 through 29. The phase plane plots, on which the control sector for $\zeta = 60$ is given for reference, show that the angular deviations approach exponential functions as t approaches t_f with time constants $\gamma_9 = 22$ minutes, $\gamma_{16} = 27.55$ minutes, respectively. The plot for $\delta\phi_{12}$ is omitted since:

$$\delta\phi_{12}(t) \doteq 0 \quad (5-14)$$

(b) Controlled motion: $\zeta = 60$ (Figures 30-49)

Use of the control system described in section II to maintain configuration control produces rapid changes in the spin rate deviation of the m_i for which the control is activated, as shown in Figure 30 for $\delta\dot{\phi}_9$. Each point resembling a jump discontinuity corresponds to a point of control system activation, as seen by comparison with the graph of the switching function Δ_9 in Figure 31. The first cluster of control pulses is expanded in Figure 32 for clarity. This clearly shows the nature of this switching function as consisting largely of a set of one-second pulses, separated by intervals of at least 4 seconds. Figures 33 through 35 display the corresponding information for m_{18} , except that Figure 35 expands the final cluster of control pulses of Figure 34, rather than the initial cluster. The effect on the spin rate deviations for the remainder of the structure is seen by comparison of Figures 36 through 44 with Figures 15 through 23, respectively. In particular, Figures 36 and 37 show the direct effect of the control on the spin rate deviation of line masses lying on the dipole leg between the rhombic and the leg periphery. The primary effect of the control is an arrestment of the divergent fundamental motion that previously appeared in the deviations for masses on or close to the dipole leg, so that the peripheral masses m_i now remain within their distortion circles as indicated by the radial motion of Figure 45 and the tangential motion shown in Figures 46 through 49. Due to the monotonic character of the fundamental free motion for $\delta\phi_9$ and $\delta\phi_{18}$, the control is unidirectional for each controlled mass:

$$\Delta_9 \geq 0 \quad (5-15)$$

$$\Delta_{18} \leq 0 \quad (5-16)$$

The phase plane trajectories of Figures 47 and 49 in conjunction with the graphs of the switching functions in Figures 31 and 34 show that the control is applied in a series of pulses rather than continuously for a certain duration, similar to the "chattering" phenomenon observed in second order bang-bang control systems. The fuel requirements are summarized in Table 4, using the calculations based on equations (2-49) through (2-51).

(3) Rhombic peripheral mass: 1.01ω

(a) Free motion (Figures 50-70)

If the perturbations remain small, the qualitative features of the natural response to tangential thrust perturbations of one of the peripheral rhombic masses are the same for different size perturbations. The radial distance deviations representative of the response are shown in Figures 50 through 54. Since these deviations for masses on the dipole leg are very small ($\leq 0.0104 \delta_{M_i}$), they are not shown. The empirical observations:

$$\delta_{1_4}(t) = \delta_{1_{12}}(t) + \pi \quad (5-17)$$

$$\delta_{1_i}^{(k)}(t) = \delta_{1_j}^{(k)}(t) \quad (i=2,3,14,13; j=6,5,10,11; k=1) \quad (5-18)$$

$$\delta_{1_i}^{(k)}(t) = \delta_{1_j}^{(k)}(t) + \pi \quad (i=2,3,14,13; j=6,5,10,11; k=2) \quad (5-19)$$

allow the remaining δ_{1_i} of the rhombic masses to be deduced from Figures 50 through 54. The higher harmonics of the rhombic leg masses are superposed on the fundamental oscillation of that rhombic peripheral mass on the same side of the dipole leg, and have much lower amplitudes on the side away from the perturbation. The spin rate deviations for rhombic masses are markedly different on opposite sides of the dipole leg, as shown in Figures 55 through 64, the primary difference being the greater amplitude of the second harmonic for masses on the perturbed side of the dipole leg. The relation between the spin rate deviations of the rhombic tip masses:

$$\delta\dot{\phi}_4^{(2)}(t) = \delta\dot{\phi}_{12}^{(2)}(t) + \pi \quad (5-20)$$

is observed to hold, where both deviations oscillate about a fundamental motion $f(t)$ given approximately by:

$$f(t) = -\delta\dot{\phi}_9(t) + 0.877 \times 10^{-5} \text{ sec}^{-1} \quad (5-21)$$

The spin rate deviations of the remaining rhombic masses, in turn, contain higher harmonics superposed on the rhombic tip mass motion. The angular position deviations of the tip masses and the corresponding phase plane trajectories, shown in Figures 65 through 70, show a non-periodic fundamental motion with the superposed harmonic $\delta\phi_{12}(t)$, which combine to exceed the limits of the position sector for the dipole tip masses. The harmonic $\delta\phi_{12}(t)$, for the unperturbed rhombic tip mass, is a pure sinusoidal oscillation, as seen from Figures 67 and 68.

Since the dipole leg peripheral masses leave the position sector in free motion under a 1.01ω rhombic perturbation, activation of the control system is needed for configuration control. Several values of the error rate constant ζ were chosen for comparison of control system performance.

(b) Controlled motion: $\zeta = 60$ (Figures 71-95)

The study of the free motion for this case shows that deviations in radial distance, spin rate and angular position consist generally of a non-periodic fundamental motion modulated by one or more harmonics. The primary effect of the control system is to change the character of the fundamental motion. Although the frequencies of the superposed harmonics are not affected, their amplitudes are changed, the latter effect being most pronounced for spin rate deviations of masses on the dipole leg exterior to the rhombic. The radial distance deviations shown in Figures 71 through 75 show that the moderate changes in each δ_{1i} compared to the free motion of Figures 50 through 54 do not carry any mass outside of its distortion circle radially. The spin rate deviations are shown by Figures 76 through 81, 84, 85, 88, and 89, while the control switching functions are shown in Figures 82, 83, 86, and 87. The amplitude changes in spin rate deviation due to control application for masses on the dipole leg are clearly shown in Figures 80 and 84. Since the free motion of the $\delta\dot{\phi}_i$ is not monotonic, in contrast to case D, Δ_i assumes both signs. The angular position deviations and the associated phase plane trajectories of Figures 90 through 95 show that all controlled tangential motion for the peripheral masses occurs within the closure of the position sector. The final burst of control pulses shown for Δ_{16} in Figure 86 and expanded in Figure 87 is seen from Figures 94 and 95 to be due to the presence of a large magnitude of $\delta\dot{\phi}_{16}$ near the boundary of R_{16} .

Table 4 shows the fuel consumption data for this case, where it is seen that m_{16} governs the satellite lifetime in accordance with (2-51) since it requires the most thrusting time of the peripheral masses.

(c) Controlled motion: $\zeta = 10$ (Figures 96-120)

Reduction of the value of the error-rate constant by a factor of 6 more closely approximates a control package employing pure position control. The results indicate that this reduction is undesirable. The radial distance deviations of Figures 96 through 100 show a large peak reaching an amplitude of $0.51 \delta_{Mi}$ for all masses. The spin rate deviation and switching function graphs for this case, corresponding to Figures 76 through 89, are given in Figures 101 through 114. The plots for the dipole leg masses, however, in Figures 105 through 112, indicate an instability of the control system which causes the switching function to alternate in sign, with an increasing pulse duration. The angular position deviation and phase plane trajectories of Figures 115 through 120 show the high $\dot{\delta}\varphi_i$ rates near the control sector boundaries which generate the large control pulses required to maintain the tangential motion within the position sector. Figure 118 shows that the former pure sinusoidal motion of the unperturbed rhombic peripheral mass has been altered. The fuel consumption data in Table 4 shows that the control of m_9 is now the governing factor for satellite lifetime. The time history and phase plane trajectories of $\delta\varphi_i$ indicate that control pulses of long duration are generated by allowing large magnitudes of $\dot{\delta}\varphi_i$ to occur near the boundary of the control sector. One way of improving this situation is to increase the value of the error-rate constant, ζ .

(d) Controlled motion: $\zeta = 120$ (Figures 121-145)

Increasing the error-rate constant by a factor of 2 from the original choice in case G improves the control system performance markedly. Figures 121 through 125 show that the radial distance deviations compared with Figures 71 through 75 are only slightly affected. The spin rate deviation and switching function graphs of Figures 126 through 139 indicate the control system is stable. The amplitudes of the harmonics induced by the control pulses are greatly reduced for masses on the dipole leg exterior to the rhombic. The angular position deviations and phase plane plots given in Figures 140 through 145 show that the $\dot{\delta}\varphi_i$ rates near the boundary of R_i have been reduced in magnitude, and that pure sinusoidal motion for $\delta\varphi_{12}$ has been re-established.

3. Large perturbations from equilibrium

a. Contact perturbations

(1) Rhombic peripheral mass: 1.05ω

(a) Free motion

The free motion of the model under this large perturbation was observed to be very similar qualitatively to that observed for the smaller 1.01ω perturbation. Accordingly, no figures for this case are presented. Quantitatively, the radial distance deviations for all masses are interior to their distortion circles, although the peak amplitudes for the rhombic line masses increase by nearly a factor of 5. The angular position deviations extend beyond the position sector boundaries for all of the non-reference peripheral masses, so that configuration control is required.

(b) Controlled motion: $\zeta = 60$ (Figures 146-157)

Figures 146 through 157 show the angular position deviation time history, phase plane diagram and switching function time history for m_9 , m_{12} , and m_{18} , respectively. The perturbation is sufficiently large that the control systems for the dipole leg peripheral masses are both activated within 5 seconds after perturbation cut-off, and that for the unperturbed rhombic peripheral mass within 20 seconds. The fuel consumption, from Table 4, is such that the effective satellite lifetime is reduced by nearly a factor of 10 compared to case E. The utility of this result lies in its relation to the deployment problem. Let the large tangential disturbances of a reference satellite be viewed, not as a perturbation from some nominal configuration, but rather as a method of changing the steady state spin rate, with configuration control maintained by the subsatellite control system. In the extreme case, when the initial spin rate is zero, one has the deployment problem of spin-up from rest. These results indicate that a spin-up method that applies thrust exclusively to a reference satellite is inefficient. This observation is the motivation for a coordinated thrusting procedure which applies uniform thrust to each subsatellite during the thrusting phase.

4. Deployment (Figures 158-183)

Coordinated tangential thrust applied to each peripheral mass in spin-up from the rest configuration results in oscillatory motion about the free space equilibrium configuration that is symmetric relative to m_0 in the same sense that was observed for case B, so that equations (5-1) and (5-2) are valid. Figures 158 through 165 show that the radial distance deviations display a large transient peak that approaches 300 feet for rhombic line masses near the dipole leg, but subsequently assume oscillations about the free space equilibrium distance with amplitudes that are interior to their respective distortion circles measured from equilibrium. The cause of these large transient peaks and their "apparent damping" to a satisfactory steady state amplitude is seen, by a comparison of Figure 158, for the motion of the rhombic peripheral mass, with Figures 159, 160, 164, and 165 for the line masses. The rhombic peripheral masses, which initially move inward toward m_0 from the rest configuration with zero spring tension, giving rise to negative strain values for the rhombic legs and the resultant large changes in radial distance deviations, must eventually move radially outward toward the free space equilibrium configuration corresponding to the final spin rate ω and the parameters of the initial rest configuration to satisfy the laws of motion. When this happens, the spring tension is increased, providing the mechanism for the "apparent damping" observed. Figures 166 through 173 show the representative spin rate deviations which display slightly different behavior. The motion of the peripheral masses are truncated ramp functions, given by:

$$R_T(t) = (A_1 t + A_2) \{u(t) - u(t-t_T)\} \quad (5-22)$$

where

$$A_1 = 0.976 \times 10^{-6} \text{ sec}^{-2}$$

$$A_2 = -1.745 \times 10^{-3} \text{ sec}^{-1}$$

with $u(t)$ defined as in equation (2-3). The remaining spin rate deviations oscillate about $R_T(t)$ without displaying a transient peaking as observed in the $\delta_{1_i}(t)$ plots. A very encouraging result is that the angular position deviations

do not leave their respective position sectors during or after spin-up thrusting. Since the symmetric relations (5-7) and (5-8) hold for this case also, Figures 174 and 175 represent the time history and phase plane diagram for the angular position deviation, and clearly illustrate this result. Consequently no activation of the control system after thrust termination is required. Figures 176 through 183 are full structure diagrams of the structure at designated instants during the thrusting phase, and show that the major structural distortion due to the early transient peaking in $\delta_{1i}(t)$ disappears by thrust termination time. The fuel and thrusting time required for spin-up deployment are shown in Table 4.

Section VI: APPLICABILITY

The results obtained for the lumped mass model are encouraging. One can specify certain characteristic parameters of a desired operational configuration, compute the exact free space equilibrium configuration and the associated rest configuration corresponding to these specifications, and then deliver the system, in the presence of the gravitational field, from the rest configuration into a configuration which is sufficiently close to the specified configuration that:

- (i) the allowable structural distortion limits are not exceeded, and
- (ii) no active control for configuration adjustment is required in the absence of further perturbations, at least for high operational altitudes.

The effect of thrust perturbations likely to be encountered if all thrusters are not terminated simultaneously has been determined by a study of contact perturbations, and a simple control system which can counteract small perturbation effects for a satisfactory operational lifetime has been demonstrated.

Several remarks should now be made concerning the extent to which one may view the results obtained for this lumped mass model as applicable to the actual KWOT structure. First, the duration of time for which the motion has been studied is only a few hundredths of one percent of the least useful lifetime envisioned for KWOT. Thus, a classification of "non-periodic" applied to a certain motion, such as the fundamental motion of many of the deviations, is evidently premature. The conclusion of an "infinite" lifetime for the model under the influence of those perturbations which did not produce free motion exterior to the distortion circles of each mass, such as the pure gravitational field perturbation, is similarly premature.

Second, the oscillations that occur due to field or contact perturbations from equilibrium persist in most cases in a steady state condition resembling neutral stability for the model, which does not incorporate provisions for damping. The actual structure, however, will undoubtedly have some degree of natural damping. This can be expected to reduce the amount of fuel required for configuration control due to portions of the structure exceeding their distortion limits.

Third, the assumption that the relative motion of the structure does not affect the motion of the center of mass is equivalent to the assumption that the central observatory has infinite mass, which is clearly not true. In fact, the ratio m_i/m_o of equation (2-1) computed for one of the SMS units alone is expected to be of the order of 10^{-1} for the actual structure, so that assumptions II-1 and II-8 are not really justified. Of the results obtained for the model, the one which appears most sensitive to the validity of these assumptions is the result for case D which indicates instability of the dipole leg to tangential thrust perturbations. The motion that occurs is characterized by a lack of coupling through the central mass m_o , and by the fact that the actual center of mass position, as the motion evolves in time, deviates a significant distance from its assumed position coincident with m_o . These considerations cast doubt on the instability conclusion for structures similar to the model with relatively large m_i/m_o ratios.

Finally, it should be observed that these results have been obtained with a very simple control system, for which no systematic optimization studies have been conducted. Other control concepts, such as a sampled data system, could be expected to perform as well, if not better.

REFERENCES

1. Haddock, F.T., Phase I Final Report, Engineering Feasibility Study of a Kilometer Wave Orbiting Telescope, University of Michigan Radio Astronomy Observatory, Ann Arbor, Michigan, October, 1966.
2. Crist, S.A., Motion and Stability of a Spinning Cable-Connected System in Orbit, UM-RAO Report 67-7, University of Michigan Radio Astronomy Observatory, Ann Arbor, Michigan, June, 1967.
3. Greenwood, D.T., Principles of Dynamics, Prentice-Hall, Englewood Cliffs, New Jersey, 1965.
4. Collatz, L., The Numerical Treatment of Differential Equations, Springer-Verlag, Berlin, 1960.

Appendix A: GLOSSARY OF TERMSRoman letters - lower case

a	Radius of model in equilibrium configuration
b_i	Rate of fuel ejection from thruster associated with m_i
c_j	Characteristic of linear damper in parallel with j^{th} spring
\underline{e}_j	Unit vector acting in direction of instantaneous strain
f_i	Component of total force at a point in direction of positive x_i
\underline{f}_{E_i}	Force vector due to i^{th} spring
\underline{f}_{G_i}	Force vector acting on m_i due to m_E
g_0	Gravitational acceleration at surface of earth
h	Step size for Runge-Kutta integration
h_i	Function representing the equation of free motion for m_i
\underline{k}_i	i^{th} auxiliary vector function for Runge-Kutta integration
k_j	Linear characteristic of j^{th} spring
l_i	Distance of m_i from m_0
l_{R_i}	Reference distance of m_i from m_0
m_E	Mass of earth
m_i	i^{th} point mass of lumped mass model
\underline{q}	Generalized coordinate vector
r	Distance of m_0 from earth center
s	Laplace transform variable
s_j	Length of j^{th} spring
s_{j0}	Value of s_j at zero strain
t	Time
t_f	Problem termination time
t_k	Value of t at k^{th} step of Runge-Kutta integration
t_0	Problem initiation time
t_{s_i}	Start time for plot type VI of Δ_i
t_T	Thrust duration for thrust perturbations
\underline{x}_k	State vector \underline{x} at k^{th} step of Runge-Kutta integration
$\underline{x}(k)$	Vector \underline{x} at k^{th} stage of Newton's method iteration
x_i	Cartesian position coordinate
Y_i	Position vector of m_i relative to m_0
\underline{z}_i	Position vector of m_i relative to earth center

Roman letters - upper case

A_D	Cross-sectional area of continuous wire comprising dipole legs
A_R	Cross-sectional area of continuous wire comprising rhombic legs
D	Rayleigh dissipation function
E_D	Modulus of elasticity of continuous wire comprising dipole legs
E_R	Modulus of elasticity of continuous wire comprising rhombic legs
\underline{F}	Vector function representing general second order equation of motion
F_{C_i}	Fuel capacity of SMS unit associated with m_i
F_i	Fuel used for configuration control
F_{T_i}	Fuel used for thrust perturbations
G	Universal gravitational constant
I_{sp}	Specific impulse of thruster propellant
K_j	Non-linear characteristic of j^{th} spring
L	Lagrangian function
M	Total mass of lumped mass model
P_i	Position sector associated with m_i
Q	Generalized force vector
Q_R	Generalized force not derivable from a potential or dissipation function
Q_v	Generalized force derivable from a dissipation function
R_i	Control sector associated with m_i
R_i^+	Region exterior to R_i requiring $\Delta_i > 0$
R_i^-	Region exterior to R_i requiring $\Delta_i < 0$
T	Total kinetic energy
T_{m_i}	Thrust level for thruster associated with m_i
T_i	Thrust produced by thruster associated with m_i
V	Total potential energy
V_E	Potential energy associated with elastic forces
V_G	Potential energy associated with gravitational forces
W	Work
W_i	Weight of SMS unit associated with m_i

Greek letters - lower case

α	Rhombic half-angle defined by $m_0 - m_4 - m_1$ in the equilibrium configuration
β_i	Half-angle subtended by distortion circle of m_i at m_0
γ_i	Time constants for motion of $\delta\phi_i$
δ_{1i}	Radial distance deviation for m_i
δ_{M_i}	Radius of distortion circle for m_i
$\delta\dot{\phi}_i$	Spin rate deviation for m_i
$\delta\dot{\phi}_i(j)$	j^{th} harmonic component of $\delta\dot{\phi}_i$
$\delta\phi_i$	Angular position deviation for m_i
ϵ_A	Convergence parameter for iteration process A
ϵ_{B_i}	Convergence parameter for i^{th} equation for iteration process B
ϵ_{db_i}	Radius of position sector for tangential motion of m_i
ϵ_{E_j}	Instantaneous strain of j^{th} spring
ϵ_i	Angle between rhombic major axis and spring connecting m_i to a principal axis of the structure in equilibrium
ϵ_0	Radius of ball about the true solution containing initial guesses for which Newton's method converges
ζ_i	Error rate constant for control system for m_i
θ	Angular position of m_0 measured at earth center
θ_i	Acute angle defining the deviation from a straight rhombic leg configuration for the spring connecting a rhombic leg mass m_i to a principal axis of the structure in equilibrium
μ_E	Earth gravitational constant
μ_i	Acute angle defined by γ_i and the normal to the spring which connects m_i to a principal axis of the structure in equilibrium
ρ_D	Volume density of continuous wire comprising dipole legs
ρ_R	Volume density of continuous wire comprising rhombic legs
σ	Uniform spacing of point masses along rhombic leg in equilibrium configuration
τ_{A_i}	Cumulative activation time for thruster associated with m_i
τ_{C_i}	Time duration for plot type VI of Δ_i
τ_j	Tension in j^{th} spring
ϕ_i	Angular position of m_i measured at m_0
ϕ_R	Reference value for ϕ_i

ψ_i	Acute angle between two adjacent springs at m_i
ω	Angular velocity of model about m_0 in the equilibrium configuration
ω_R	Reference spin rate for m_i relative to m_0

Greek letters - upper case

Γ_{L_i}	Left boundary of P_i
Γ_{R_i}	Right boundary of P_i
Γ_{+i}	Left boundary of R_i
Γ_{-i}	Right boundary of R_i
Δ_i	Control switching function for control thruster associated with m_i

Special symbols

ϕ	Phase angle
$ \underline{x} $	Euclidean norm of the vector \underline{x} defined by $\sqrt{\sum_{i=1}^n x_i^2}$

Appendix B: ELASTIC POTENTIAL DERIVATIVES

The elastic potential $V_E(\underline{q}, t)$ is defined by equations (2-3), (2-13), (2-14), and (2-15). The derivatives $\partial V_E / \partial q_i$, expressed in terms of the generalized coordinates are listed below for completeness:

$\partial V_E / \partial l_i$ ($i=1 \dots 16$):

$$\partial V_E / \partial l_1 = k_1 u \{ s_1 - s_{10} \} \left(1 - \frac{s_{10}}{s_1} \right) \left[l_1 - l_2 \cos(\varphi_2 - \varphi_1) \right] + k_{15} u \{ s_{15} - s_{150} \} \left(1 - \frac{s_{150}}{s_{15}} \right) \left[l_1 - l_{14} \cos(\varphi_1 - \varphi_{14}) \right]$$

$$+ k_{18} u \{ s_{18} - s_{180} \} \left(1 - \frac{s_{180}}{s_{18}} \right) \left[l_1 - l_{15} \cos(\varphi_{15} - \varphi_1) \right] + k_{18} u \{ s_{18} - s_{180} \} (s_{18} - s_{180})$$

$$\partial V_E / \partial l_2 = k_1 u \{ s_1 - s_{10} \} \left(1 - \frac{s_{10}}{s_1} \right) \left[l_2 - l_1 \cos(\varphi_2 - \varphi_1) \right] + k_2 u \{ s_2 - s_{20} \} \left(1 - \frac{s_{20}}{s_2} \right) \left[l_2 - l_3 \cos(\varphi_3 - \varphi_2) \right]$$

$$\partial V_E / \partial l_3 = k_2 u \{ s_2 - s_{20} \} \left(1 - \frac{s_{20}}{s_2} \right) \left[l_3 - l_2 \cos(\varphi_3 - \varphi_2) \right] + k_3 u \{ s_3 - s_{30} \} \left(1 - \frac{s_{30}}{s_3} \right) \left[l_3 - l_4 \cos(\varphi_4 - \varphi_3) \right]$$

$$\partial V_E / \partial l_4 = k_3 u \{ s_3 - s_{30} \} \left(1 - \frac{s_{30}}{s_3} \right) \left[l_4 - l_3 \cos(\varphi_4 - \varphi_3) \right] + k_4 u \{ s_4 - s_{40} \} \left(1 - \frac{s_{40}}{s_4} \right) \left[l_4 - l_5 \cos(\varphi_5 - \varphi_4) \right]$$

$$\partial V_E / \partial l_5 = k_4 u \{ s_4 - s_{40} \} \left(1 - \frac{s_{40}}{s_4} \right) \left[l_5 - l_4 \cos(\varphi_5 - \varphi_4) \right] + k_5 u \{ s_5 - s_{50} \} \left(1 - \frac{s_{50}}{s_5} \right) \left[l_5 - l_6 \cos(\varphi_6 - \varphi_5) \right]$$

$$\partial V_E / \partial l_6 = k_5 u \{ s_5 - s_{50} \} \left(1 - \frac{s_{50}}{s_5} \right) \left[l_6 - l_5 \cos(\varphi_6 - \varphi_5) \right] + k_6 u \{ s_6 - s_{60} \} \left(1 - \frac{s_{60}}{s_6} \right) \left[l_6 - l_7 \cos(\varphi_7 - \varphi_6) \right]$$

$$\partial V_E / \partial l_7 = k_6 u \{ s_6 - s_{60} \} \left(1 - \frac{s_{60}}{s_6} \right) \left[l_7 - l_6 \cos(\varphi_7 - \varphi_6) \right] + k_7 u \{ s_7 - s_{70} \} (s_7 - s_{70}) + k_8 u \{ s_8 - s_{80} \} \left(1 - \frac{s_{80}}{s_8} \right)$$

$$\times \left[l_7 - l_8 \cos(\varphi_8 - \varphi_7) \right] + k_{10} u \{ s_{10} - s_{100} \} \left(1 - \frac{s_{100}}{s_{10}} \right) \left[l_7 - l_{10} \cos(\varphi_{10} - \varphi_7) \right]$$

$$\partial V_E / \partial l_8 = k_8 u \{ s_8 - s_{80} \} \left(1 - \frac{s_{80}}{s_8} \right) \left[l_8 - l_7 \cos(\varphi_8 - \varphi_7) \right] + k_9 u \{ s_9 - s_{90} \} \left(1 - \frac{s_{90}}{s_9} \right) \left[l_8 - l_9 \cos(\varphi_9 - \varphi_8) \right]$$

$$\partial V_E / \partial l_9 = k_9 u \{ s_9 - s_{90} \} \left(1 - \frac{s_{90}}{s_9} \right) \left[1_9 - 1_8 \cos(\varphi_9 - \varphi_8) \right]$$

$$\partial V_E / \partial l_{10} = k_{11} u \{ s_{11} - s_{110} \} \left(1 - \frac{s_{110}}{s_{11}} \right) \left[1_{10} - 1_{11} \cos(\varphi_{11} - \varphi_{10}) \right] + k_{10} u \{ s_{10} - s_{100} \} \left(1 - \frac{s_{100}}{s_{10}} \right) \left[1_{10} - 1_7 \right. \\ \left. \times \cos(\varphi_{10} - \varphi_7) \right]$$

$$\partial V_E / \partial l_{11} = k_{11} u \{ s_{11} - s_{110} \} \left(1 - \frac{s_{110}}{s_{11}} \right) \left[1_{11} - 1_{10} \cos(\varphi_{11} - \varphi_{10}) \right] + k_{12} u \{ s_{12} - s_{120} \} \left(1 - \frac{s_{120}}{s_{12}} \right) \left[1_{11} - 1_{12} \right. \\ \left. \times \cos(\varphi_{12} - \varphi_{11}) \right]$$

$$\partial V_E / \partial l_{12} = k_{12} u \{ s_{12} - s_{120} \} \left(1 - \frac{s_{120}}{s_{12}} \right) \left[1_{12} - 1_{11} \cos(\varphi_{12} - \varphi_{11}) \right] + k_{13} u \{ s_{13} - s_{130} \} \left(1 - \frac{s_{130}}{s_{13}} \right) \left[1_{12} - 1_{13} \right. \\ \left. \times \cos(\varphi_{13} - \varphi_{12}) \right]$$

$$\partial V_E / \partial l_{13} = k_{13} u \{ s_{13} - s_{130} \} \left(1 - \frac{s_{130}}{s_{13}} \right) \left[1_{13} - 1_{12} \cos(\varphi_{13} - \varphi_{12}) \right] + k_{14} u \{ s_{14} - s_{140} \} \left(1 - \frac{s_{140}}{s_{14}} \right) \left[1_{13} - 1_{14} \right. \\ \left. \times \cos(\varphi_{14} - \varphi_{13}) \right]$$

$$\partial V_E / \partial l_{14} = k_{14} u \{ s_{14} - s_{140} \} \left(1 - \frac{s_{140}}{s_{14}} \right) \left[1_{14} - 1_{13} \cos(\varphi_{14} - \varphi_{13}) \right] + k_{15} u \{ s_{15} - s_{150} \} \left(1 - \frac{s_{150}}{s_{15}} \right) \left[1_{14} - 1_1 \right. \\ \left. \times \cos(\varphi_1 - \varphi_{14}) \right]$$

$$\partial V_E / \partial l_{15} = k_{15} u \{ s_{15} - s_{150} \} \left(1 - \frac{s_{150}}{s_{15}} \right) \left[1_{15} - 1_1 \cos(\varphi_{15} - \varphi_1) \right] + k_{17} u \{ s_{17} - s_{170} \} \left(1 - \frac{s_{170}}{s_{17}} \right) \left[1_{15} - 1_{16} \right. \\ \left. \times \cos(\varphi_{16} - \varphi_{15}) \right]$$

$$\partial V_E / \partial l_{16} = k_{17} u \{ s_{17} - s_{170} \} \left(1 - \frac{s_{170}}{s_{17}} \right) \left[1_{16} - 1_{15} \cos(\varphi_{16} - \varphi_{15}) \right]$$

$$\underline{\partial V_E / \partial \varphi_i} \quad (i=1 \dots 16)$$

$$\begin{aligned} \partial V_E / \partial \varphi_1 = & l_1 \left\{ -k_1 u \{s_1 - s_{10}\} \left(1 - \frac{s_{10}}{s_1}\right) \left[l_2 \sin(\varphi_2 - \varphi_1) \right] + k_{15} u \{s_{15} - s_{150}\} \left(1 - \frac{s_{150}}{s_{15}}\right) \left[l_{14} \sin \right. \right. \\ & \left. \left. (\varphi_1 - \varphi_{14}) \right] - k_{16} u \{s_{16} - s_{160}\} \left(1 - \frac{s_{160}}{s_{16}}\right) \left[l_{15} \sin(\varphi_{15} - \varphi_1) \right] \right\} \end{aligned}$$

$$\partial V_E / \partial \varphi_2 = l_2 \left\{ k_1 u \{s_1 - s_{10}\} \left(1 - \frac{s_{10}}{s_1}\right) \left[l_1 \sin(\varphi_2 - \varphi_1) \right] - k_2 u \{s_2 - s_{20}\} \left(1 - \frac{s_{20}}{s_2}\right) \left[l_3 \sin(\varphi_3 - \varphi_2) \right] \right\}$$

$$\partial V_E / \partial \varphi_3 = l_3 \left\{ k_2 u \{s_2 - s_{20}\} \left(1 - \frac{s_{20}}{s_2}\right) \left[l_2 \sin(\varphi_3 - \varphi_2) \right] - k_3 u \{s_3 - s_{30}\} \left(1 - \frac{s_{30}}{s_3}\right) \left[l_4 \sin(\varphi_4 - \varphi_3) \right] \right\}$$

$$\partial V_E / \partial \varphi_4 = l_4 \left\{ k_3 u \{s_3 - s_{30}\} \left(1 - \frac{s_{30}}{s_3}\right) \left[l_3 \sin(\varphi_4 - \varphi_3) \right] - k_4 u \{s_4 - s_{40}\} \left(1 - \frac{s_{40}}{s_4}\right) \left[l_5 \sin(\varphi_5 - \varphi_4) \right] \right\}$$

$$\partial V_E / \partial \varphi_5 = l_5 \left\{ k_4 u \{s_4 - s_{40}\} \left(1 - \frac{s_{40}}{s_4}\right) \left[l_4 \sin(\varphi_5 - \varphi_4) \right] - k_5 u \{s_5 - s_{50}\} \left(1 - \frac{s_{50}}{s_5}\right) \left[l_6 \sin(\varphi_6 - \varphi_5) \right] \right\}$$

$$\partial V_E / \partial \varphi_6 = l_6 \left\{ k_5 u \{s_5 - s_{50}\} \left(1 - \frac{s_{50}}{s_5}\right) \left[l_5 \sin(\varphi_6 - \varphi_5) \right] - k_6 u \{s_6 - s_{60}\} \left(1 - \frac{s_{60}}{s_6}\right) \left[l_7 \sin(\varphi_7 - \varphi_6) \right] \right\}$$

$$\begin{aligned} \partial V_E / \partial \varphi_7 = & l_7 \left\{ k_6 u \{s_6 - s_{60}\} \left(1 - \frac{s_{60}}{s_6}\right) \left[l_6 \sin(\varphi_7 - \varphi_6) \right] - k_8 u \{s_8 - s_{80}\} \left(1 - \frac{s_{80}}{s_8}\right) \left[l_8 \sin(\varphi_8 - \varphi_7) \right] \right. \\ & \left. - k_{10} u \{s_{10} - s_{100}\} \left(1 - \frac{s_{100}}{s_{10}}\right) \left[l_{10} \sin(\varphi_{10} - \varphi_7) \right] \right\} \end{aligned}$$

$$\partial V_E / \partial \varphi_8 = l_8 \left\{ k_8 u \{s_8 - s_{80}\} \left(1 - \frac{s_{80}}{s_8}\right) \left[l_7 \sin(\varphi_8 - \varphi_7) \right] - k_9 u \{s_9 - s_{90}\} \left(1 - \frac{s_{90}}{s_9}\right) \left[l_9 \sin(\varphi_9 - \varphi_8) \right] \right\}$$

$$\partial V_E / \partial \varphi_9 = l_9 \left\{ k_9 u \{s_9 - s_{90}\} \left(1 - \frac{s_{90}}{s_9}\right) \left[l_8 \sin(\varphi_9 - \varphi_8) \right] \right\}$$

$$\frac{\partial V_E}{\partial \varphi_{10}} = l_{10} \left\{ k_{10} u \{ s_{10} - s_{100} \} \left(1 - \frac{s_{100}}{s_{10}} \right) \left[l_7 \sin(\varphi_{10} - \varphi_7) \right] - k_{11} u \{ s_{11} - s_{110} \} \left(1 - \frac{s_{110}}{s_{11}} \right) \left[l_{11} \right. \right. \\ \left. \left. \times \sin(\varphi_{11} - \varphi_{10}) \right] \right\}$$

$$\frac{\partial V_E}{\partial \varphi_{11}} = l_{11} \left\{ k_{11} u \{ s_{11} - s_{110} \} \left(1 - \frac{s_{110}}{s_{11}} \right) \left[l_{10} \sin(\varphi_{11} - \varphi_{10}) \right] - k_{12} u \{ s_{12} - s_{120} \} \left(1 - \frac{s_{120}}{s_{12}} \right) \left[l_{12} \right. \right. \\ \left. \left. \times \sin(\varphi_{12} - \varphi_{11}) \right] \right\}$$

$$\frac{\partial V_E}{\partial \varphi_{12}} = l_{12} \left\{ k_{12} u \{ s_{12} - s_{120} \} \left(1 - \frac{s_{120}}{s_{12}} \right) \left[l_{11} \sin(\varphi_{12} - \varphi_{11}) \right] - k_{13} u \{ s_{13} - s_{130} \} \left(1 - \frac{s_{130}}{s_{13}} \right) \left[l_{13} \right. \right. \\ \left. \left. \times \sin(\varphi_{13} - \varphi_{12}) \right] \right\}$$

$$\frac{\partial V_E}{\partial \varphi_{13}} = l_{13} \left\{ k_{13} u \{ s_{13} - s_{130} \} \left(1 - \frac{s_{130}}{s_{13}} \right) \left[l_{12} \sin(\varphi_{13} - \varphi_{12}) \right] - k_{14} u \{ s_{14} - s_{140} \} \left(1 - \frac{s_{140}}{s_{14}} \right) \left[l_{14} \right. \right. \\ \left. \left. \times \sin(\varphi_{14} - \varphi_{13}) \right] \right\}$$

$$\frac{\partial V_E}{\partial \varphi_{14}} = l_{14} \left\{ k_{14} u \{ s_{14} - s_{140} \} \left(1 - \frac{s_{140}}{s_{14}} \right) \left[l_{13} \sin(\varphi_{14} - \varphi_{13}) \right] - k_{15} u \{ s_{15} - s_{150} \} \left(1 - \frac{s_{150}}{s_{15}} \right) \left[l_{15} \right. \right. \\ \left. \left. \times \sin(\varphi_{15} - \varphi_{14}) \right] \right\}$$

$$\frac{\partial V_E}{\partial \varphi_{15}} = l_{15} \left\{ k_{15} u \{ s_{15} - s_{150} \} \left(1 - \frac{s_{150}}{s_{15}} \right) \left[l_{14} \sin(\varphi_{15} - \varphi_{14}) \right] - k_{17} u \{ s_{17} - s_{170} \} \left(1 - \frac{s_{170}}{s_{17}} \right) \left[l_{17} \right. \right. \\ \left. \left. \times \sin(\varphi_{17} - \varphi_{15}) \right] \right\}$$

$$\frac{\partial V_E}{\partial \varphi_{16}} = l_{16} \left\{ k_{17} u \{ s_{17} - s_{170} \} \left(1 - \frac{s_{170}}{s_{17}} \right) \left[l_{15} \sin(\varphi_{16} - \varphi_{15}) \right] \right\}$$

Appendix C: Incorporation of Artificial Damping

In this appendix, the equations governing the motion of a model similar to that of Figure 2 incorporating damping are derived. Consider the structure of Figure 2 with the additional feature that a linear damper with characteristic c_j is connected between each point mass in parallel with the spring k_j . Although equation (2-4) may be used directly to generate the equations of motion, with the viscous dissipation forces computed as part of the generalized force vector \underline{Q} , another form of (2-4) may be obtained by introducing the Rayleigh dissipation function $D(\underline{q}, \dot{\underline{q}}, t)$, defined by:

$$D(\underline{q}, \dot{\underline{q}}, t) = \frac{1}{2} \left\{ \text{Rate of energy dissipation in system} \right\}$$

as described in reference 3. The generalized forces due to viscous dissipation may thus be separated as:

$$\underline{Q}_v = - \frac{\partial D}{\partial \dot{\underline{q}}} \quad (\text{C-1})$$

so that

$$\underline{Q} = \underline{Q}_R - \frac{\partial D}{\partial \dot{\underline{q}}} \quad (\text{C-2})$$

Lagrange's equations may now be expressed in the form:

$$\frac{d}{dt} \left(\frac{\partial L}{\partial \dot{\underline{q}}} \right) + \frac{\partial D}{\partial \dot{\underline{q}}} - \frac{\partial L}{\partial \underline{q}} = \underline{Q}_R \quad (\text{C-3})$$

The dissipation function for the model described is given by:

$$D(\underline{q}, \dot{\underline{q}}, t) = \frac{1}{2} \sum_{k=1}^{18} c_k \dot{s}_k^2(\underline{q}, \dot{\underline{q}}, t) \quad (\text{C-4})$$

If s_k is the length of the spring connecting m_i and m_j , it is expressed in terms of the generalized coordinates by equations (2-14) and (2-15), and its derivative is given by:

$$\dot{s}_k = \left(\frac{1}{r_k}\right) \left\{ \left[1_i - 1_j \cos(\varphi_i - \varphi_j) \right] \dot{1}_i + \left[1_j - 1_i \cos(\varphi_i - \varphi_j) \right] \dot{1}_j + \left[1_i 1_j \sin(\varphi_i - \varphi_j) \right] \dot{\varphi}_i - \left[1_i 1_j \sin(\varphi_i - \varphi_j) \right] \dot{\varphi}_j \right\} \quad (C-5)$$

When the necessary manipulations are completed, in accordance with equation (C-3), the equations of motion for each mass m_i become:

$$\ddot{1}_i - 1_i \dot{\varphi}_i^2 - \frac{\mu 1_i}{2r^3} \left[1 + 3 \cos 2(\theta - \varphi_i) \right] + \left(\frac{1}{m_i} \right) \left[\frac{\partial V_E}{\partial 1_i} + \frac{\partial D}{\partial 1_i} \right] = 0 \quad (i=1 \dots 16) \quad (C-6)$$

$$1_i \ddot{\varphi}_i + 2 \dot{1}_i \dot{\varphi}_i - \frac{3\mu 1_i}{2r^3} \sin 2(\theta - \varphi_i) + \left(\frac{1}{m_i 1_i} \right) \left[\frac{\partial V_E}{\partial \varphi_i} + \frac{\partial D}{\partial \varphi_i} - Q_{Ri} \right] = 0 \quad (i=1 \dots 16) \quad (C-7)$$

The forces Q_{Ri} are given by equation (2-17). The derivatives, $\partial D / \partial \dot{1}_i$, $\partial D / \partial \dot{\varphi}_i$ are listed below for completeness:

$\partial D / \partial \dot{1}_i$ ($i=1 \dots 16$)

$$\frac{\partial D}{\partial \dot{1}_1} = \left(\frac{c \dot{s}}{s_1} \right) \left[1_1 - 1_2 \cos(\varphi_2 - \varphi_1) \right] + \left(\frac{c \dot{s}}{s_{15}} \right) \left[1_1 - 1_{14} \cos(\varphi_1 - \varphi_{14}) \right] + \left(\frac{c \dot{s}}{s_{16}} \right) \times \left[1_1 - 1_{15} \cos(\varphi_{15} - \varphi_1) \right] + (c \dot{s}_{18})$$

$$\frac{\partial D}{\partial \dot{1}_2} = \left(\frac{c \dot{s}}{s_1} \right) \left[1_2 - 1_1 \cos(\varphi_2 - \varphi_1) \right] + \left(\frac{c \dot{s}}{s_2} \right) \left[1_2 - 1_3 \cos(\varphi_3 - \varphi_2) \right]$$

$$\frac{\partial D}{\partial \dot{1}_3} = \left(\frac{c \dot{s}}{s_2} \right) \left[1_3 - 1_2 \cos(\varphi_3 - \varphi_2) \right] + \left(\frac{c \dot{s}}{s_3} \right) \left[1_3 - 1_4 \cos(\varphi_4 - \varphi_3) \right]$$

$$\frac{\partial D}{\partial \dot{1}_4} = \left(\frac{c \dot{s}}{s_3} \right) \left[1_4 - 1_3 \cos(\varphi_4 - \varphi_3) \right] + \left(\frac{c \dot{s}}{s_4} \right) \left[1_4 - 1_5 \cos(\varphi_5 - \varphi_4) \right]$$

$$\frac{\partial D}{\partial \dot{1}_5} = \left(\frac{c \dot{s}}{s_4} \right) \left[1_5 - 1_4 \cos(\varphi_5 - \varphi_4) \right] + \left(\frac{c \dot{s}}{s_5} \right) \left[1_5 - 1_6 \cos(\varphi_6 - \varphi_5) \right]$$

$$\partial D / \partial \dot{i}_5 = \left(\frac{c \dot{s}_5}{s_5} \right) [1_5 - 1_5 \cos(\varphi_6 - \varphi_5)] + \left(\frac{c \dot{s}_6}{s_6} \right) [1_8 - 1_7 \cos(\varphi_7 - \varphi_6)]$$

$$\begin{aligned} \partial D / \partial \dot{i}_7 = & \left(\frac{c \dot{s}_6}{s_6} \right) [1_7 - 1_6 \cos(\varphi_7 - \varphi_6)] + (c \dot{s}_7) + \left(\frac{c \dot{s}_8}{s_8} \right) [1_7 - 1_8 \cos(\varphi_8 - \varphi_7)] + \frac{c \dot{s}_{10}}{s_{10}} \\ & \times [-1_7 - 1_{10} \cos(\varphi_{10} - \varphi_7)] \end{aligned}$$

$$\partial D / \partial \dot{i}_8 = \left(\frac{c \dot{s}_8}{s_8} \right) [1_8 - 1_7 \cos(\varphi_8 - \varphi_7)] + \left(\frac{c \dot{s}_9}{s_9} \right) [1_8 - 1_9 \cos(\varphi_9 - \varphi_8)]$$

$$\partial D / \partial \dot{i}_9 = \left(\frac{c \dot{s}_9}{s_9} \right) [1_9 - 1_8 \cos(\varphi_9 - \varphi_8)]$$

$$\partial D / \partial \dot{i}_{10} = \left(\frac{c \dot{s}_{10}}{s_{10}} \right) [1_{10} - 1_7 \cos(\varphi_{10} - \varphi_7)] + \left(\frac{c \dot{s}_{11}}{s_{11}} \right) [1_{10} - 1_{11} \cos(\varphi_{11} - \varphi_{10})]$$

$$\partial D / \partial \dot{i}_{11} = \left(\frac{c \dot{s}_{11}}{s_{11}} \right) [1_{11} - 1_{10} \cos(\varphi_{11} - \varphi_{10})] + \left(\frac{c \dot{s}_{12}}{s_{12}} \right) [1_{11} - 1_{12} \cos(\varphi_{12} - \varphi_{11})]$$

$$\partial D / \partial \dot{i}_{12} = \left(\frac{c \dot{s}_{12}}{s_{12}} \right) [1_{12} - 1_{11} \cos(\varphi_{12} - \varphi_{11})] + \left(\frac{c \dot{s}_{13}}{s_{13}} \right) [1_{12} - 1_{13} \cos(\varphi_{13} - \varphi_{12})]$$

$$\partial D / \partial \dot{i}_{13} = \left(\frac{c \dot{s}_{13}}{s_{13}} \right) [1_{13} - 1_{12} \cos(\varphi_{13} - \varphi_{12})] + \left(\frac{c \dot{s}_{14}}{s_{14}} \right) [1_{13} - 1_{14} \cos(\varphi_{14} - \varphi_{13})]$$

$$\partial D / \partial \dot{i}_{14} = \left(\frac{c \dot{s}_{14}}{s_{14}} \right) [1_{14} - 1_{13} \cos(\varphi_{14} - \varphi_{13})] + \left(\frac{c \dot{s}_{15}}{s_{15}} \right) [1_{14} - 1_1 \cos(\varphi_1 - \varphi_{14})]$$

$$\partial D / \partial \dot{i}_{15} = \left(\frac{c \dot{s}_{15}}{s_{15}} \right) [1_{15} - 1_1 \cos(\varphi_{15} - \varphi_1)] + \left(\frac{c \dot{s}_{17}}{s_{17}} \right) [1_{15} - 1_{16} \cos(\varphi_{16} - \varphi_{15})]$$

$$\partial D / \partial \dot{i}_{16} = \left(\frac{c \dot{s}_{17}}{s_{17}} \right) [1_{16} - 1_{15} \cos(\varphi_{16} - \varphi_{15})]$$

$$\underline{\partial D / \partial \dot{\phi}_i} \quad (i=1 \dots 16)$$

$$\partial D / \partial \dot{\phi}_1 = 1_1 \left\{ \left(\frac{c_{15} \dot{s}_{15}}{s_{15}} \right) \left[1_{14} \sin(\varphi_1 - \varphi_{14}) \right] - \left(\frac{c_{11} \dot{s}_{11}}{s_{11}} \right) \left[1_2 \sin(\varphi_2 - \varphi_1) \right] - \left(\frac{c_{16} \dot{s}_{16}}{s_{16}} \right) \left[1_{15} \sin(\varphi_{15} - \varphi_1) \right] \right\}$$

$$\partial D / \partial \dot{\phi}_2 = 1_2 \left\{ \left(\frac{c_{11} \dot{s}_{11}}{s_{11}} \right) \left[1_1 \sin(\varphi_2 - \varphi_1) \right] - \left(\frac{c_{22} \dot{s}_{22}}{s_{22}} \right) \left[1_3 \sin(\varphi_3 - \varphi_2) \right] \right\}$$

$$\partial D / \partial \dot{\phi}_3 = 1_3 \left\{ \left(\frac{c_{22} \dot{s}_{22}}{s_{22}} \right) \left[1_2 \sin(\varphi_3 - \varphi_2) \right] - \left(\frac{c_{33} \dot{s}_{33}}{s_{33}} \right) \left[1_4 \sin(\varphi_4 - \varphi_3) \right] \right\}$$

$$\partial D / \partial \dot{\phi}_4 = 1_4 \left\{ \left(\frac{c_{33} \dot{s}_{33}}{s_{33}} \right) \left[1_3 \sin(\varphi_4 - \varphi_3) \right] - \left(\frac{c_{44} \dot{s}_{44}}{s_{44}} \right) \left[1_5 \sin(\varphi_5 - \varphi_4) \right] \right\}$$

$$\partial D / \partial \dot{\phi}_5 = 1_5 \left\{ \left(\frac{c_{44} \dot{s}_{44}}{s_{44}} \right) \left[1_4 \sin(\varphi_5 - \varphi_4) \right] - \left(\frac{c_{55} \dot{s}_{55}}{s_{55}} \right) \left[1_6 \sin(\varphi_6 - \varphi_5) \right] \right\}$$

$$\partial D / \partial \dot{\phi}_6 = 1_6 \left\{ \left(\frac{c_{55} \dot{s}_{55}}{s_{55}} \right) \left[1_5 \sin(\varphi_6 - \varphi_5) \right] - \left(\frac{c_{66} \dot{s}_{66}}{s_{66}} \right) \left[1_7 \sin(\varphi_7 - \varphi_6) \right] \right\}$$

$$\partial D / \partial \dot{\phi}_7 = 1_7 \left\{ \left(\frac{c_{66} \dot{s}_{66}}{s_{66}} \right) \left[1_6 \sin(\varphi_7 - \varphi_6) \right] - \left(\frac{c_{88} \dot{s}_{88}}{s_{88}} \right) \left[1_8 \sin(\varphi_8 - \varphi_7) \right] - \left(\frac{c_{1010} \dot{s}_{1010}}{s_{1010}} \right) \left[1_{10} \sin(\varphi_{10} - \varphi_7) \right] \right\}$$

$$\partial D / \partial \dot{\phi}_8 = 1_8 \left\{ \left(\frac{c_{88} \dot{s}_{88}}{s_{88}} \right) \left[1_7 \sin(\varphi_8 - \varphi_7) \right] - \left(\frac{c_{99} \dot{s}_{99}}{s_{99}} \right) \left[1_9 \sin(\varphi_9 - \varphi_8) \right] \right\}$$

$$\partial D / \partial \dot{\phi}_9 = 1_9 \left\{ \left(\frac{c_{99} \dot{s}_{99}}{s_{99}} \right) \left[1_8 \sin(\varphi_9 - \varphi_8) \right] \right\}$$

$$\partial D / \partial \dot{\phi}_{10} = 1_{10} \left\{ \left(\frac{c_{1010} \dot{s}_{1010}}{s_{1010}} \right) \left[1_7 \sin(\varphi_{10} - \varphi_7) \right] - \left(\frac{c_{1111} \dot{s}_{1111}}{s_{1111}} \right) \left[1_{11} \sin(\varphi_{11} - \varphi_{10}) \right] \right\}$$

$$\partial D / \partial \dot{\phi}_{11} = 1_{11} \left\{ \left(\frac{c_{1111} \dot{s}_{1111}}{s_{1111}} \right) \left[1_{10} \sin(\varphi_{11} - \varphi_{10}) \right] - \left(\frac{c_{1212} \dot{s}_{1212}}{s_{1212}} \right) \left[1_{12} \sin(\varphi_{12} - \varphi_{11}) \right] \right\}$$

$$\partial D / \partial \dot{\phi}_{12} = 1_{12} \left\{ \left(\frac{c_{1212} \dot{s}_{1212}}{s_{1212}} \right) \left[1_{11} \sin(\varphi_{12} - \varphi_{11}) \right] - \left(\frac{c_{1313} \dot{s}_{1313}}{s_{1313}} \right) \left[1_{13} \sin(\varphi_{13} - \varphi_{12}) \right] \right\}$$

$$\partial D / \partial \dot{\phi}_{13} = 1_{13} \left\{ \left(\frac{c_{13} \dot{s}_{13}}{s_{13}} \right) \left[1_{12} \sin(\phi_{13} - \phi_{12}) \right] - \left(\frac{c_{14} \dot{s}_{14}}{s_{14}} \right) \left[1_{14} \sin(\phi_{14} - \phi_{13}) \right] \right\}$$

$$\partial D / \partial \dot{\phi}_{14} = 1_{14} \left\{ \left(\frac{c_{14} \dot{s}_{14}}{s_{14}} \right) \left[1_{13} \sin(\phi_{14} - \phi_{13}) \right] - \left(\frac{c_{15} \dot{s}_{15}}{s_{15}} \right) \left[1_1 \sin(\phi_1 - \phi_{14}) \right] \right\}$$

$$\partial D / \partial \dot{\phi}_{15} = 1_{15} \left\{ \left(\frac{c_{16} \dot{s}_{16}}{s_{16}} \right) \left[1_1 \sin(\phi_{15} - \phi_1) \right] - \left(\frac{c_{17} \dot{s}_{17}}{s_{17}} \right) \left[1_{16} \sin(\phi_{16} - \phi_{15}) \right] \right\}$$

$$\partial D / \partial \dot{\phi}_{16} = 1_{16} \left\{ \left(\frac{c_{17} \dot{s}_{17}}{s_{17}} \right) \left[1_{15} \sin(\phi_{16} - \phi_{15}) \right] \right\}$$

Table 1 - Configuration Specifications and Environmental ConditionsConfiguration Specifications

1. Material properties of rhombic wire	
Radius, r_R	0.01 in.
Modulus of elasticity, E_R	260,000 #/in. ²
Volume density, ρ_R	70 #/ft. ³
2. Material properties of radial wire	
Radius, r_D	0.01 in.
Modulus of elasticity, E_D	260,000 #/in. ²
Volume density, ρ_R	70 #/ft. ³
3. SMS unit characteristics	
Weight, W_i (i=4,9,12,16)	200 #
Thrust level, T_{m_i} (i=4,9,12,16)	0.1 #
4. Equilibrium condition requirements	
Angular velocity, ω	1 rev/hr.
Model radius, a	5 km.
Rhombic half-angle, α	13.3 deg.

Environmental Conditions

1. Gravitational Field characteristics	
Gravitational constant, μ	$1.407775 \cdot 10^{16} \text{ ft}^3/\text{sec}^2$
2. Orbital specifications	
Eccentricity, e	0
Period, τ	24 hr.

Other Parameters

Dead band radius, ϵ_{db_i} (i=9,12,16)	0.01 rad.
Problem termination time, t_f	1.5 hr.
Distortion circle radius, δM_i (i=1...16)	50 meters

Table 2 - Configuration SolutionsFree Space Equilibrium1. Rhombic leg shape

$$\begin{aligned}\theta_2 &= 0.10891716 \text{ deg.} \\ \theta_3 &= 0.10920864 \text{ deg.} \\ \sigma/a &= 0.34252052\end{aligned}$$

2. Spring tension

$$\begin{aligned}\tau_1 &= 0.16113813 \# \\ \tau_2 &= 0.16075628 \# \\ \tau_3 &= 0.15992107 \# \\ \tau_{15} &= 0.31144620 \# \\ \tau_{17} &= 0.31053510 \# \\ \tau_{18} &= 0.23849823 \#\end{aligned}$$

3. Generalized coordinates

$$\begin{aligned}l_1 &= 3872.0680 \text{ ft.} \\ l_2 &= 6046.1208 \text{ ft.} \\ l_3 &= 10999.684 \text{ ft.} \\ l_4 &= 16380.000 \text{ ft.} \\ l_{15} &= 10126.034 \text{ ft.} \\ l_{16} &= 16380.000 \text{ ft.} \\ \phi_2 &= 64.617149 \text{ deg} \\ \phi_3 &= 83.206874 \text{ deg}\end{aligned}$$

Rest Configuration1. Unstressed spring lengths

$$\begin{aligned}s_{10} &= 5599.4398 \text{ ft.} \\ s_{20} &= 5599.4659 \text{ ft.} \\ s_{30} &= 5599.5231 \text{ ft.} \\ s_{160} &= 3860.7950 \text{ ft.} \\ s_{170} &= 6230.2106 \text{ ft.} \\ s_{180} &= 6230.2798 \text{ ft.}\end{aligned}$$

2. Point mass values

$$\begin{aligned}m_1 &= 0.050486223 \text{ slugs} \\ m_2 &= 0.026556764 \text{ slugs} \\ m_3 &= 0.026556961 \text{ slugs} \\ m_4 &= 6.2377372 \text{ slugs} \\ m_{15} &= 0.029548449 \text{ slugs} \\ m_{16} &= 6.2259544 \text{ slugs}\end{aligned}$$

3. Generalized coordinates

$$\begin{aligned}l_{1r} &= 3860.7950 \text{ ft.} \\ l_{2r} &= 6026.8044 \text{ ft.} \\ l_{3r} &= 10974.835 \text{ ft.} \\ l_{4r} &= 16348.745 \text{ ft.} \\ l_{15r} &= 10091.006 \text{ ft.} \\ l_{16r} &= 16321.285 \text{ ft.} \\ \phi_{2r} &= 64.718194 \text{ deg.} \\ \phi_{3r} &= 83.265827 \text{ deg.}\end{aligned}$$

4. Rhombic mass deviation from rest

$$\begin{aligned}m_2 &: 22.055669 \text{ ft., } \nlessgtr \\ &35.807569 \text{ deg.} \\ m_3 &: 27.300447 \text{ ft., } \nlessgtr \\ &58.774144 \text{ deg.}\end{aligned}$$

Table 3 - Spectral Characteristics of Free Motion

Case Identifier	Harmonic Component	Amplitude (10^{-8} sec^{-1})	Period (sec)
B	$\delta\dot{\phi}_3$ (2)	0.431	2935
	$\delta\dot{\phi}_3$ (3)	0.431	212.5
	$\delta\dot{\phi}_2$ (2)	0.718	2935
	$\delta\dot{\phi}_2$ (3)	0.718	212.5
	$\delta\dot{\phi}_8$ (2)	0.1437	212.5
	$\delta\dot{\phi}_9$ (2)	0.1437	212.5
D	$\delta\dot{\phi}_9$ (2)	2.87	1800
	$\delta\dot{\phi}_{15}$ (2)	2.87	1800
	$\delta\dot{\phi}_8$ (2)	2.87	1800
	$\delta\dot{\phi}_8$ (3)	0.718	109
	$\delta\dot{\phi}_{15}$ (2)	2.87	1800
	$\delta\dot{\phi}_{15}$ (3)	0.919	109
	$\delta\dot{\phi}_7$ (2)	8.62	1800
	$\delta\dot{\phi}_1$ (2)	4.59	1800
	$\delta\dot{\phi}_{10}$ (2)	2.865	1518
	$\delta\dot{\phi}_{10}$ (3)	2.865	212.5
	$\delta\dot{\phi}_{14}$ (2)	1.438	1518
	$\delta\dot{\phi}_{14}$ (3)	1.438	212.5
	$\delta\dot{\phi}_{11}$ (2)	2.155	1518
	$\delta\dot{\phi}_{11}$ (3)	2.155	212.5
	$\delta\dot{\phi}_{13}$ (2)	1.438	1518
	$\delta\dot{\phi}_{13}$ (3)	1.438	212.5

Case Identifier	Harmonic Component	Amplitude (10^{-6} sec^{-1})	Period (sec)
F	$\delta\dot{\phi}_4$ (2)	8.7	646
	$\delta\dot{\phi}_1$ (2)	12.95	646
	$\delta\dot{\phi}_1$ (3)	0.72	19.02
	$\delta\dot{\phi}_8$ (2)	2.88	646
	$\delta\dot{\phi}_8$ (3)	2.155	109
	$\delta\dot{\phi}_{12}$ (7)	0.1062 deg.	641

Table 4 - Fuel Consumption Data

Propulsion System Parameters

$$T_{m_i} = 0.1 \text{ \#} \quad (i=4,9,12,16)$$

$$F_{c_i} = 50 \text{ \#} \quad (i=4,9,12,16)$$

$$g_0 = 32.2 \text{ ft/sec}^2$$

$$I_{sp} = 200 \text{ sec}$$

Thrust Perturbations

Type Perturbation	$\dot{\phi}_i \left(\frac{t}{\text{sec}^{-10}} \right)$	$\dot{\phi}_i \left(\frac{t}{\text{sec}^{-1T}} \right)$	τ_T (sec)	F_{T_i} (#)
{ Perturbation of m_i from equilibrium }	ω	1.005 ω	9	0.0045
	ω	1.01 ω	18	0.009
	ω	1.05 ω	97	0.0485
Spin-up from rest	0	ω	1788	3.566

Configuration Control System

Case Identifier	τ_{A_4} (sec)	τ_{A_9} (sec)	$\tau_{A_{12}}$ (sec)	$\tau_{A_{16}}$ (sec)	F_i (#)	L_f (months)
E	0	26	0	26	0.026	8.02
G	0	7	0	33	0.020	6.30
H	0	55	0	21	0.038	3.875
J	0	12	0	16	0.014	13.04
L	0	296	17	305	0.309	0.683

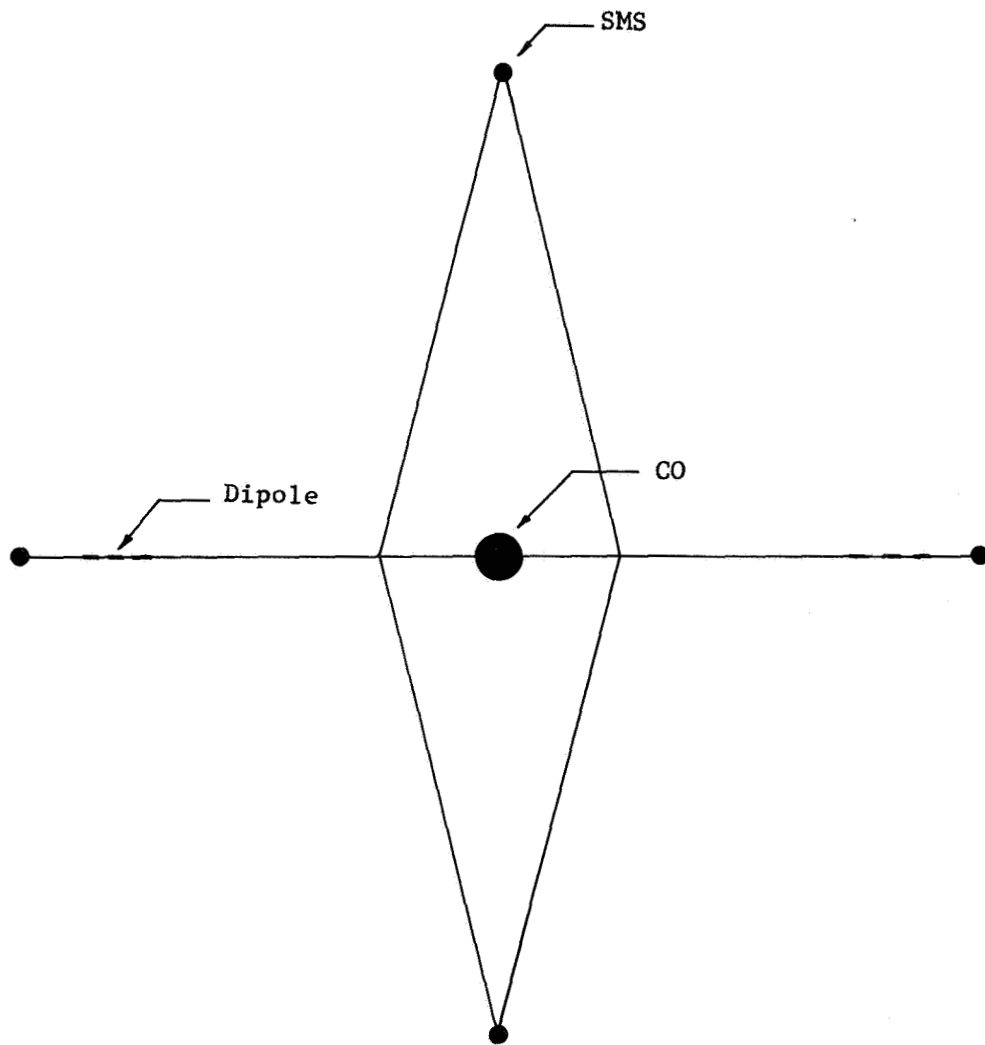


Figure 1. Continuous KWOT Structure

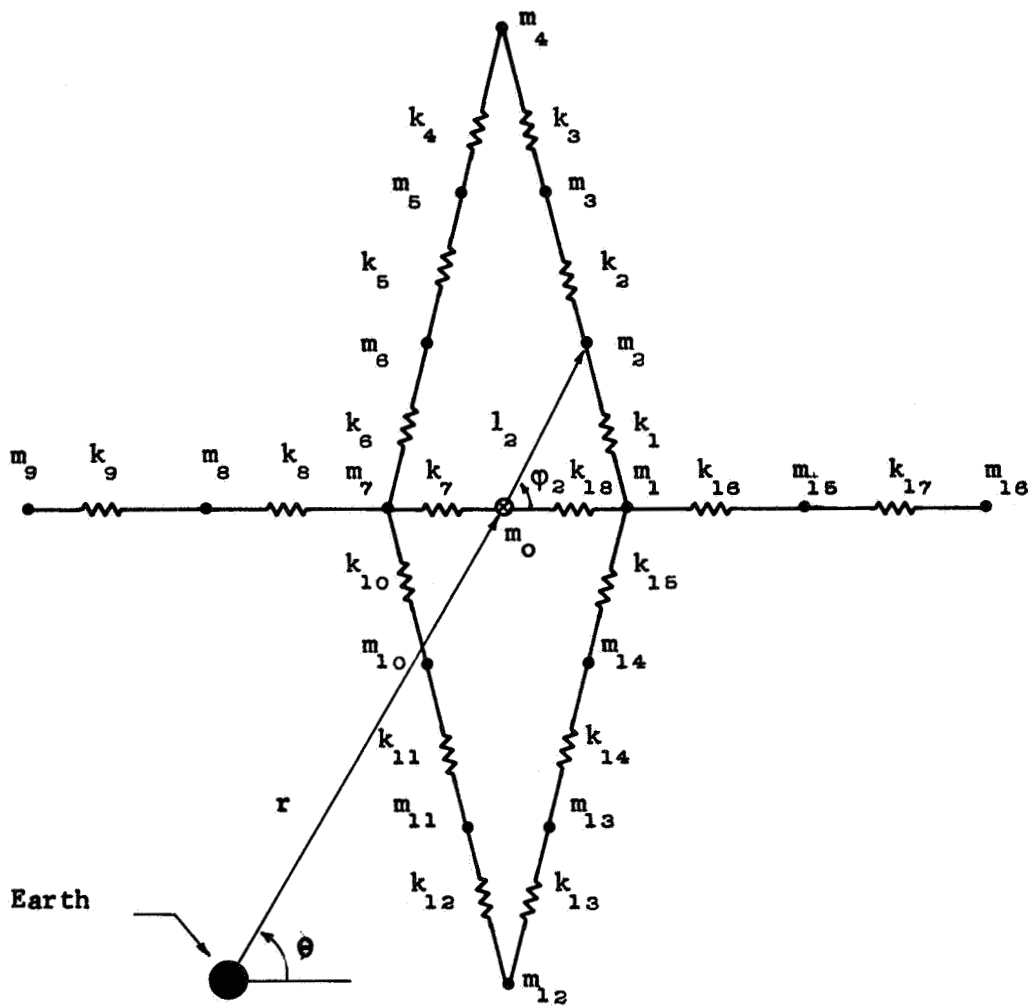


Figure 2. Lumped-mass Approximate Model of KWOT

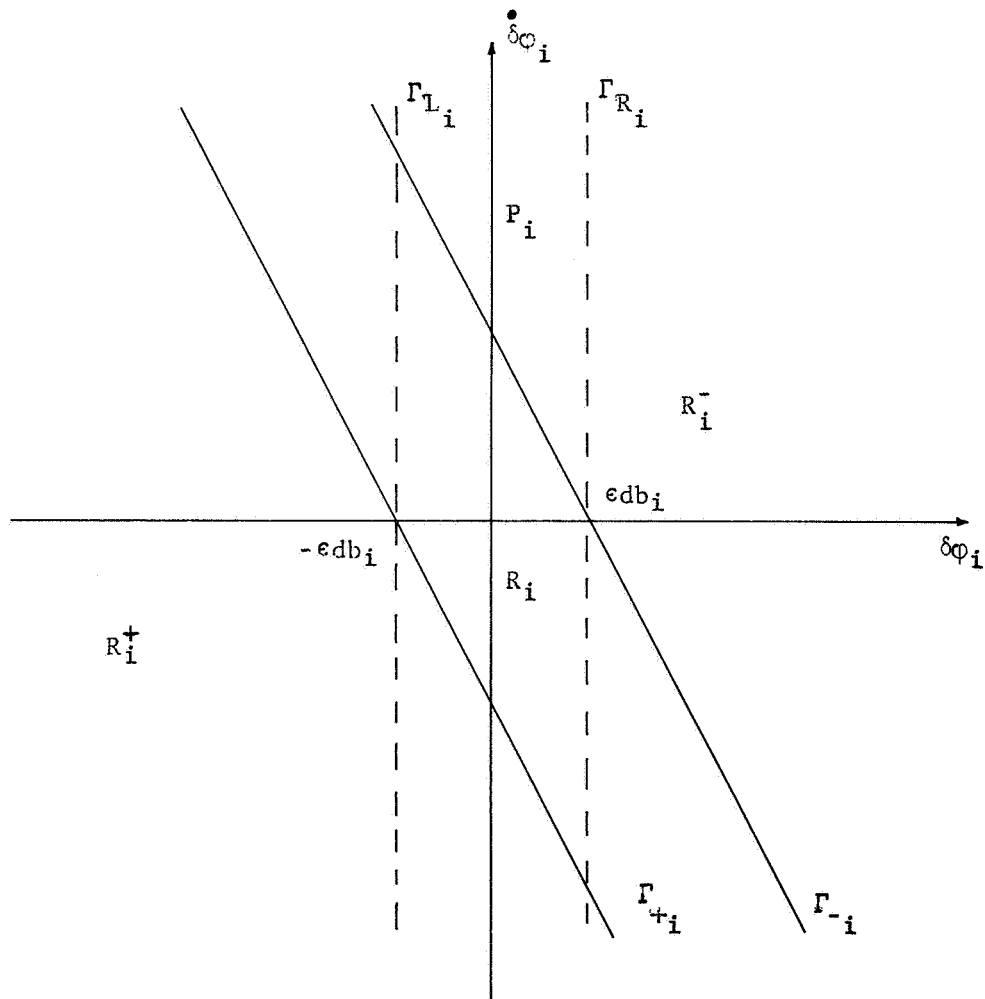


Figure 3. Control System Position and Control Sectors

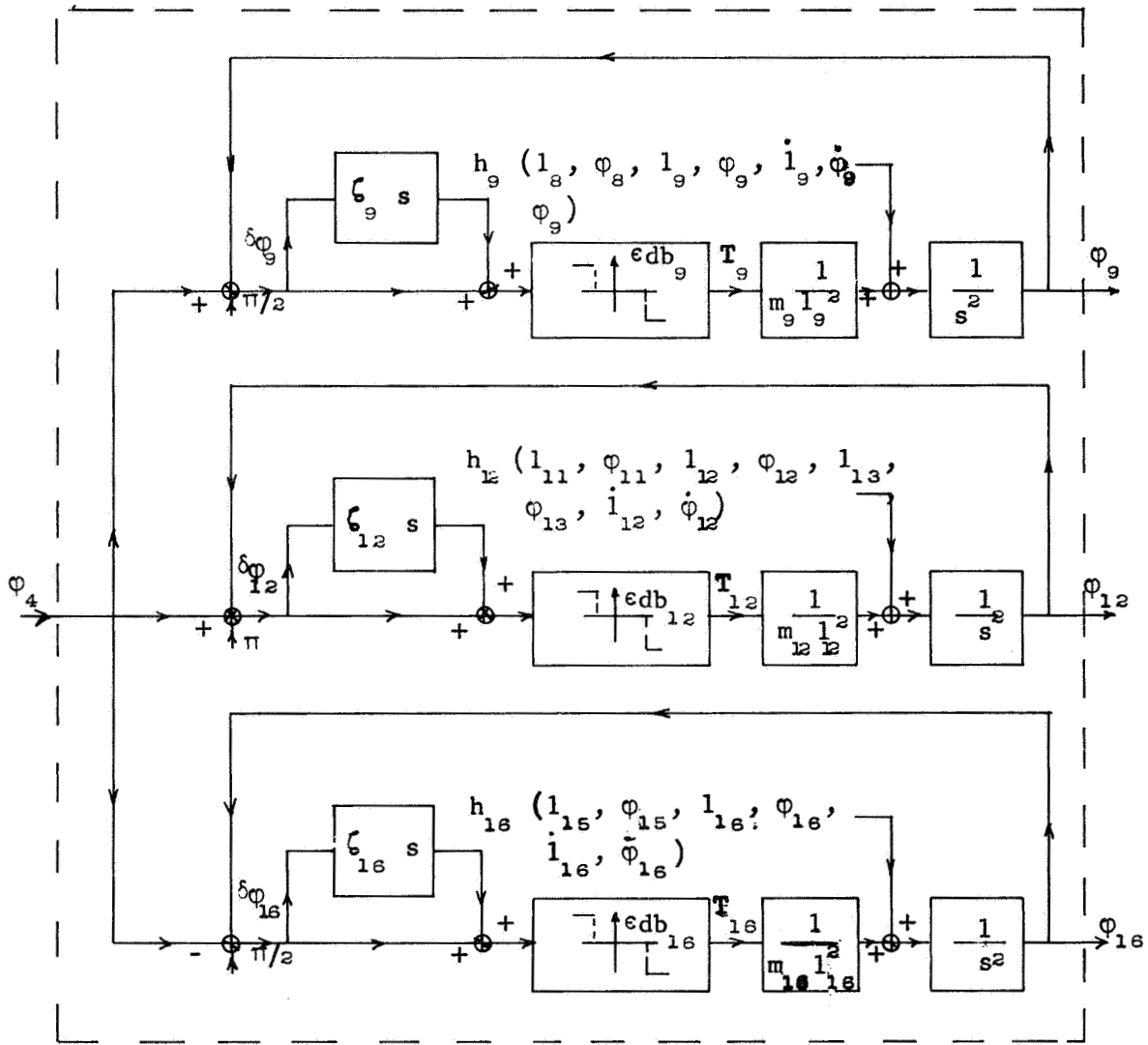


Figure 4. Control System Schematic Diagram

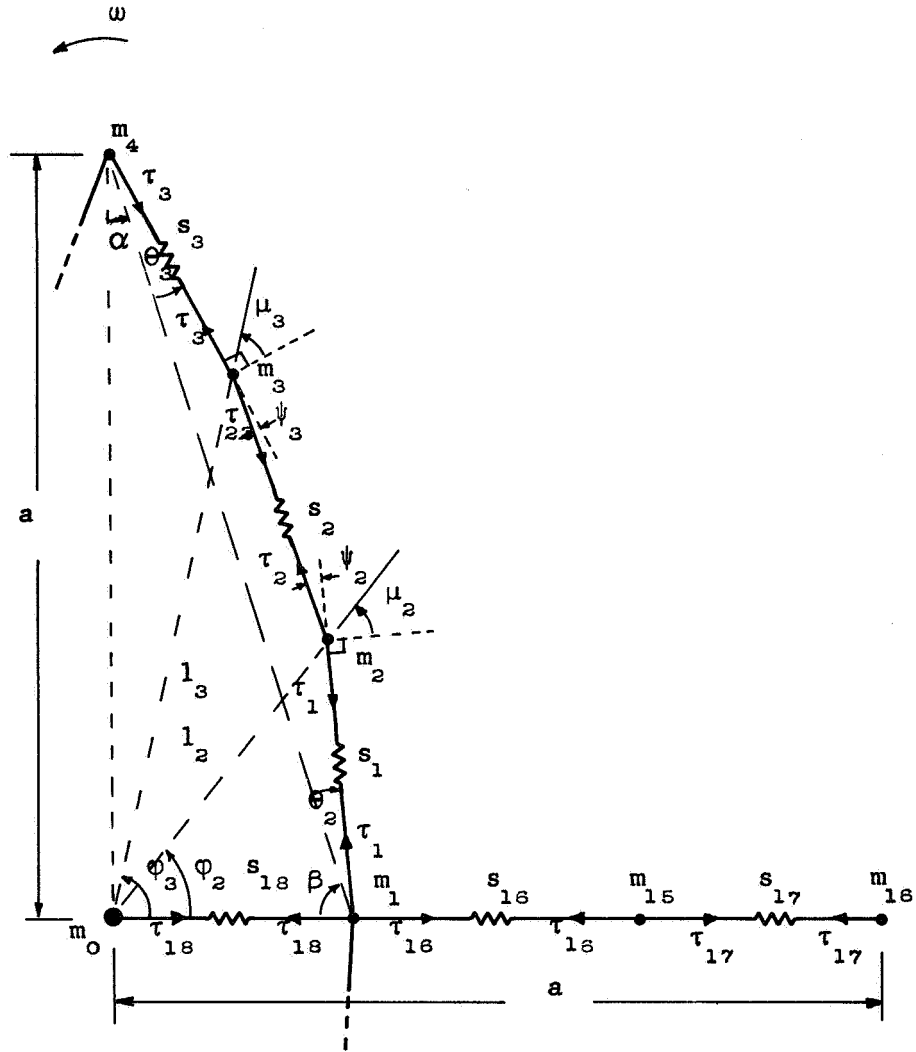
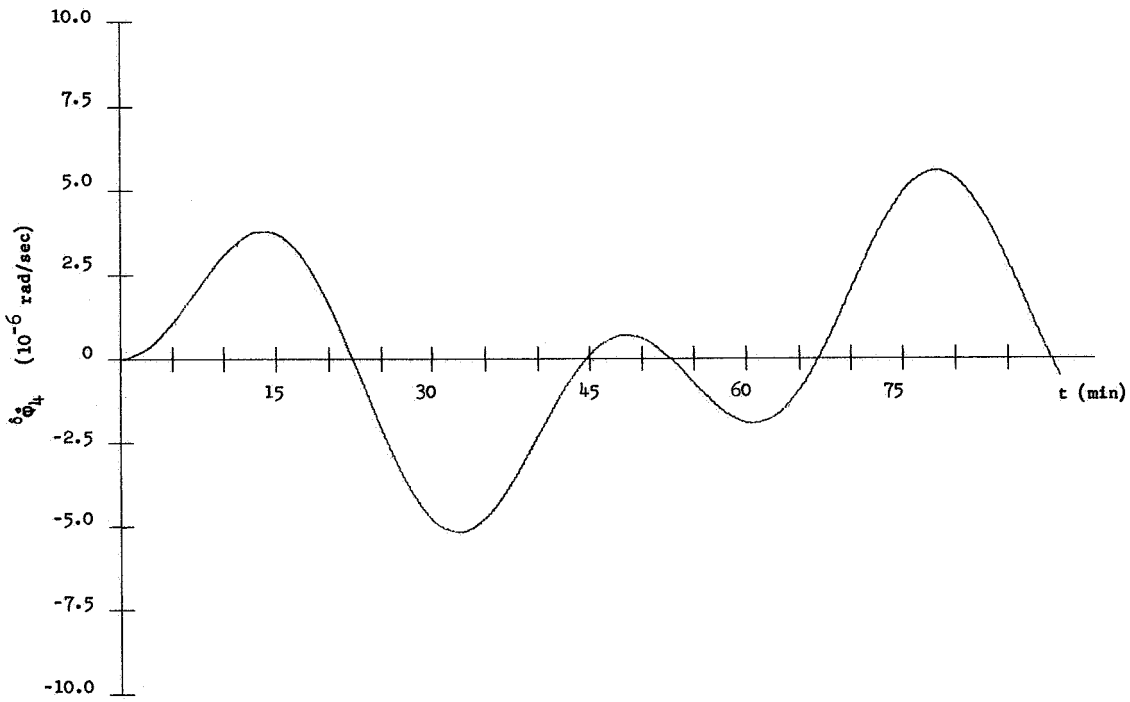
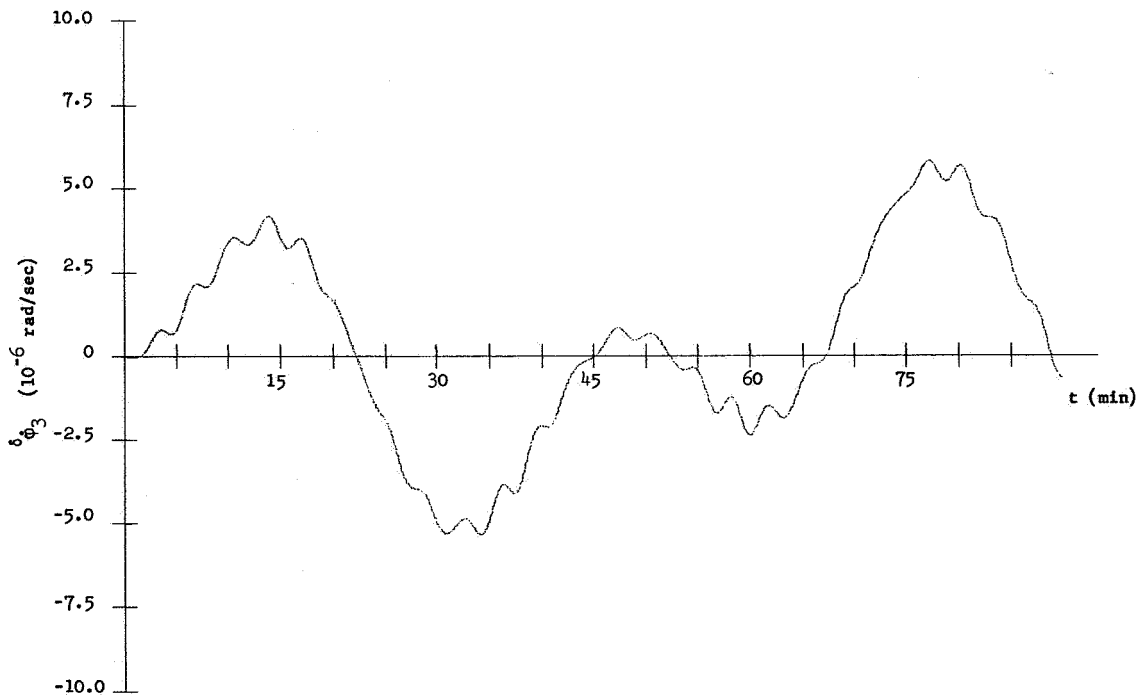


Figure 5. Free-Space Equilibrium Configuration for a Quadrant

Figure 6. Plot II-B, m_4 Figure 7. Plot II-B, m_3

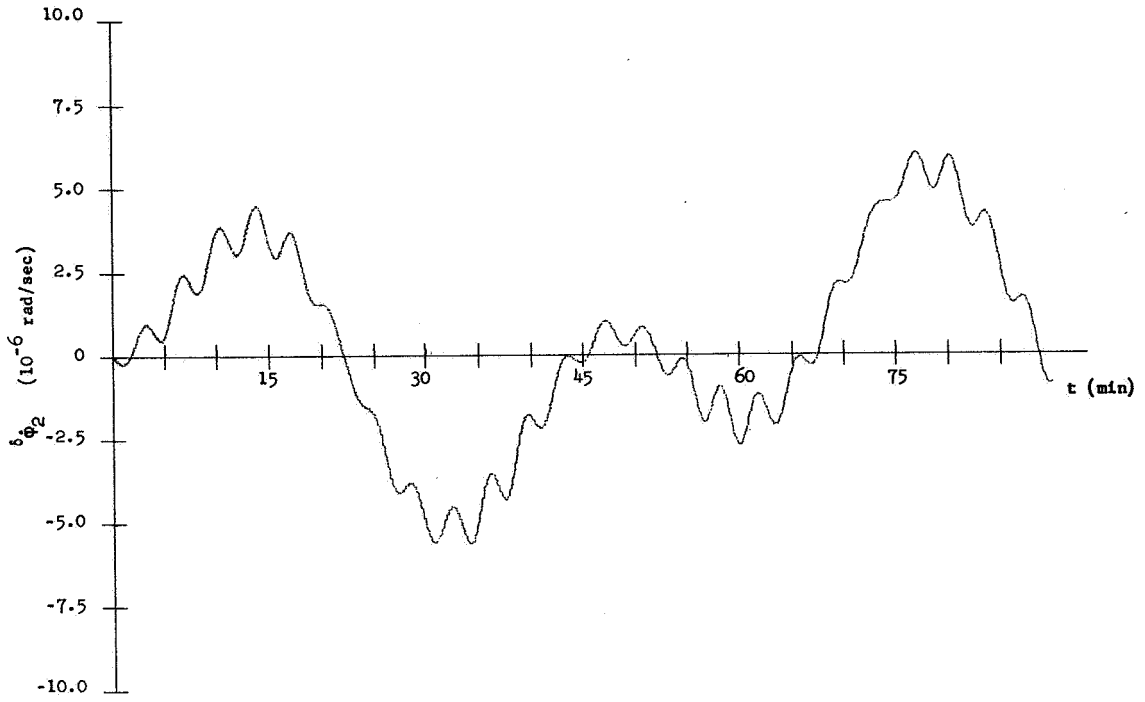


Figure 8. Plot II-B, m_2

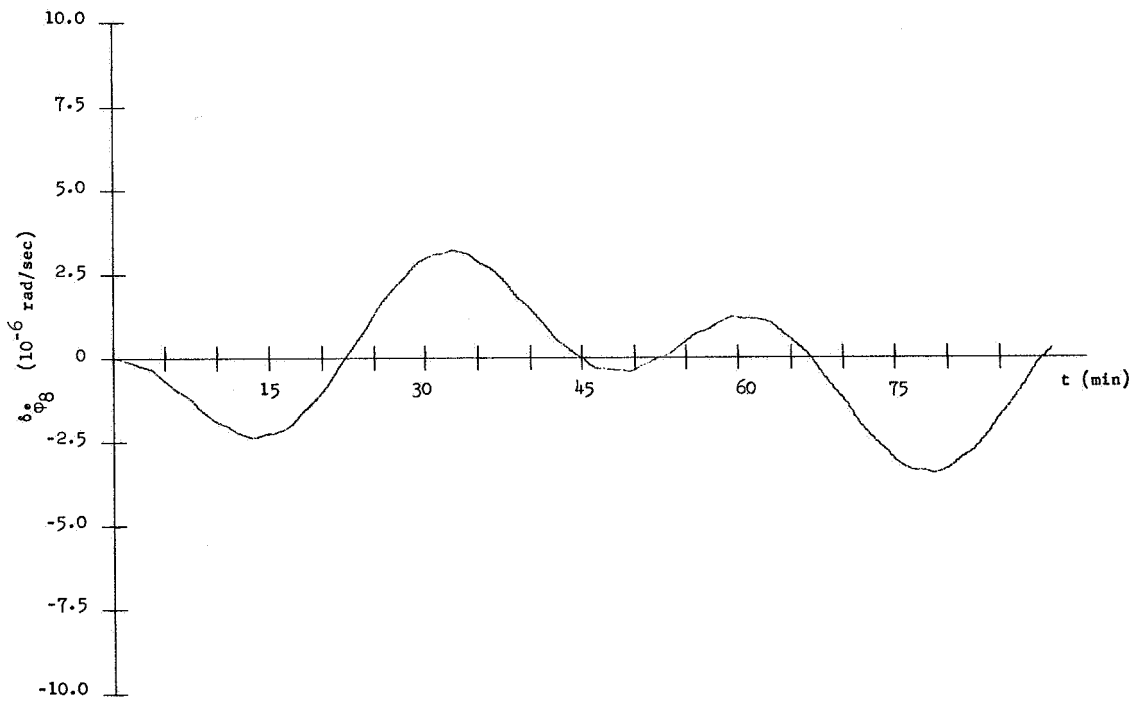
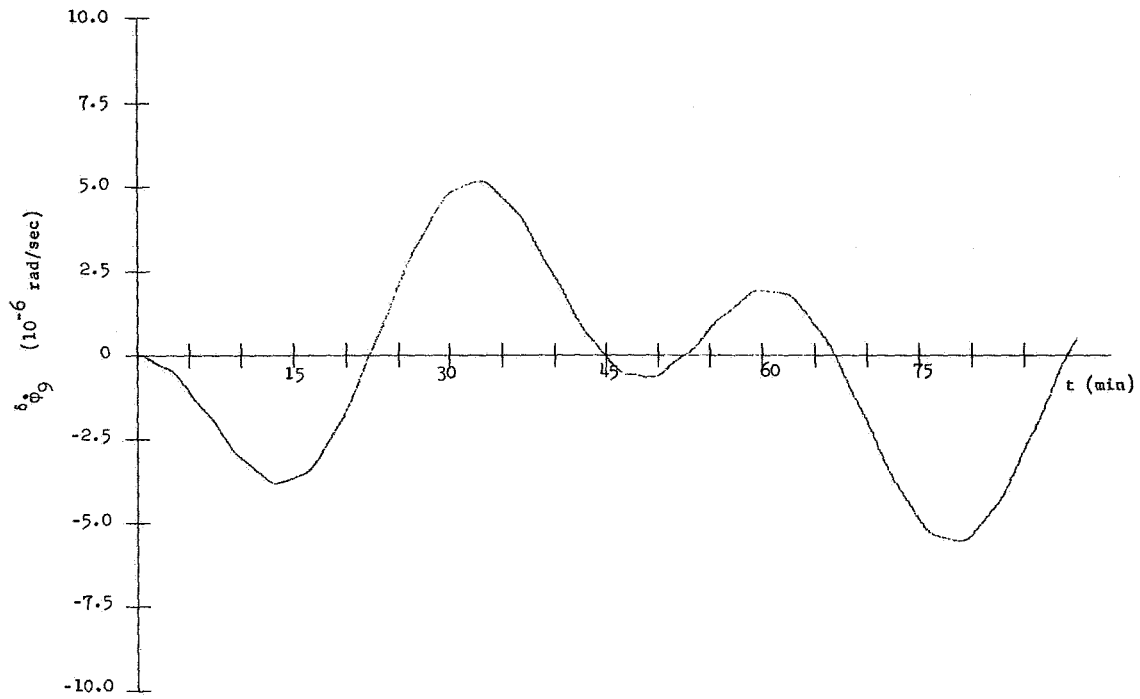
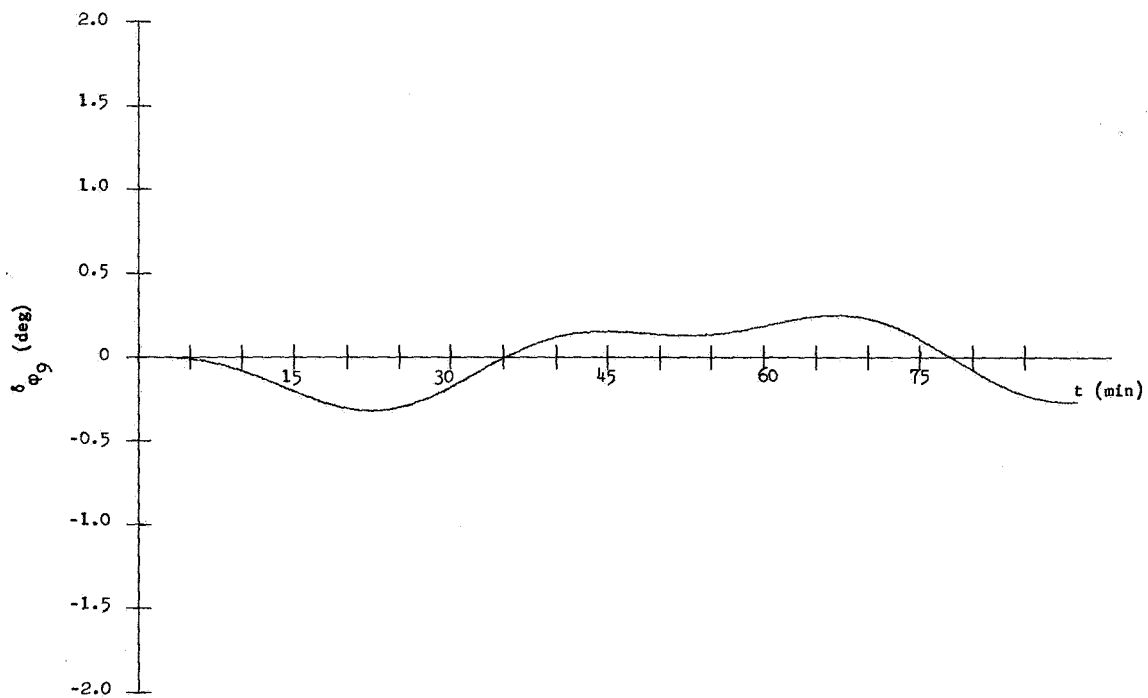
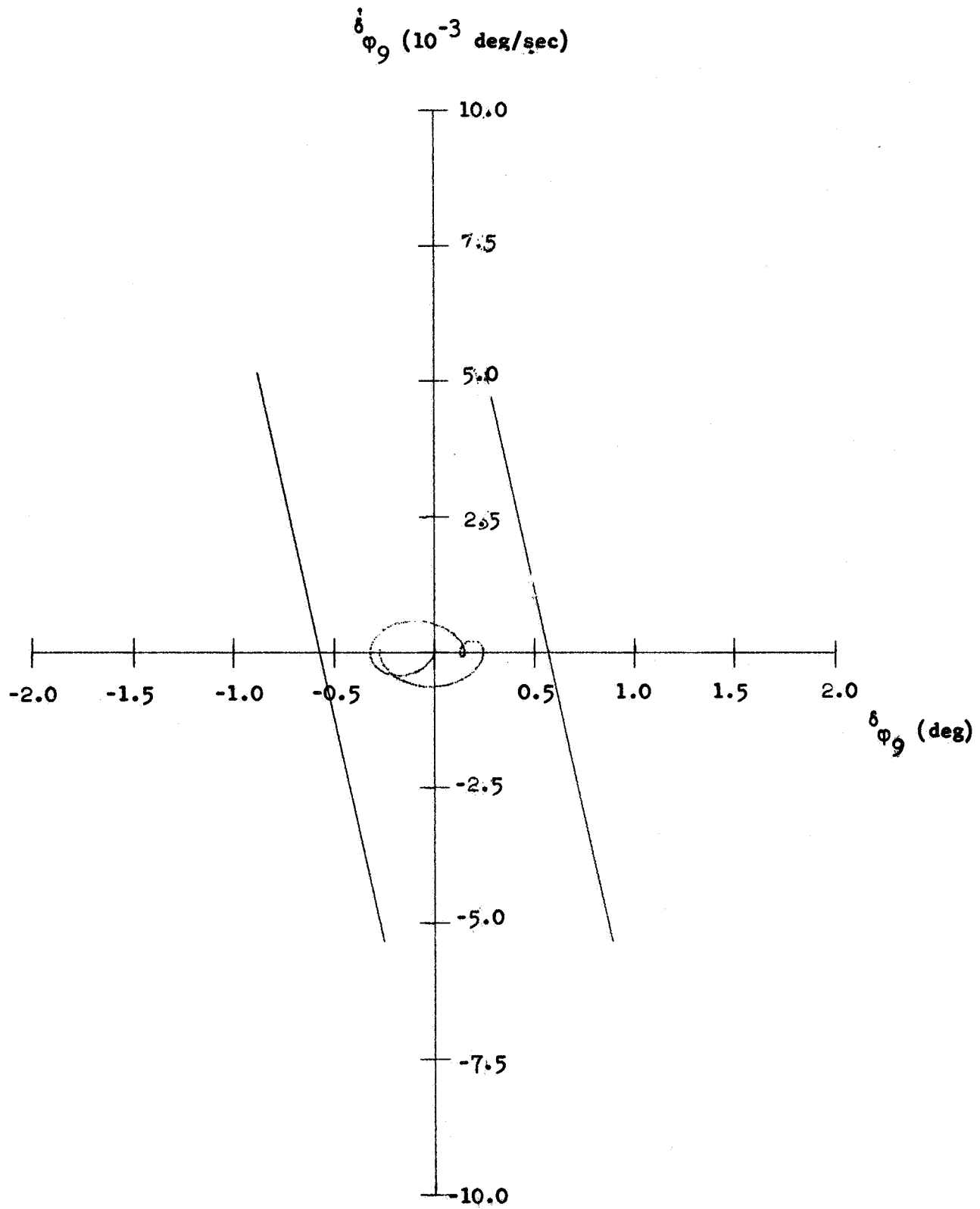
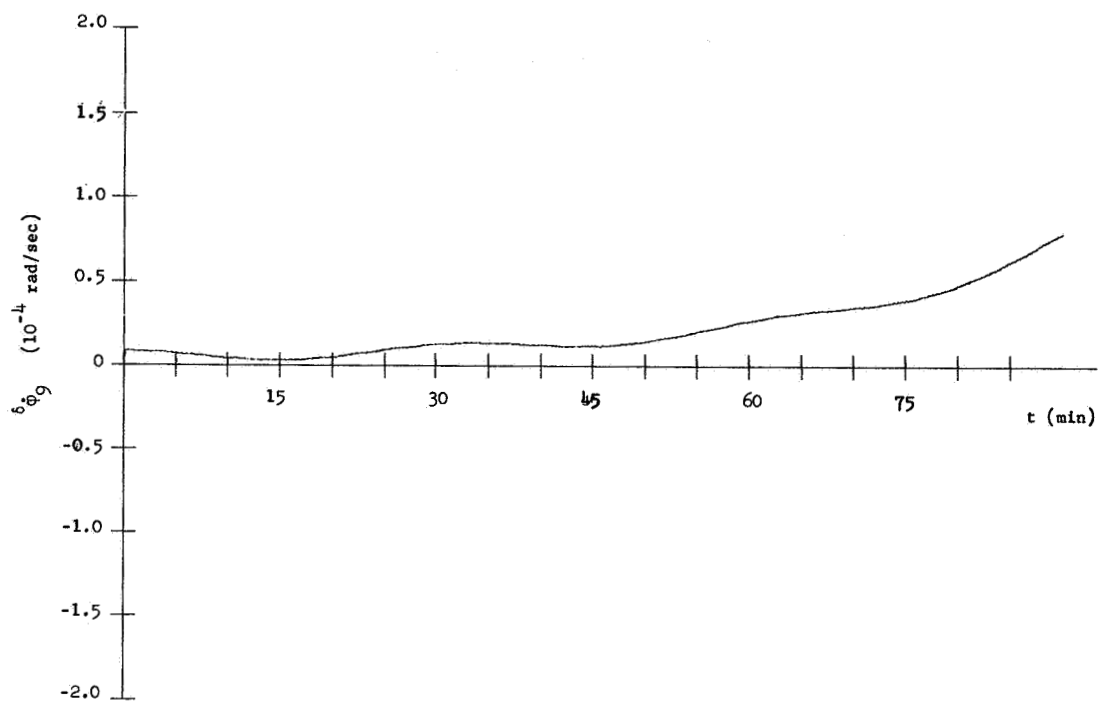
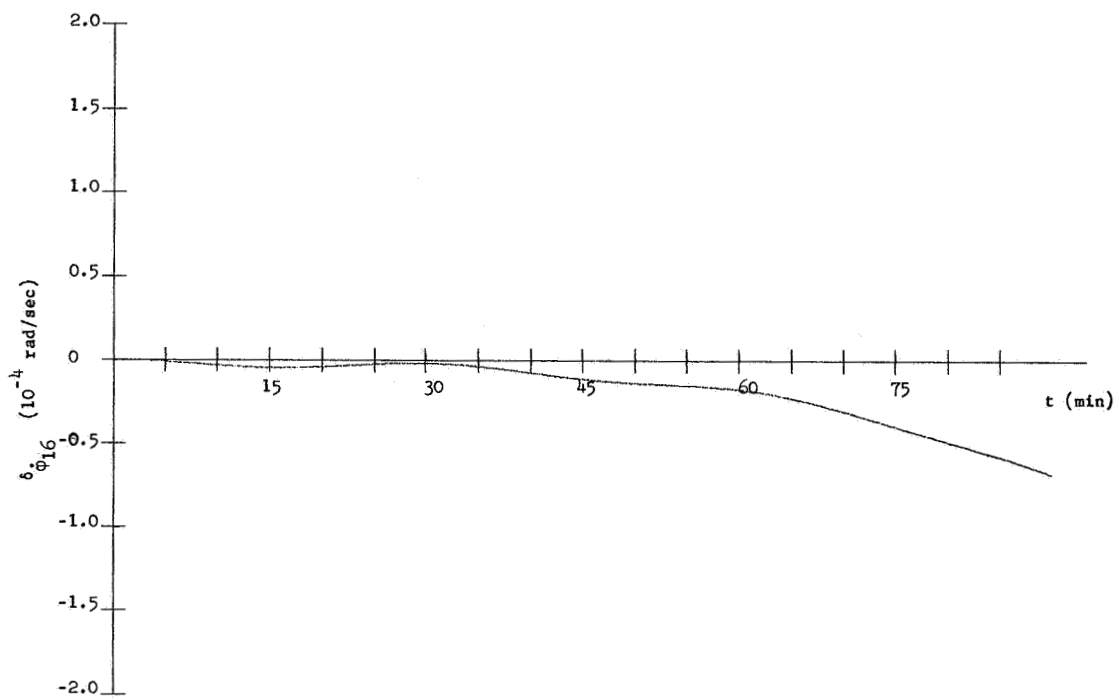
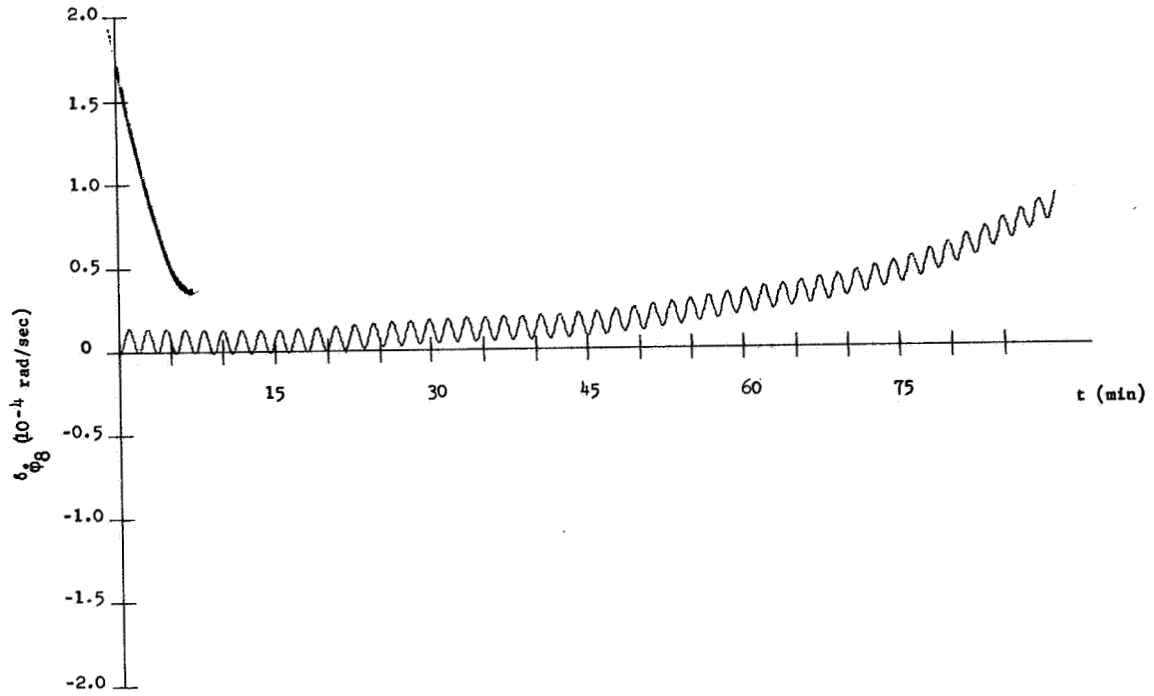
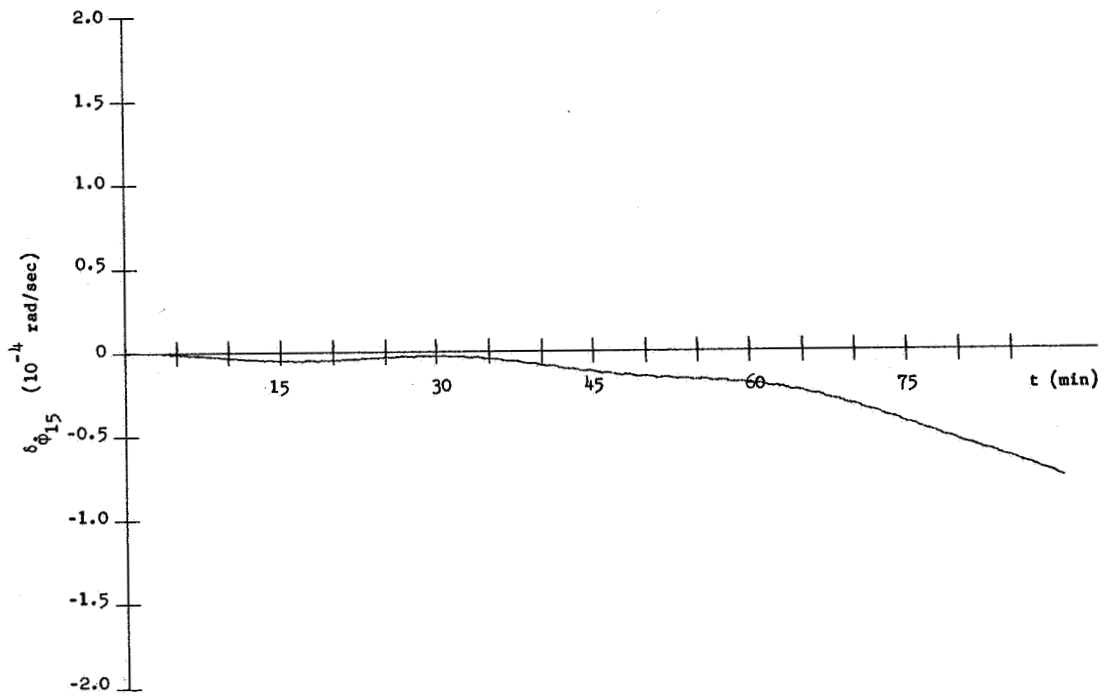


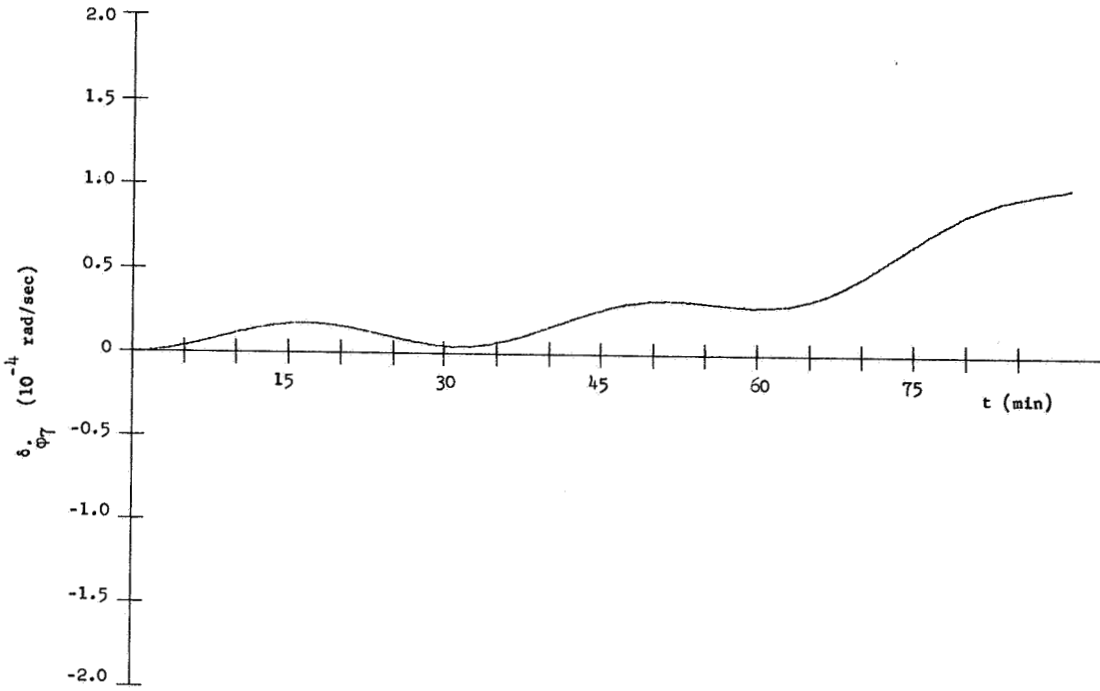
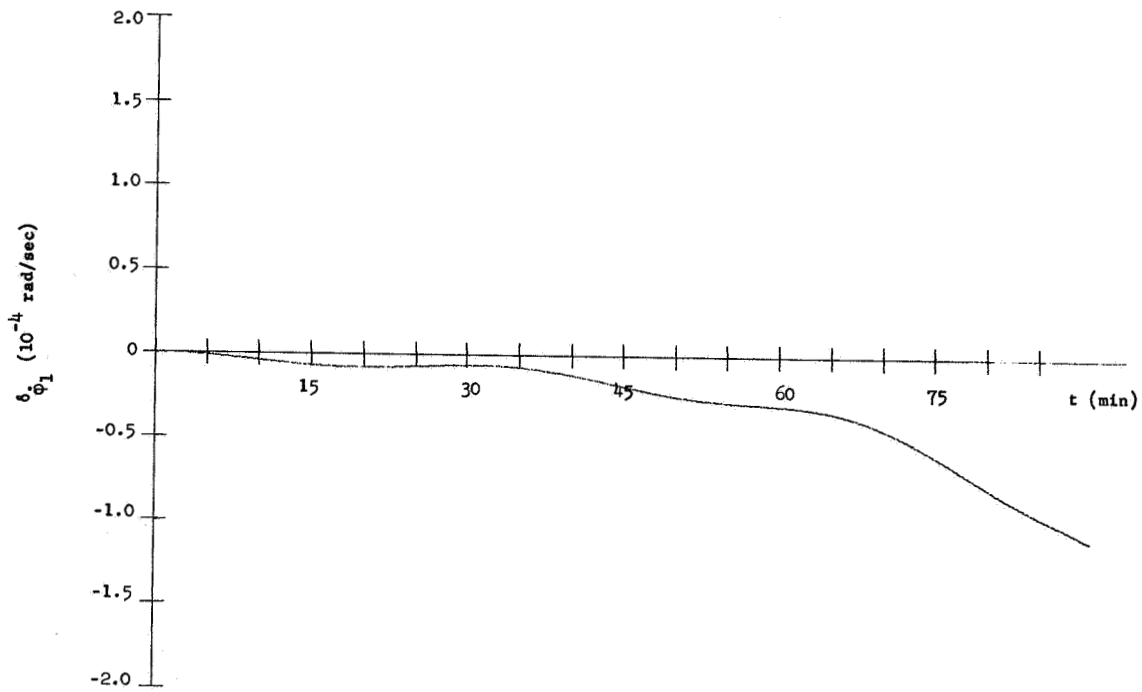
Figure 9. Plot II-B, m_B

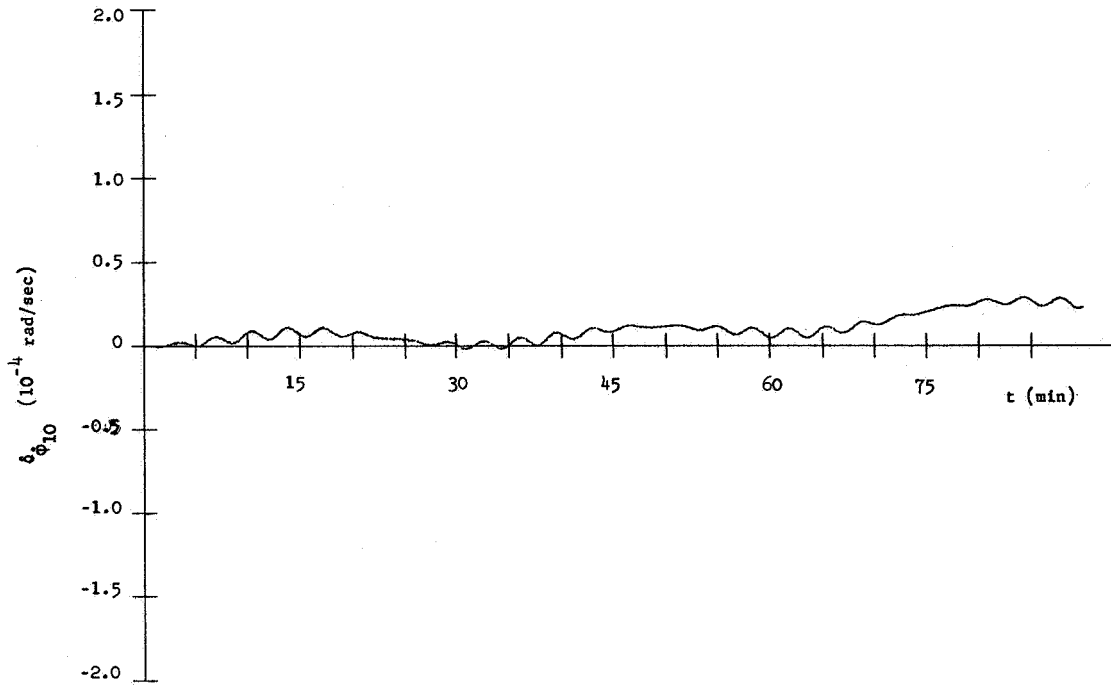
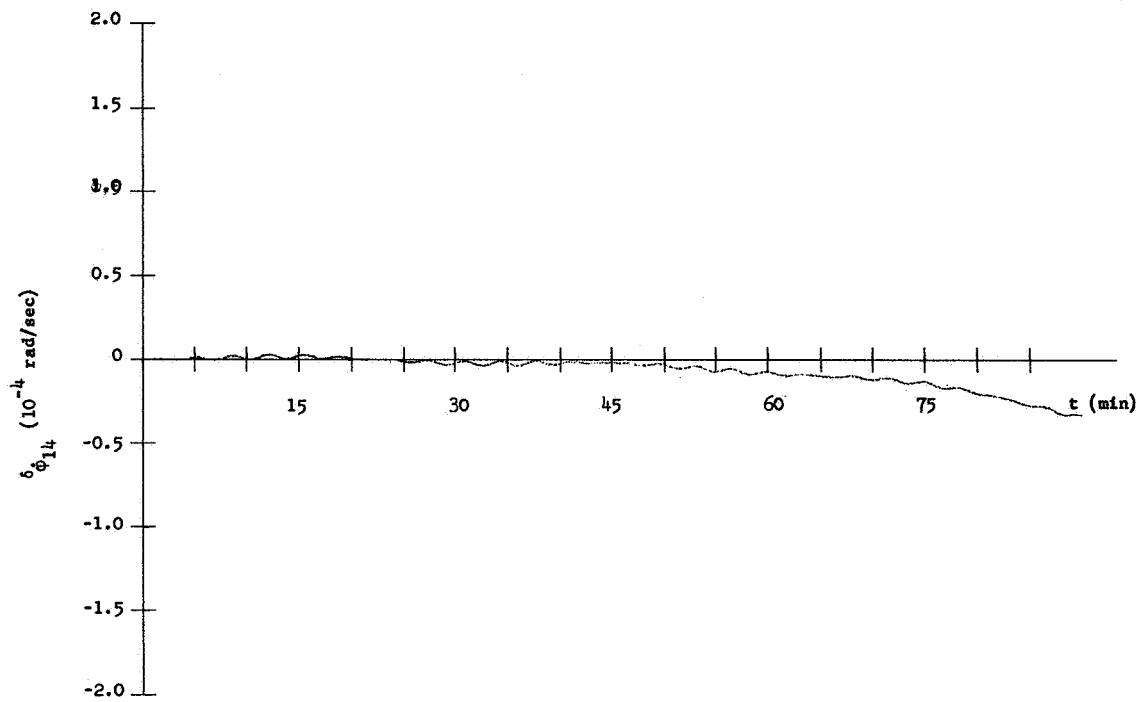
Figure 10. Plot II-B, m_g Figure 11. Plot III-B, m_g

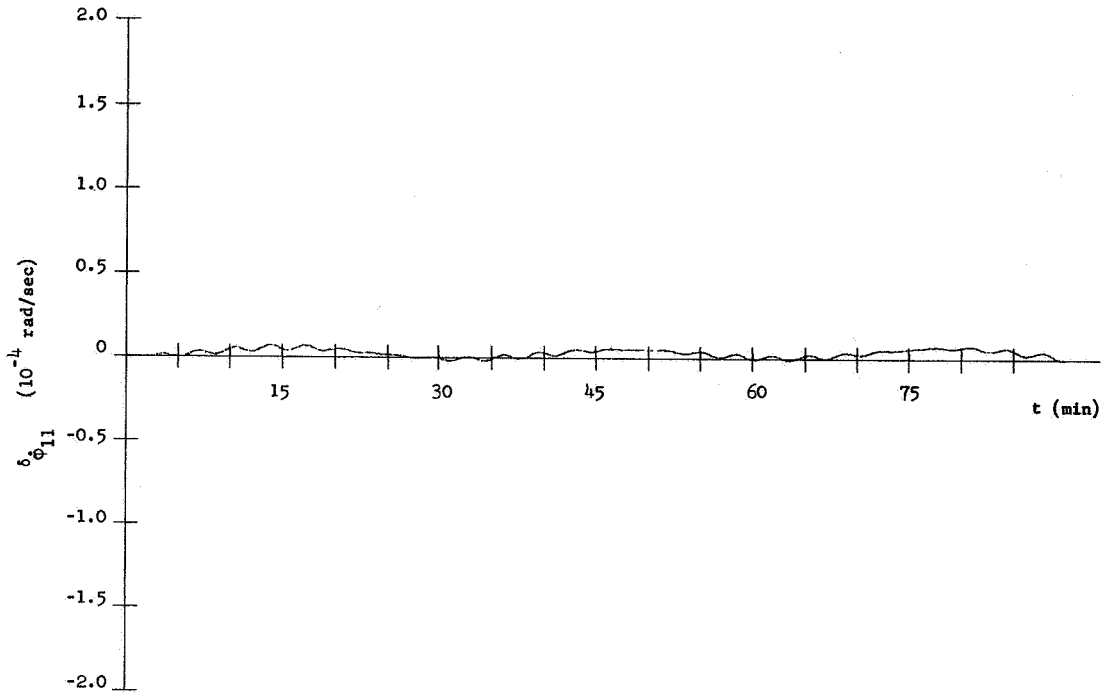
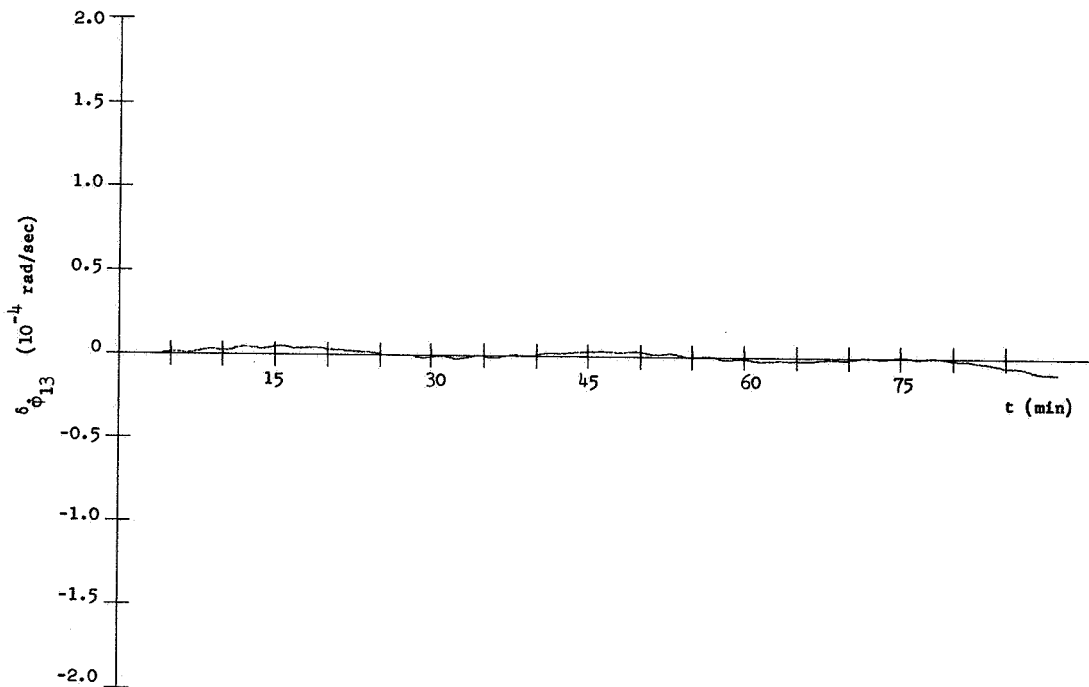
Figure 12. Plot IV-B, m_9

Figure 13. Plot II-D, m_9 Figure 14. Plot II-D, m_{16}

Figure 15. Plot II-D, m_8 Figure 16. Plot II-D, m_{15}

Figure 17. Plot II-D, m_7 Figure 18. Plot II-D, m_1

Figure 19. Plot II-D, m_{10} Figure 20. Plot II-D, m_{14}

Figure 21. Plot II-D, m_{11} Figure 22. Plot II-D, m_{13}

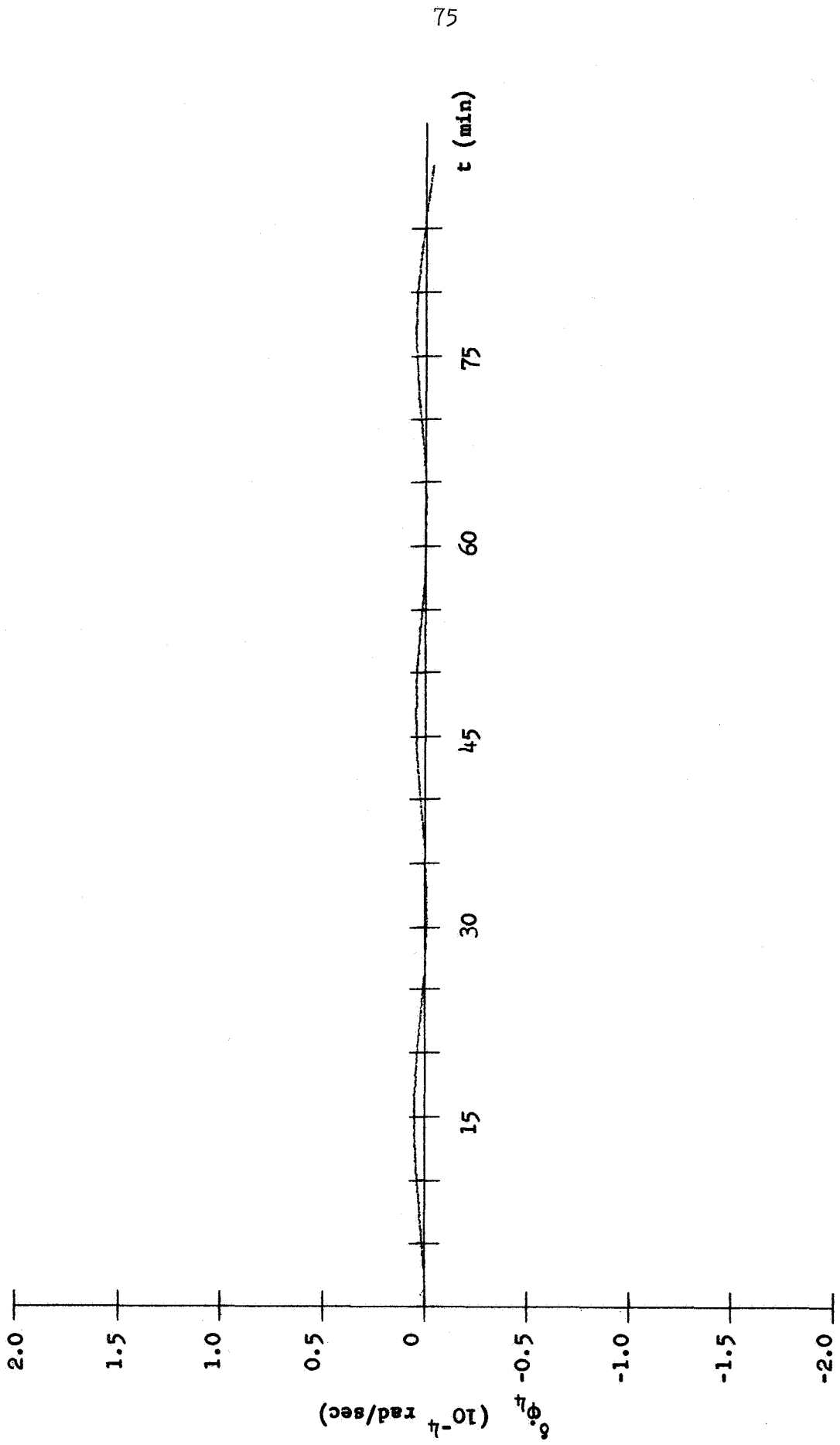


Figure 23. Plot II-D, m₄

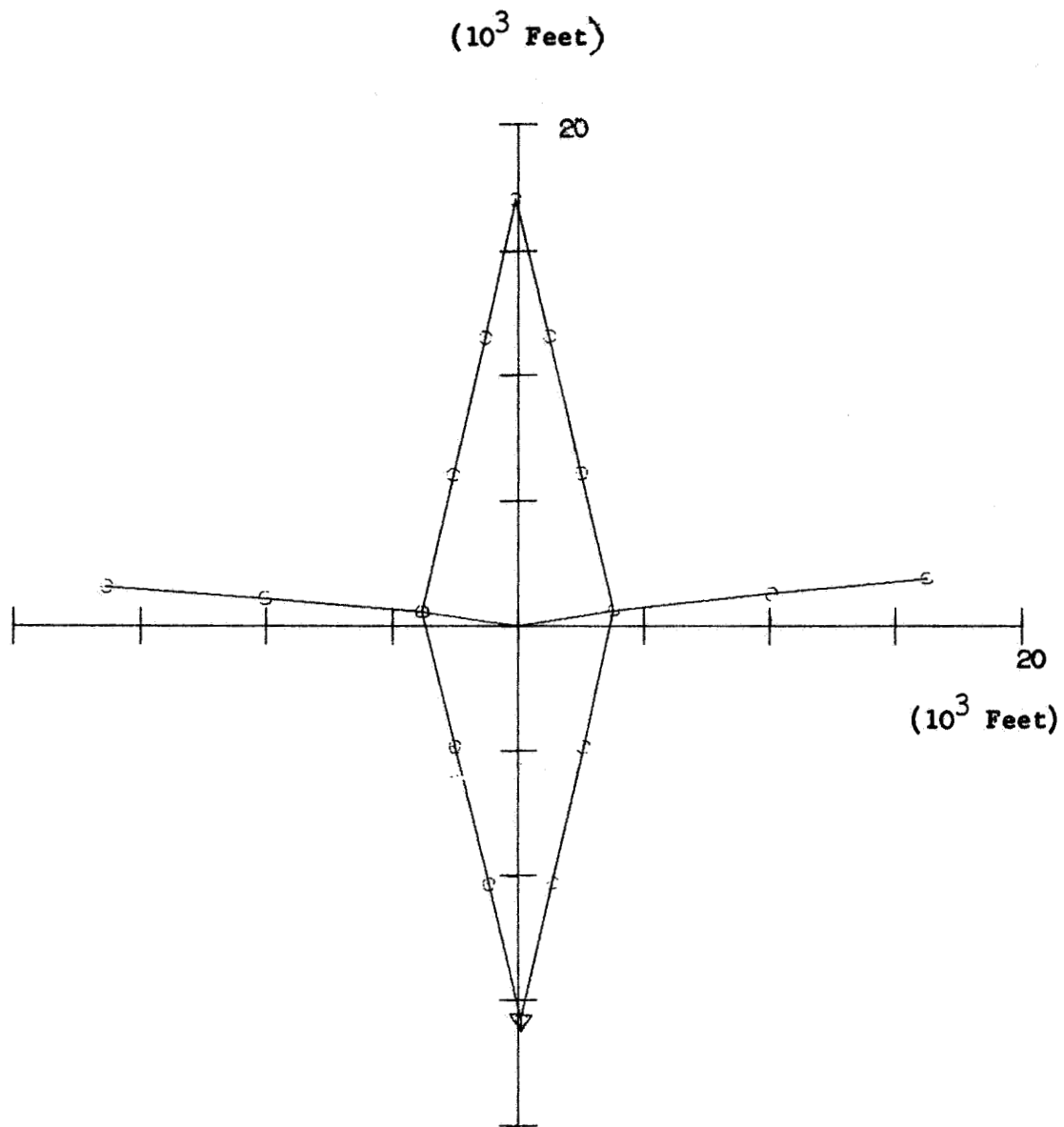
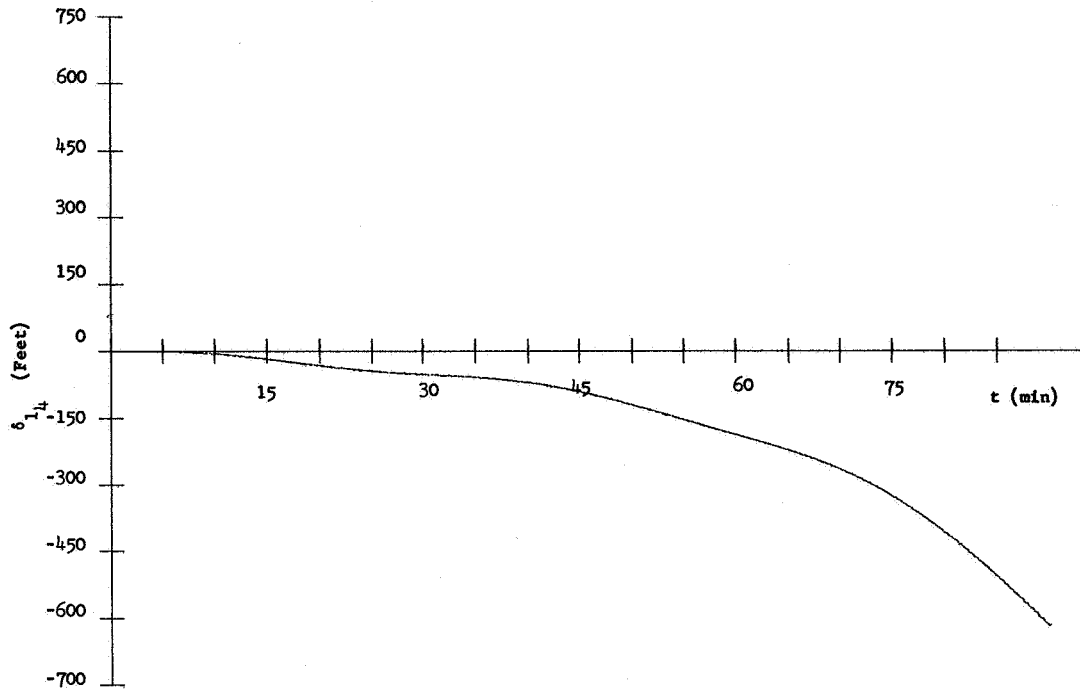
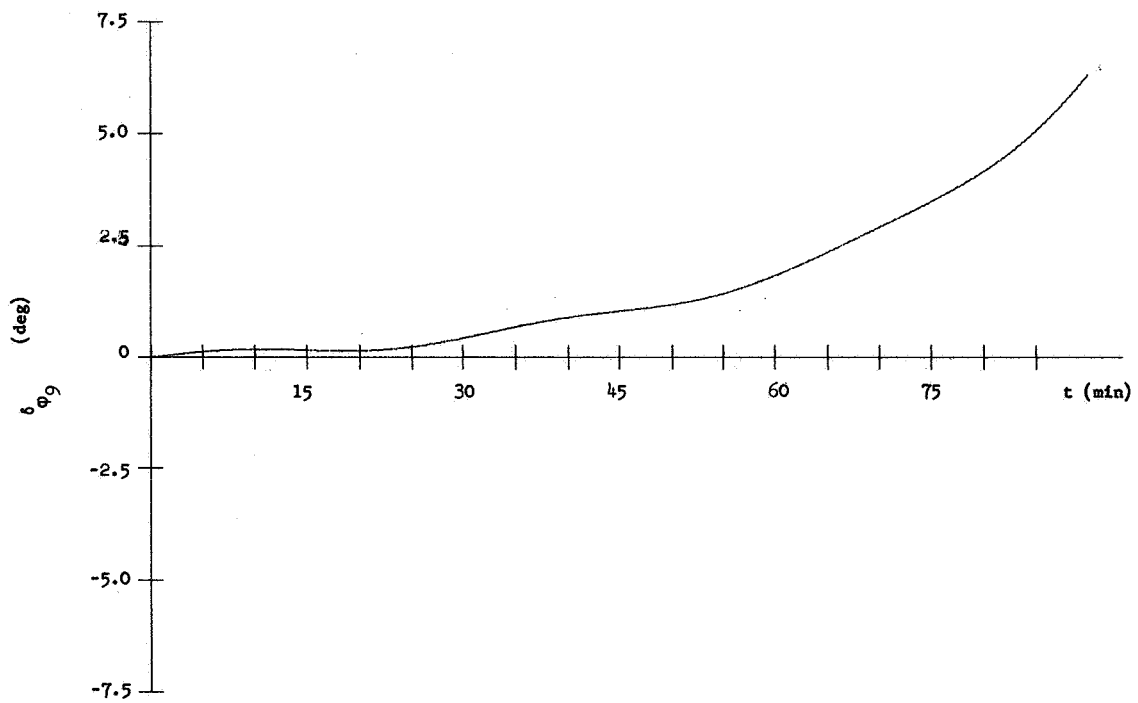
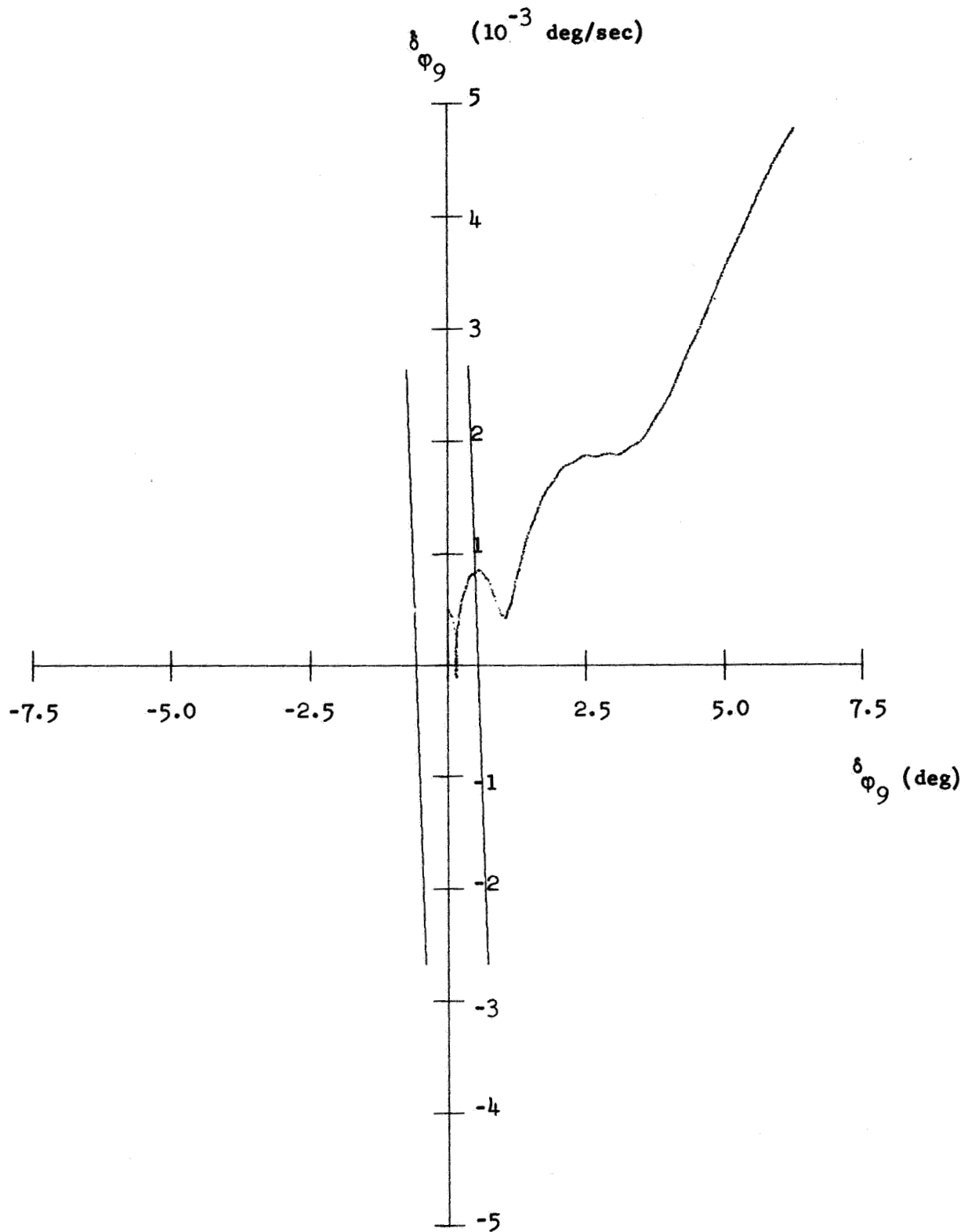


Figure 24. Structure diagram, $t=5400$ sec, Case D

Figure 25. Plot I-D, m_4 Figure 26. Plot III-D, m_9

Figure 27. Plot IV-D, m_9

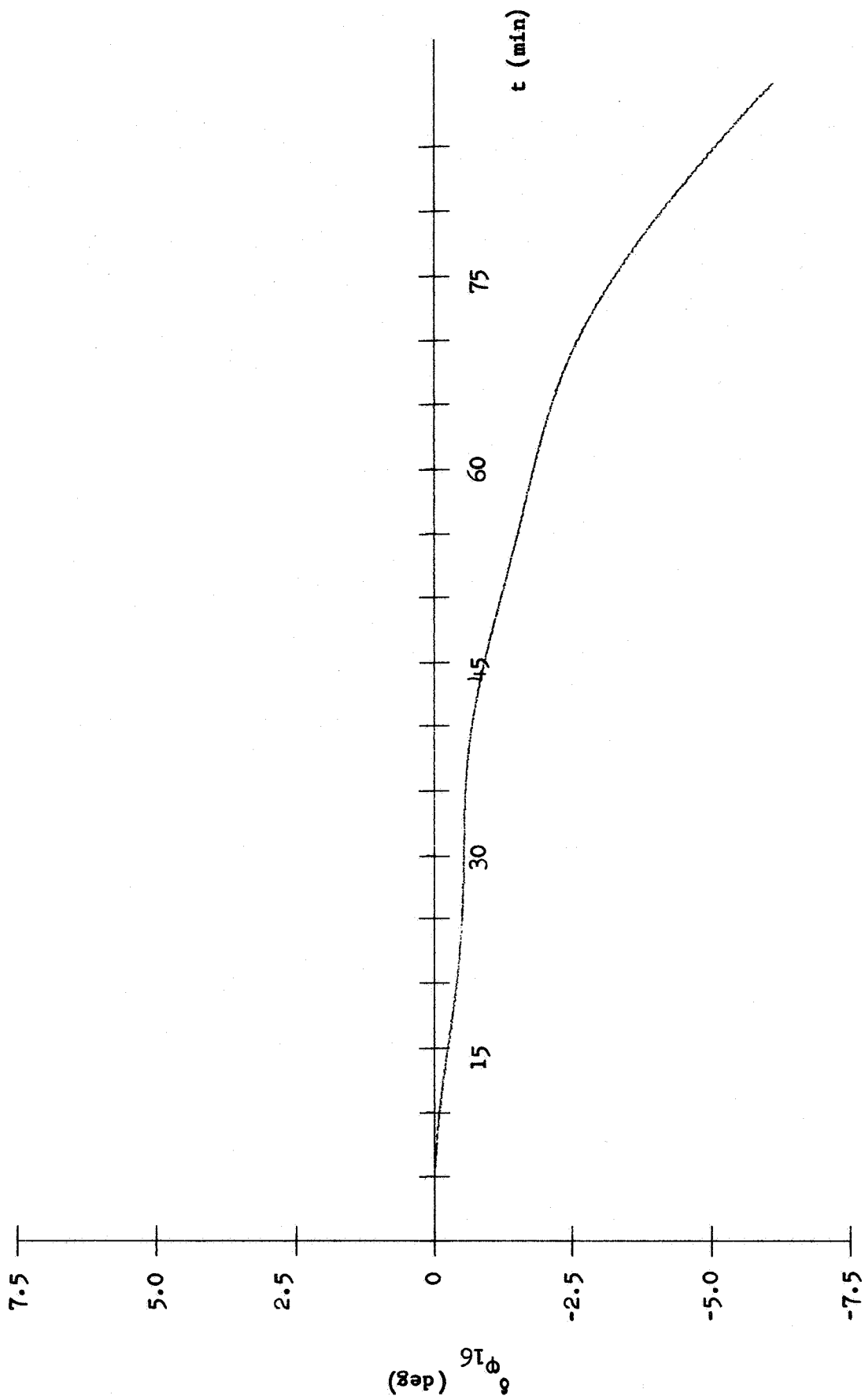
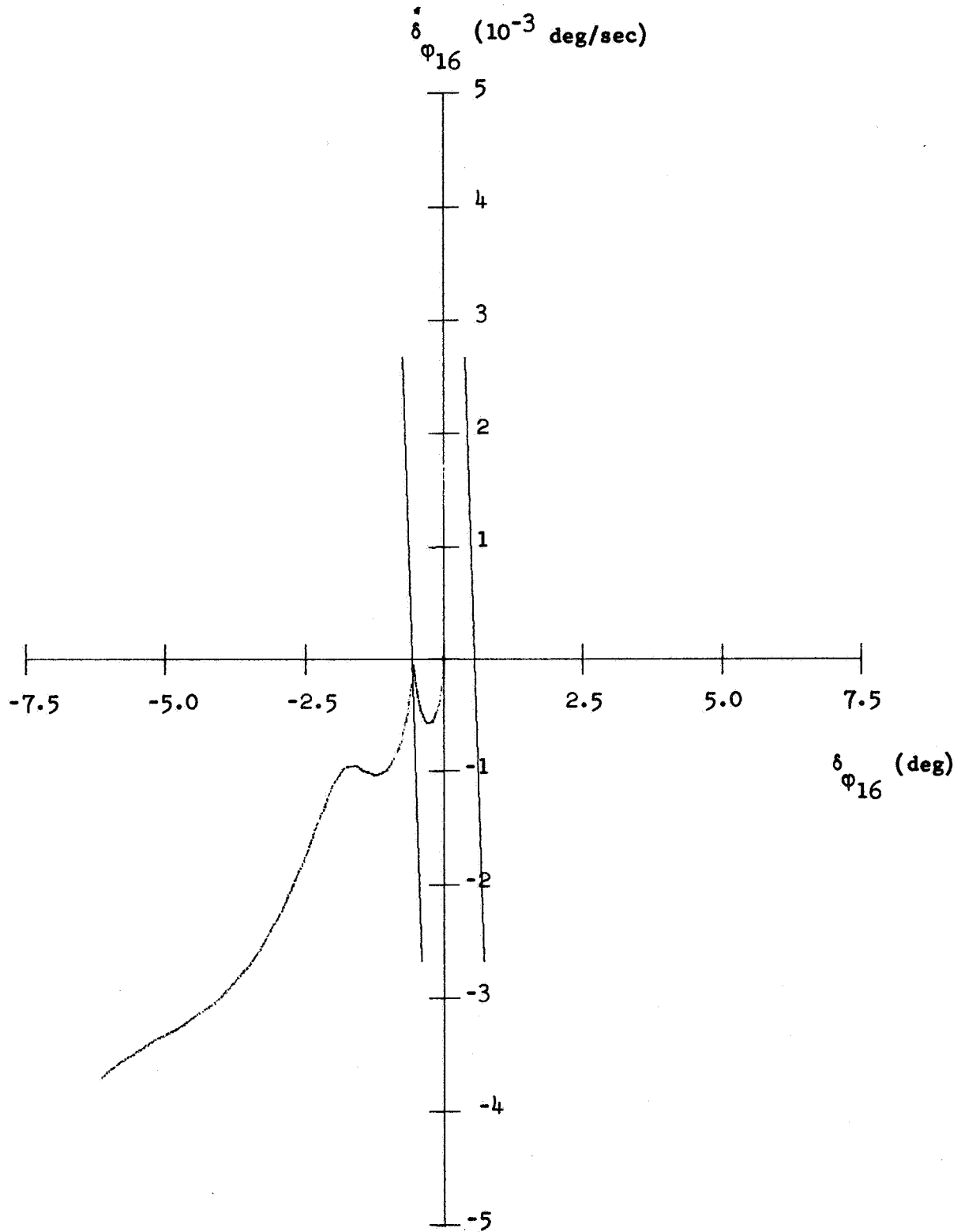
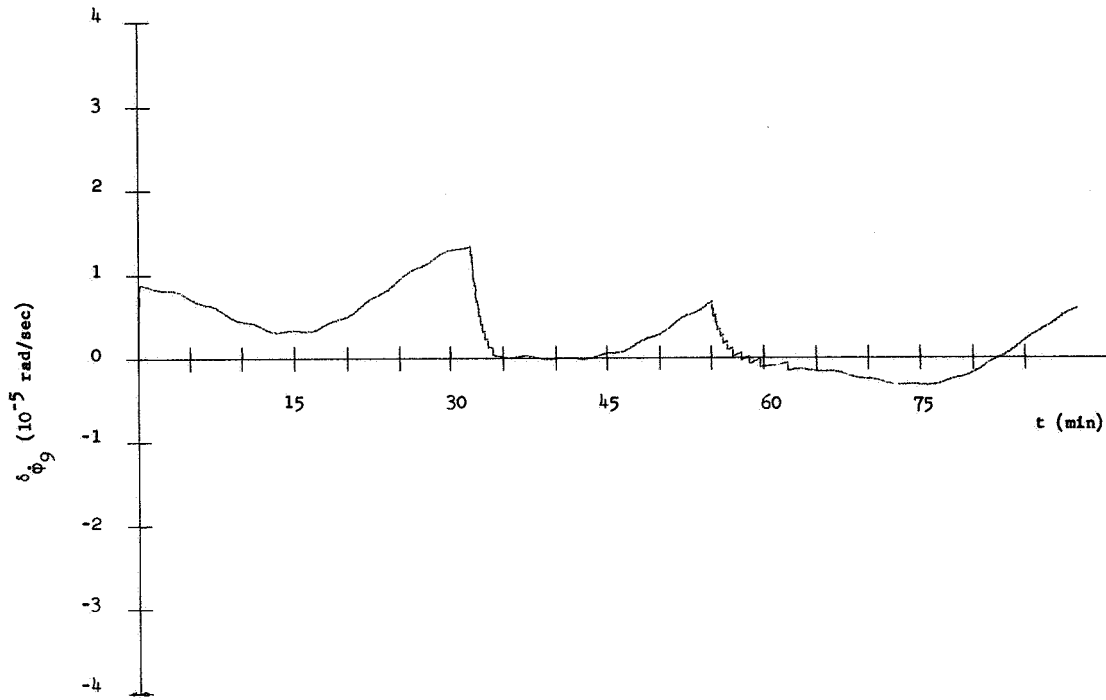
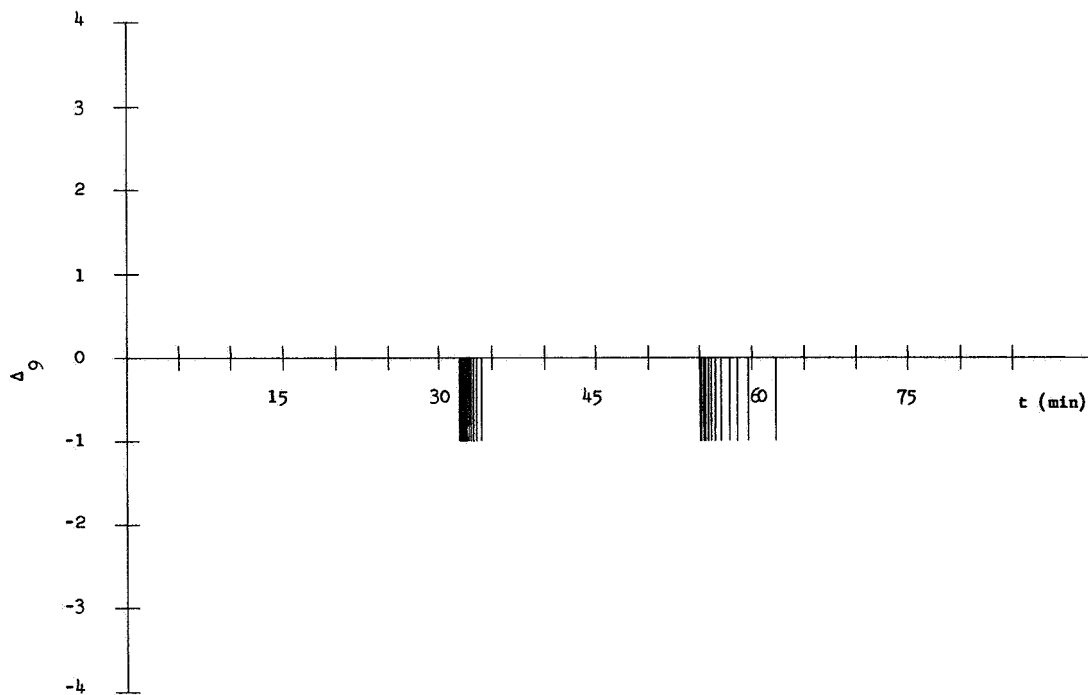
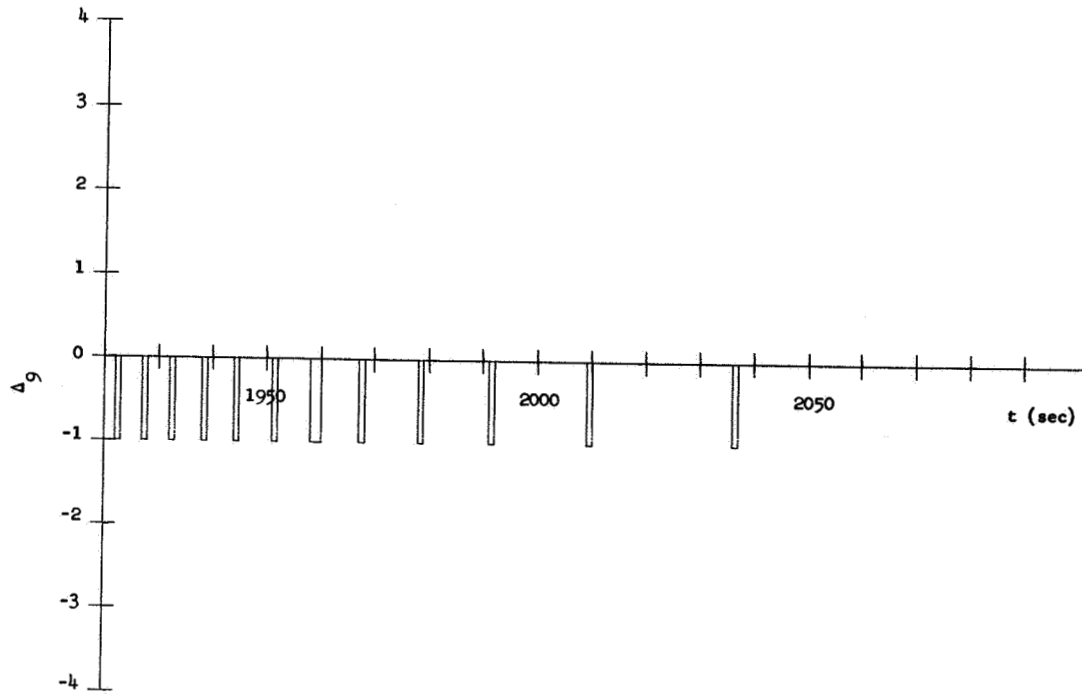
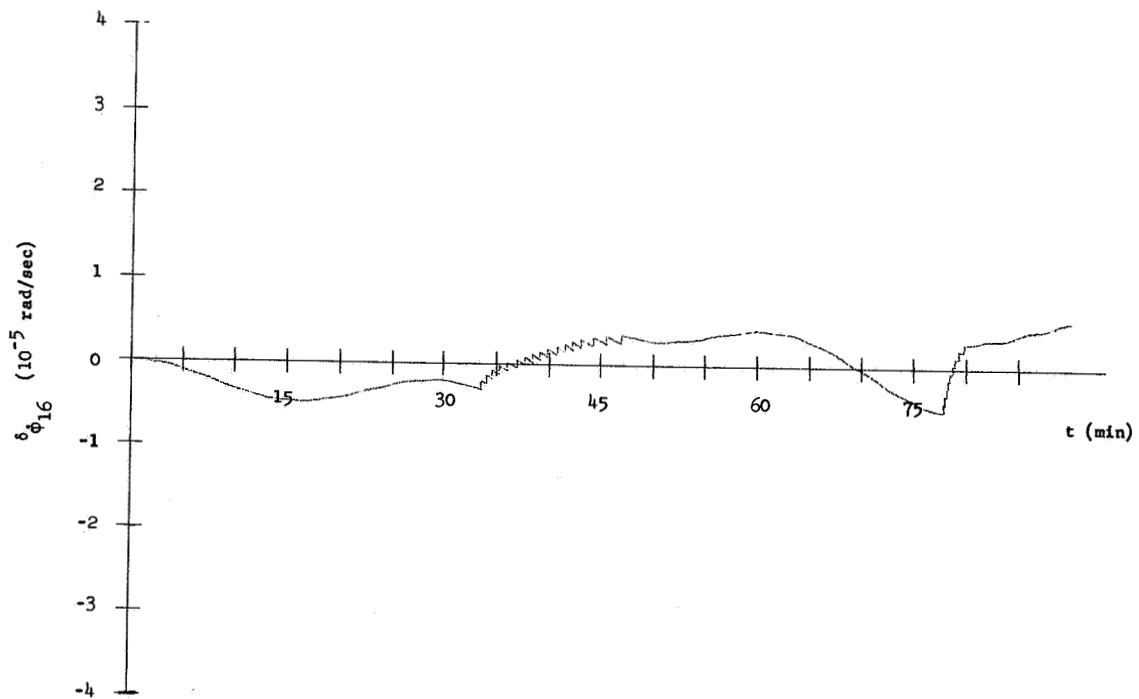


Figure 28. Plot III-D, m_{16}

Figure 29. Plot IV-D, m_{16}

Figure 30. Plot II-E, m_9 Figure 31. Plot V-E, m_9

Figure 32. Plot VI-E, m_9 Figure 33. Plot II-E, m_{16}

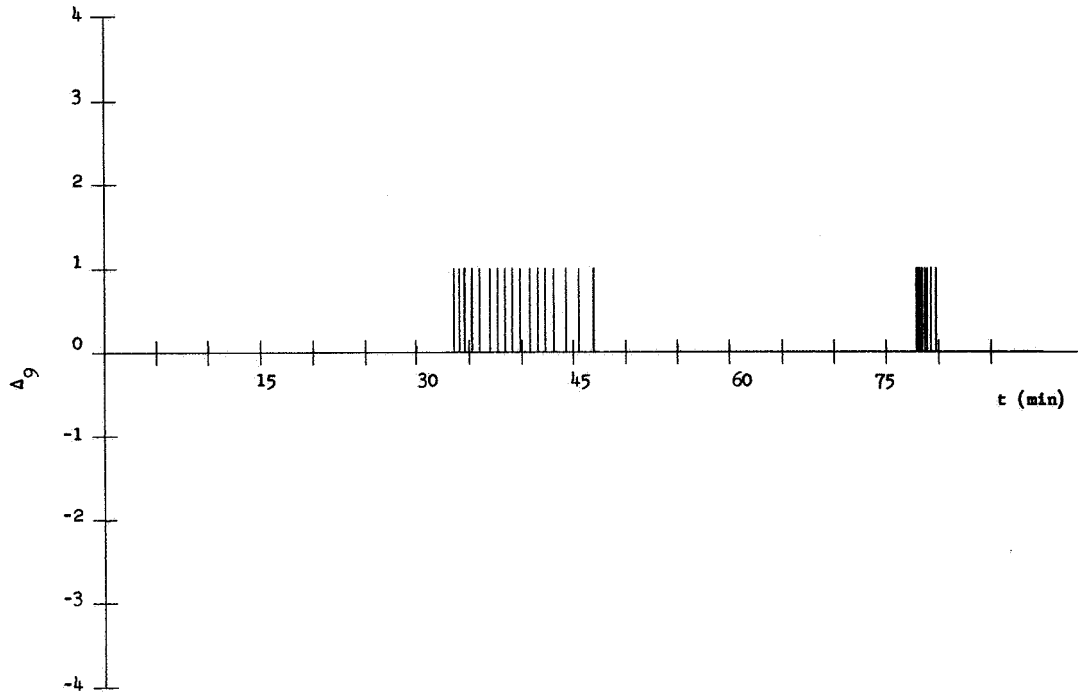


Figure 34. Plot V-E, m_{16}

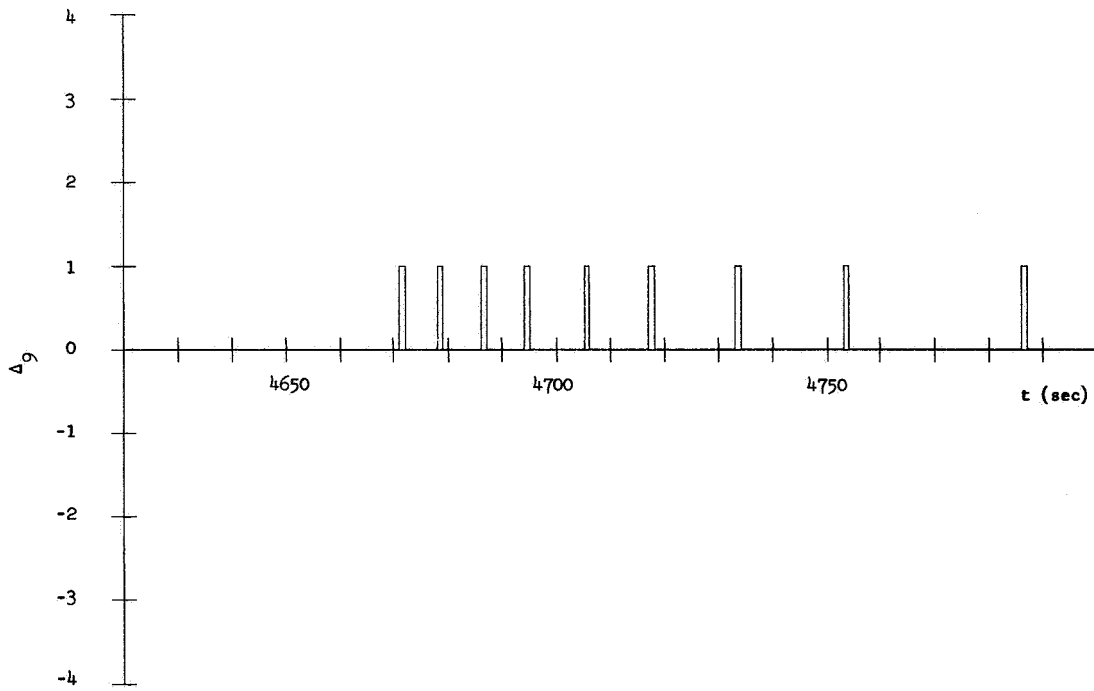
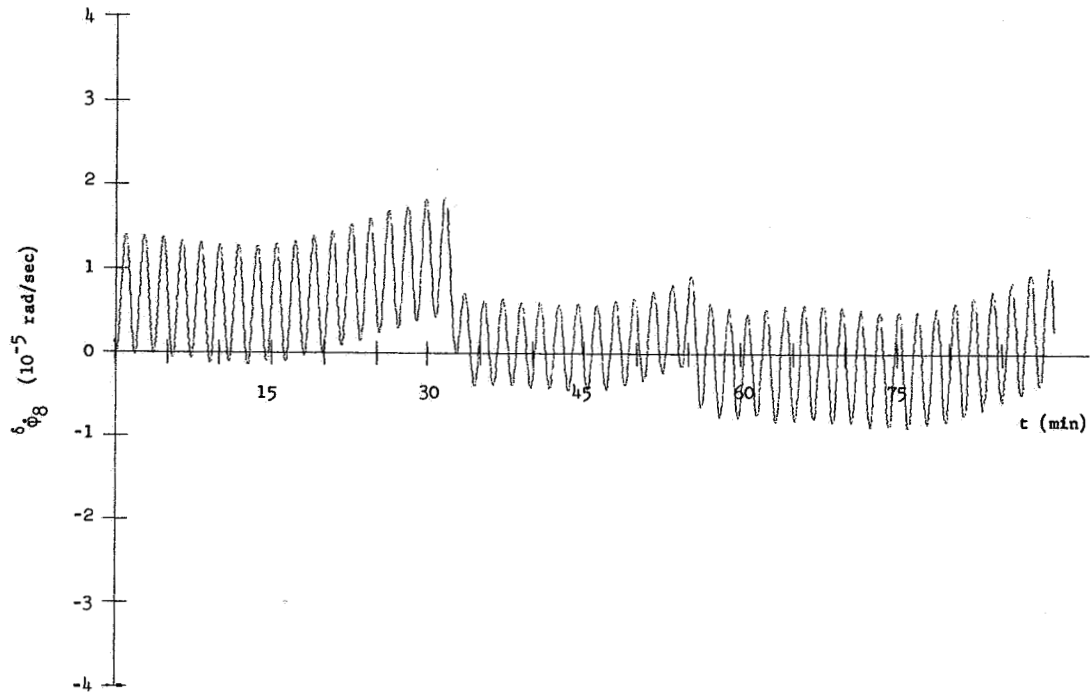
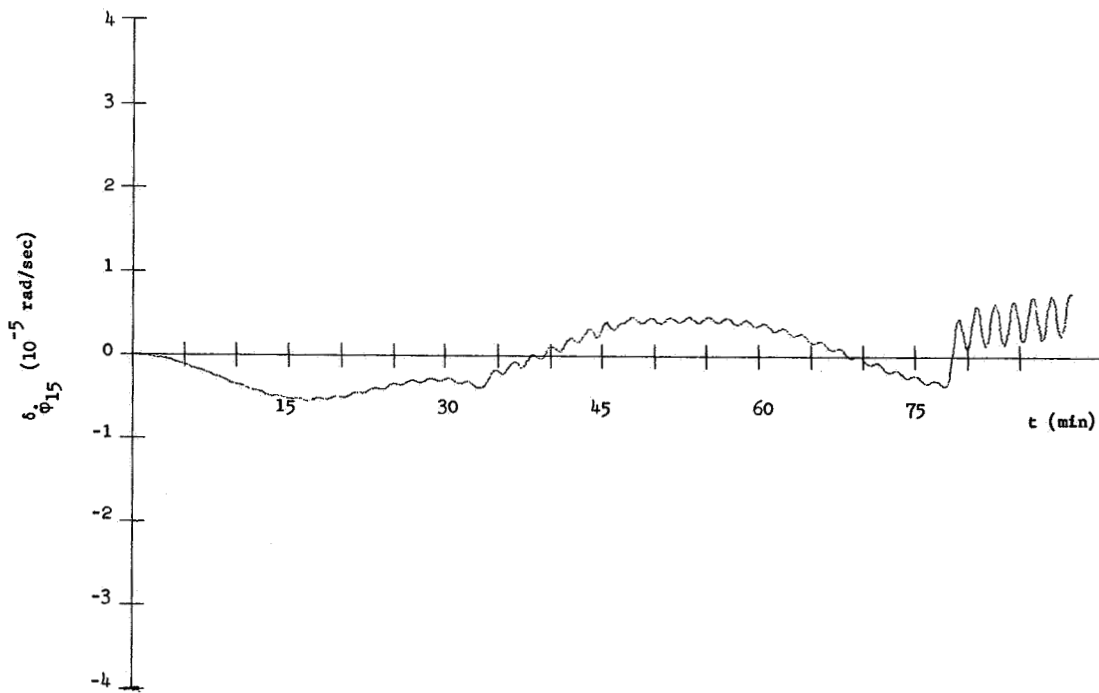
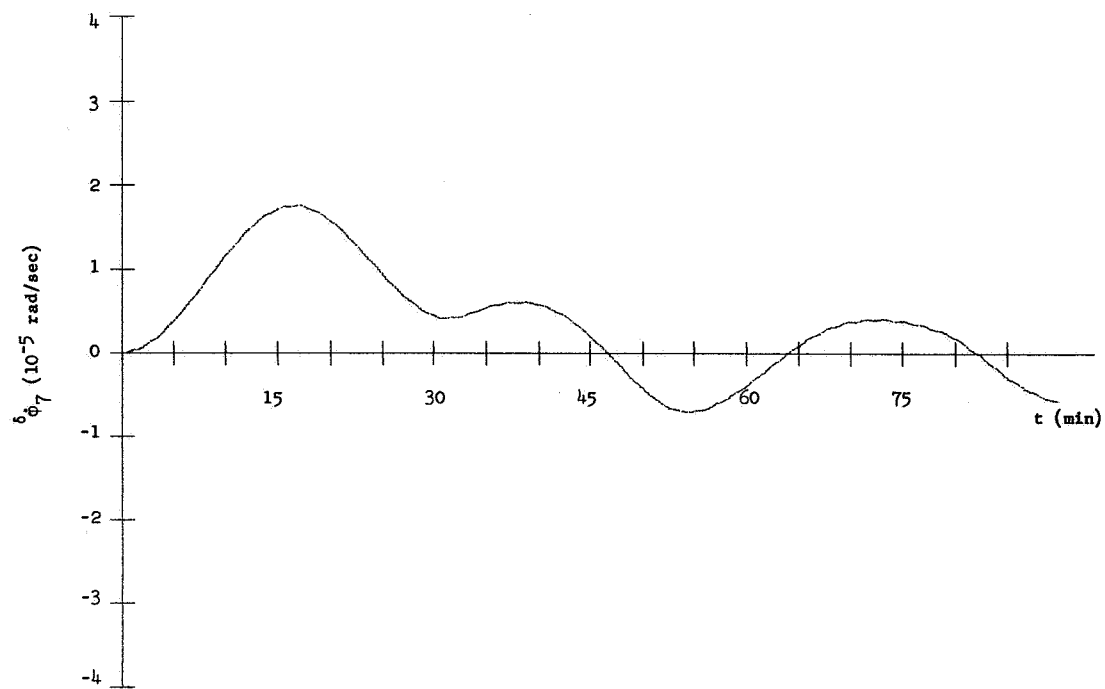
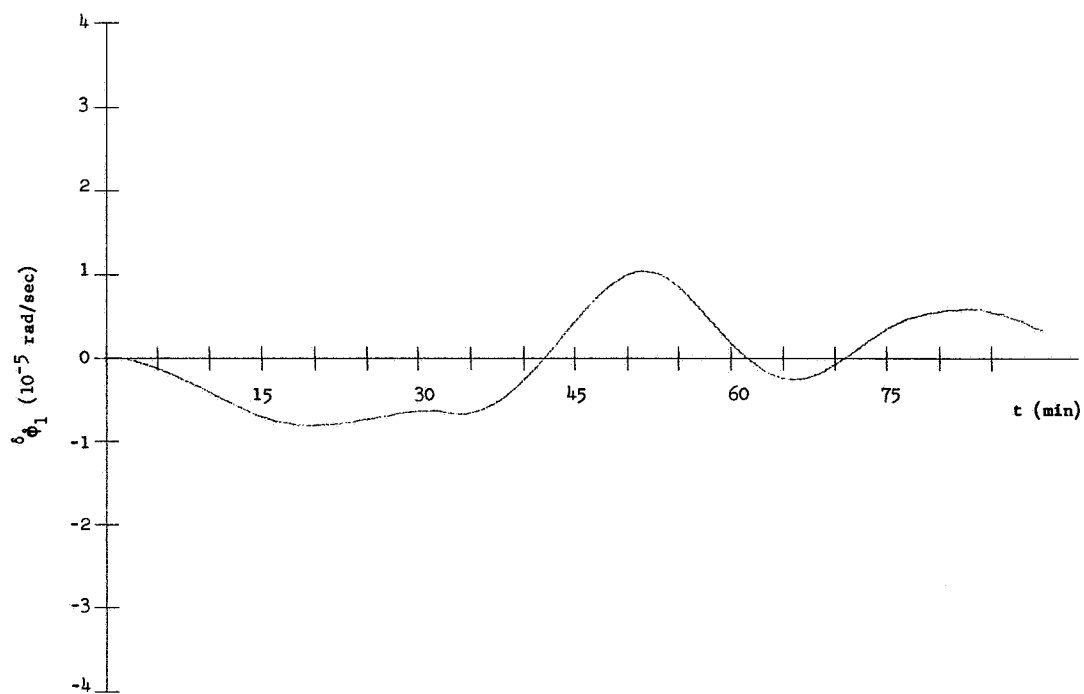
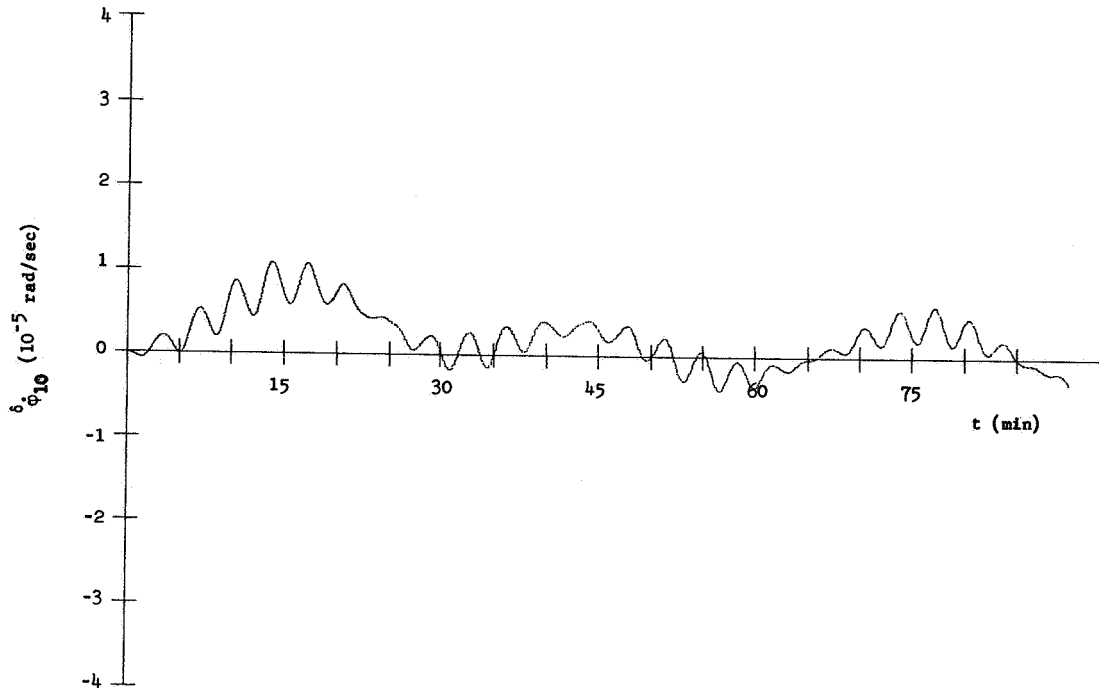
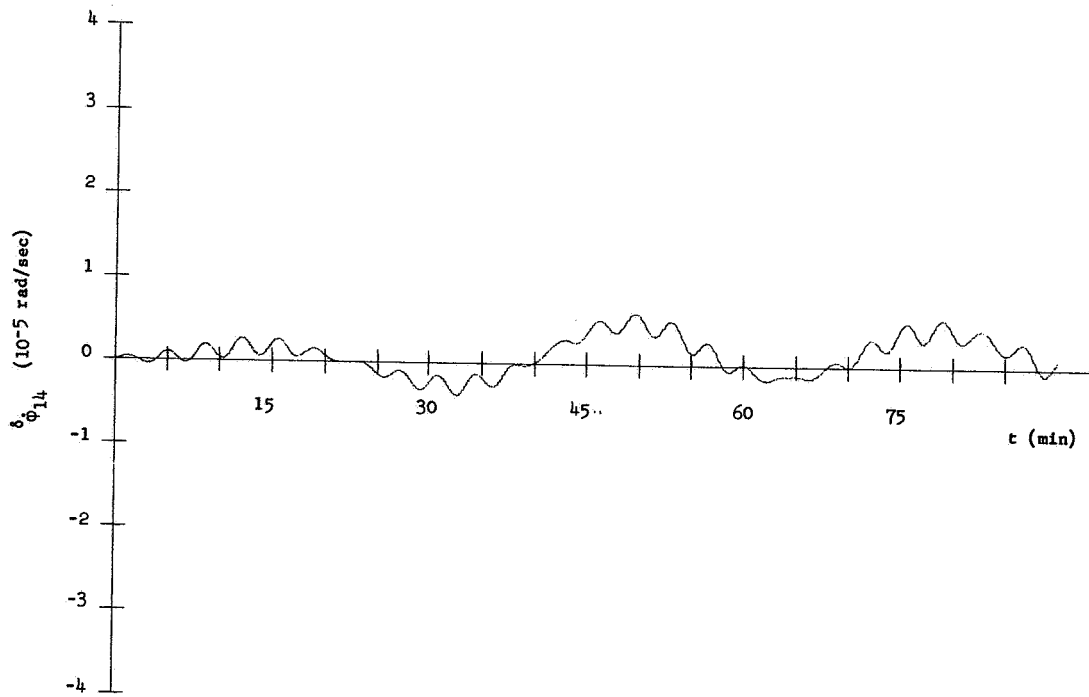
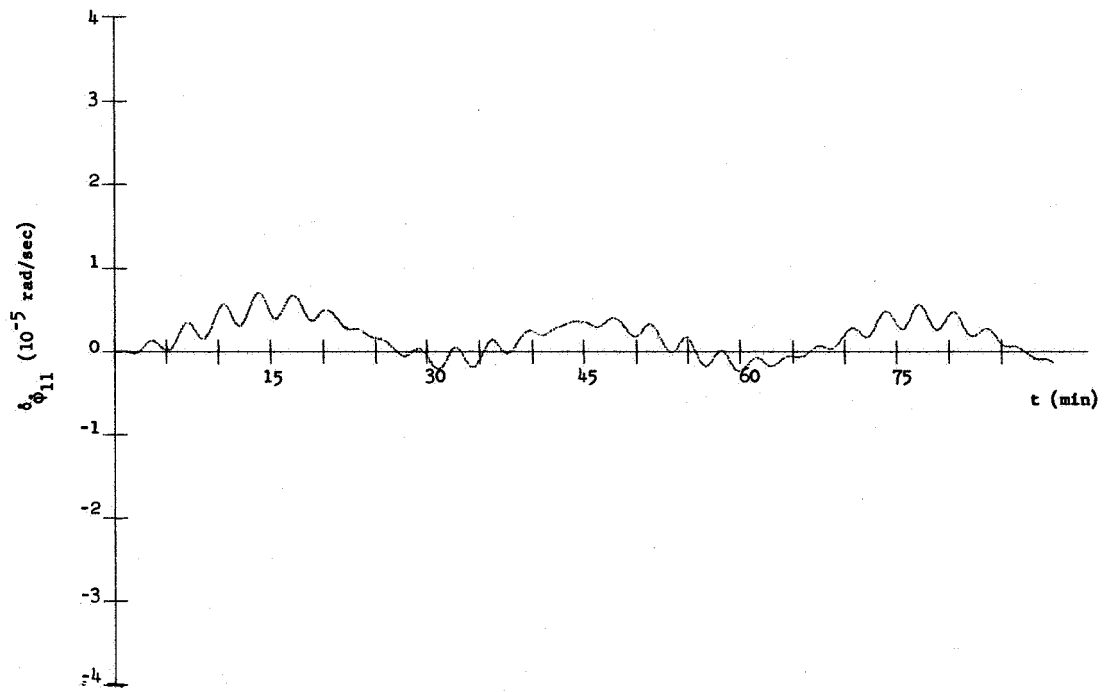
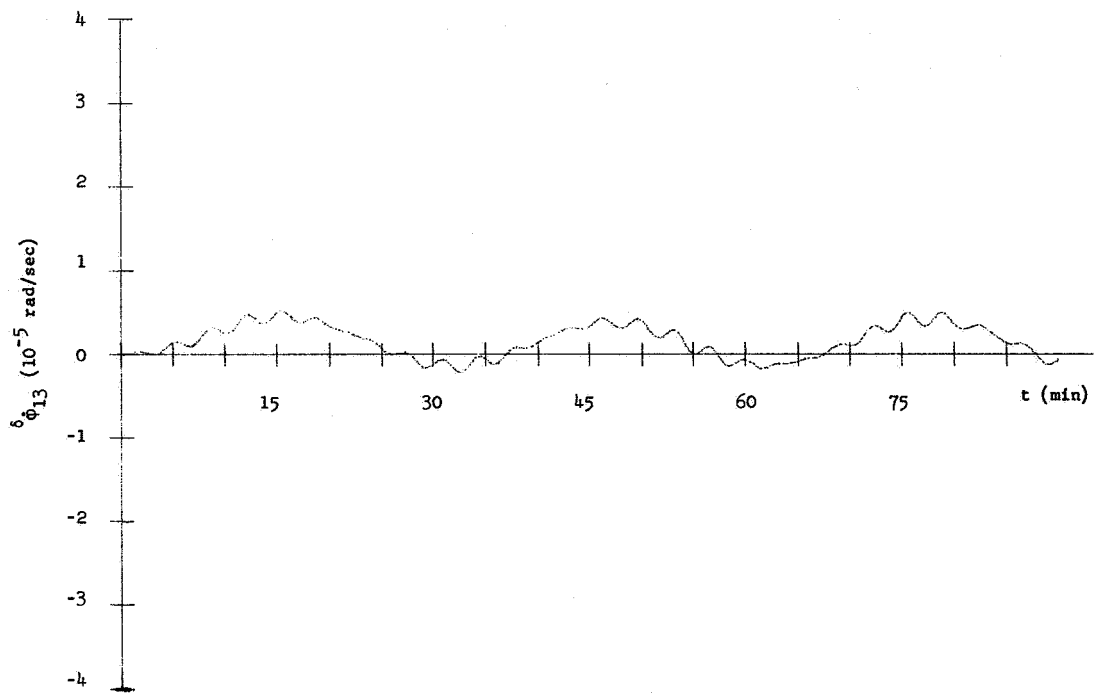


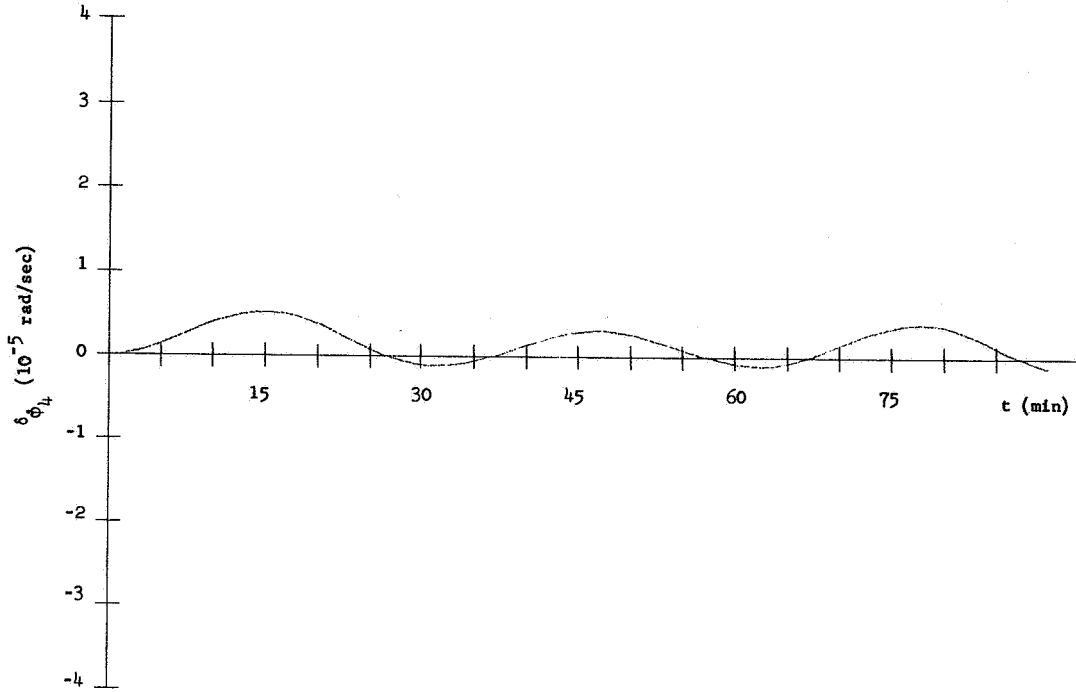
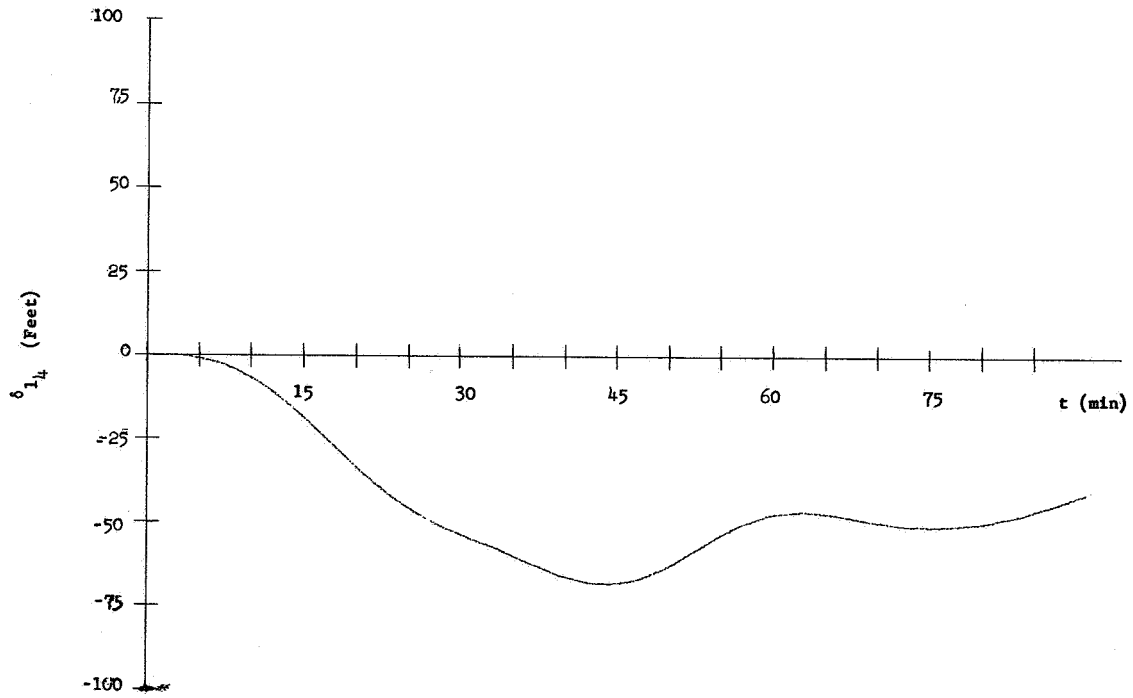
Figure 35. Plot VI-E, m_{16}

Figure 36. Plot II-E, m_8 Figure 37. Plot II-E, m_{15}

Figure 38. Plot II-E, m_7 Figure 39. Plot II-E, m_7

Figure 40. Plot II-E, m_{10} Figure 41. Plot II-E, m_{14}

Figure 42. Plot II-E, m_{11} Figure 43. Plot II-E, m_{13}

Figure 44. Plot II-E, m_4 Figure 45. Plot I-E, m_4

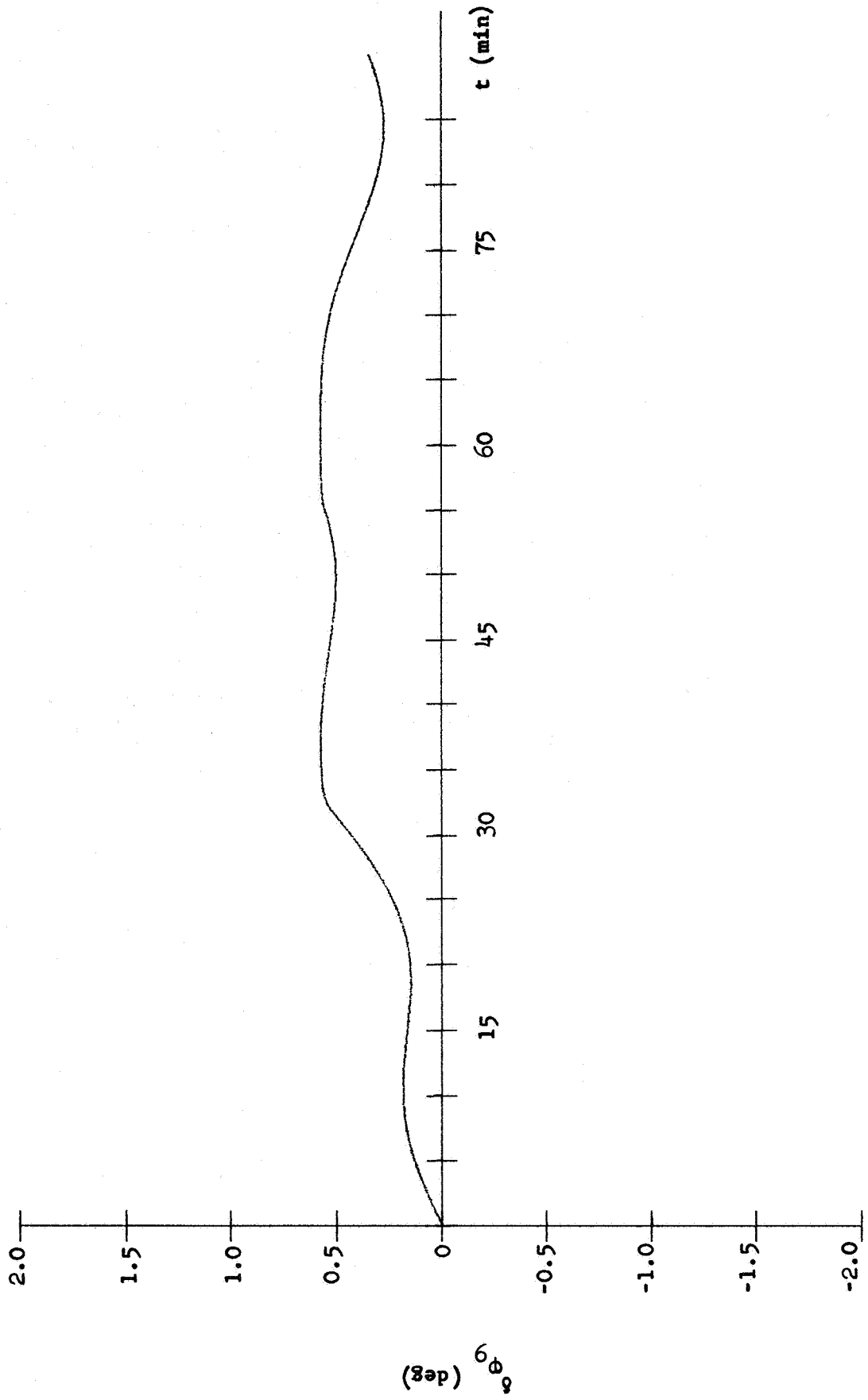
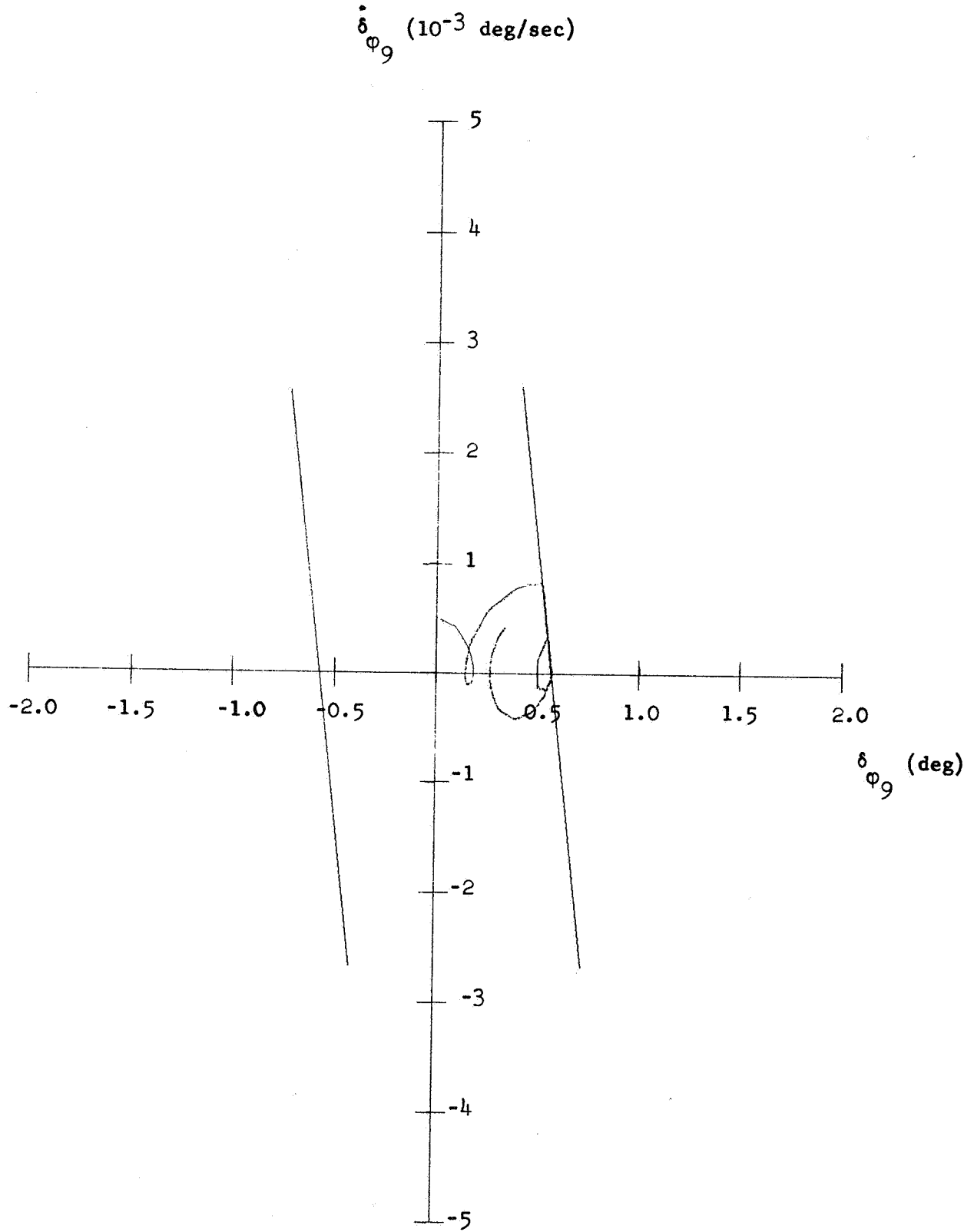


Figure 46. Plot III-E, m_9

Figure 47. Plot IV-E, m_9

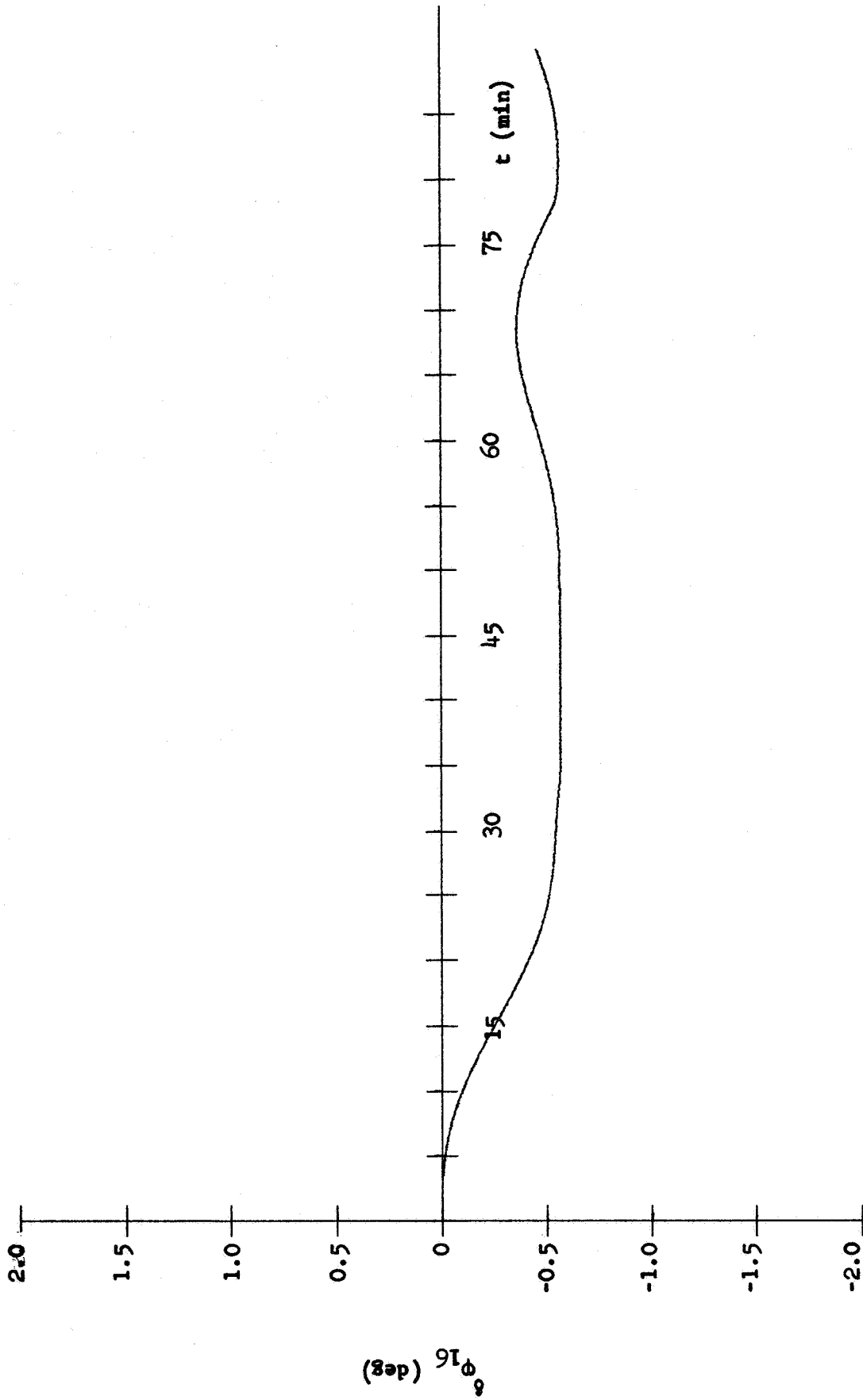
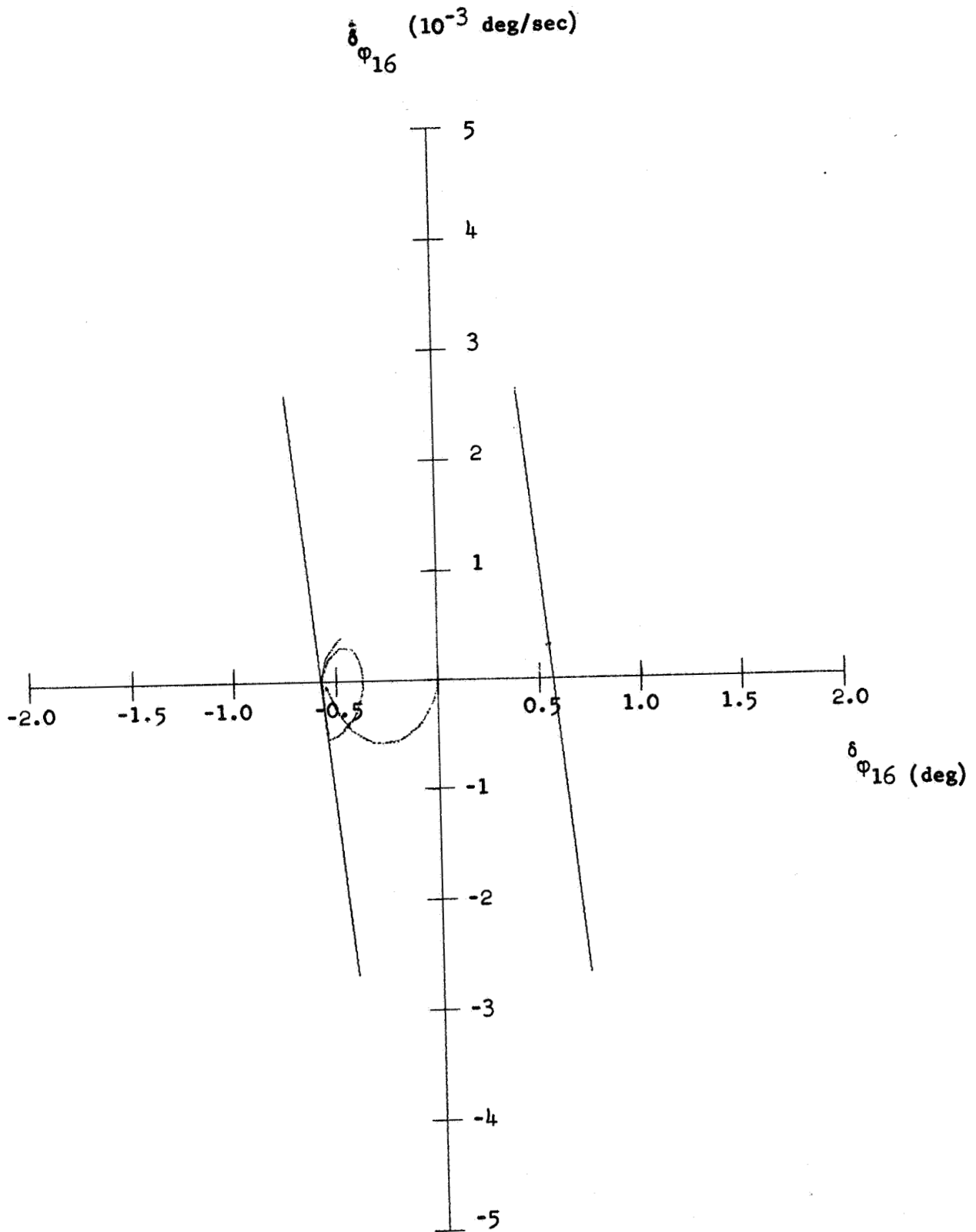
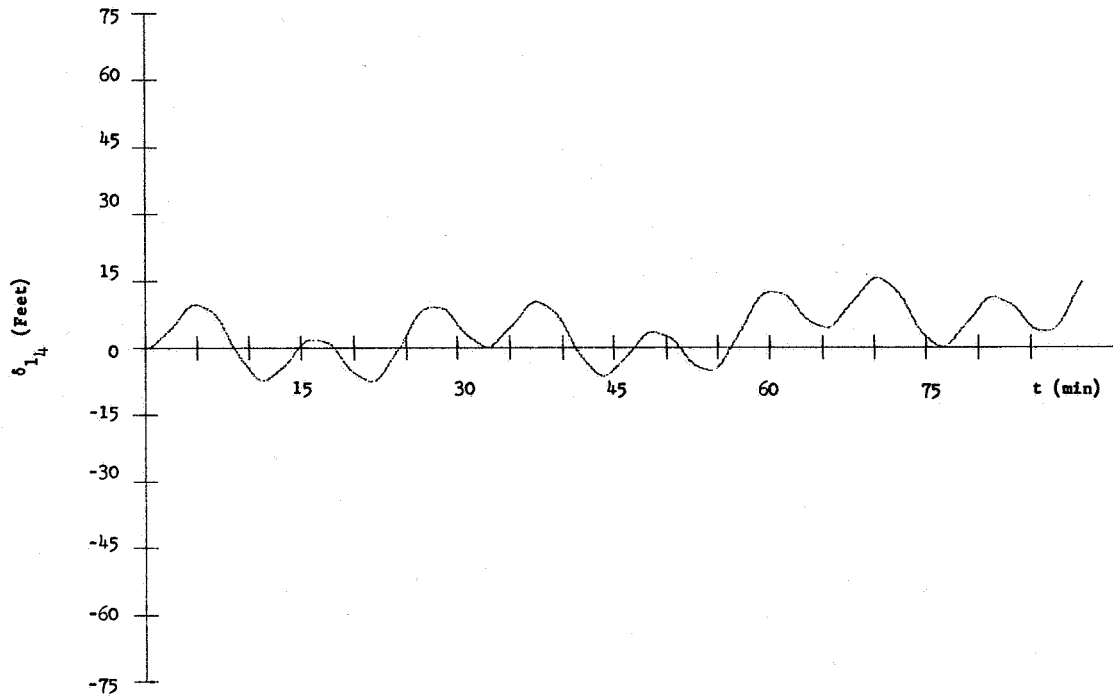
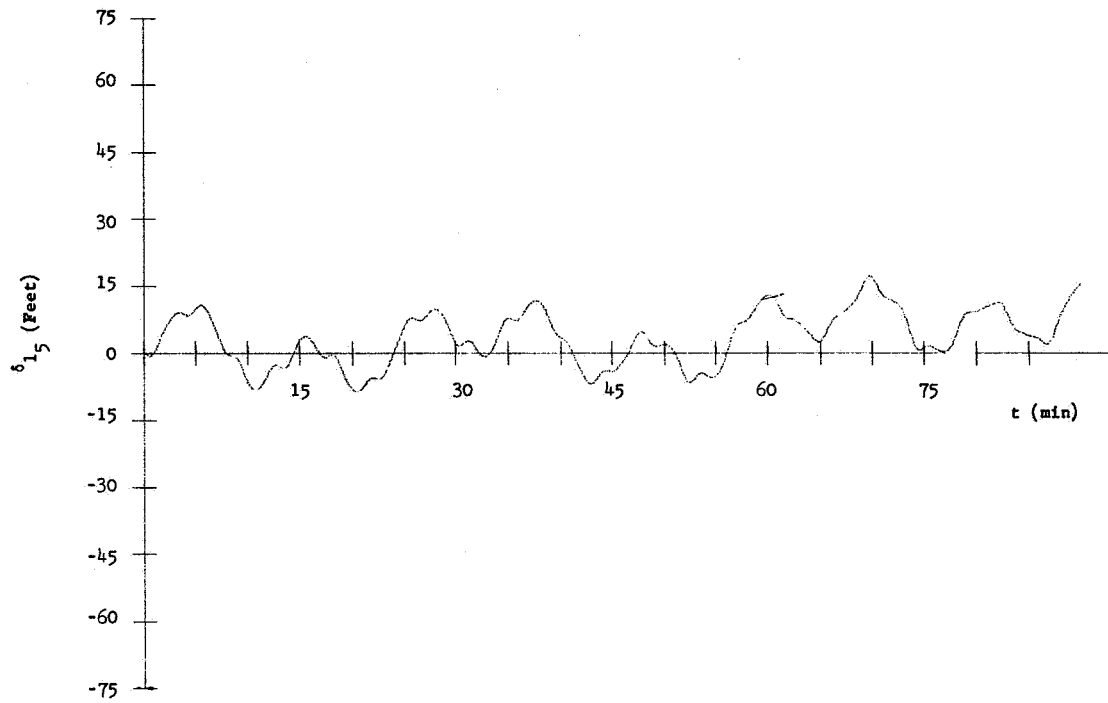


Figure 48. Plot III-E, m_{16}

Figure 49. Plot IV-E, m_{16}

Figure 50. Plot I-F, m_4 Figure 51. Plot I-F, m_5

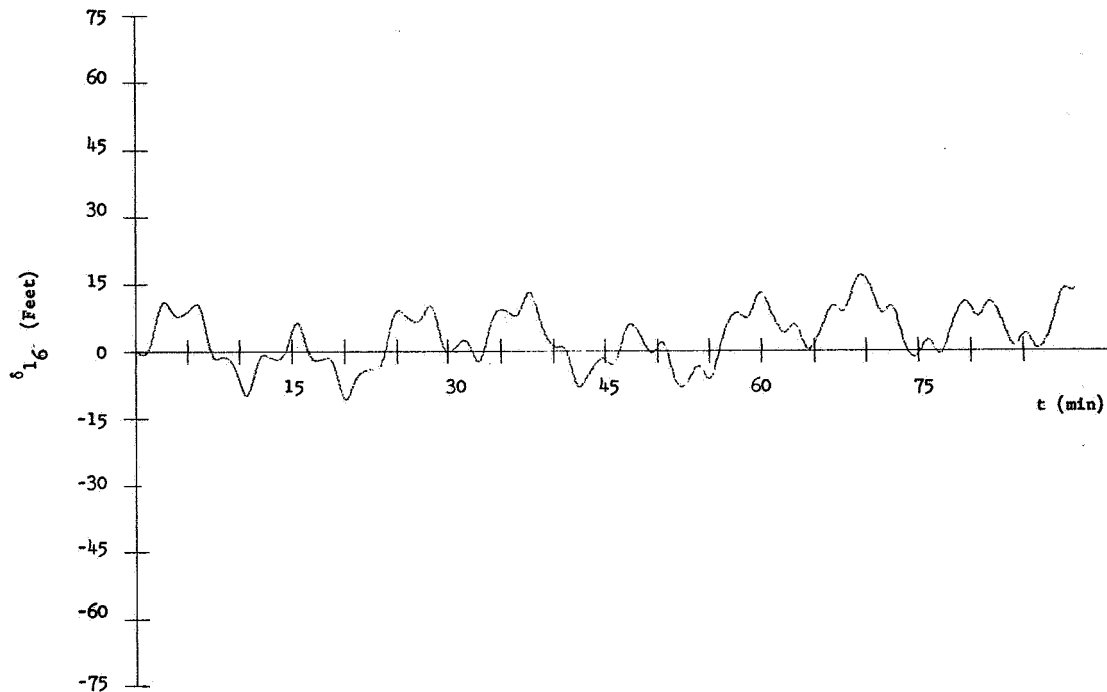


Figure 52. Plot I-F, m_6

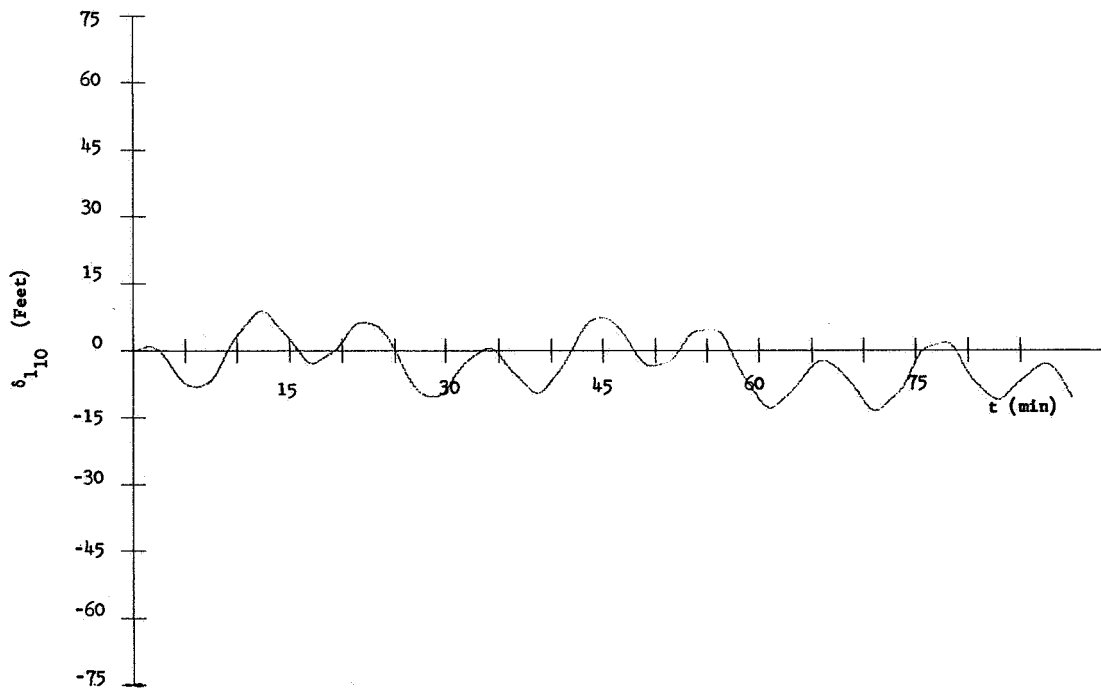
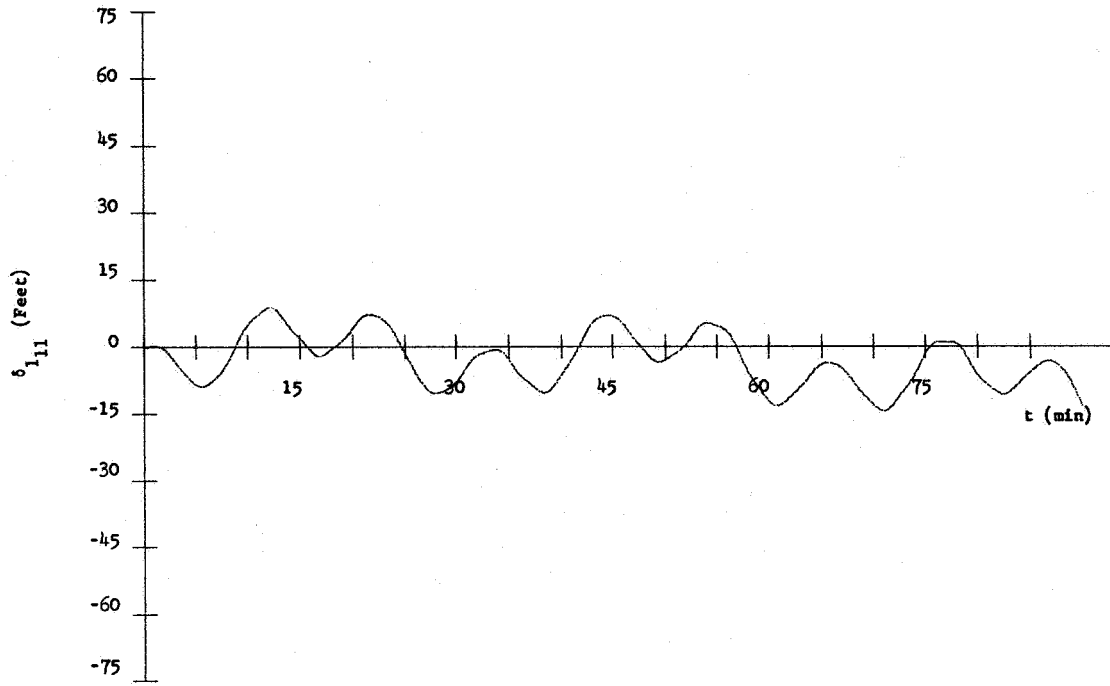
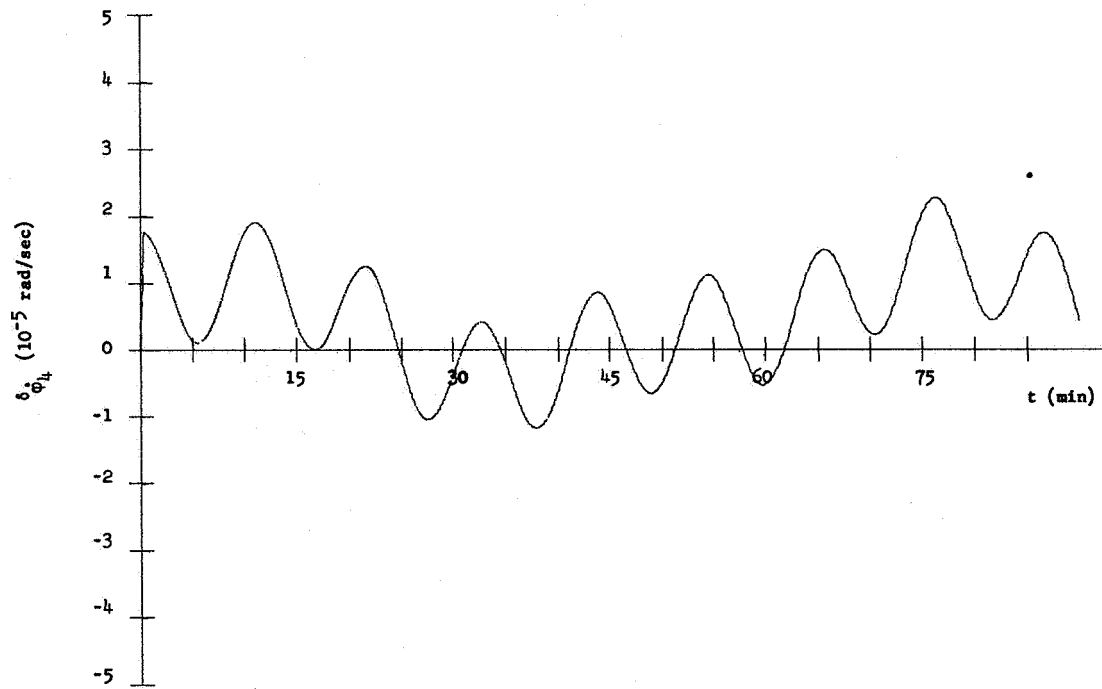
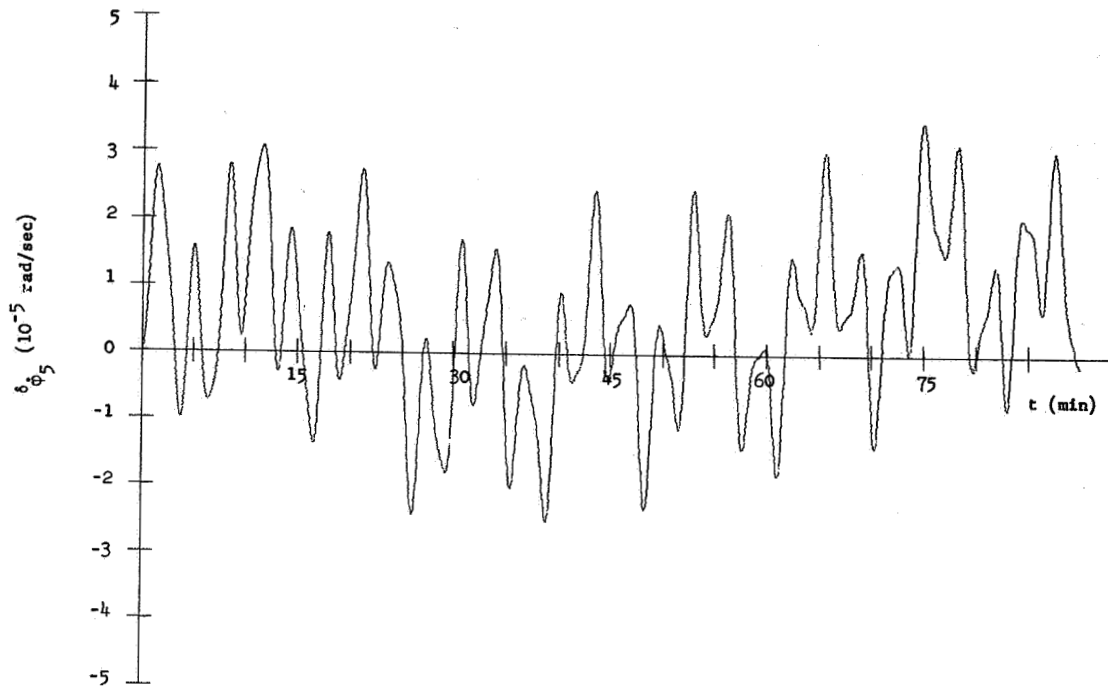
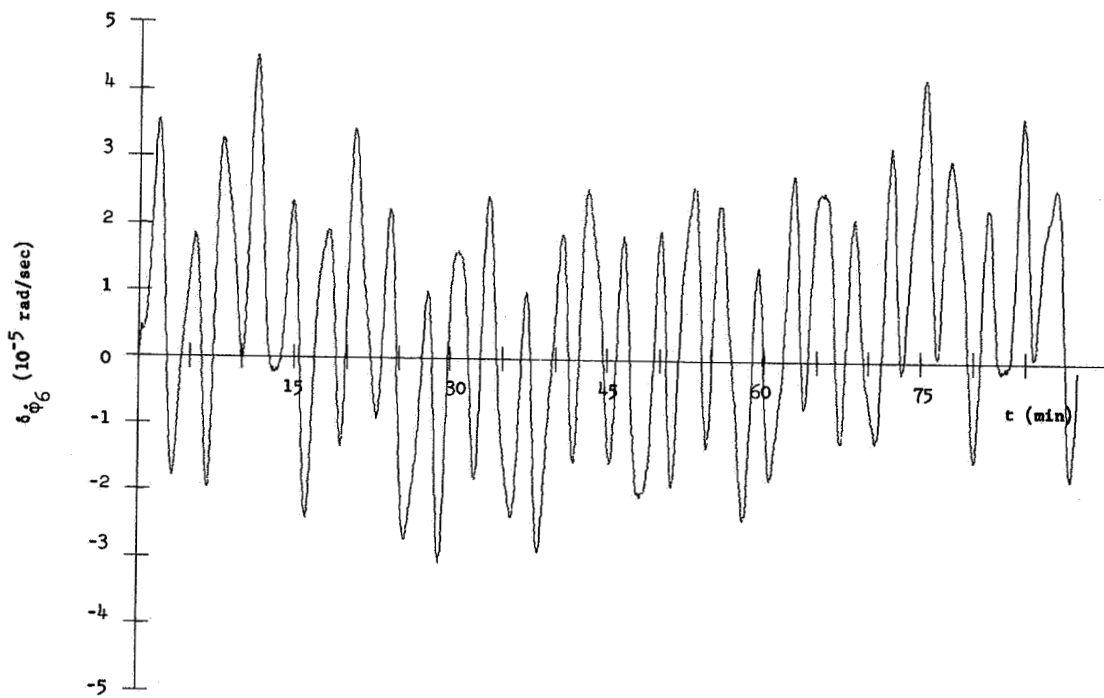
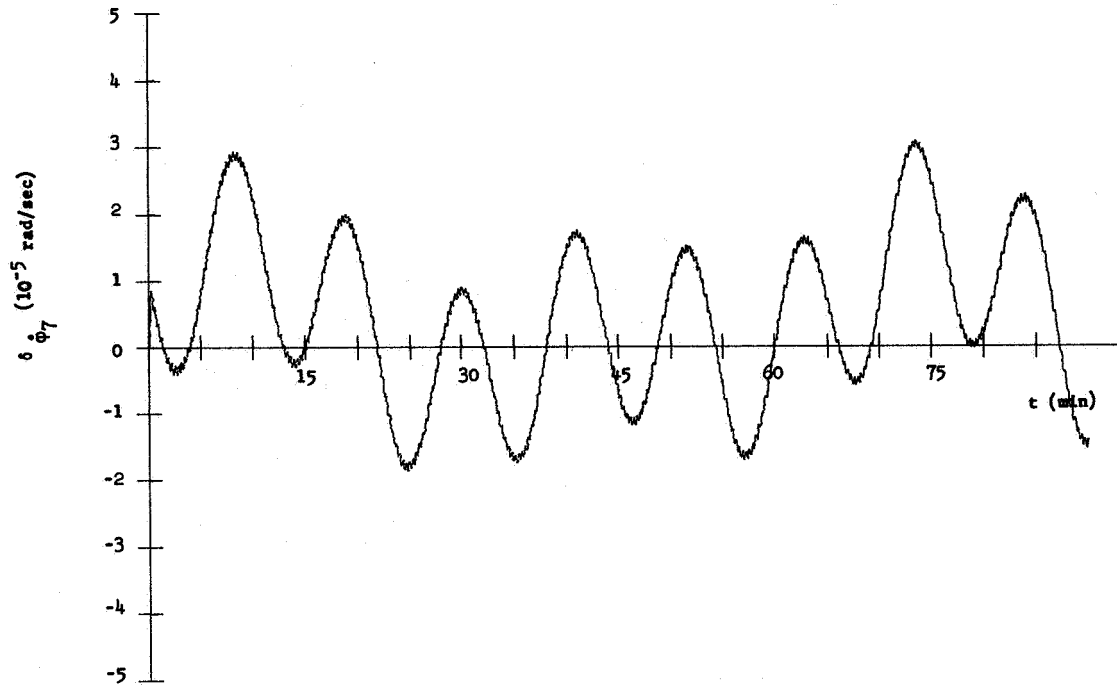
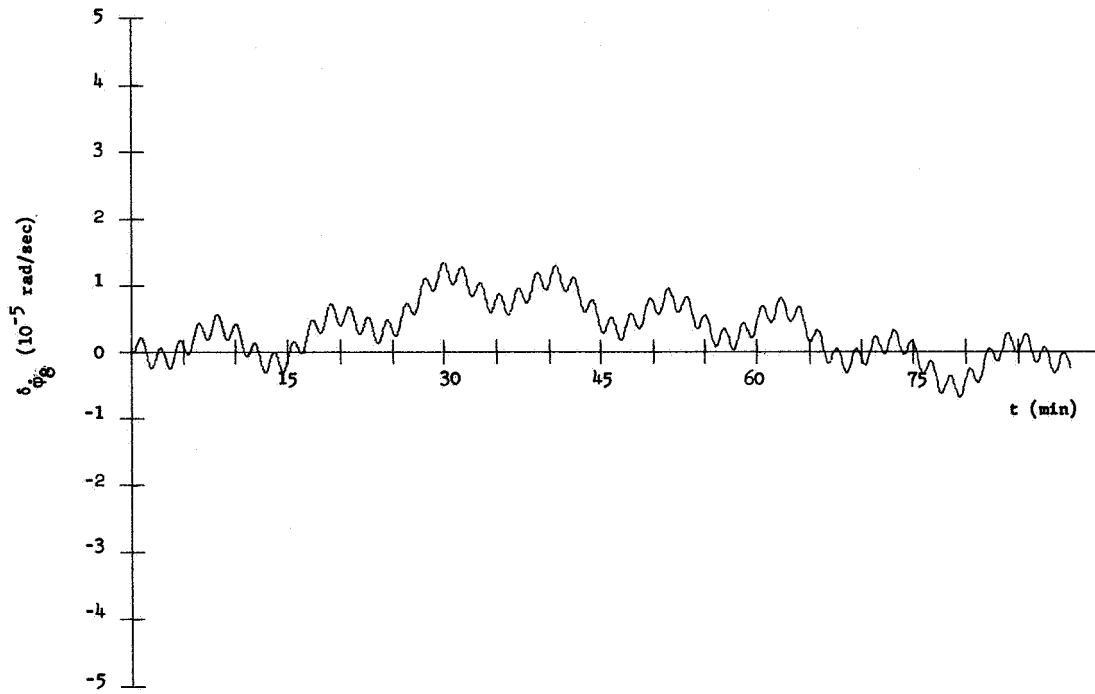
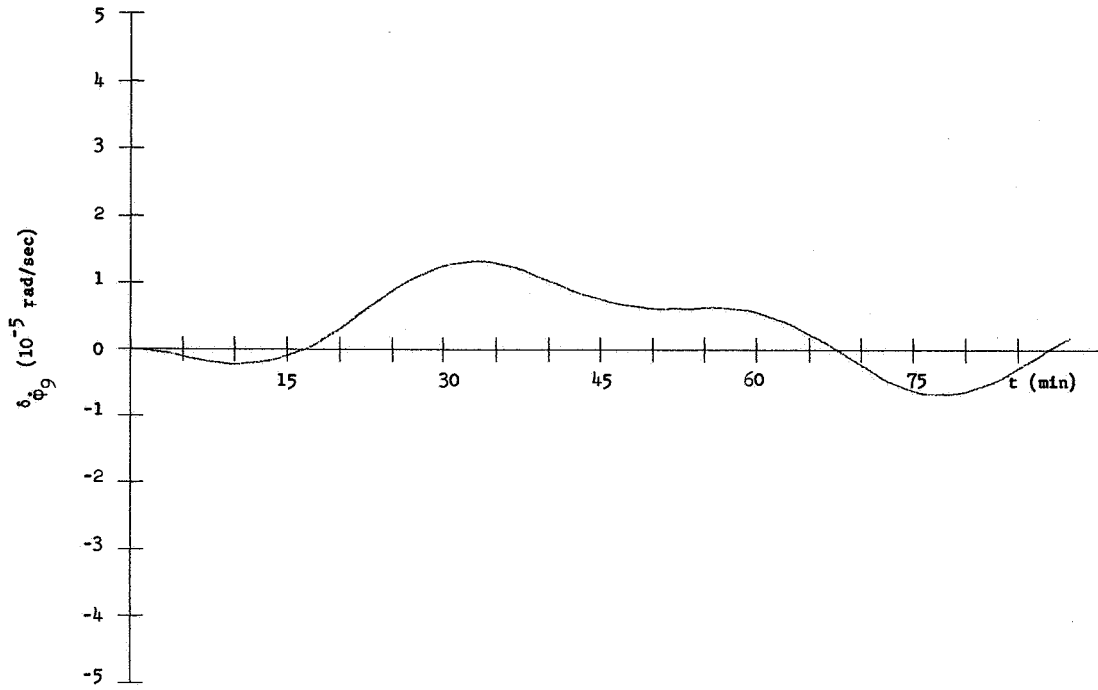
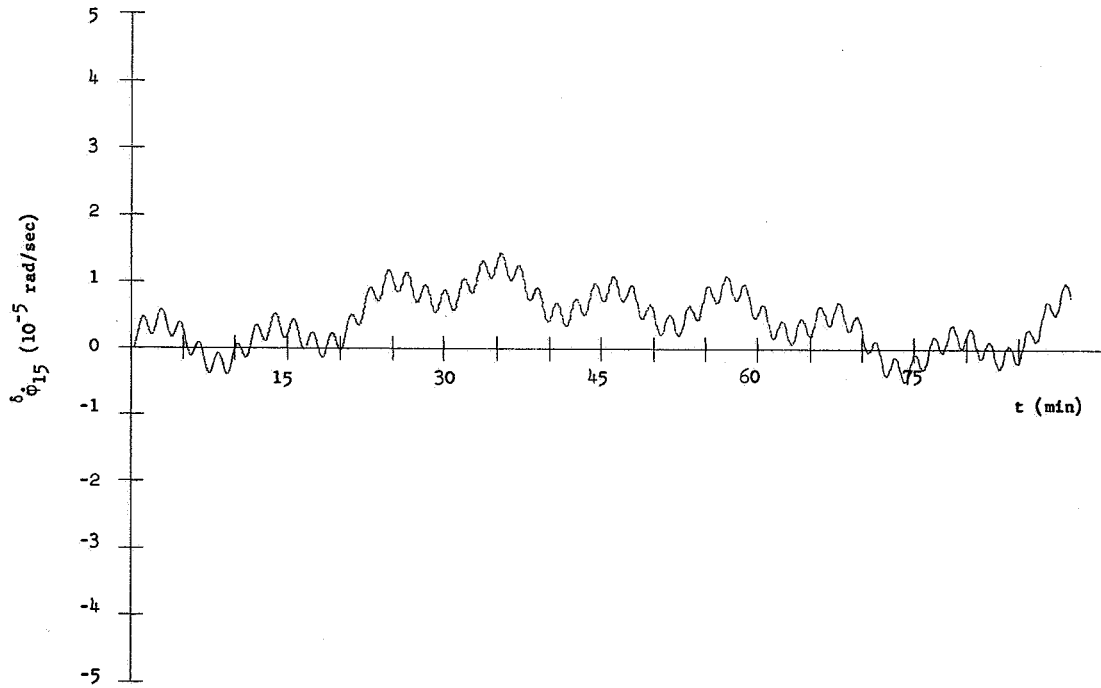


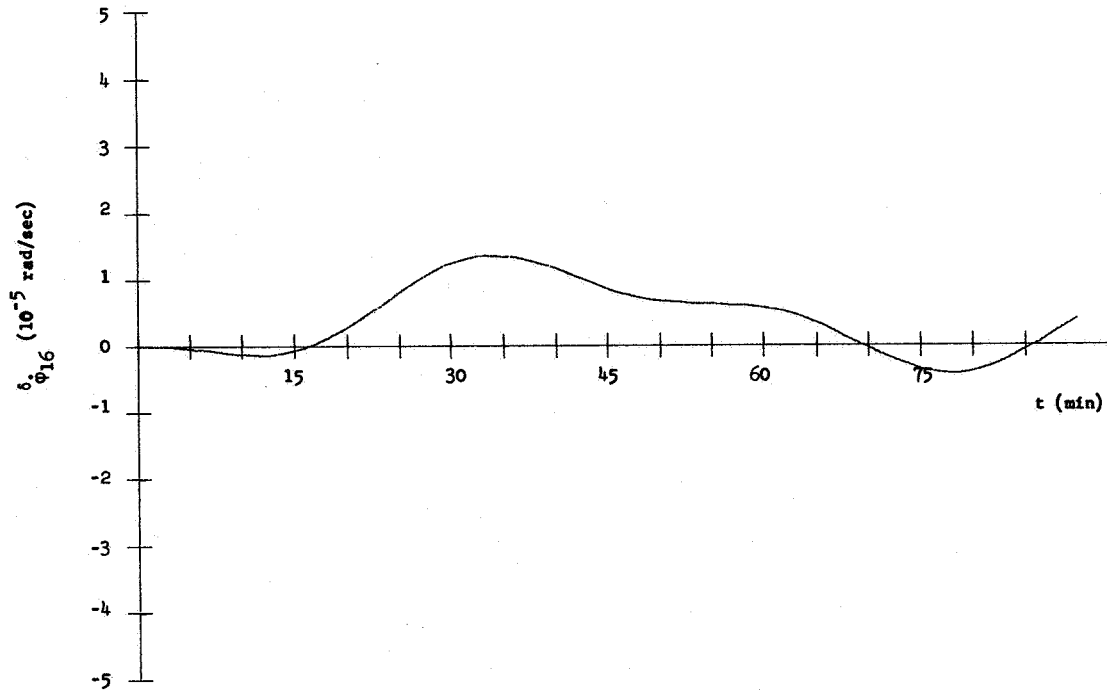
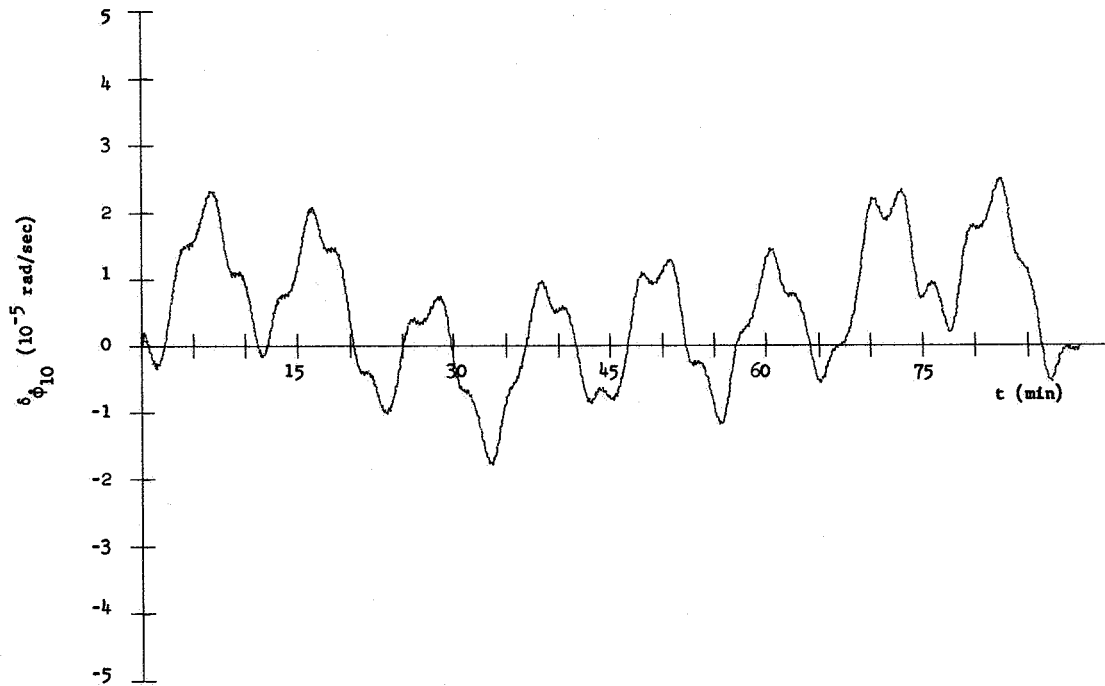
Figure 53. Plot I-F, m_{10}

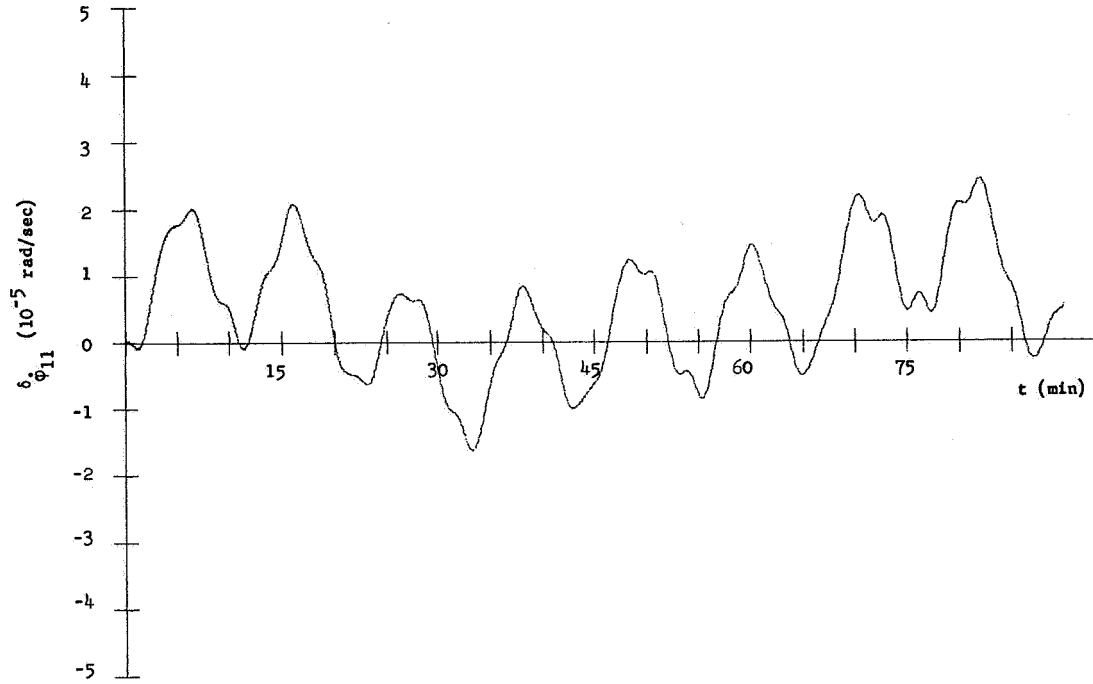
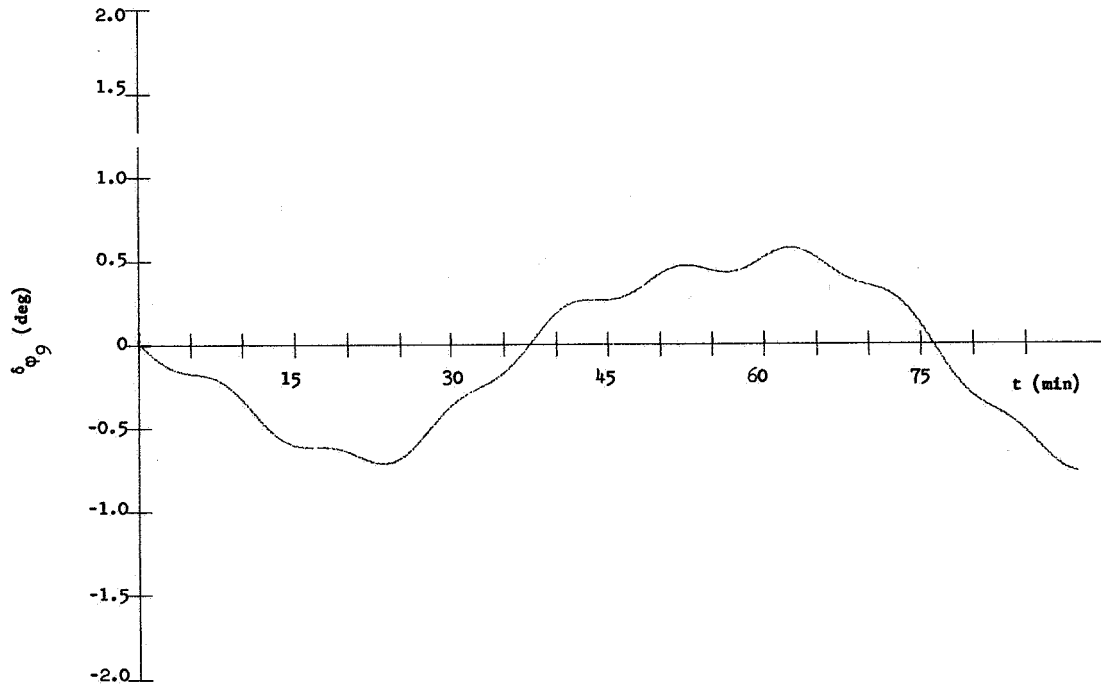
Figure 54. Plot I-F, m_{11} Figure 55. Plot II-F, m_4

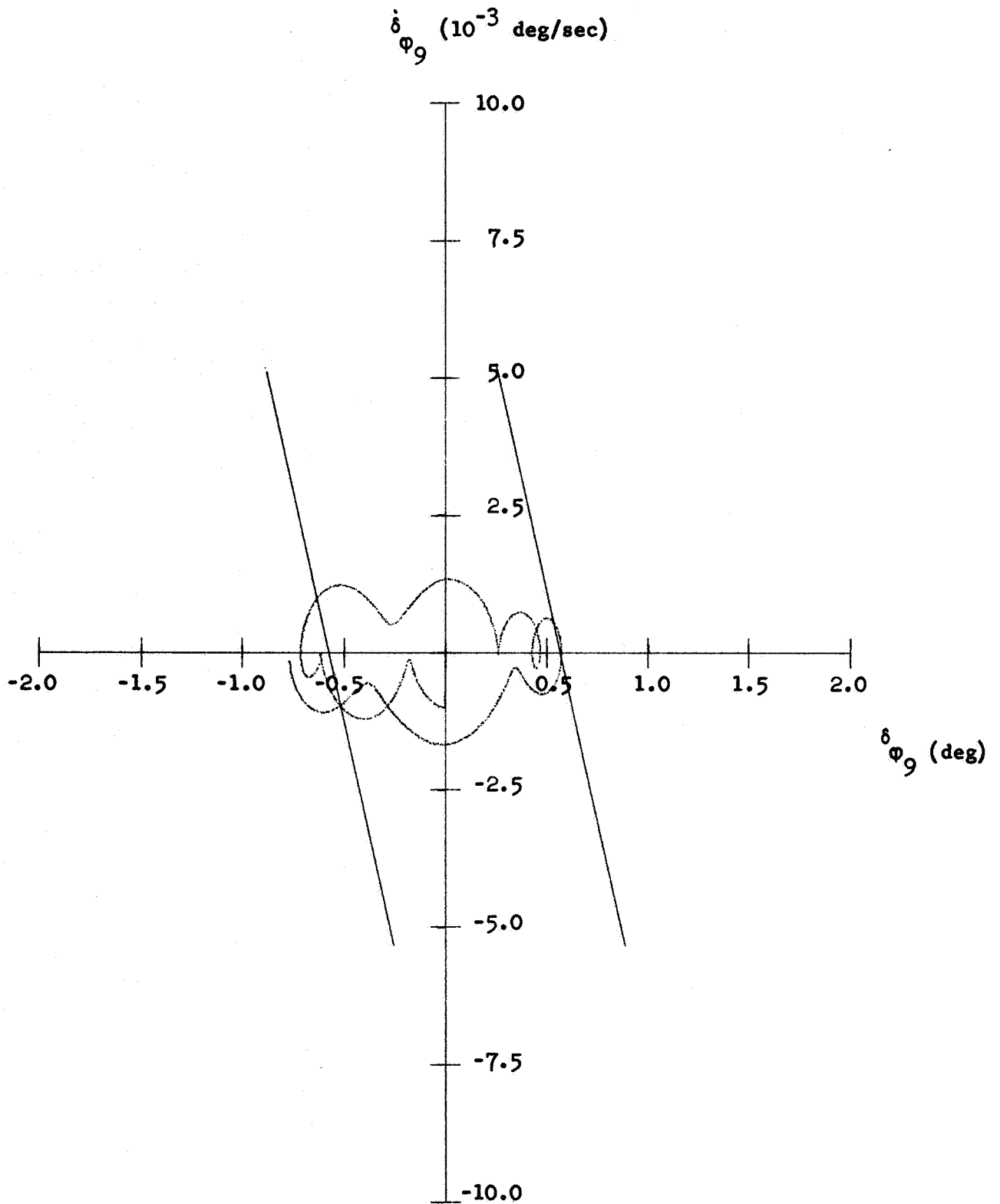
Figure 56. Plot II-F, m_5 Figure 57. Plot II-F, m_6

Figure 58. Plot II-F, n_7 Figure 59. Plot II-F, n_8

Figure 60. Plot II-F, m_9 Figure 61. Plot II-F, m_{15}

Figure 62. Plot II-F, n_{16} Figure 63. Plot II-F, n_{10}

Figure 64. Plot II-F, m_{11} Figure 65. Plot III-F, m_9

Figure 66. Plot IV-F, m_9

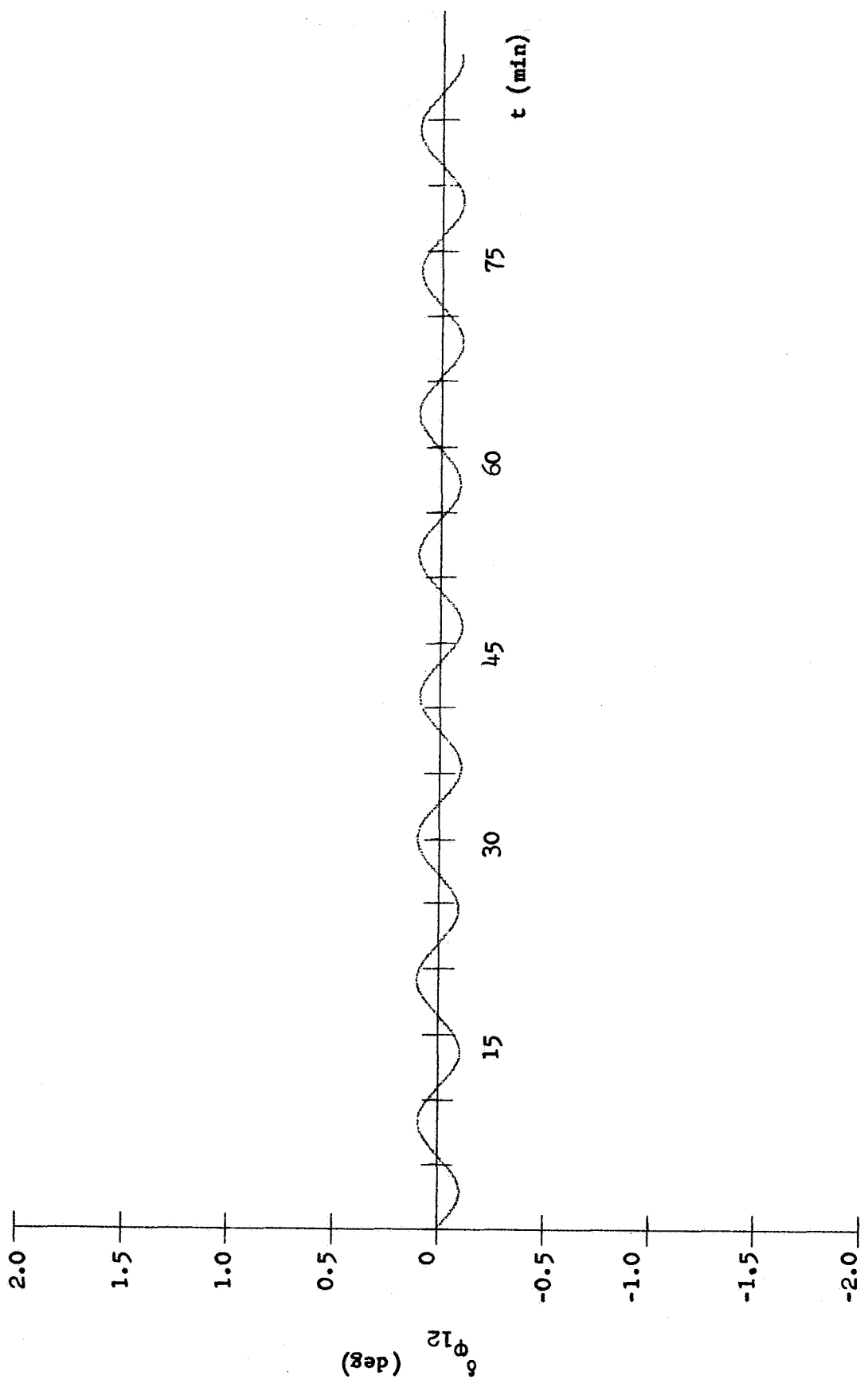
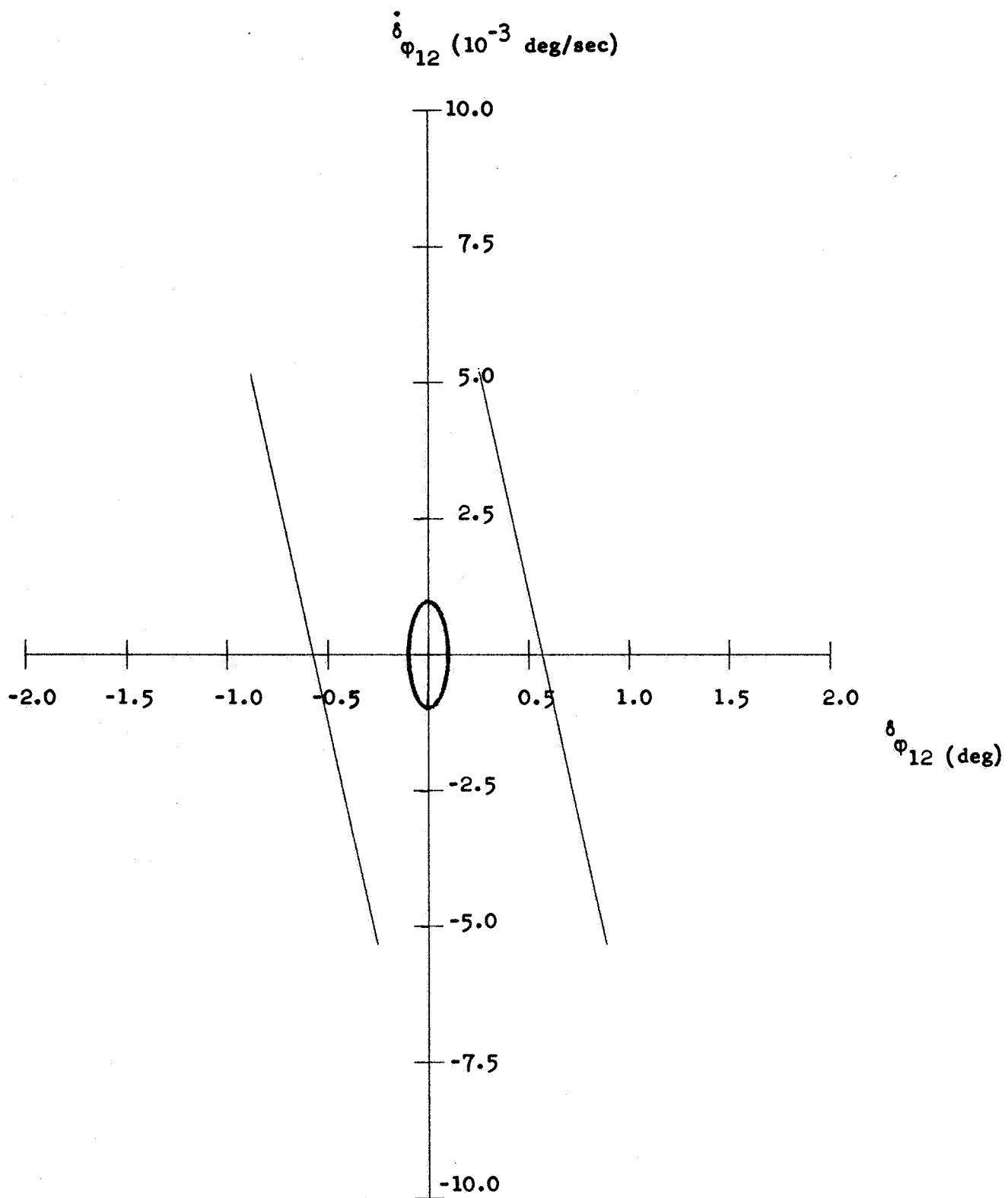


Figure 67. Plot III-F, m_{12}

Figure 68. Plot IV-F, m_{12}

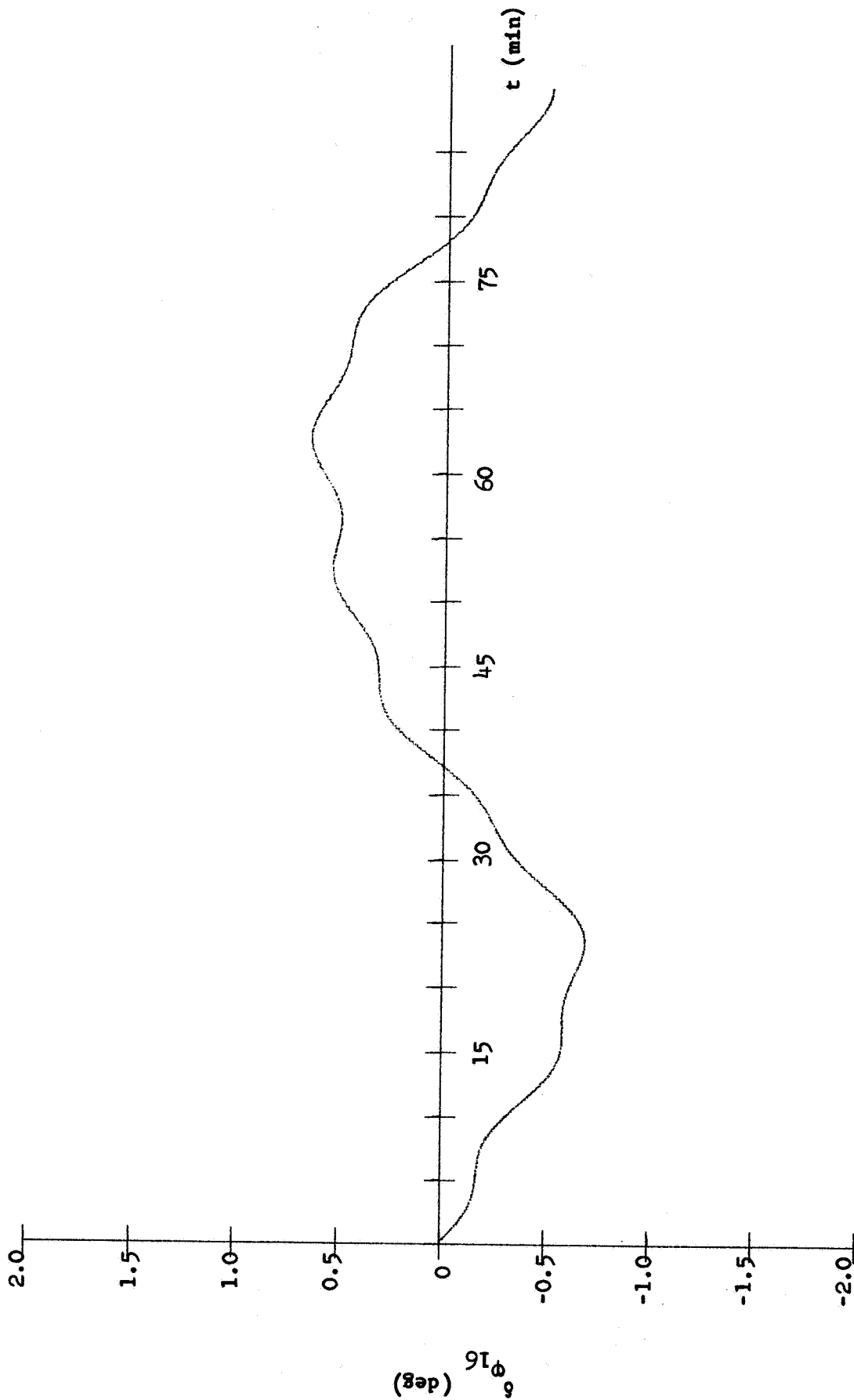
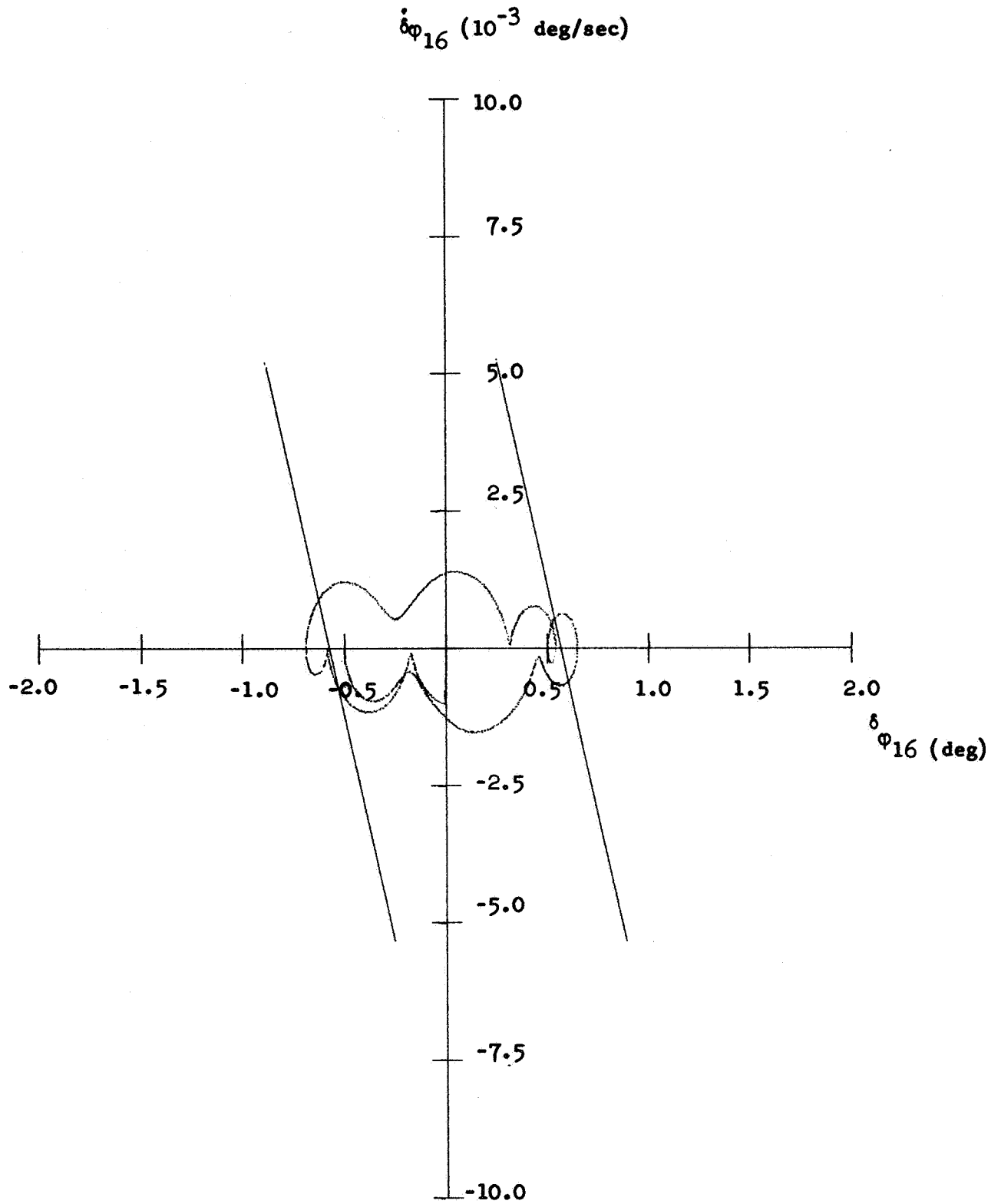
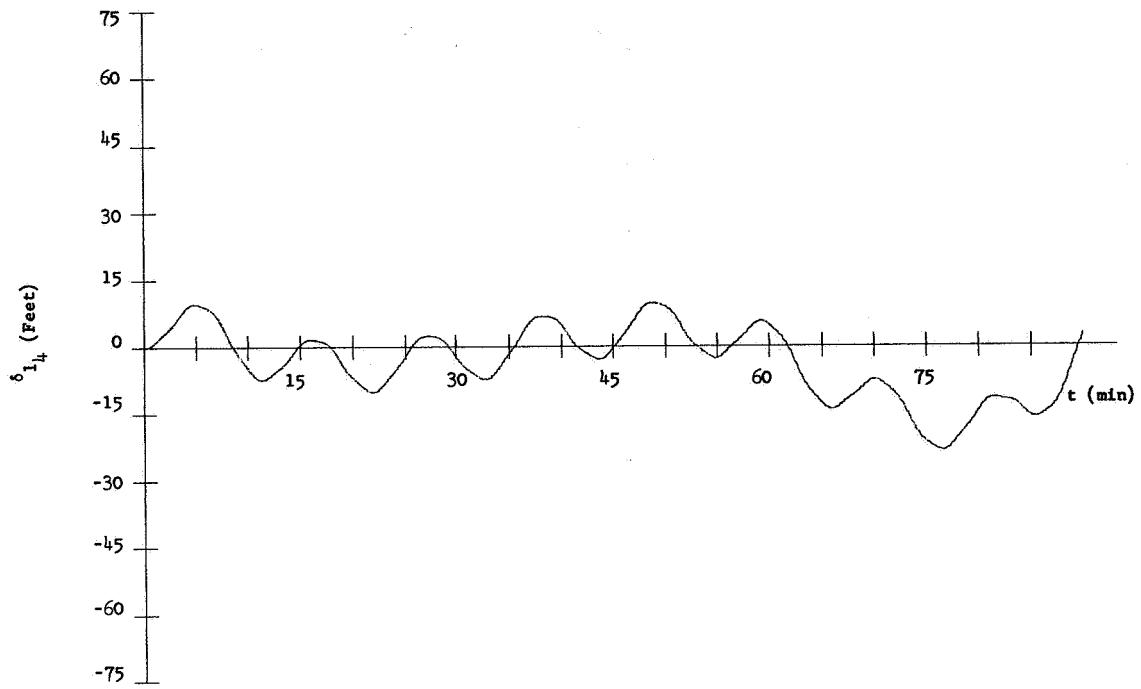
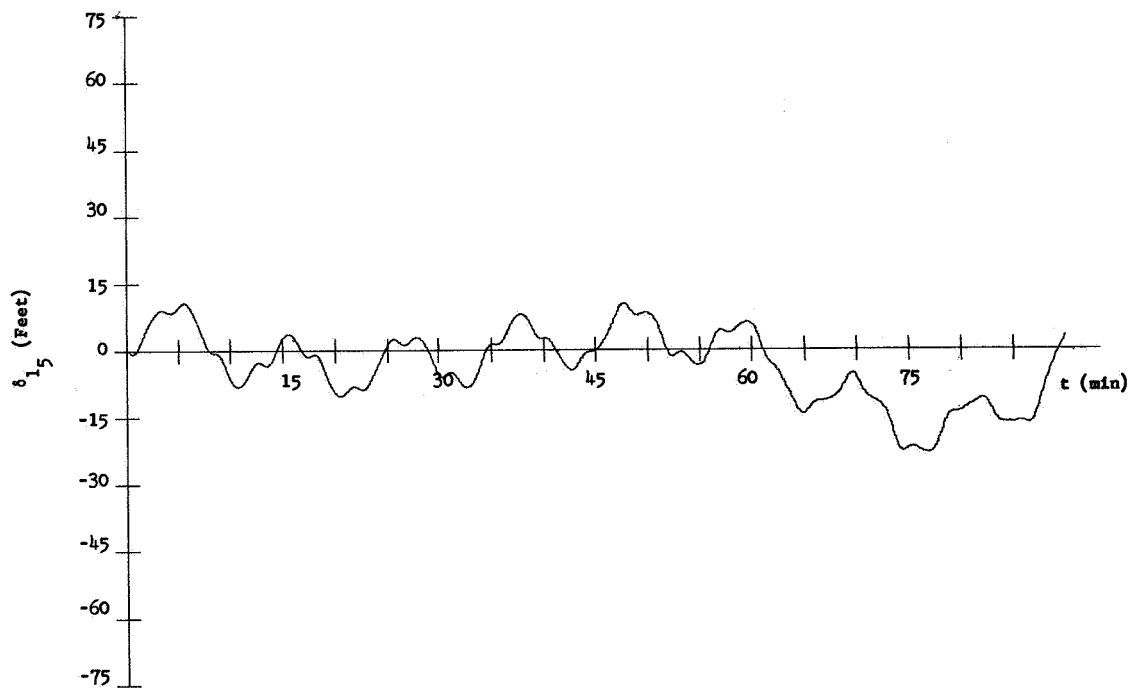


Figure 69. Plot III-F, m_{16}

Figure 70. Plot IV-F, m_{16}

Figure 71. Plot I-G, m_4 Figure 72. Plot I-G, m_5

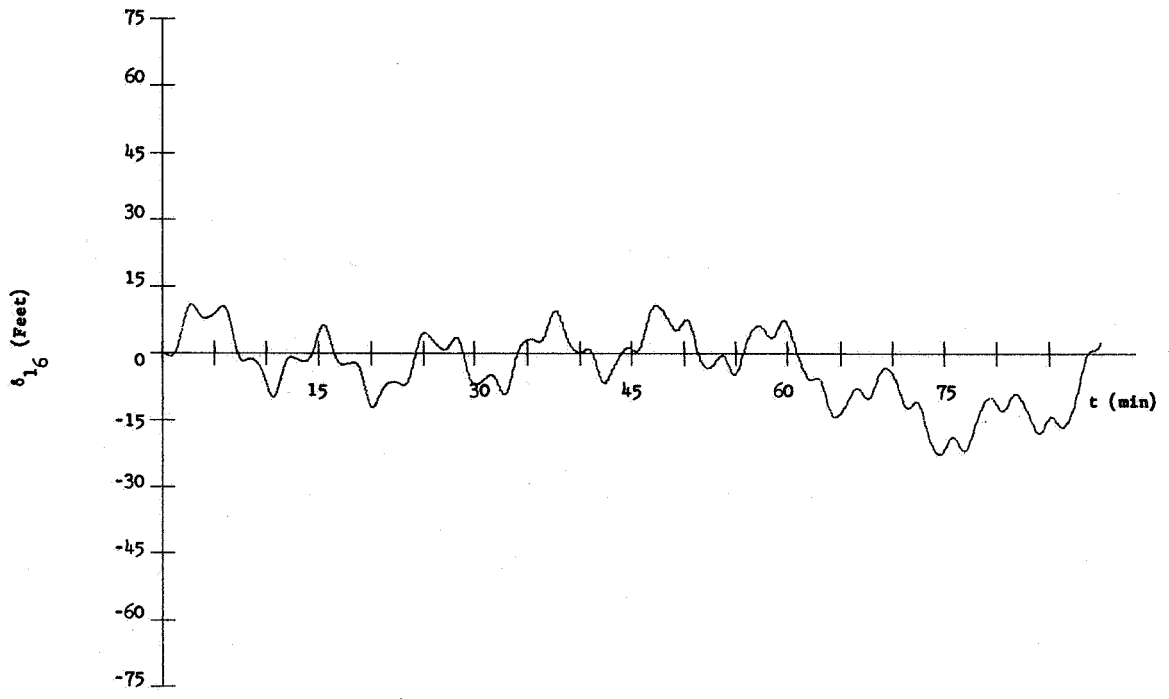


Figure 73. Plot I-G, m_6

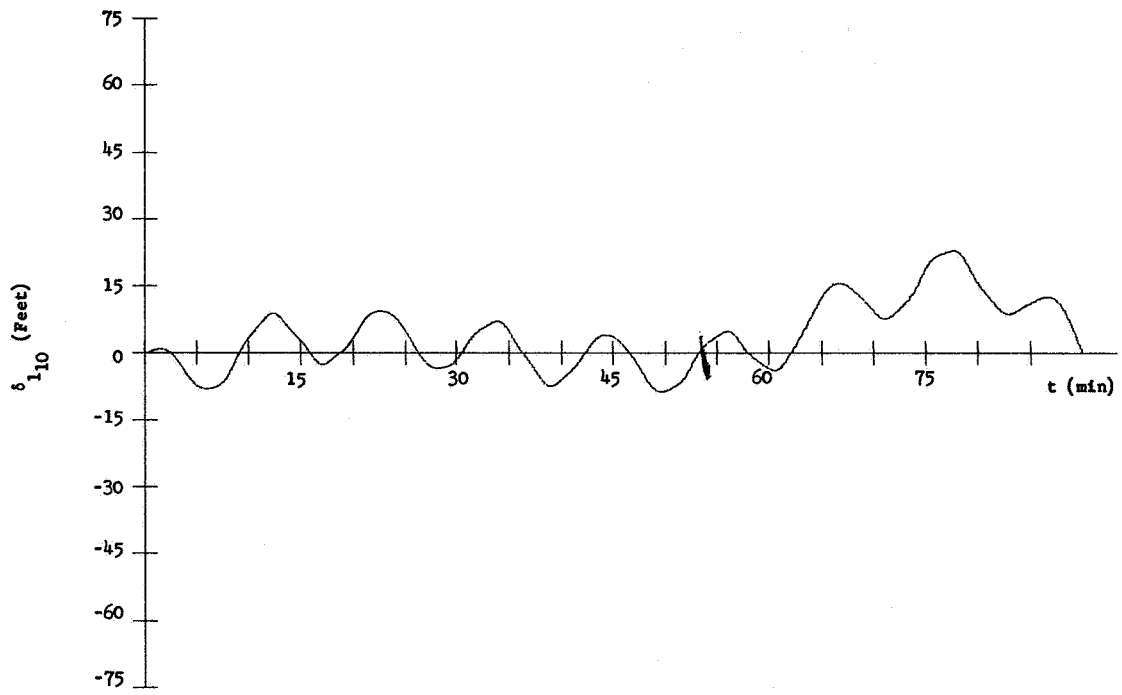
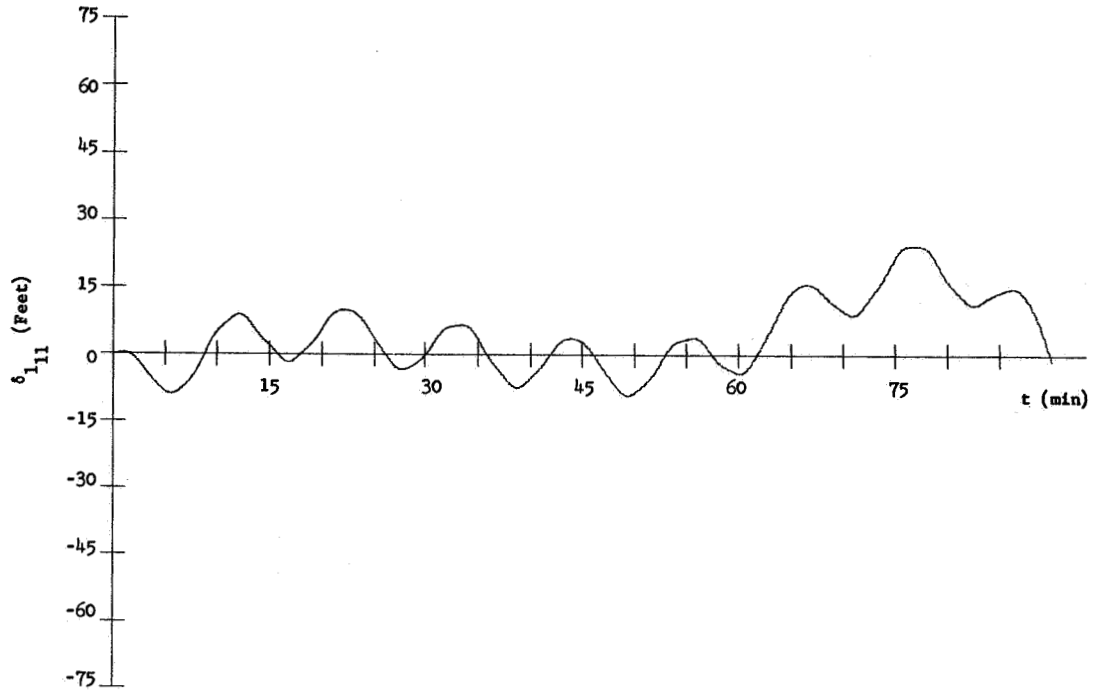
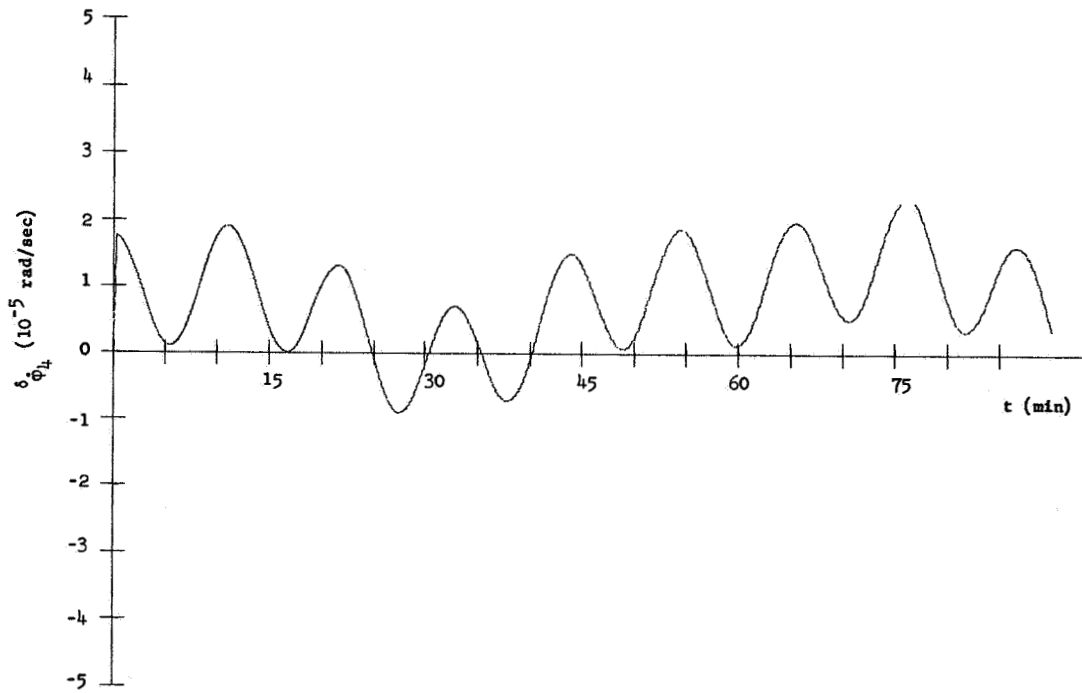
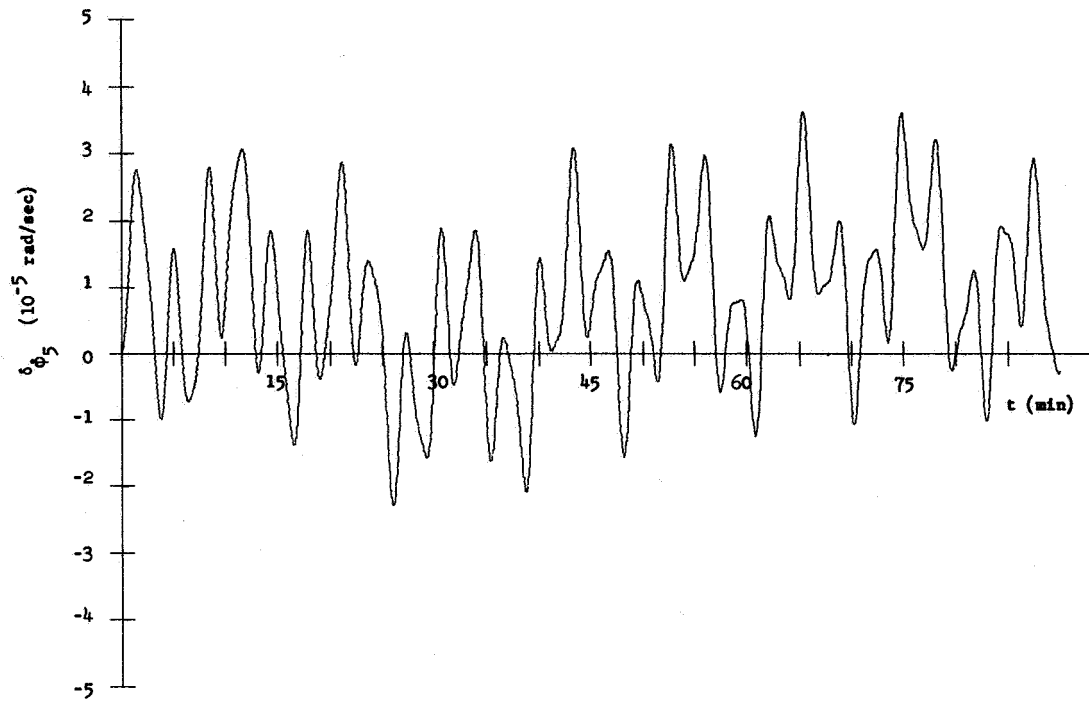
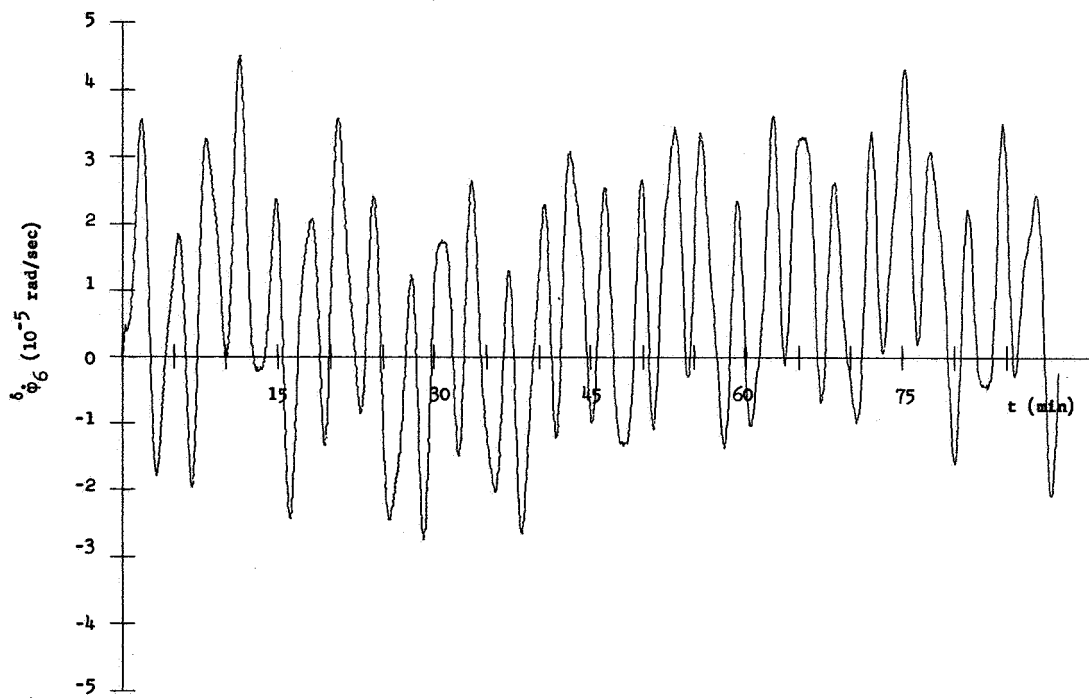
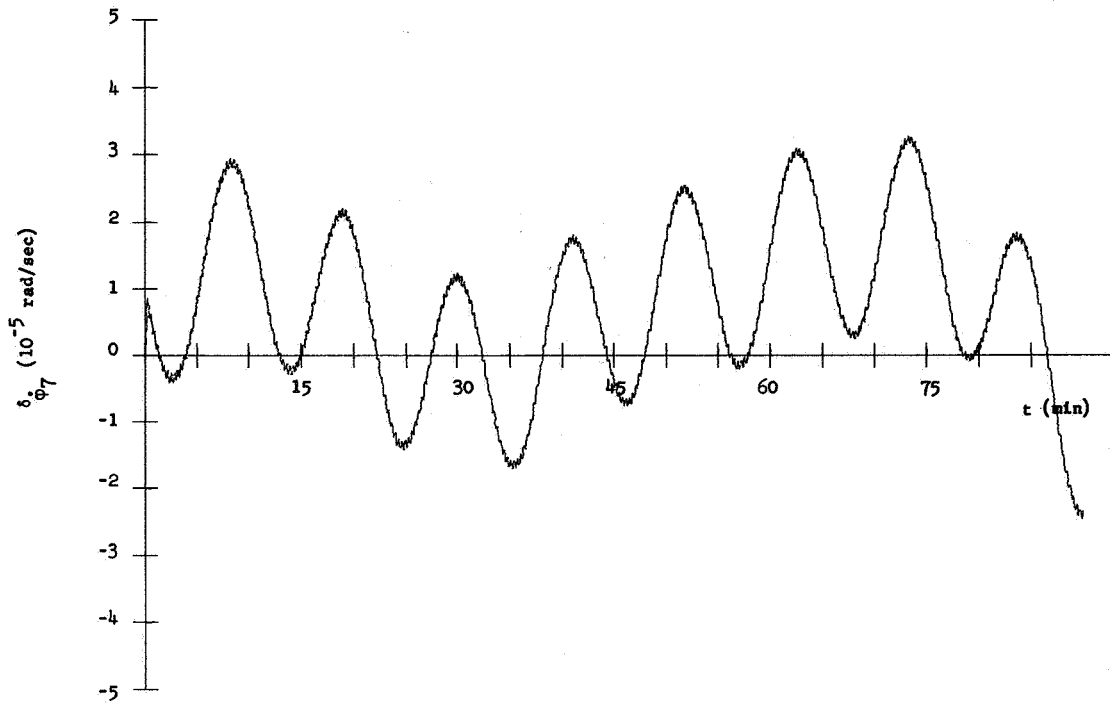
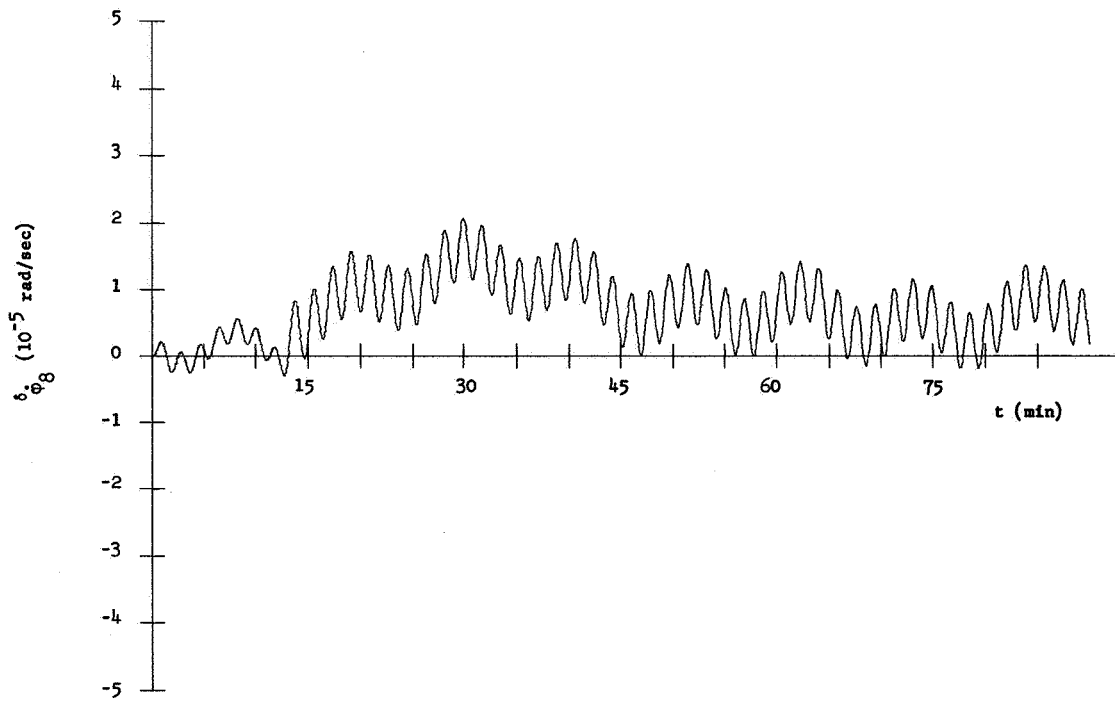
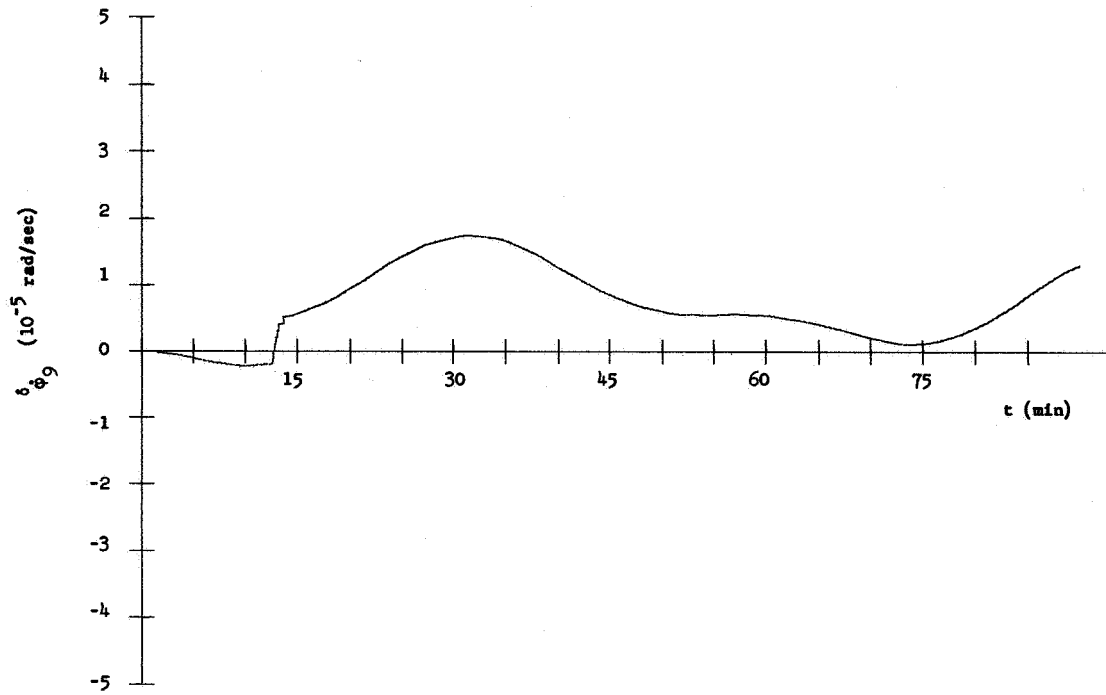
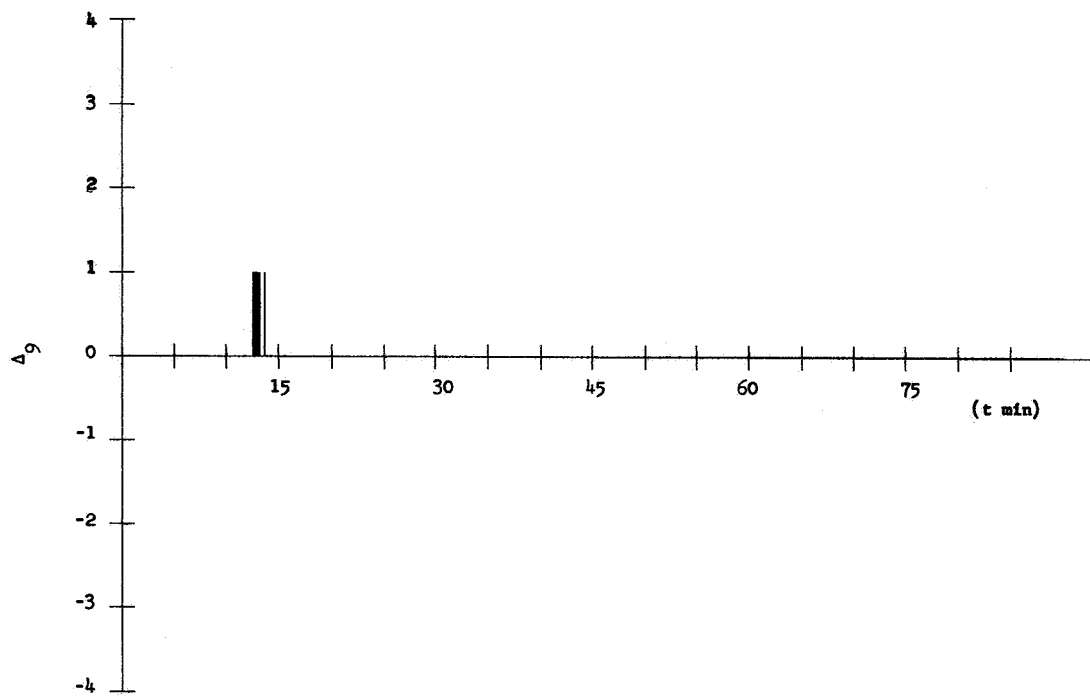


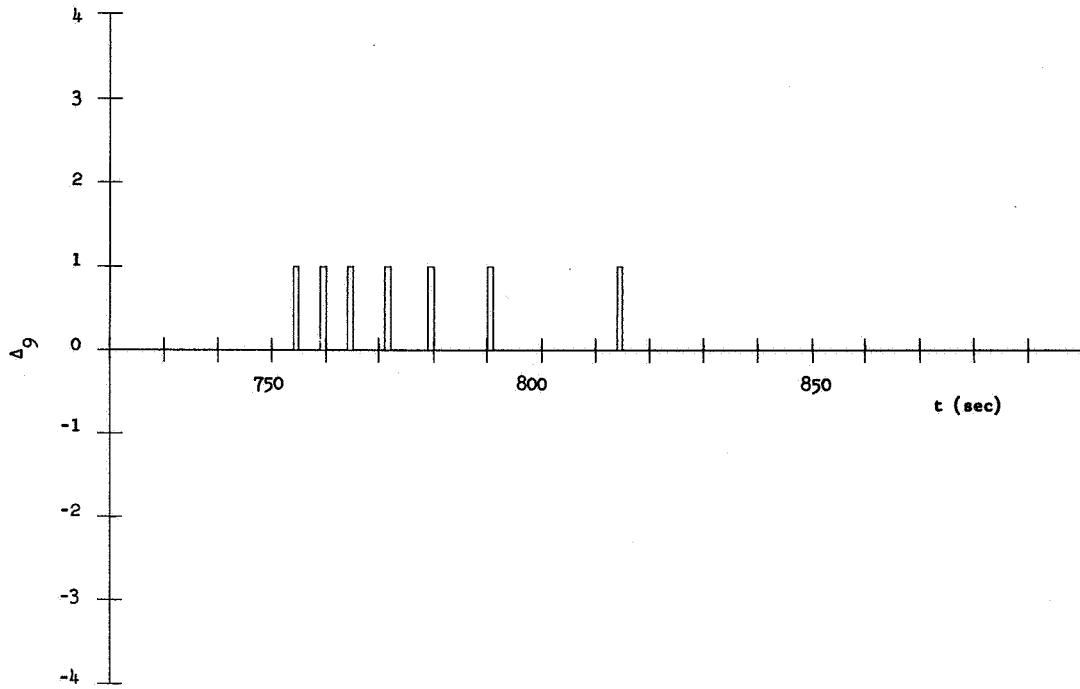
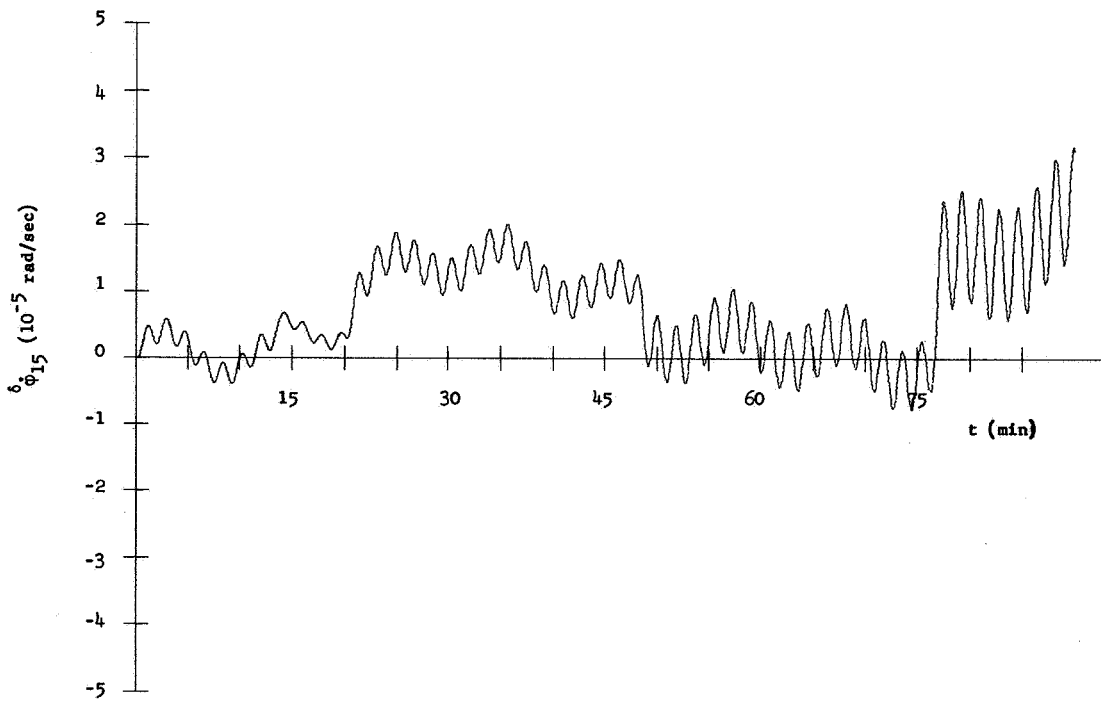
Figure 74. Plot I-G, m_{10}

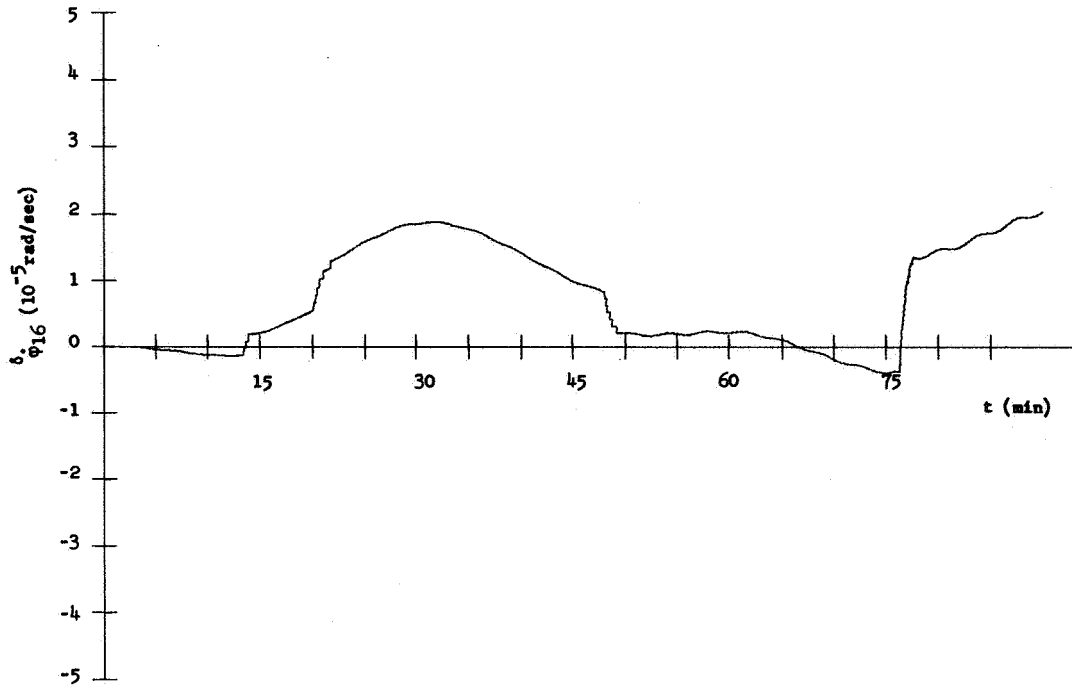
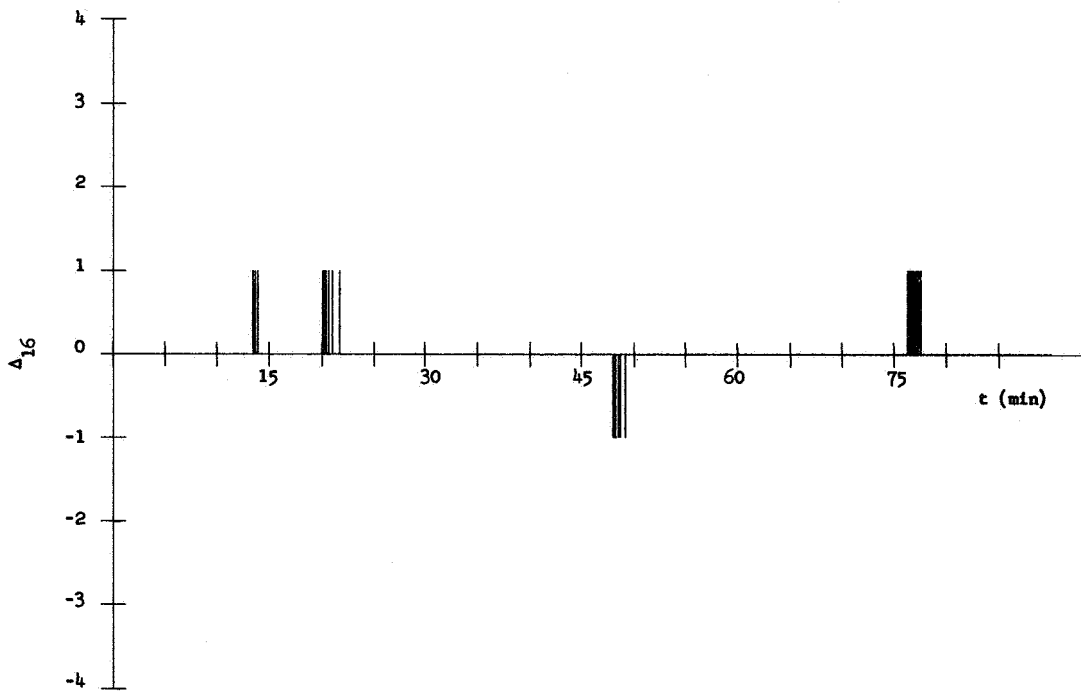
Figure 75. Plot I-G, m_{11} Figure 76. Plot II-G, m_4

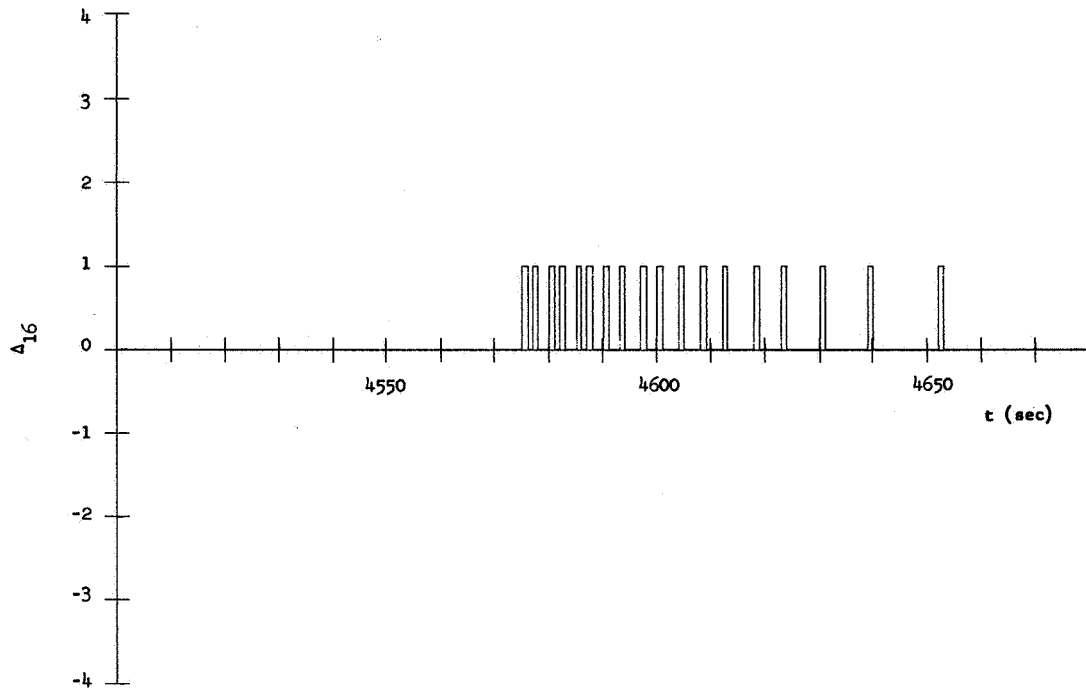
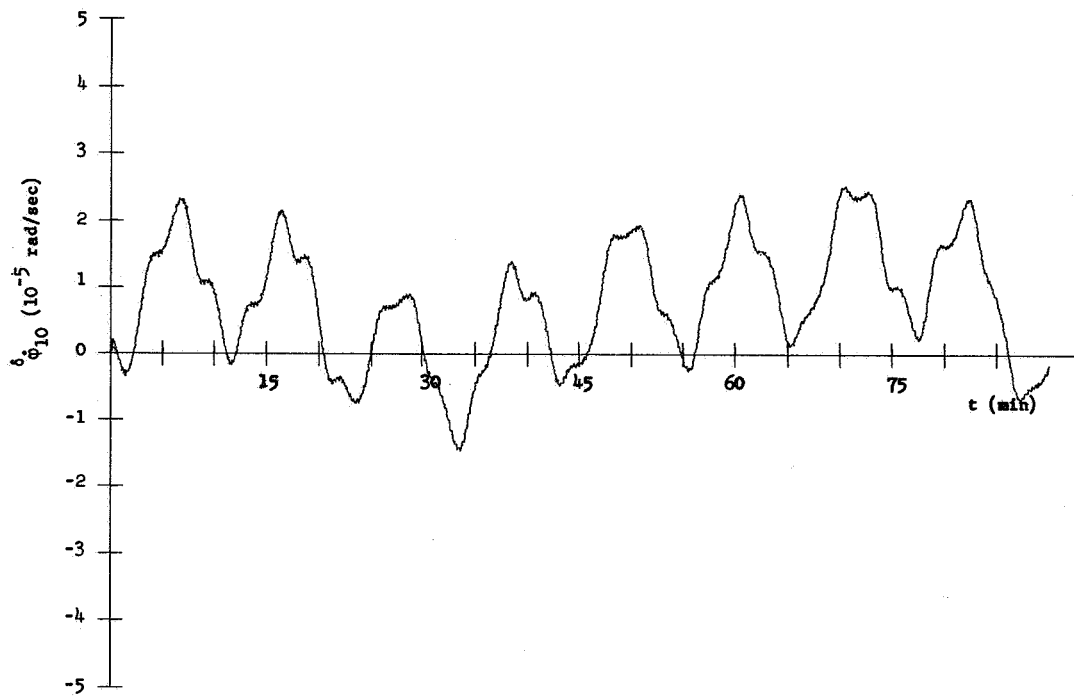
Figure 77. Plot II-G, m_5 Figure 78. Plot II-G, m_6

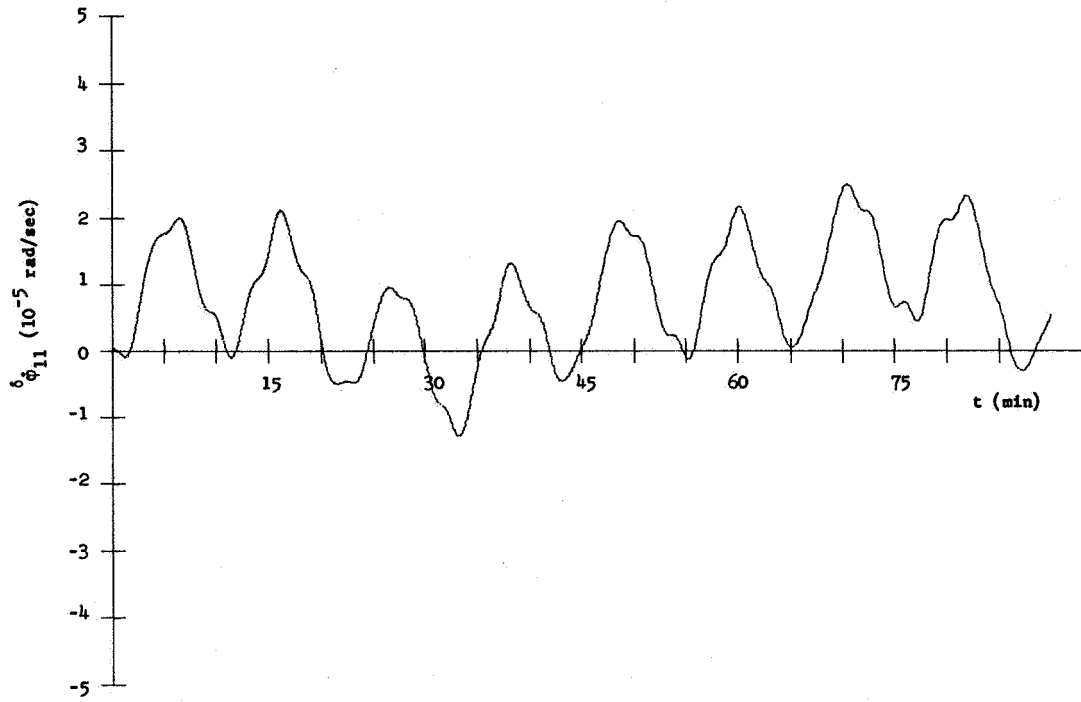
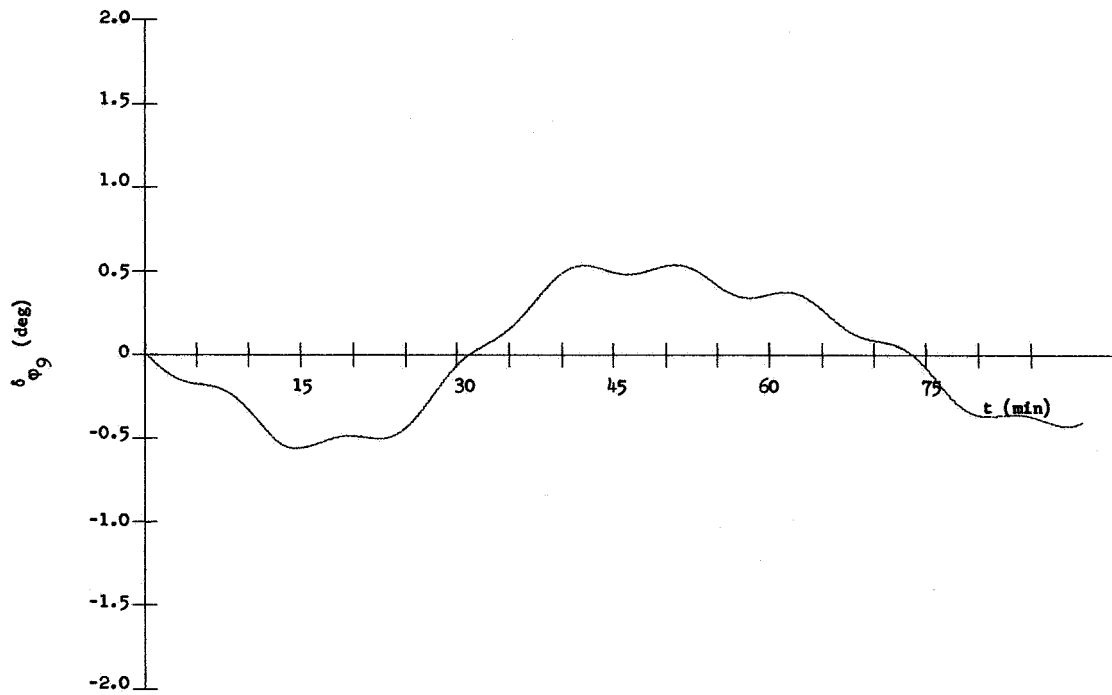
Figure 79. Plot II-G, m_7 Figure 80. Plot II-G, m_8

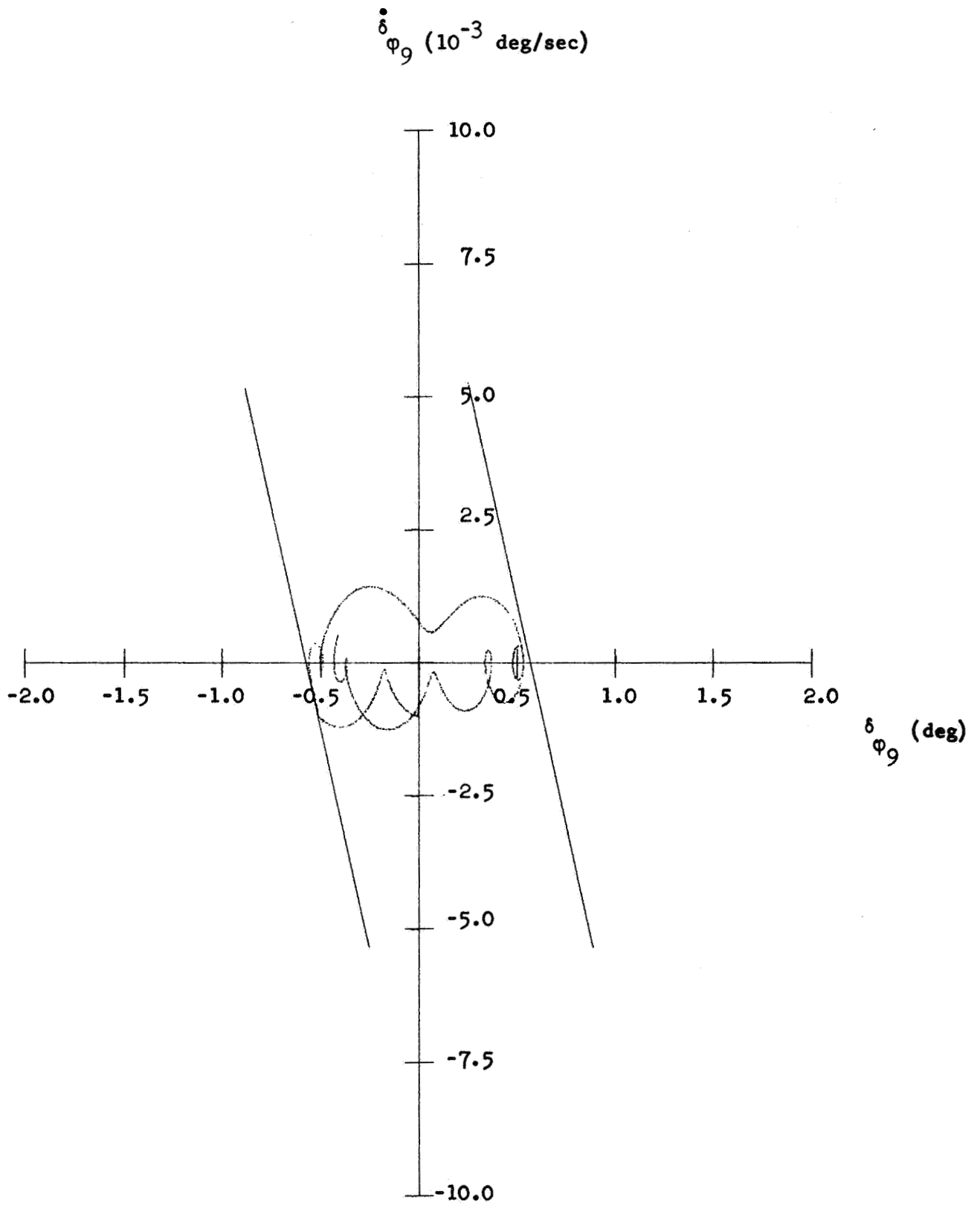
Figure 81. Plot II-G, m_9 Figure 82. Plot V-G, m_9

Figure 83. Plot VI-G, m_9 Figure 84. Plot II-G, m_{15}

Figure 85. Plot II-C, m_{16} Figure 86. Plot V-C, m_{16}

Figure 87. Plot VI-G, m_{16} Figure 88. Plot II-G, m_{10}

Figure 89. Plot II-G, m_{11} Figure 90. Plot III-G, m_9

Figure 91. Plot IV-G, m_9

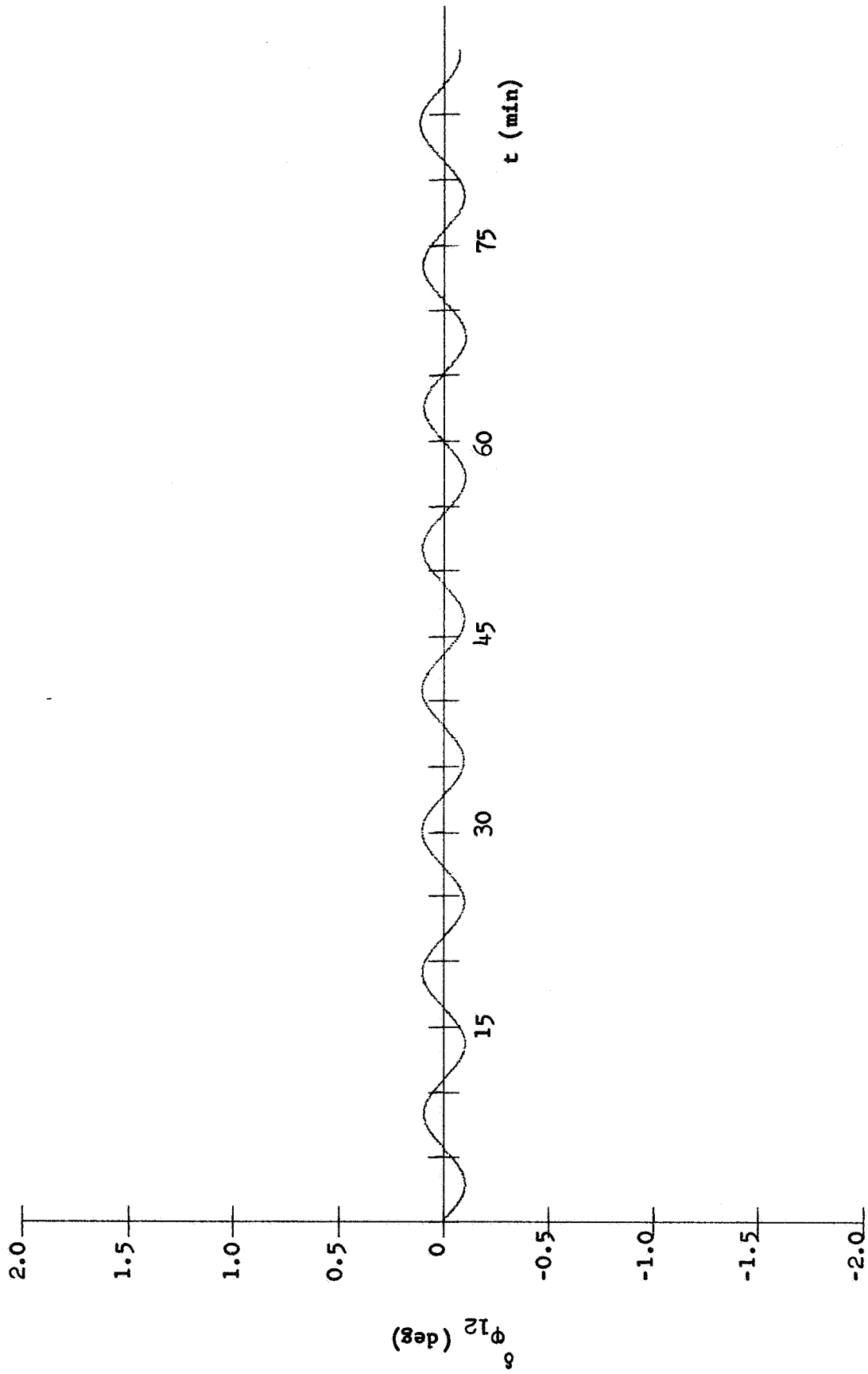
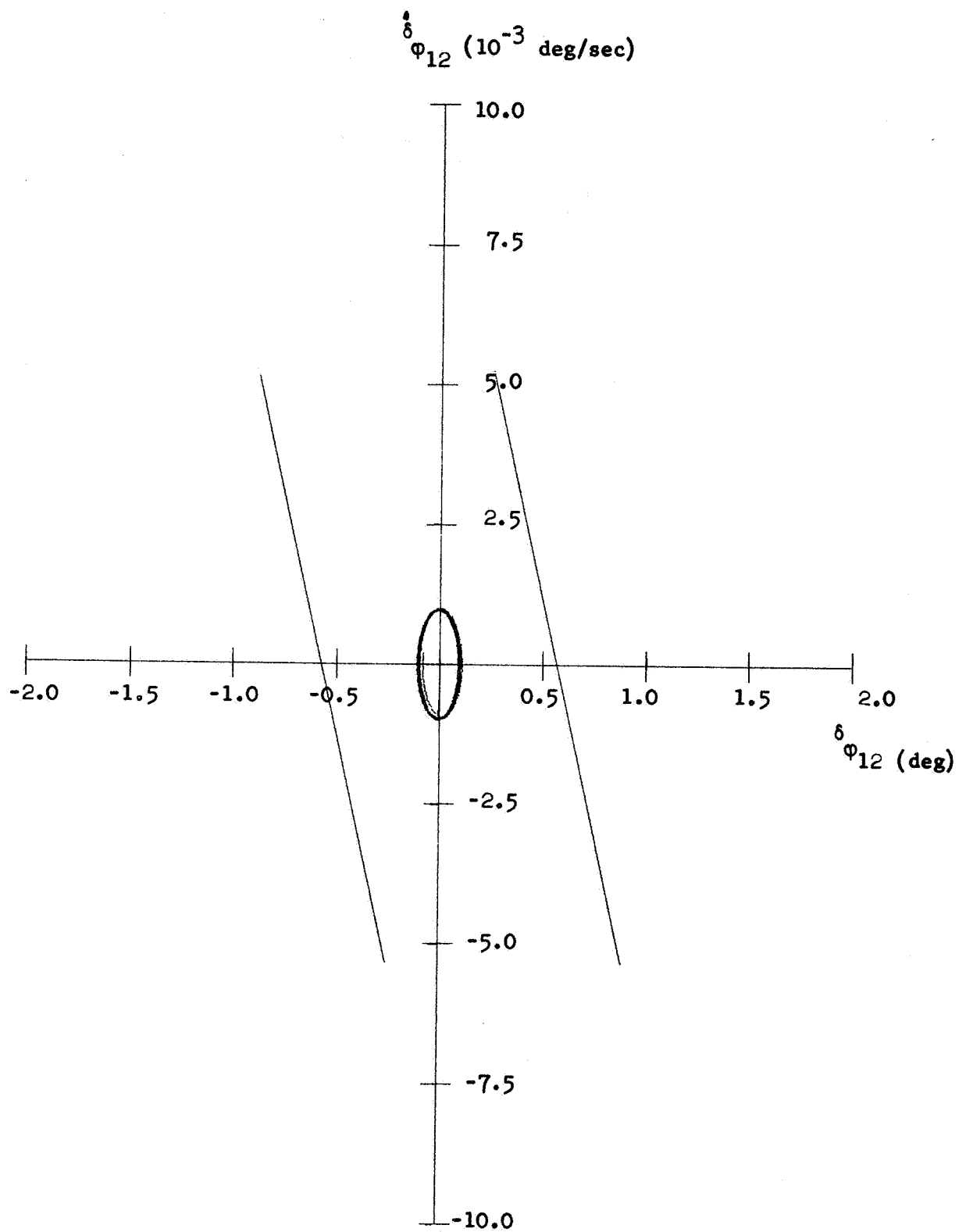


Figure 92. Plot III-G, m_{12}

Figure 93. Plot IV-G, m_{12}

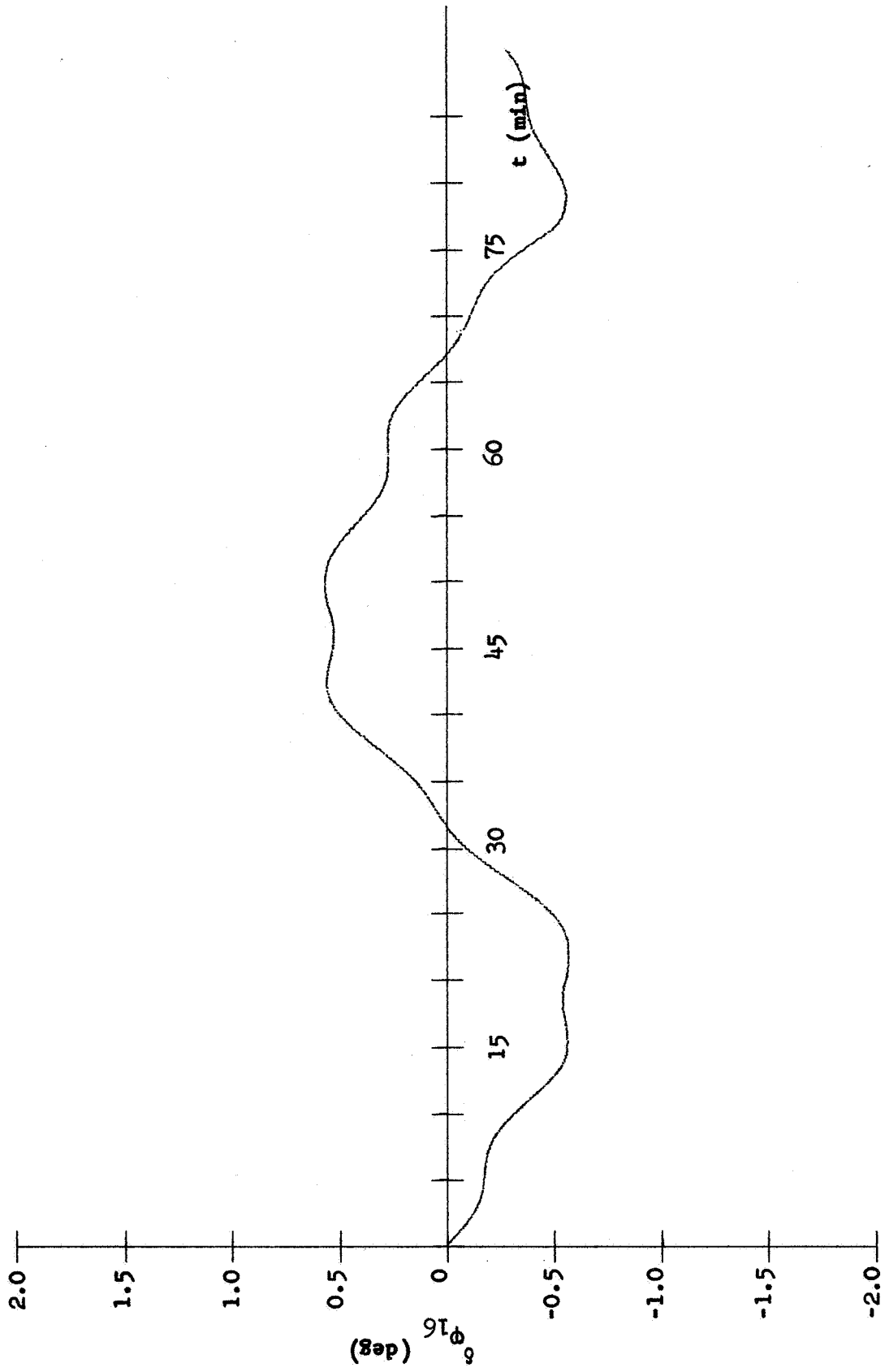
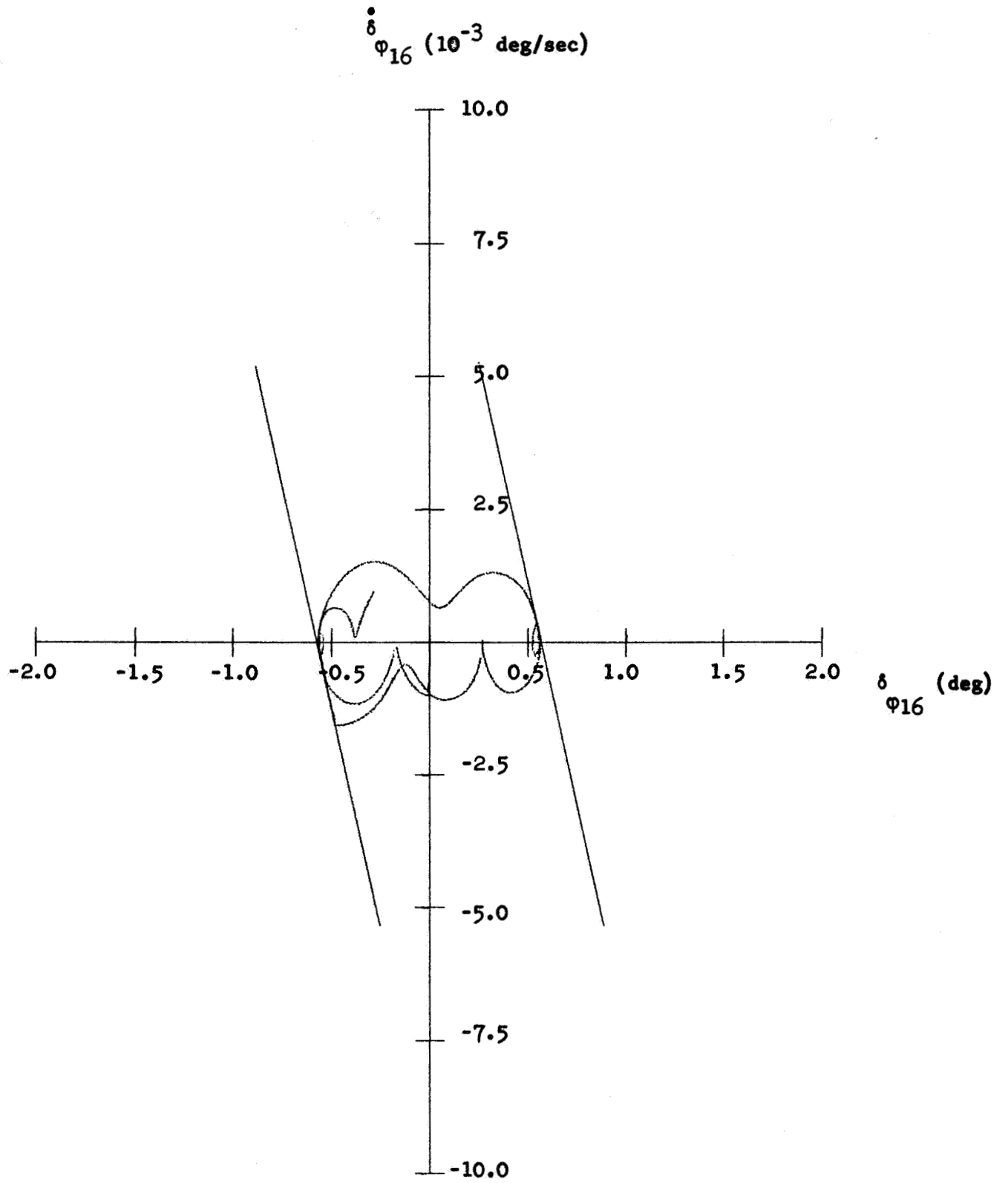
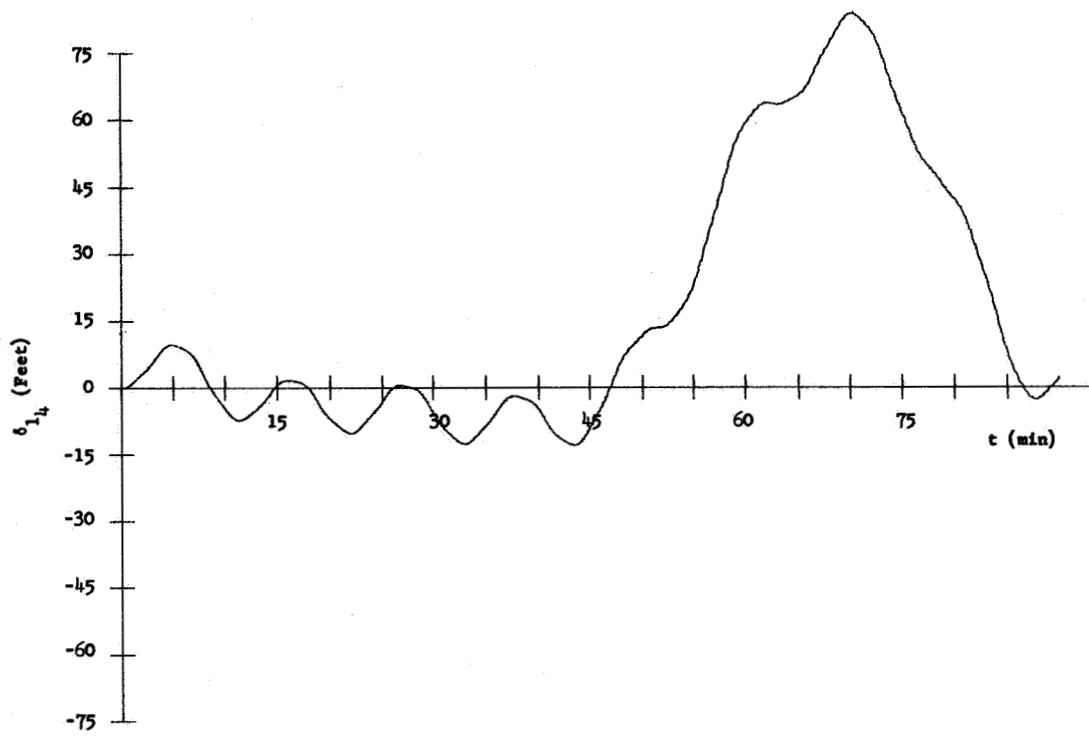
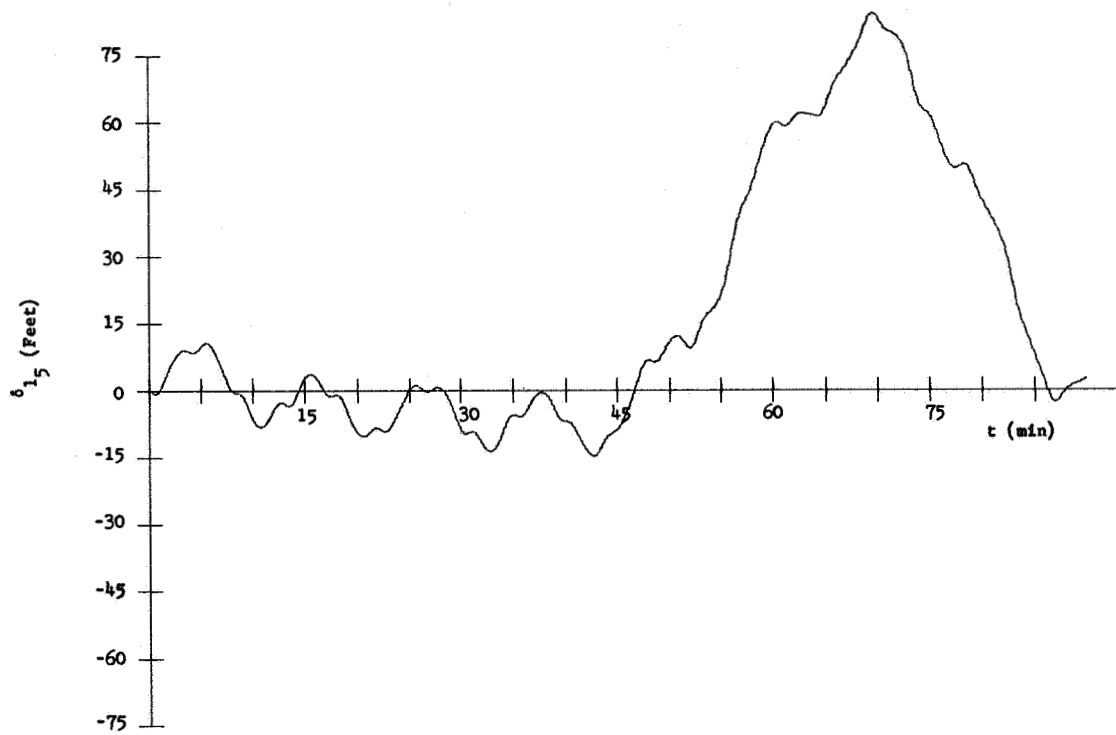
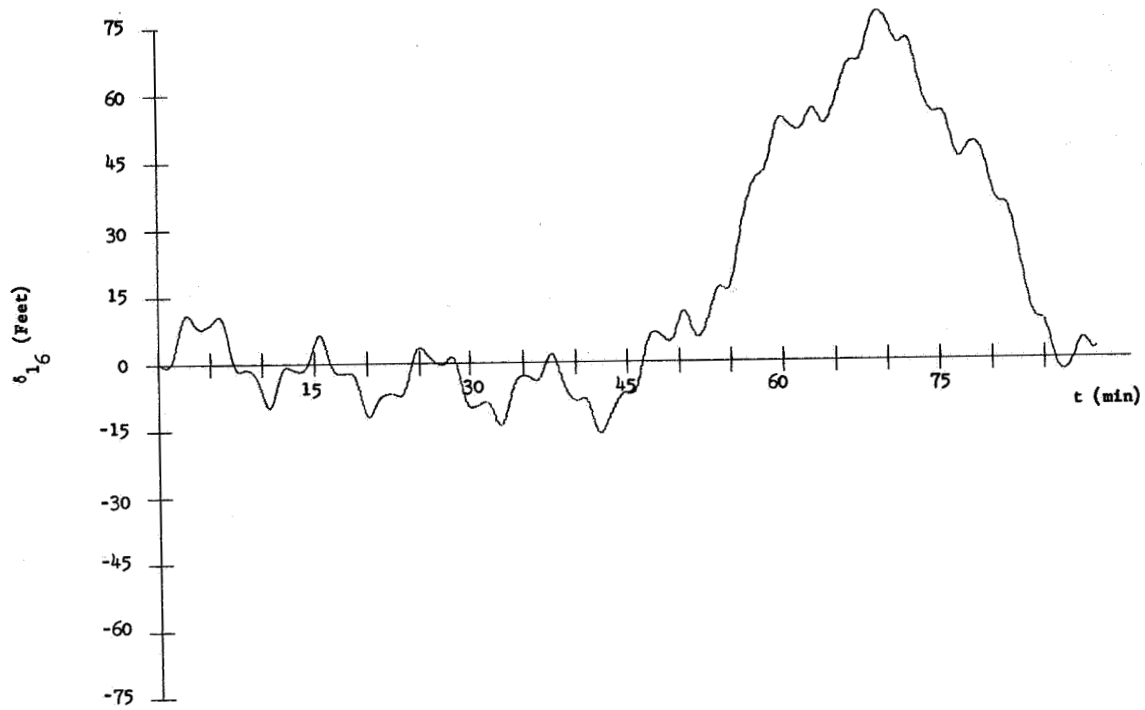
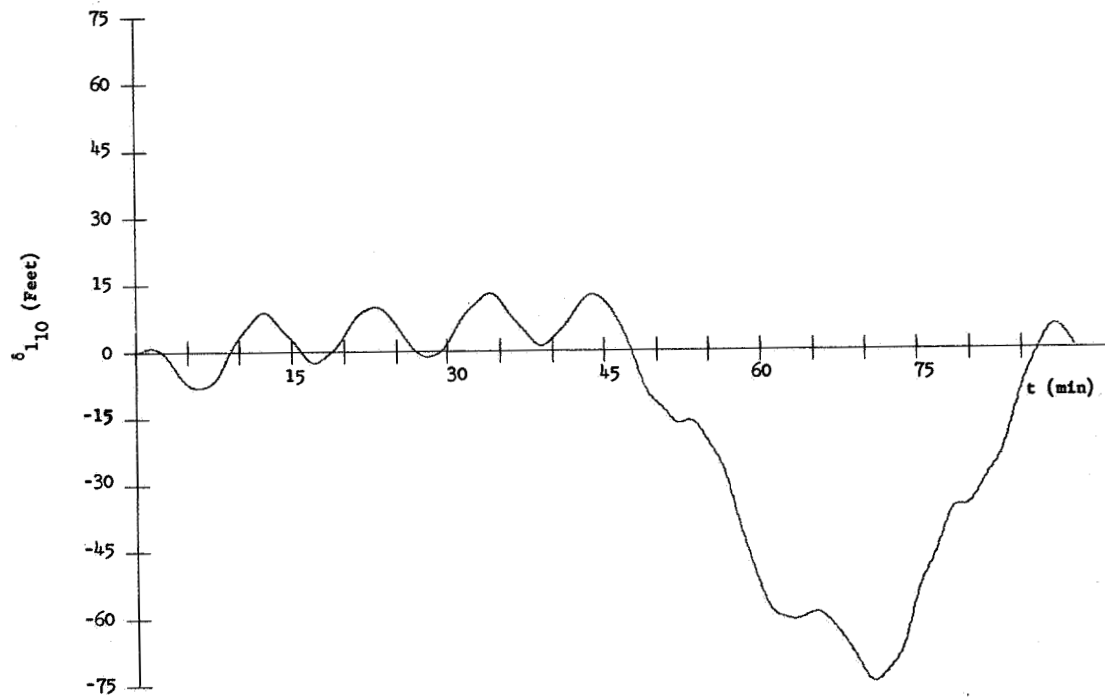
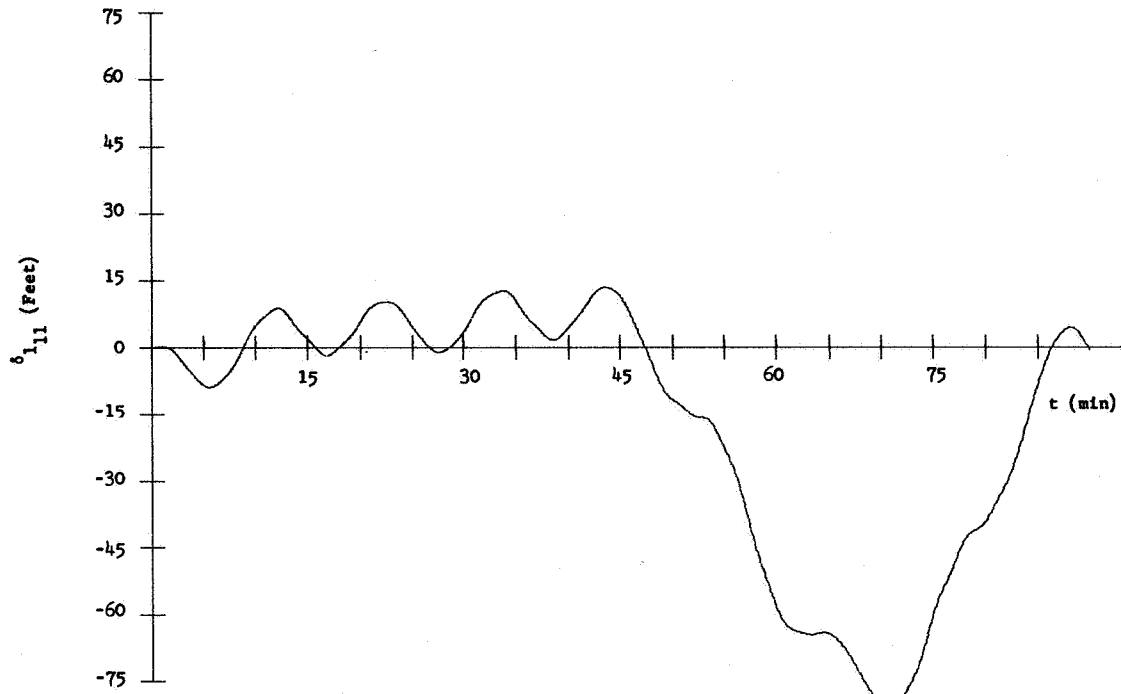
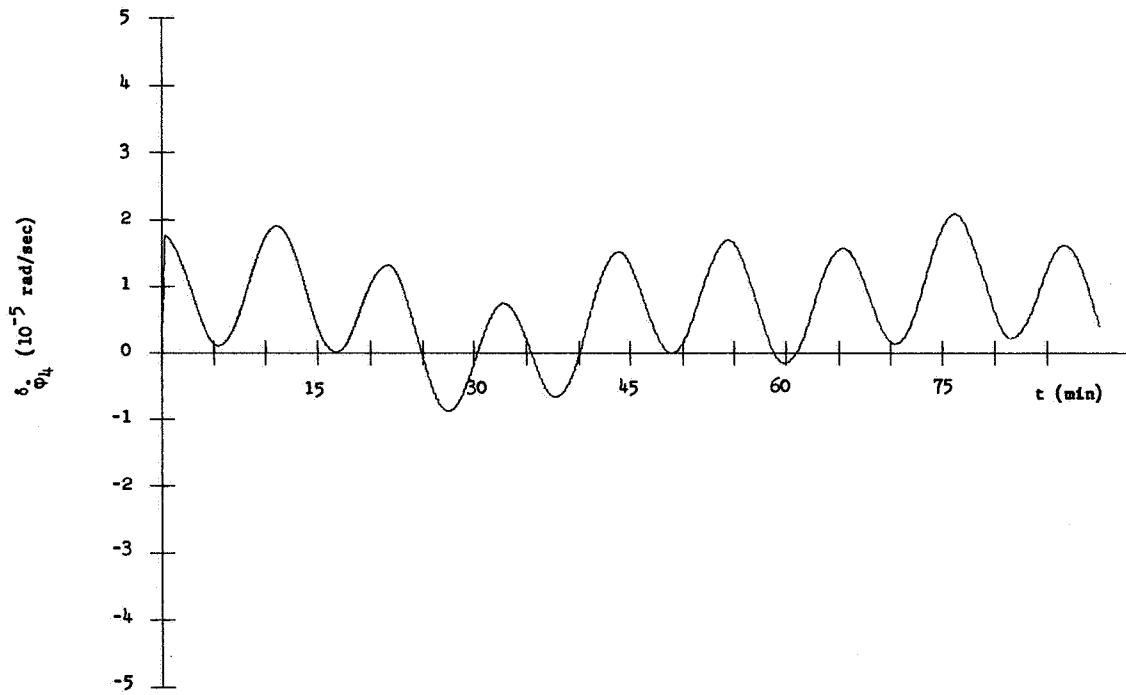


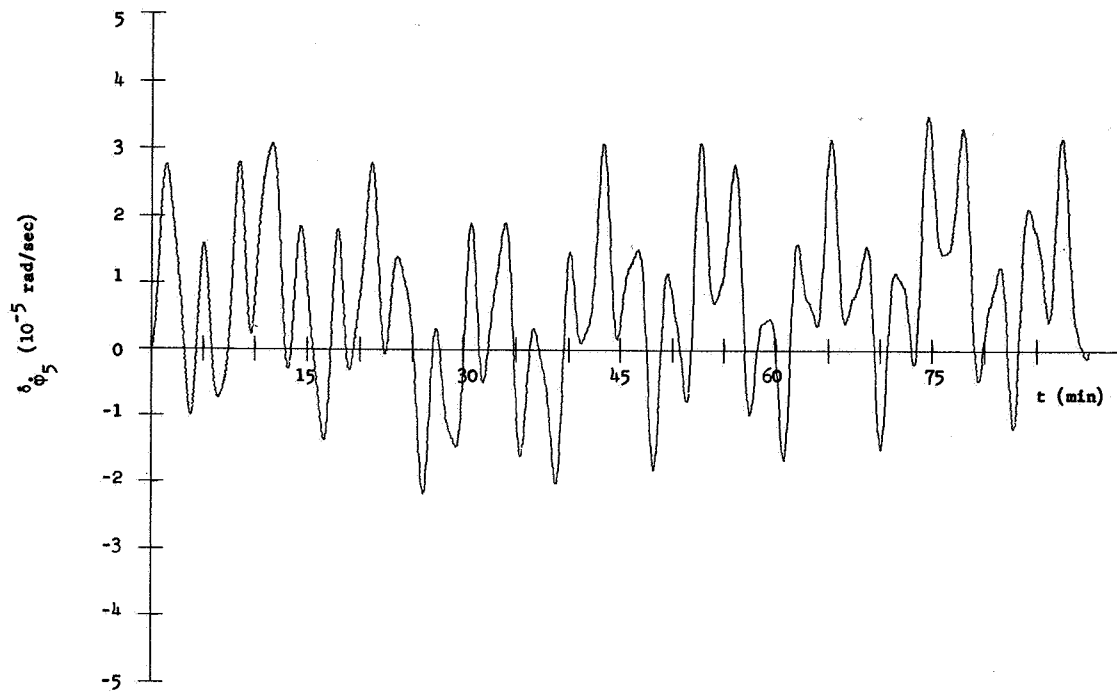
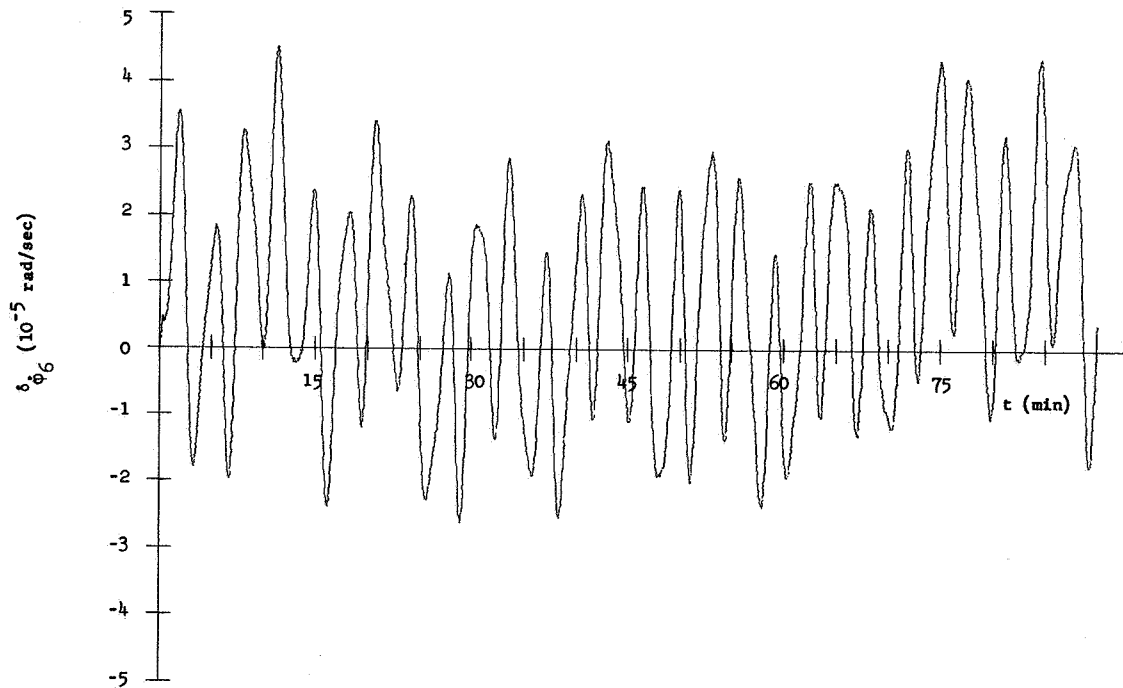
Figure 94. Plot III-G, m_{16}

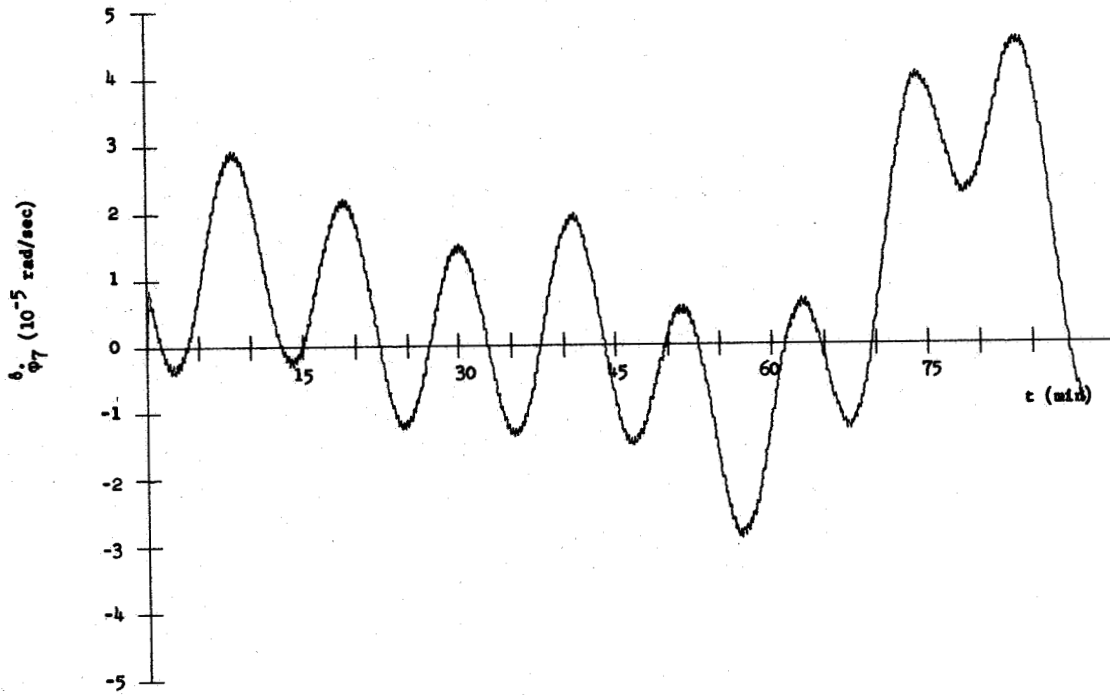
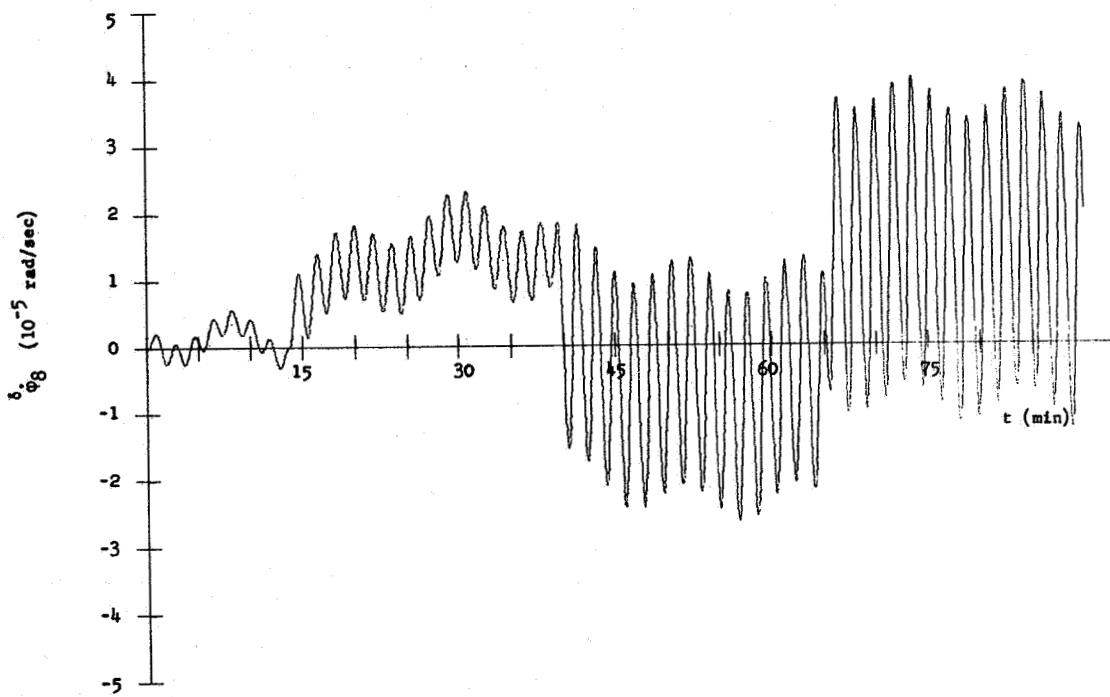
Figure 95. Plot IV-G, m_{16}

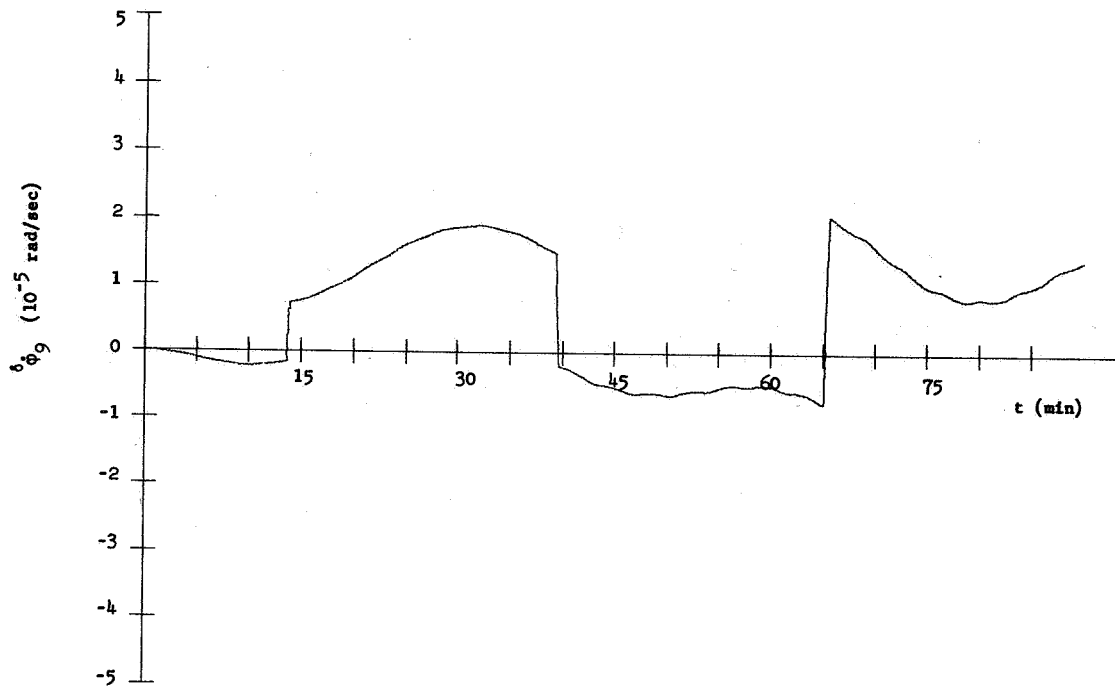
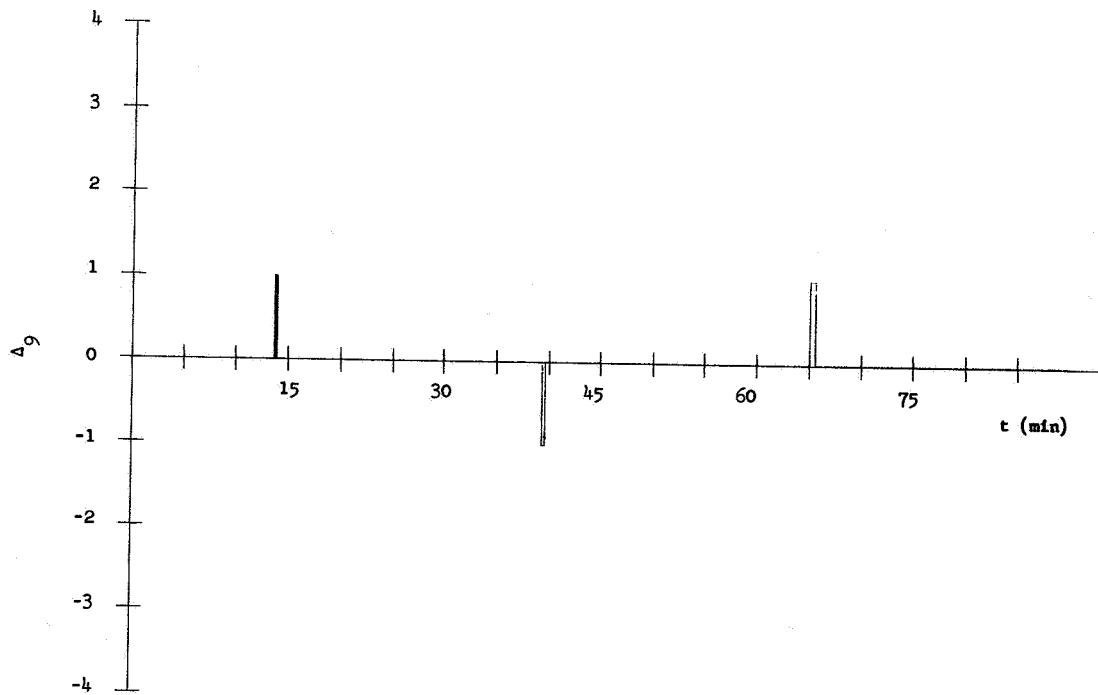
Figure 96. Plot I-H, m_4 Figure 97. Plot I-H, m_5

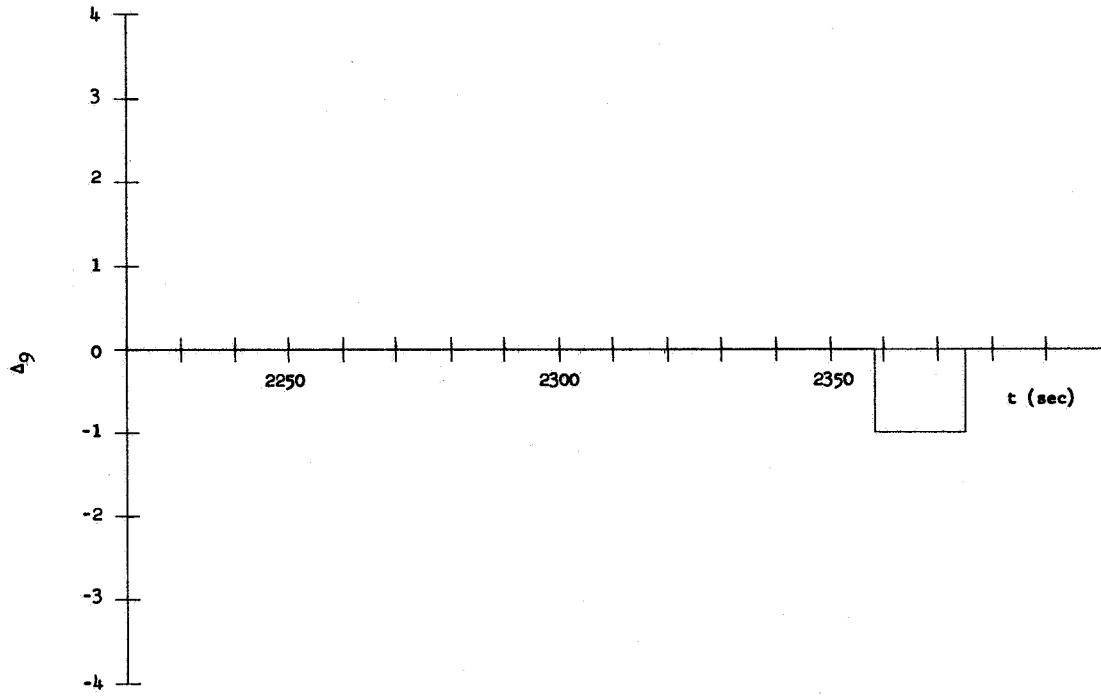
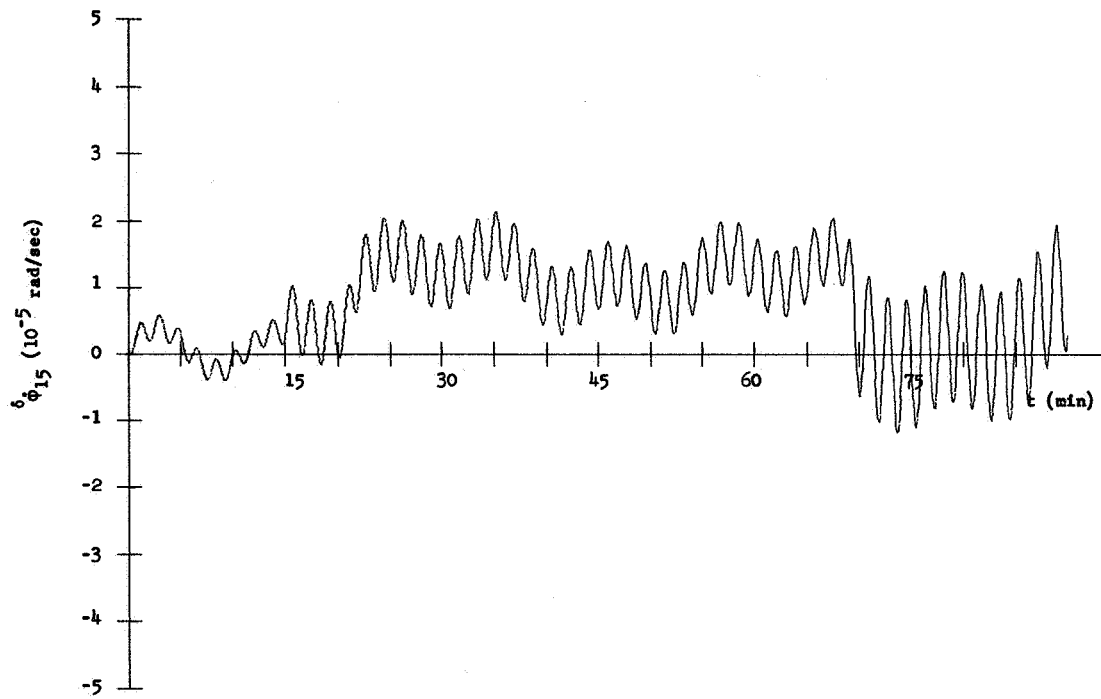
Figure 98. Plot I-H, m_6 .Figure 99. Plot I-H, m_{10} .

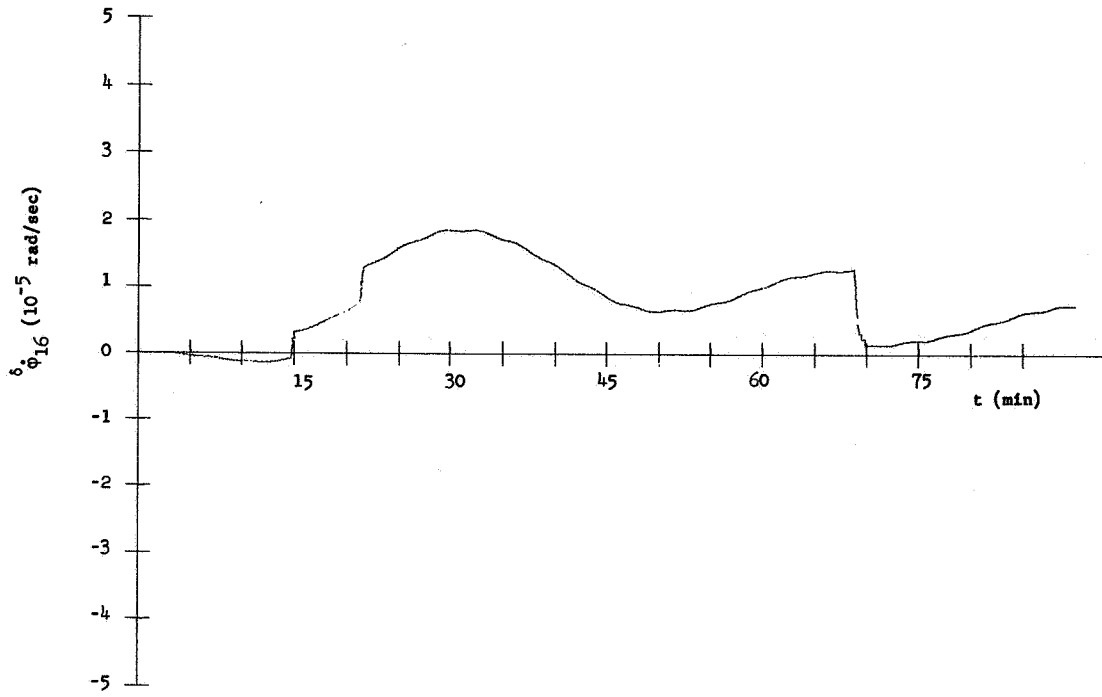
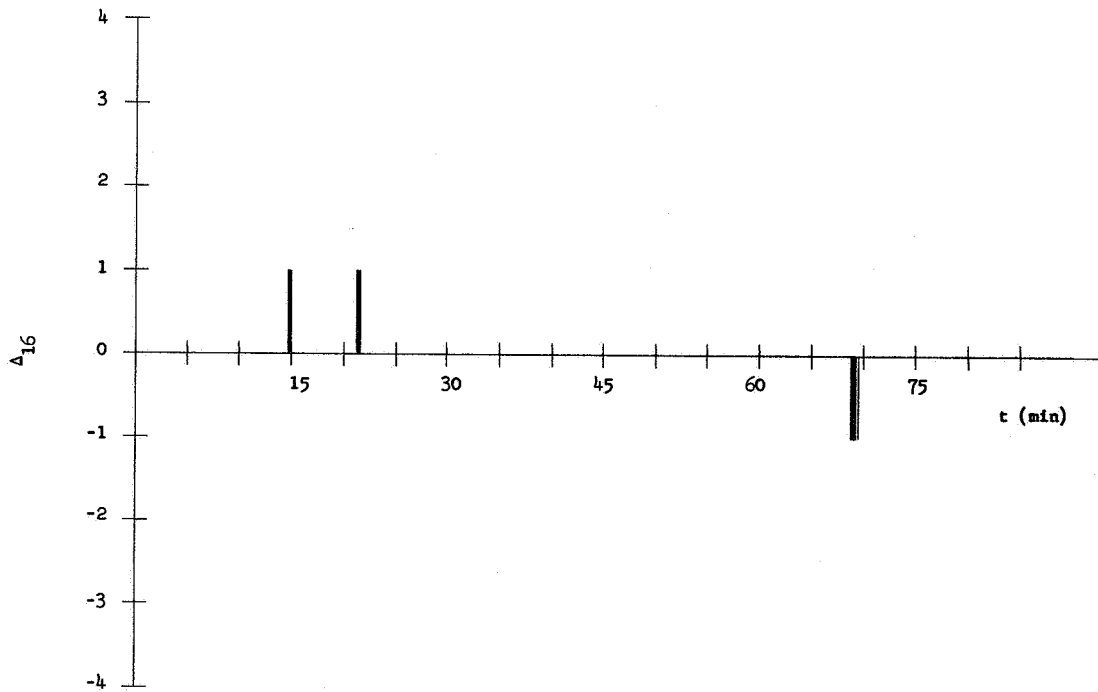
Figure 100. Plot I-H, m_{11} Figure 101. Plot II-H, m_4

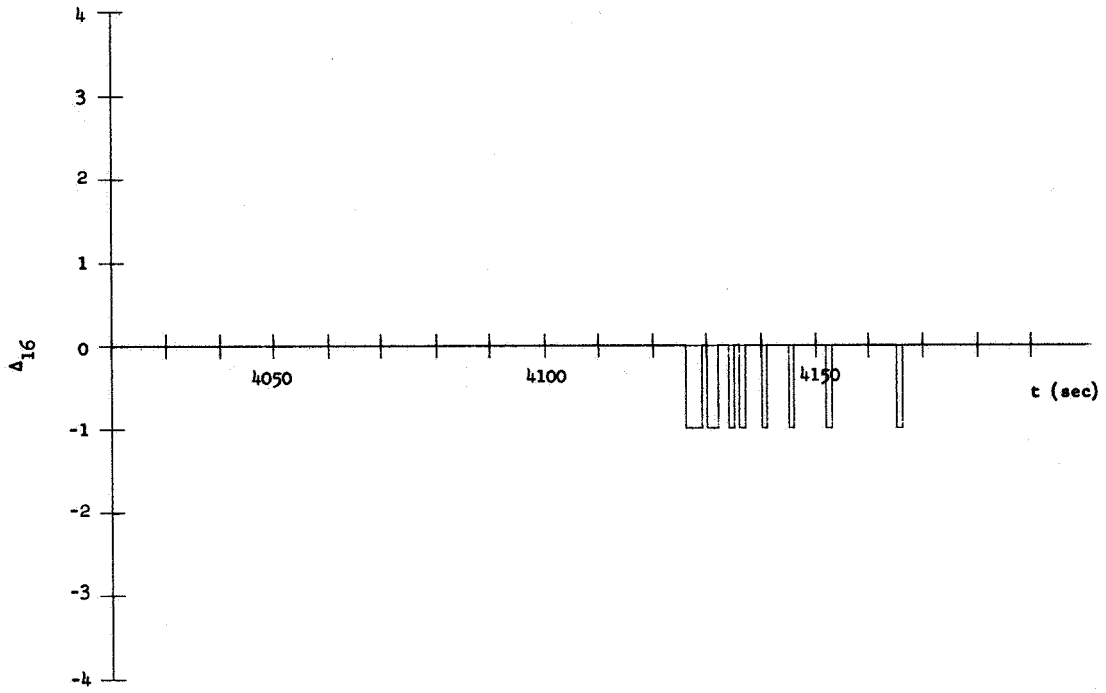
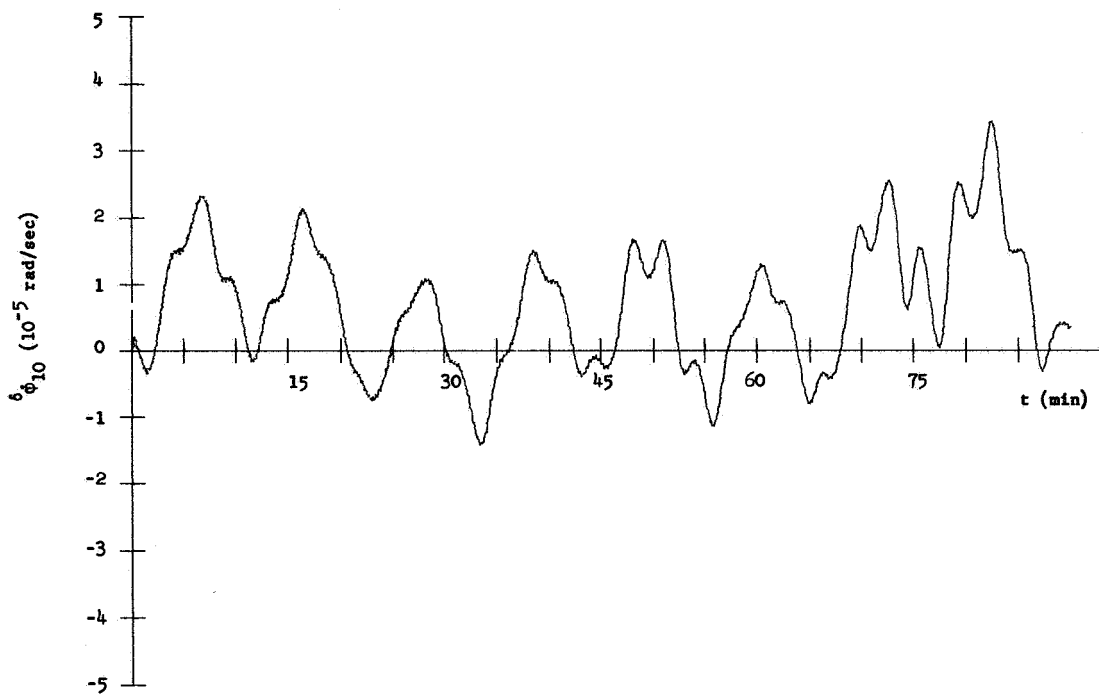
Figure 102. Plot II-H, m_5 Figure 103. Plot II-H, m_6

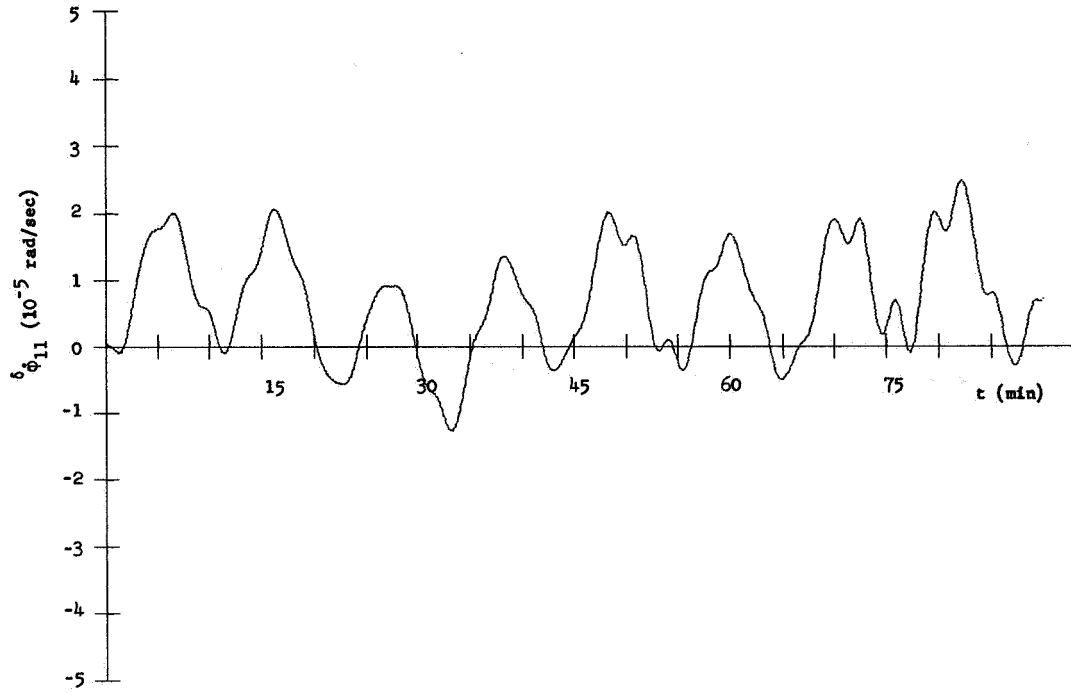
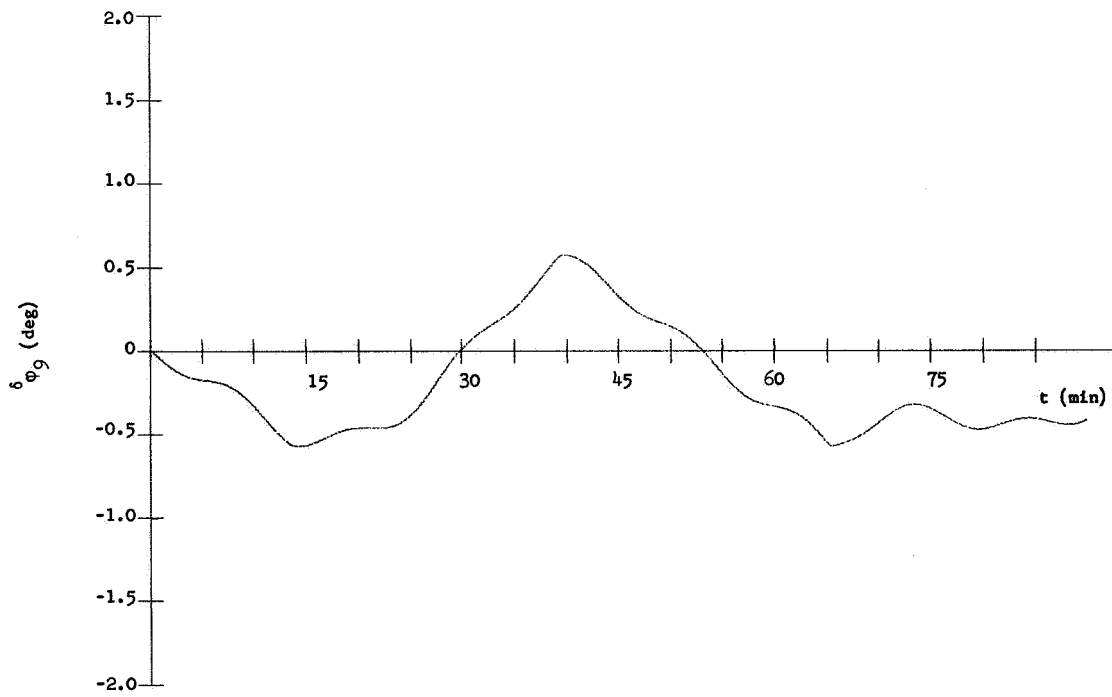
Figure 104. Plot II-H, u_7 Figure 105. Plot II-H, u_8

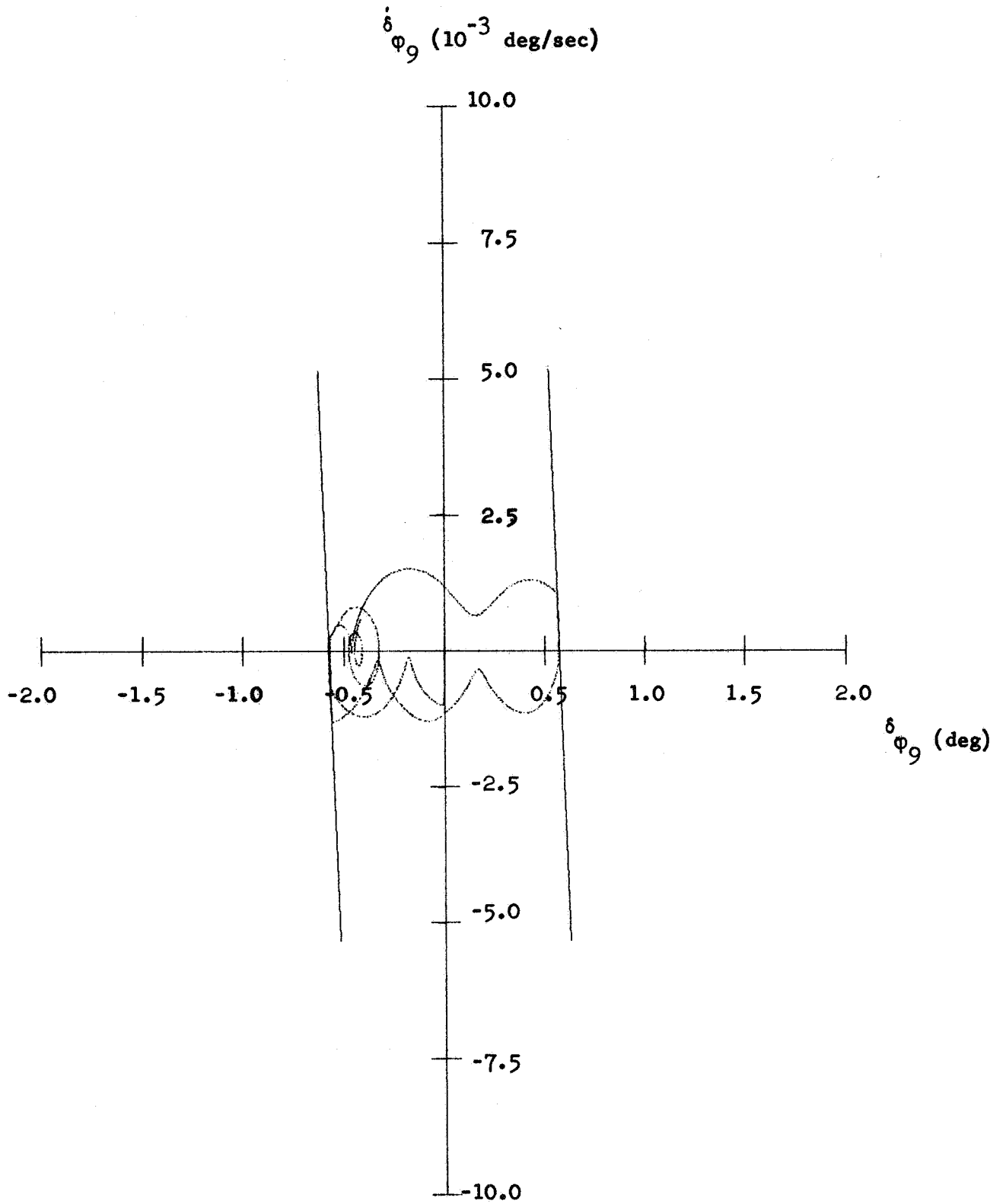
Figure 106. Plot II-H, m_9 Figure 107. Plot V-H, m_9

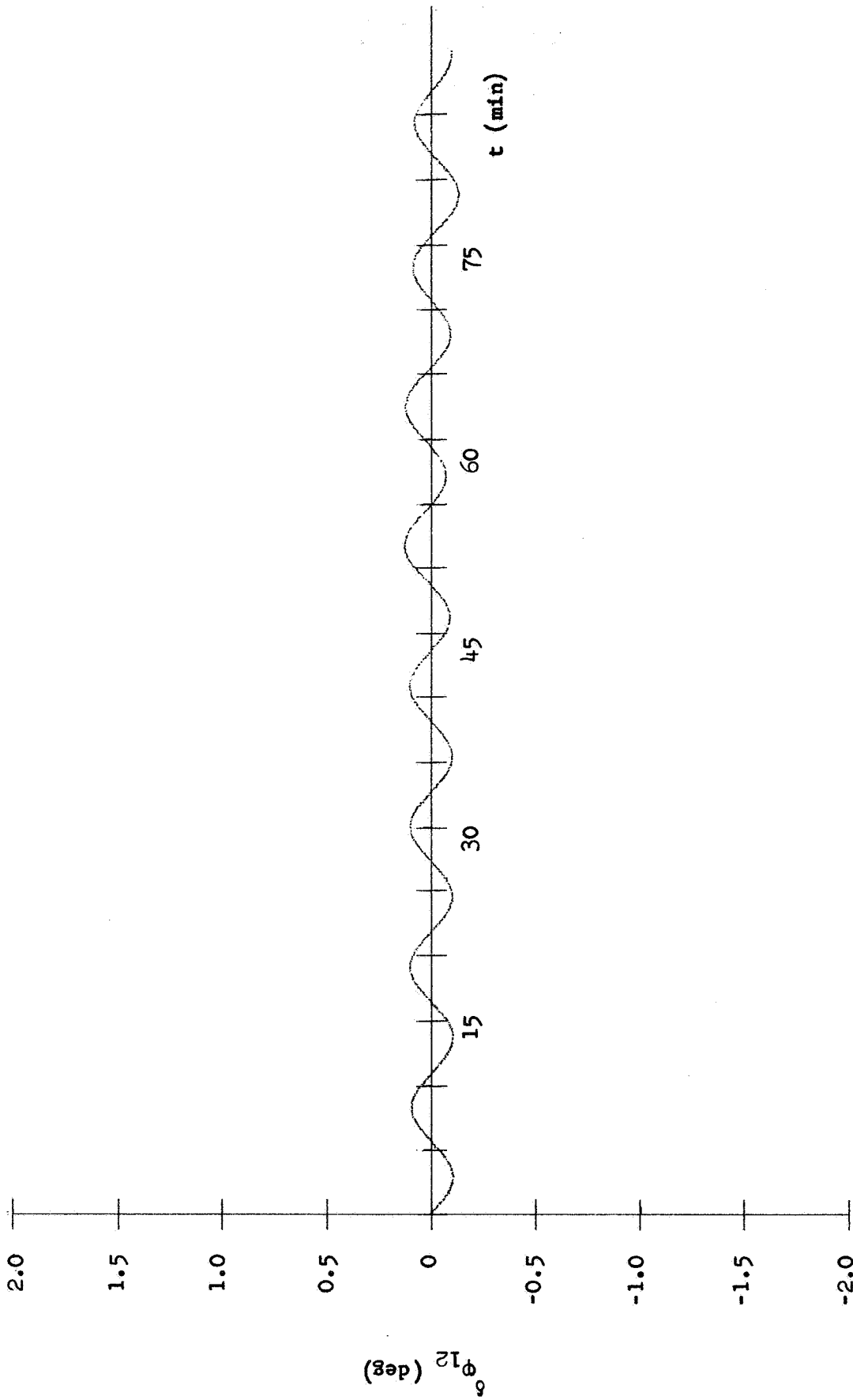
Figure 108. Plot VI-H, m_9 Figure 109. Plot II-H, m_{15}

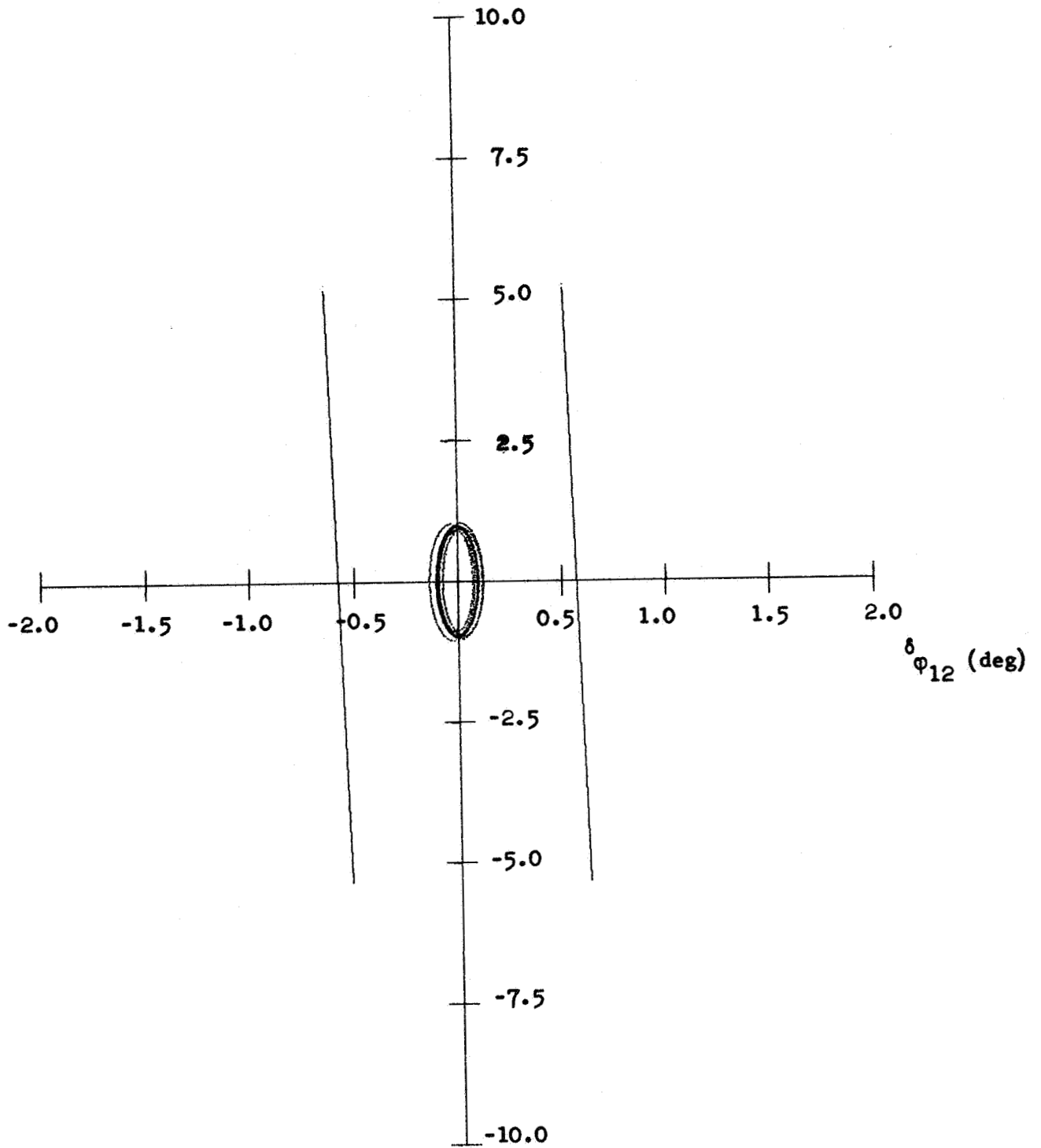
Figure 110. Plot II-H, m_{16} Figure 111. Plot V-H, m_{16}

Figure 112. Plot VI-H, m_{16} Figure 113. Plot II-H, m_{10}

Figure 114. Plot II-H, m_{11} Figure 115. Plot III-H, m_9

Figure 116. Plot IV-H, m_9

Figure 117. Plot III-H, m_{12}

$\dot{\delta}_{\phi_{12}}$ (10^{-3} deg/sec)Figure 118. Plot IV-H, m_{12}

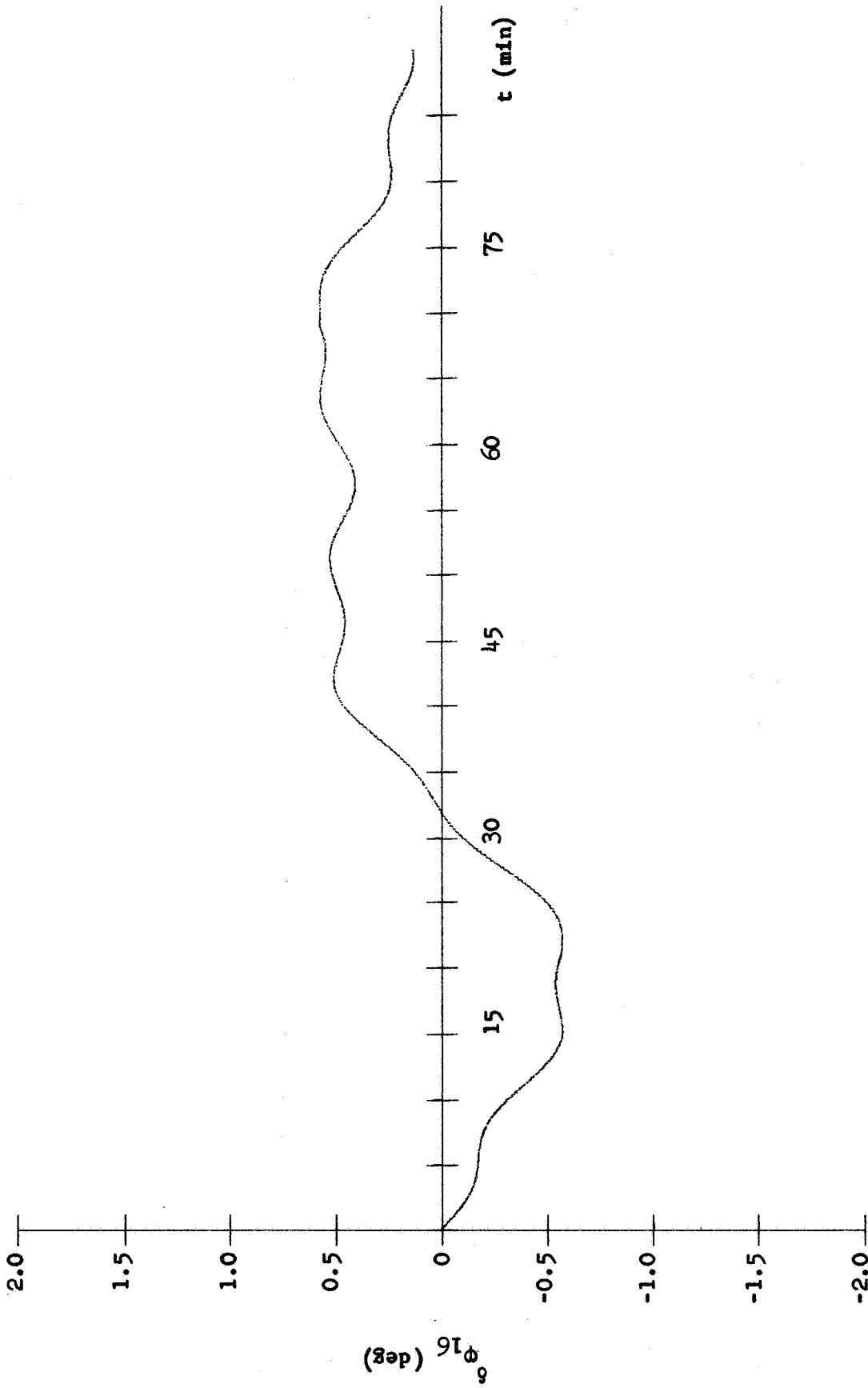
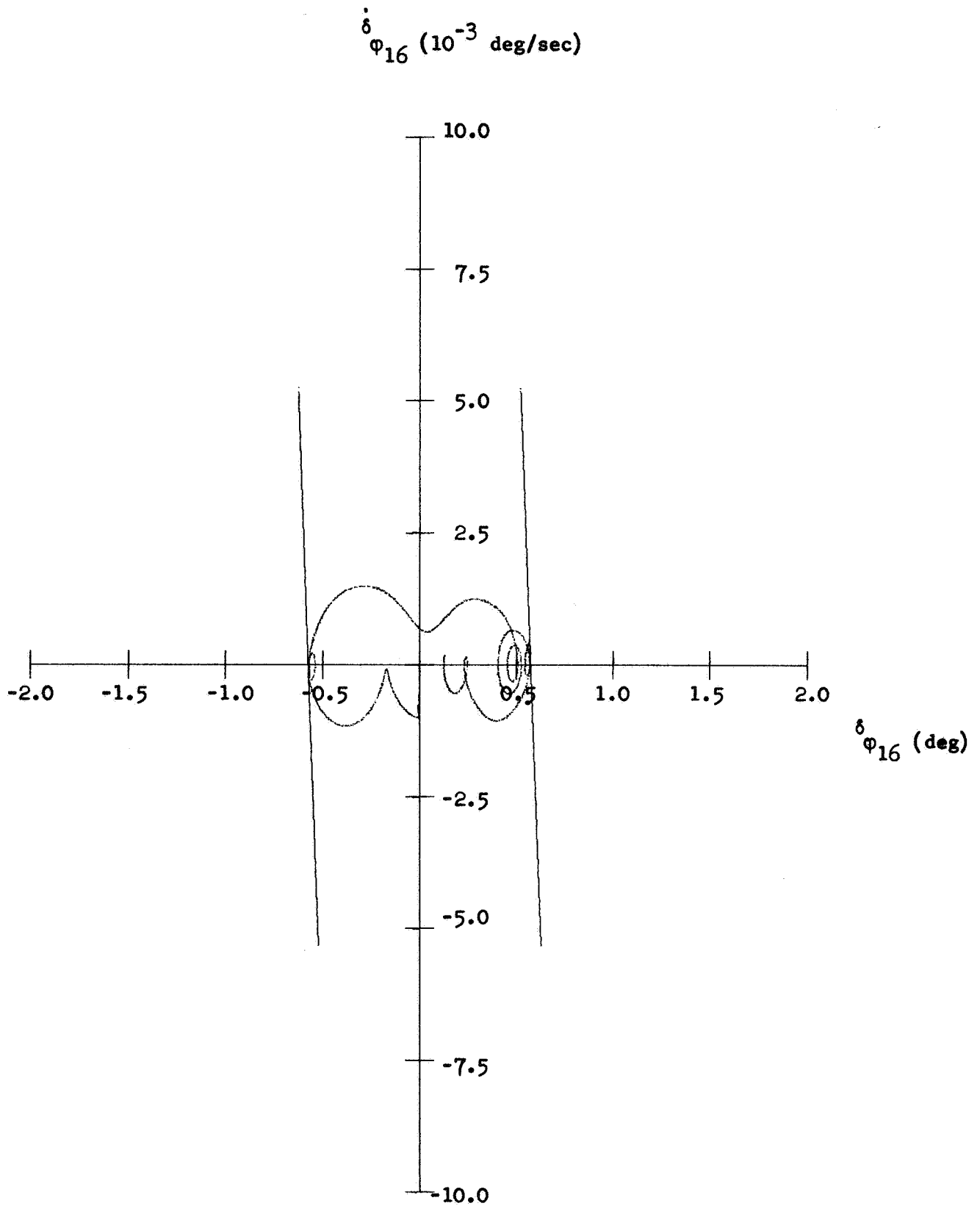
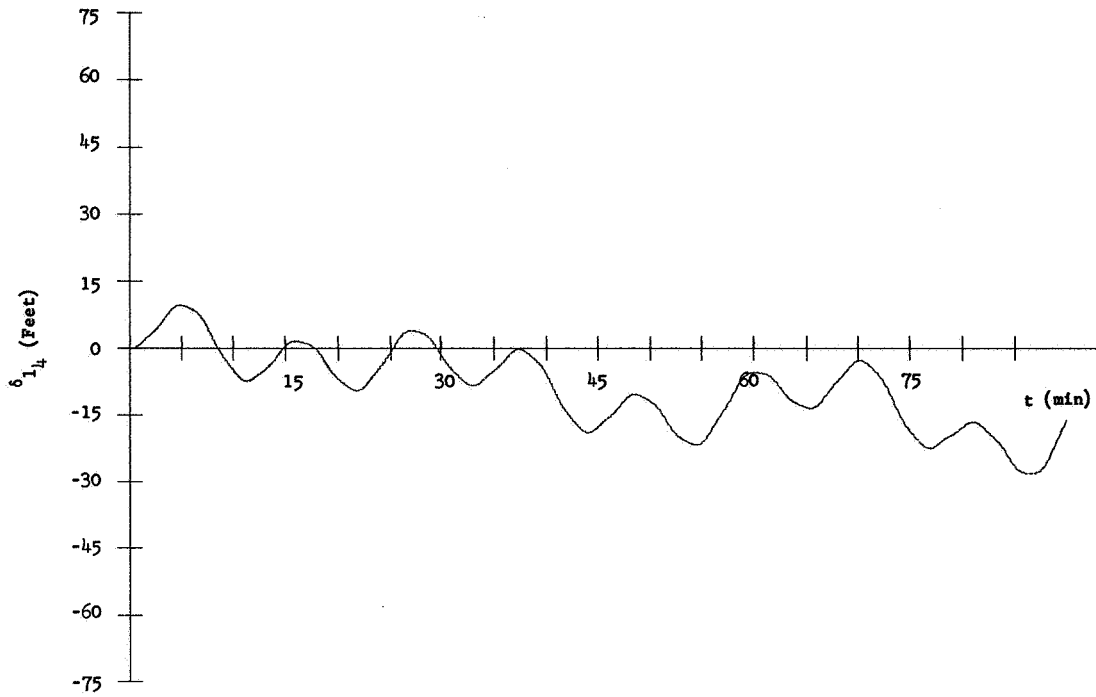
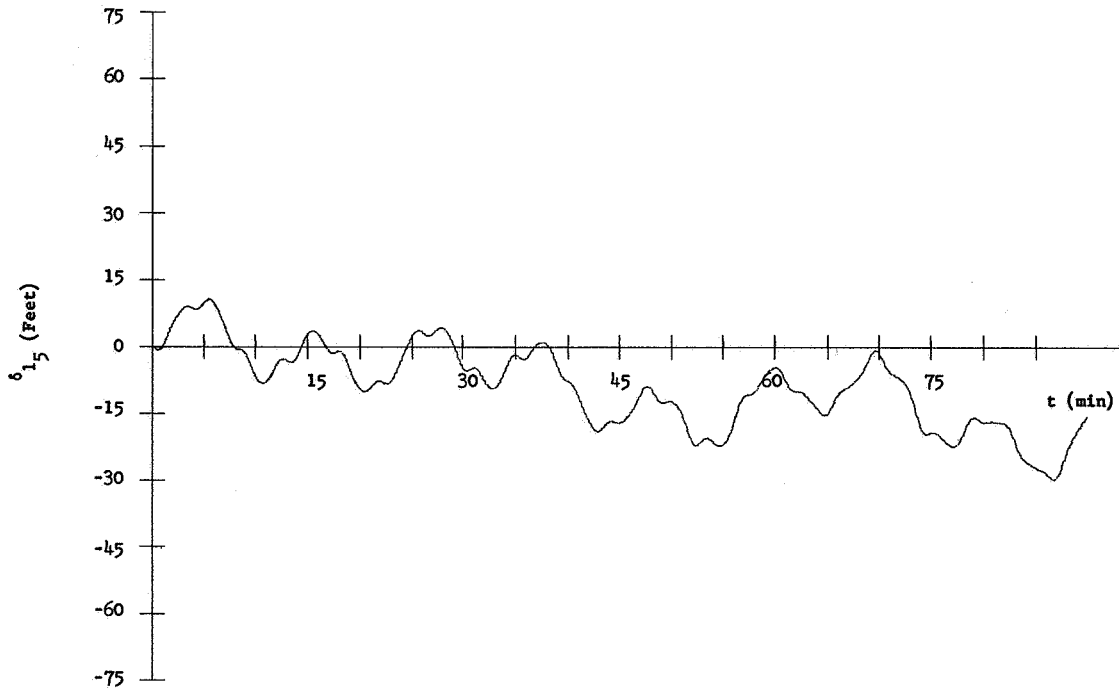


Figure 119. Plot III-H, m_{16}

Figure 120. Plot IV-H, m_{16}

Figure 121. Plot I-J, m_4 Figure 122. Plot I-J, m_5

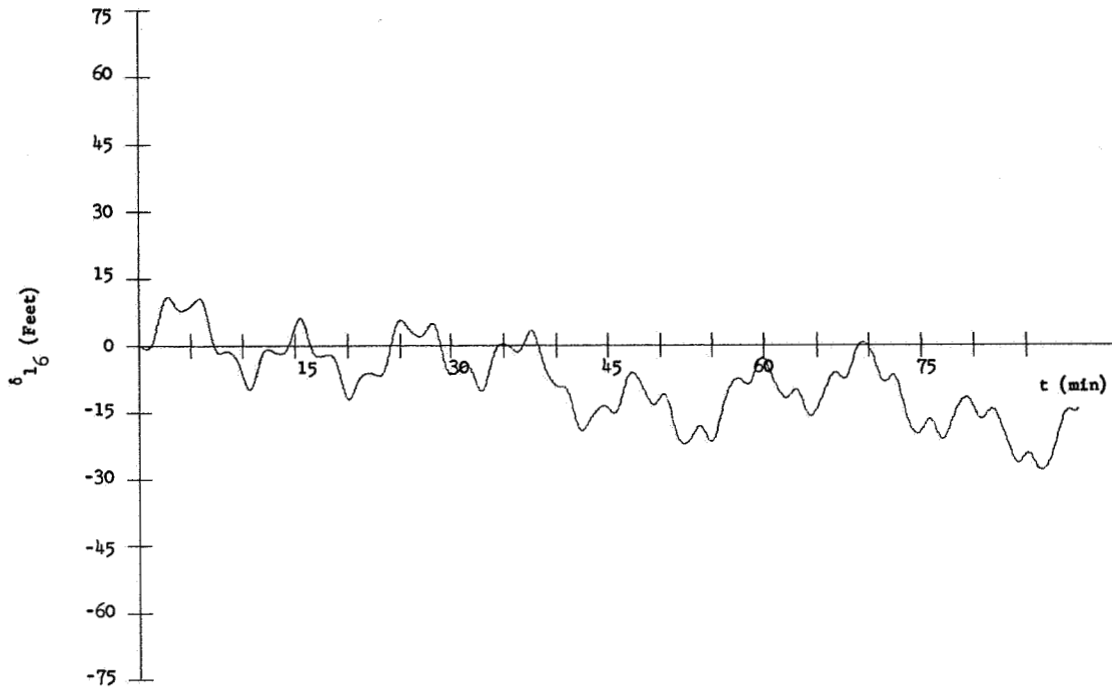


Figure 123. Plot I-J, m_6

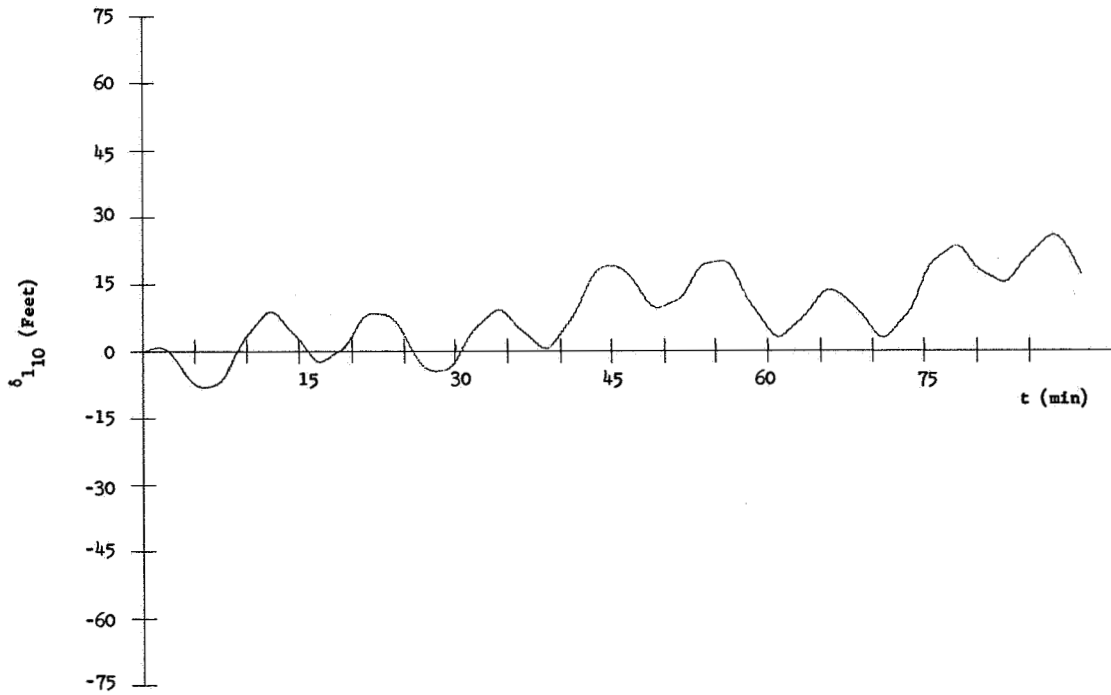
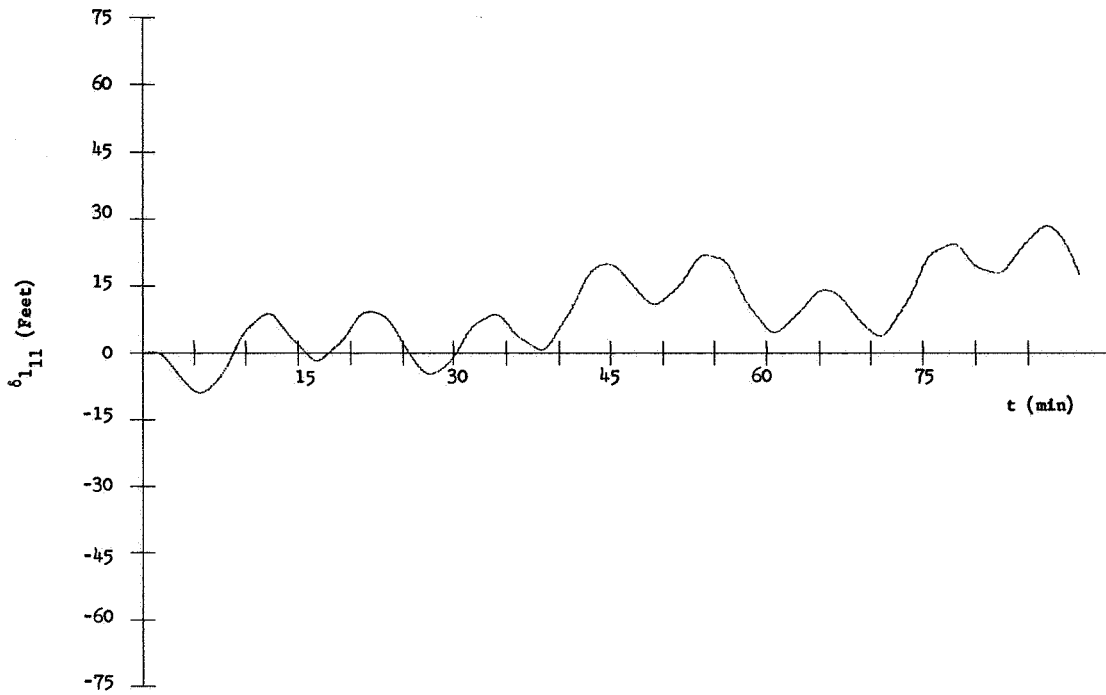
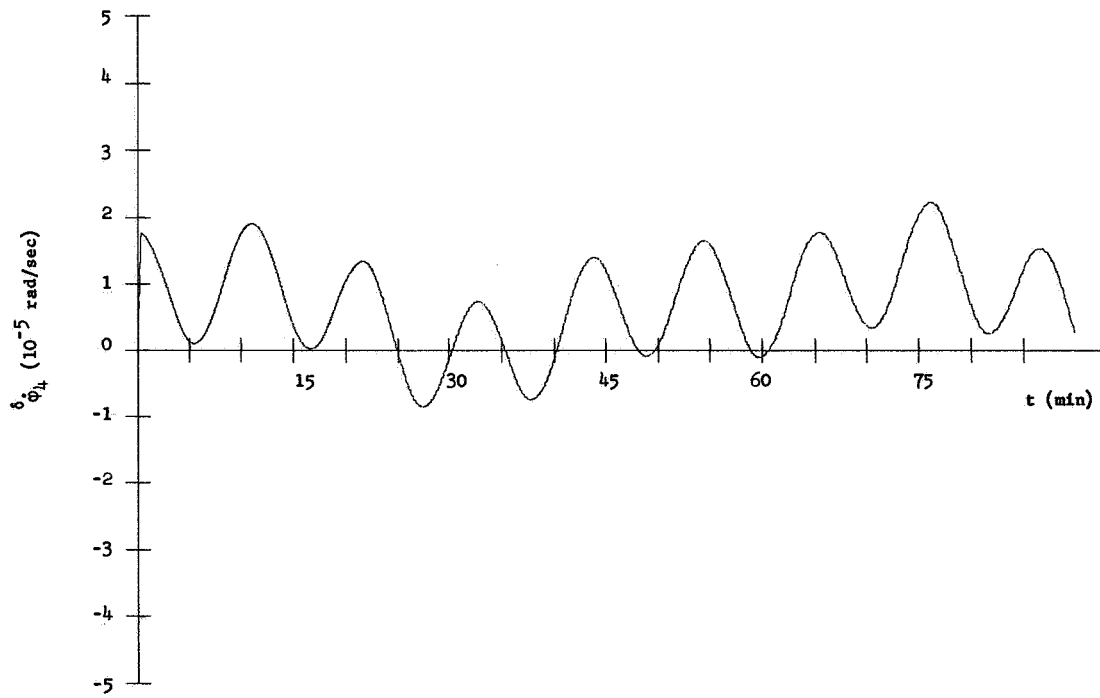
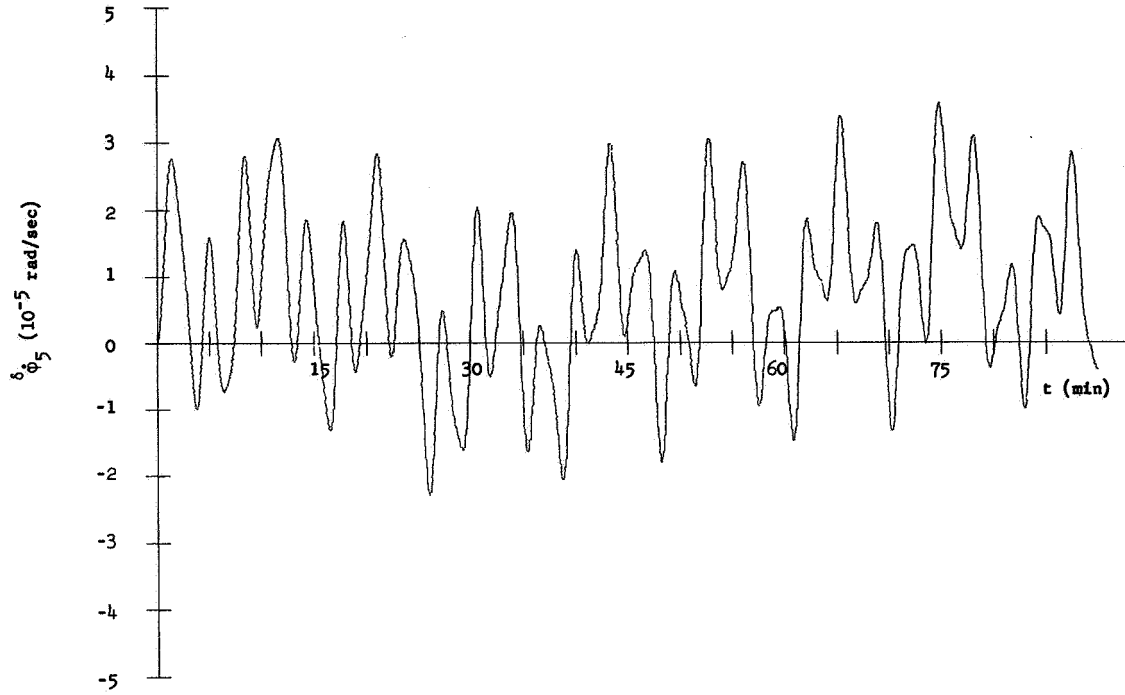
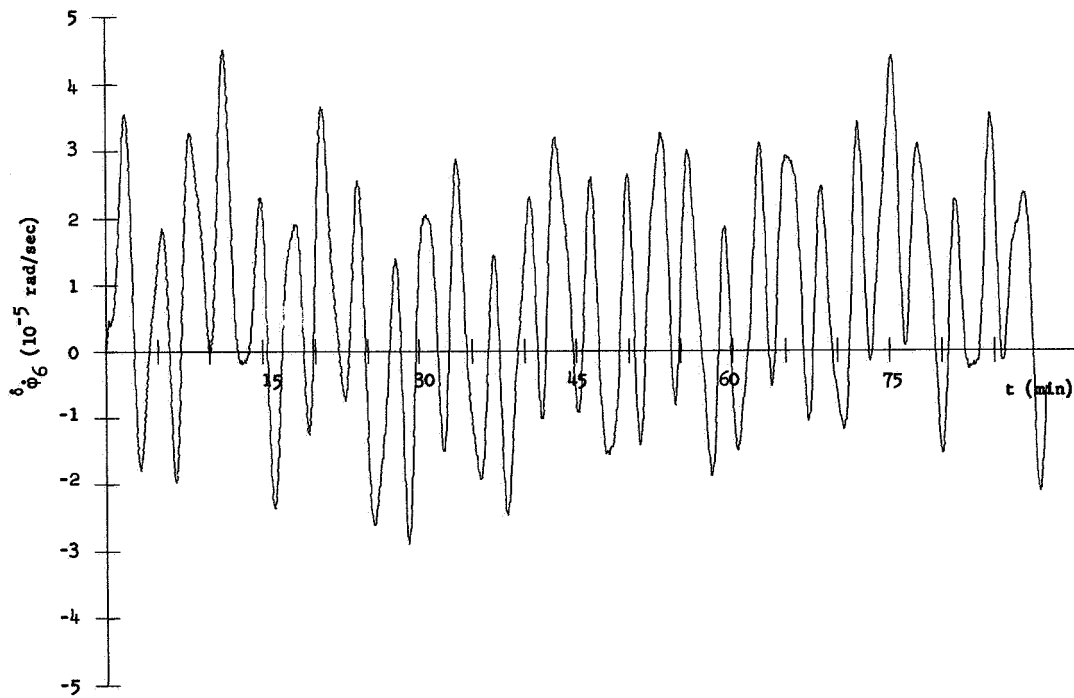
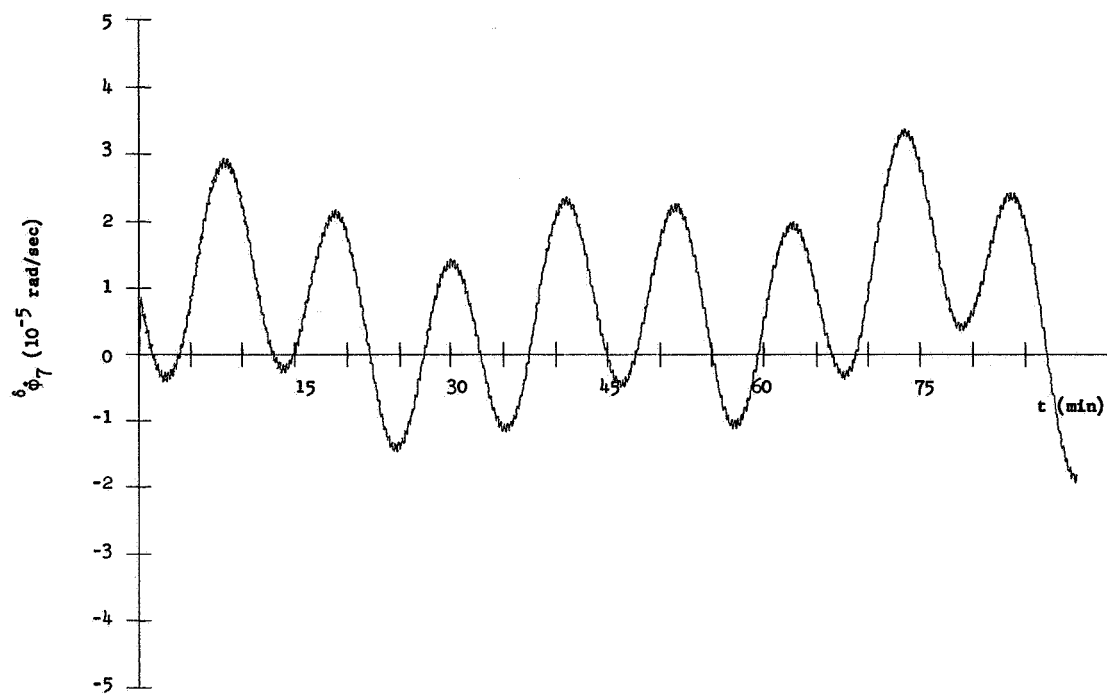
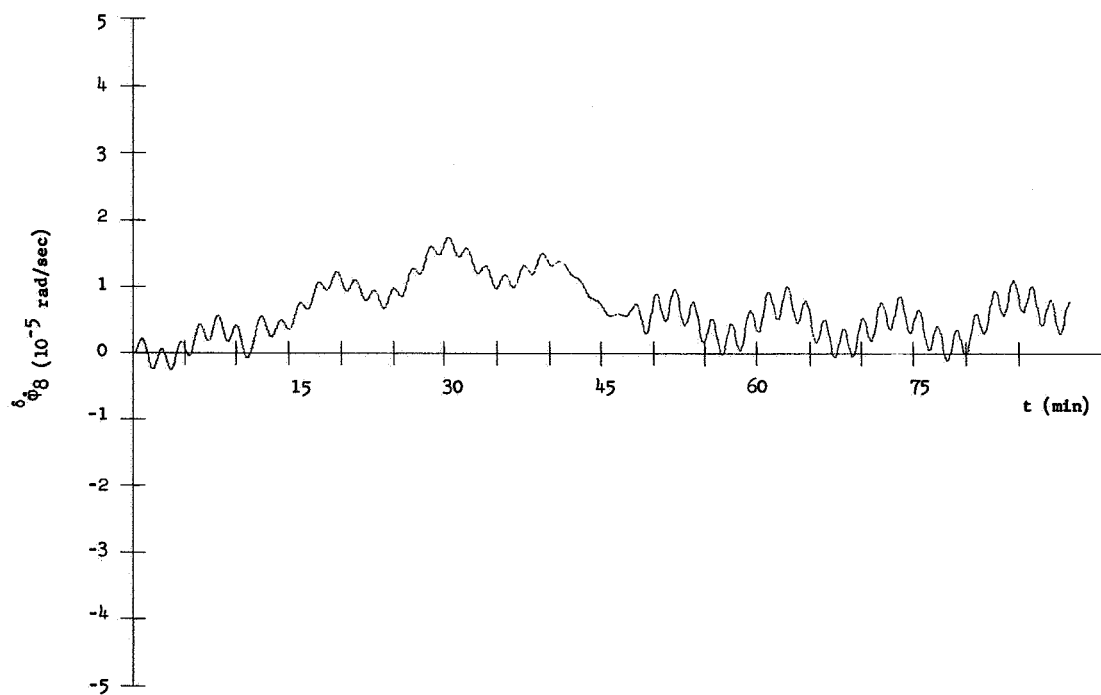
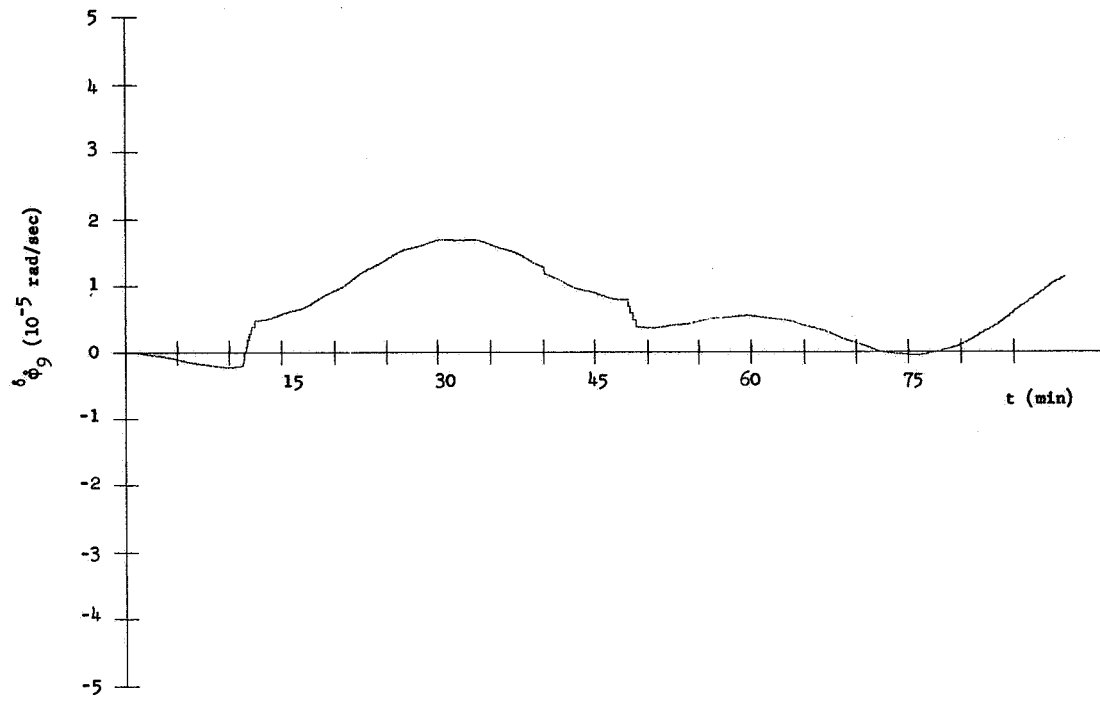
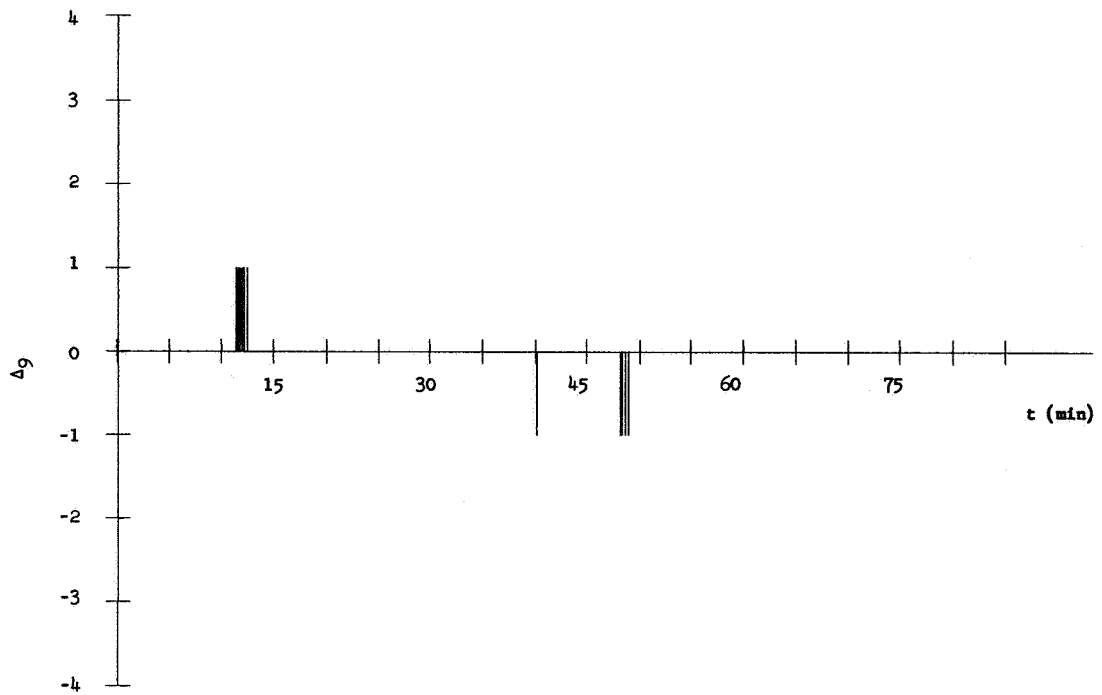


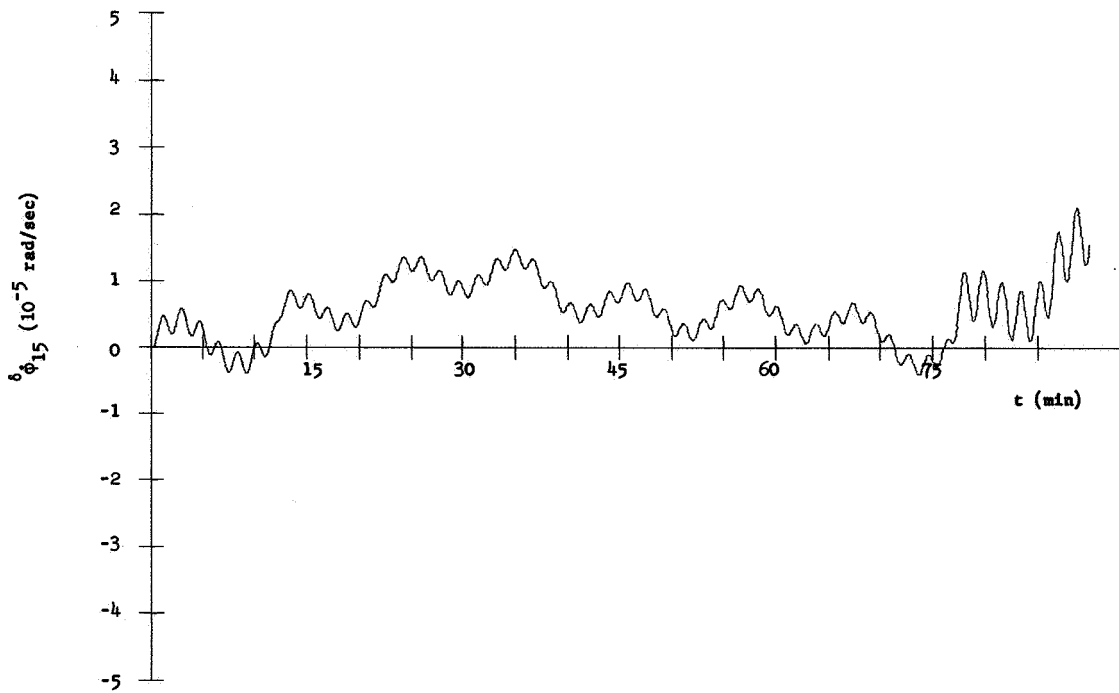
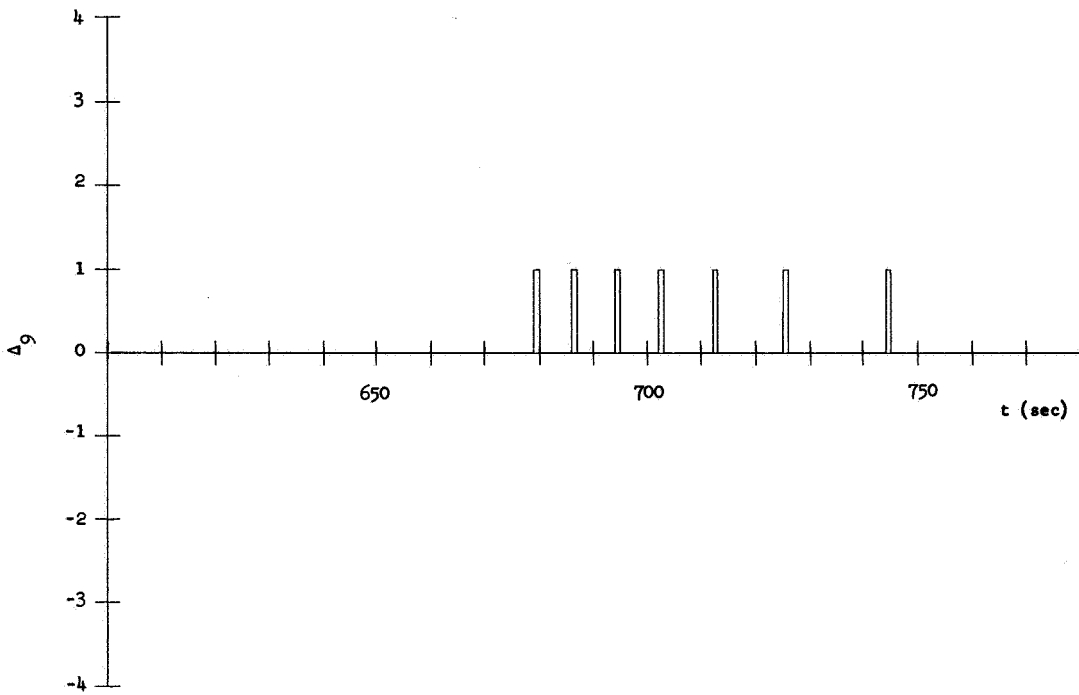
Figure 124. Plot I-J, m_{10}

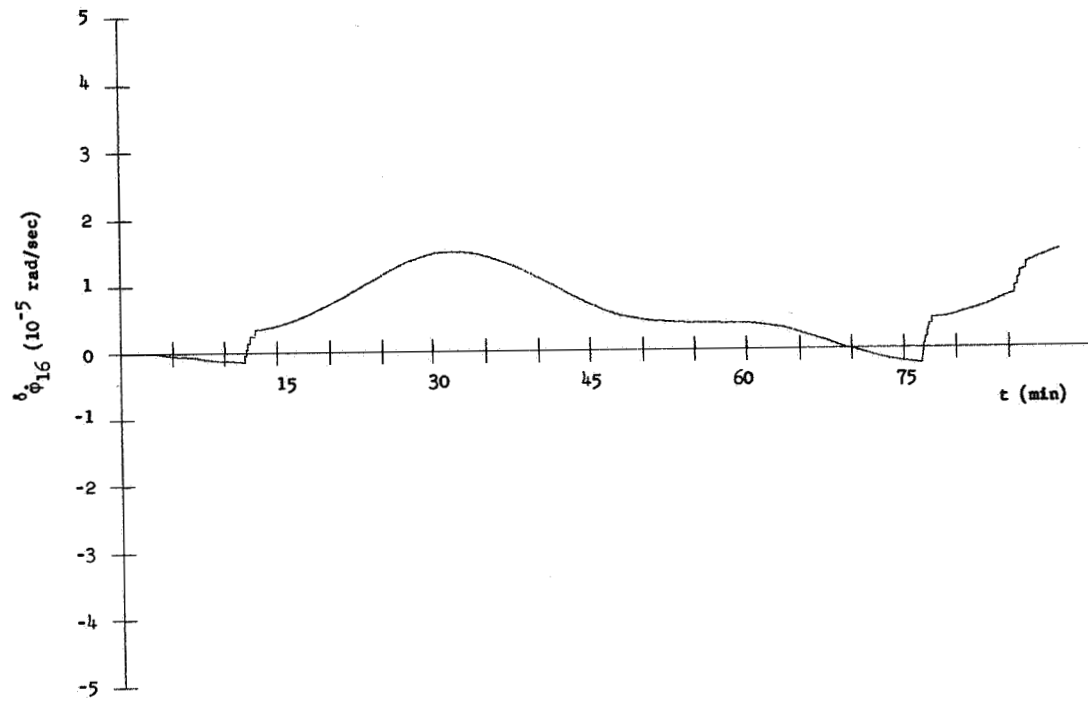
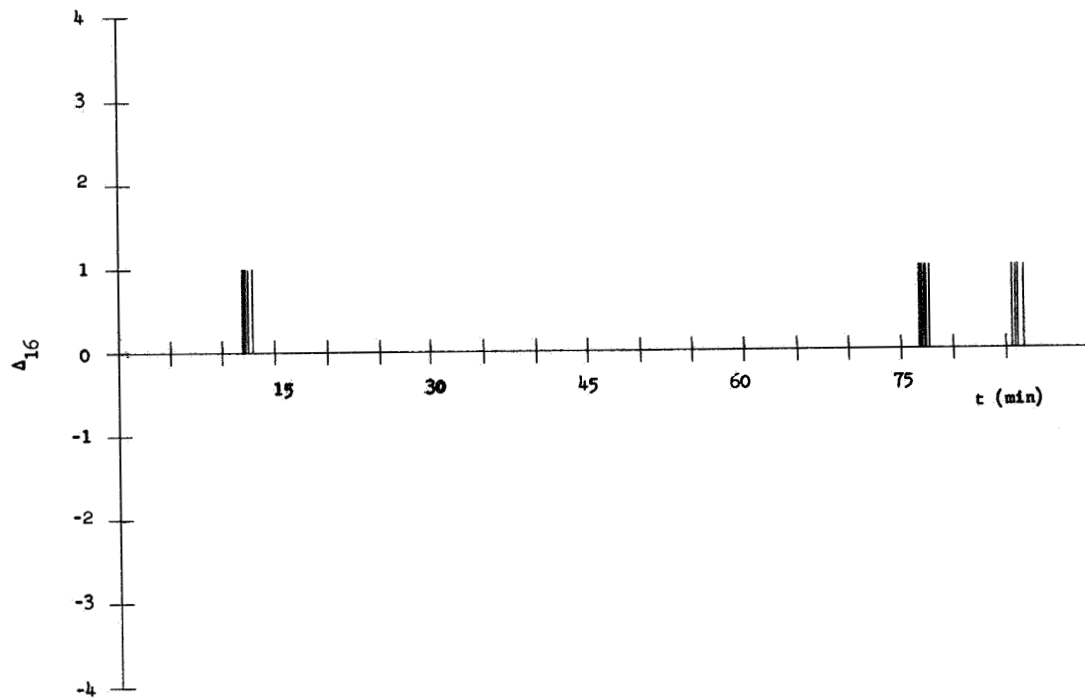
Figure 125. Plot I-J, m_{11} Figure 126. Plot II-J, m_4

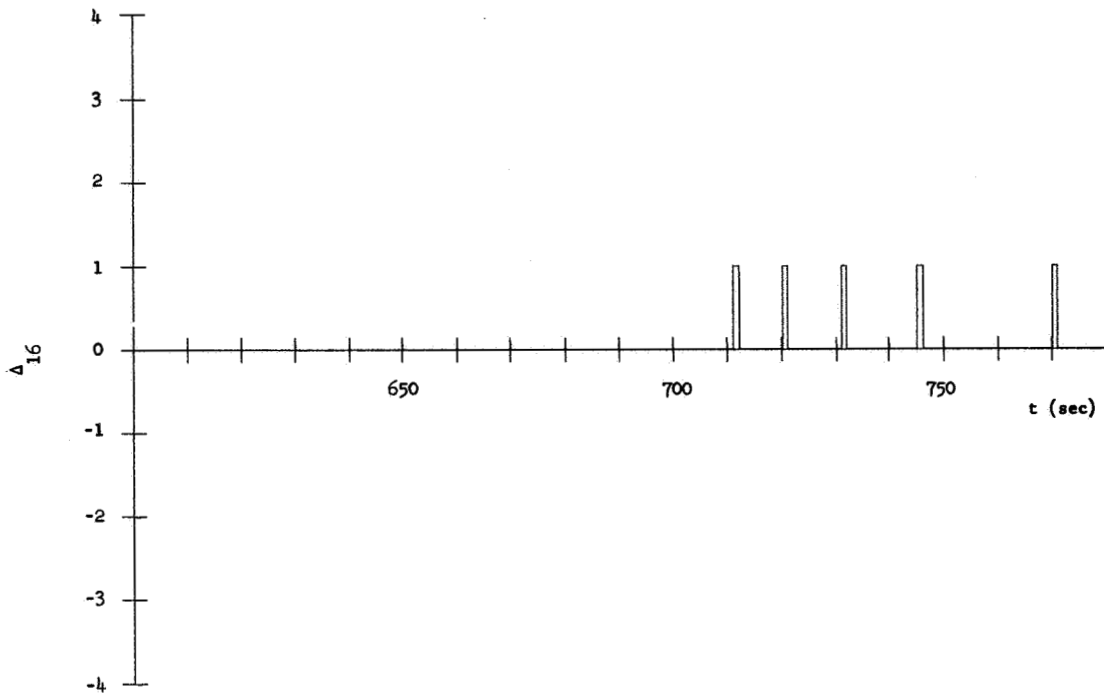
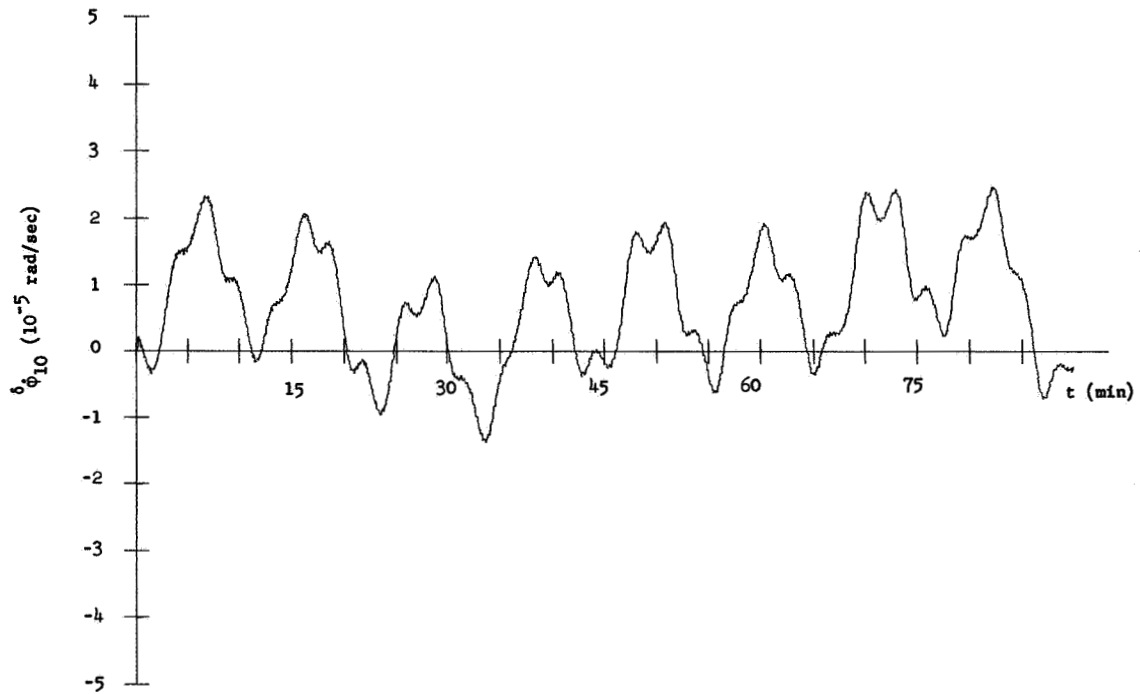
Figure 127. Plot II-J, m_5 Figure 128. Plot II-J, m_6

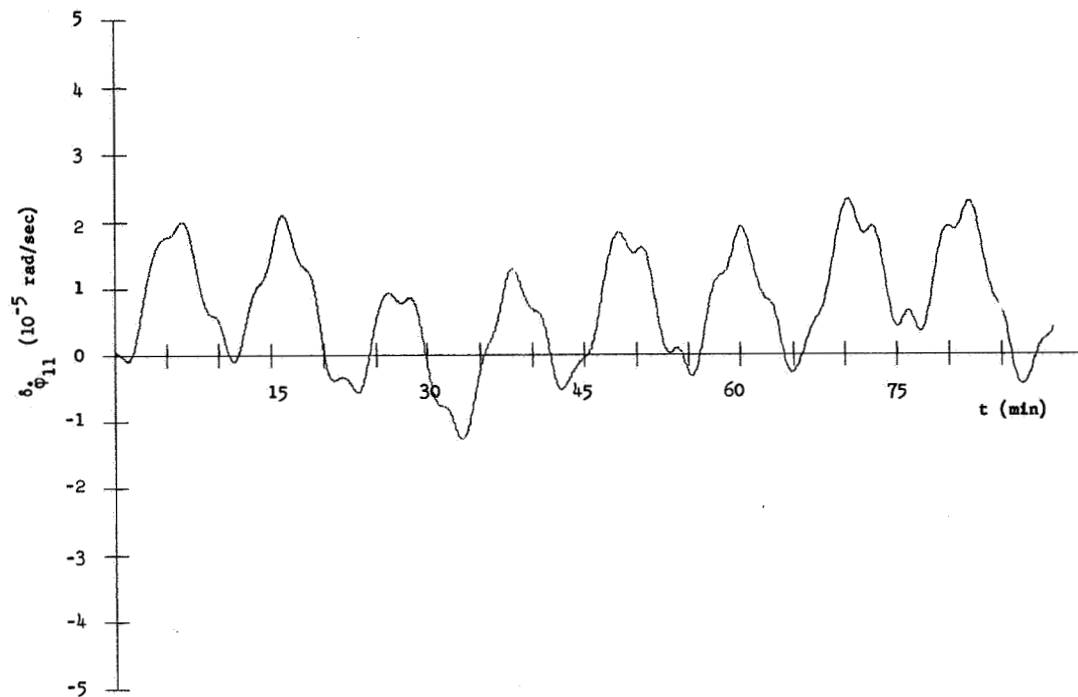
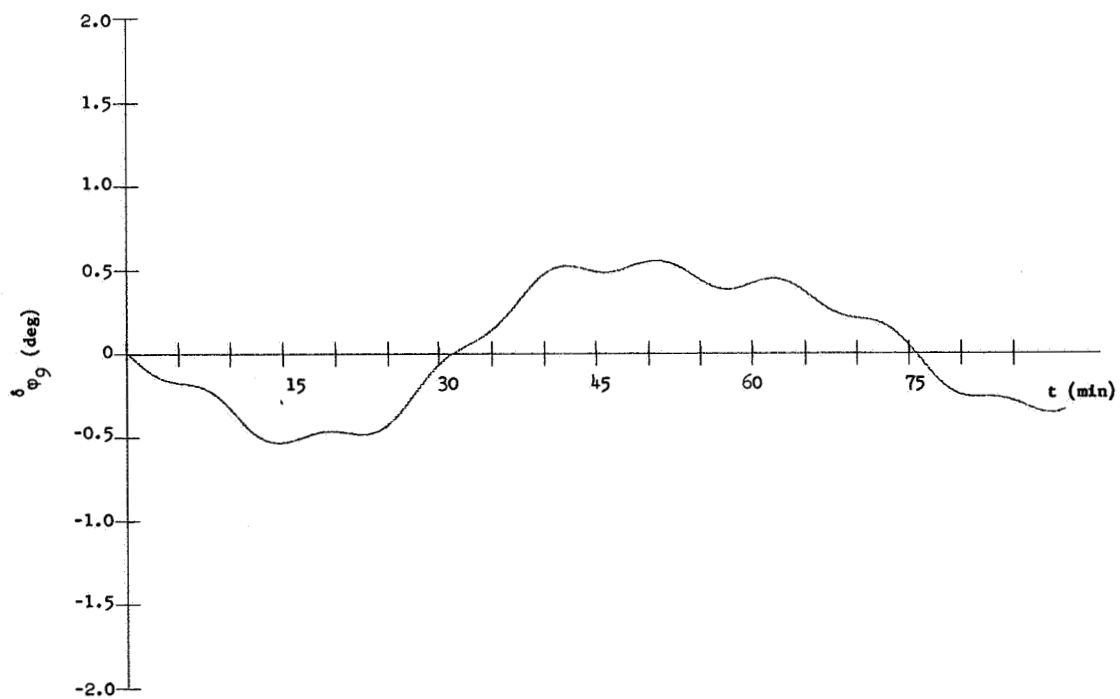
Figure 129. Plot II-J, m_7 Figure 130. Plot II-J, m_8

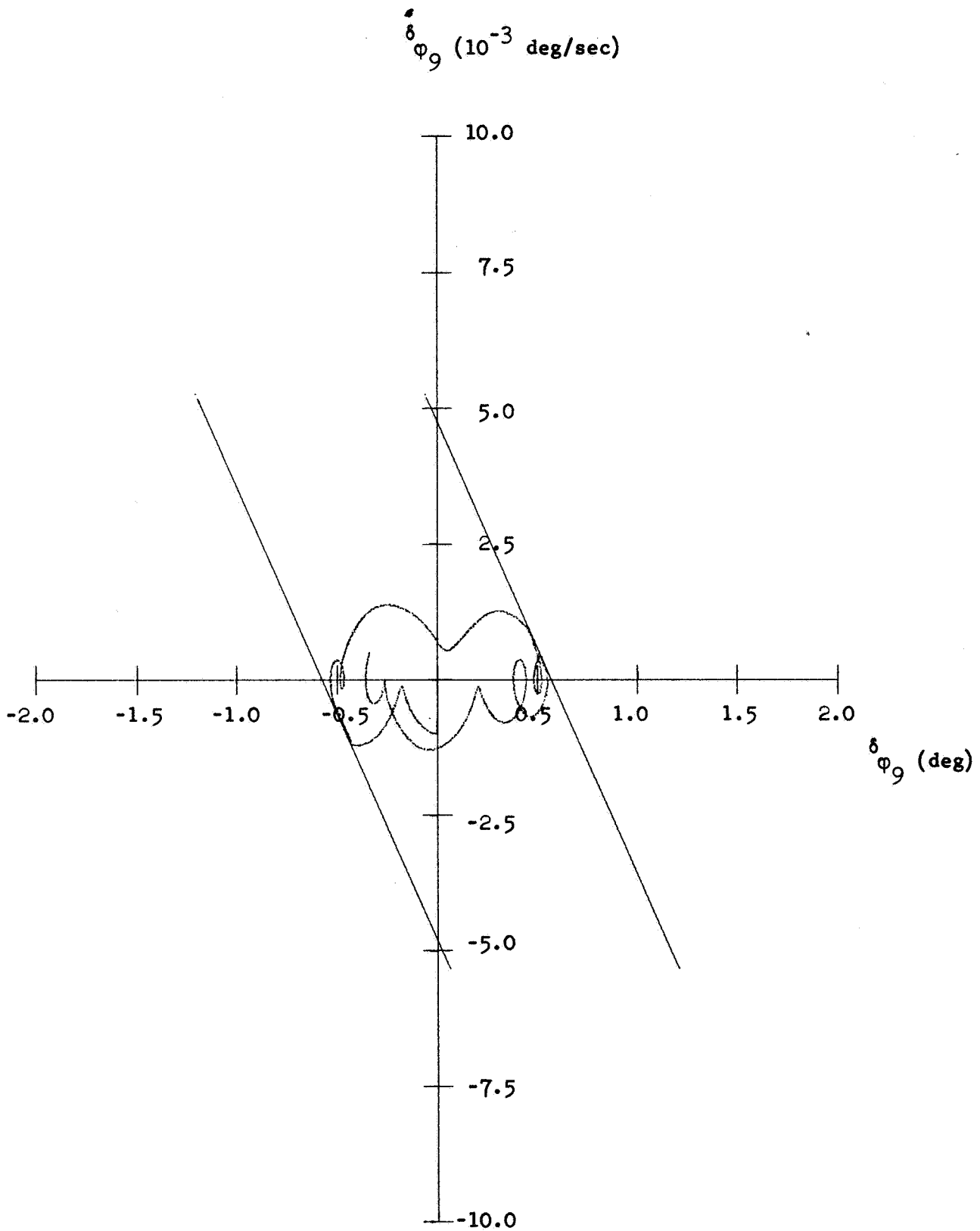
Figure 131. Plot II-J, m_9 Figure 132. Plot V-J, m_9

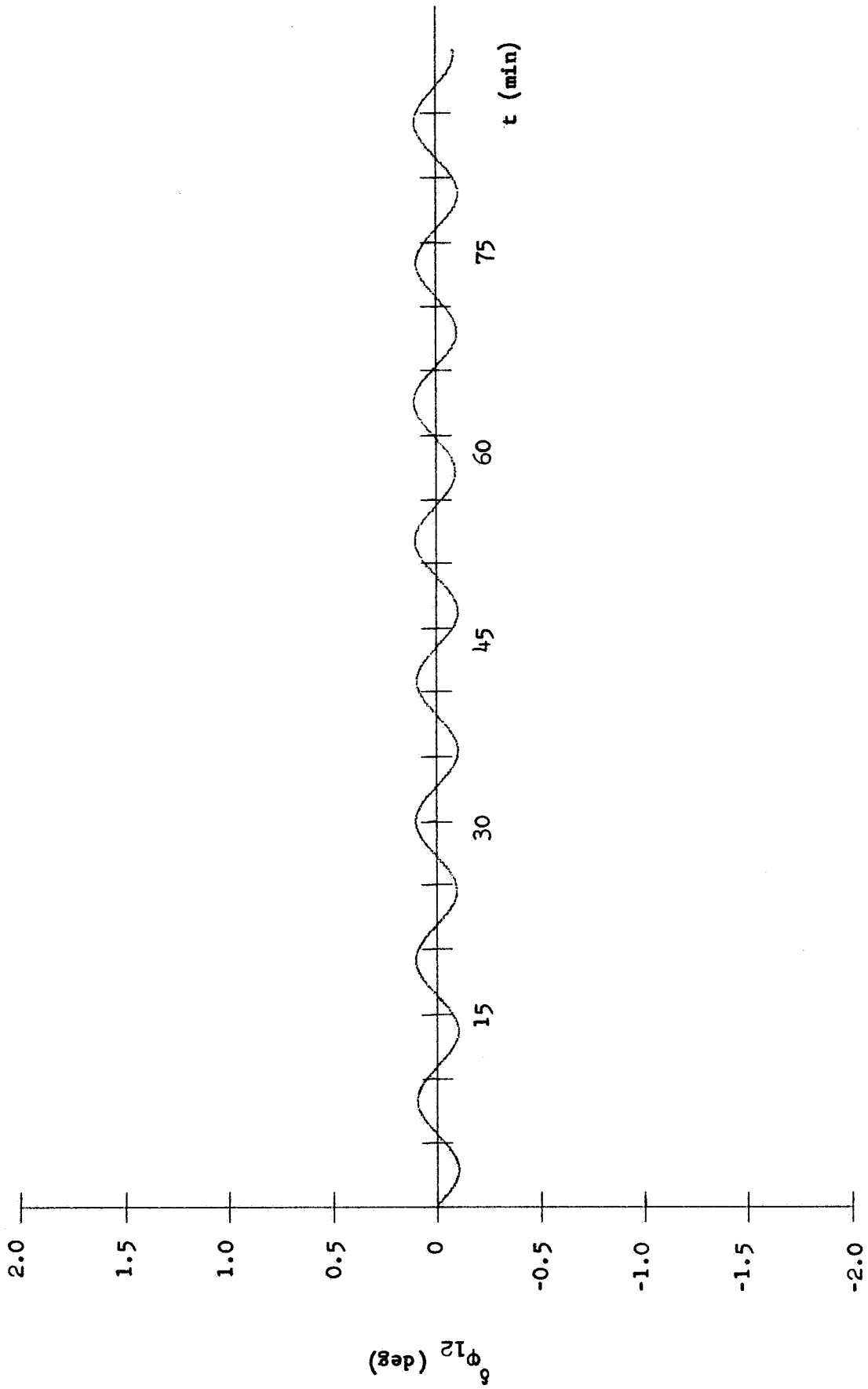


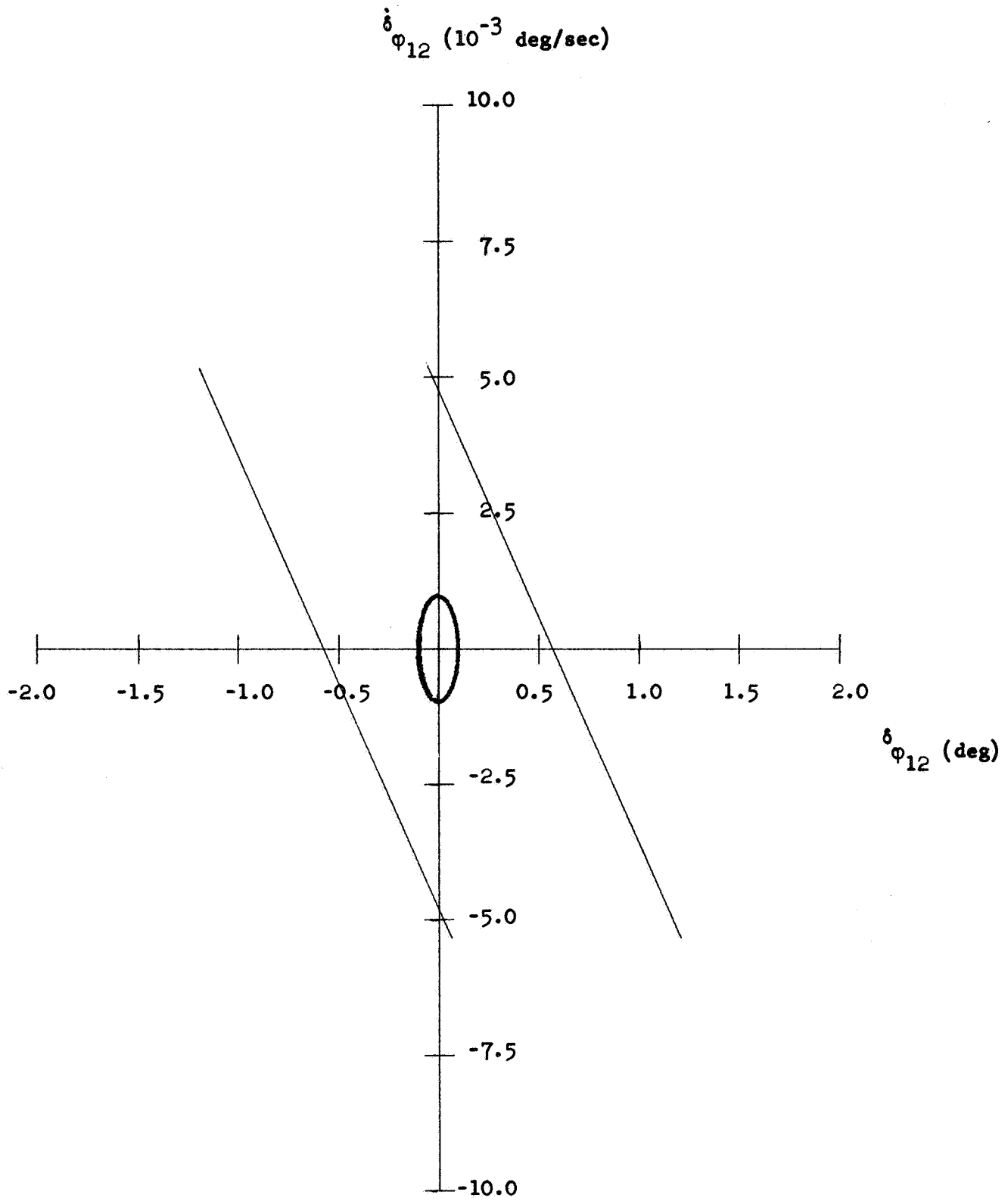
Figure 135. Plot II-J, m_{16} Figure 136. Plot V-J, m_{16}

Figure 137. Plot VI-J, m_{16} Figure 138. Plot II-J, m_{10}

Figure 139. Plot II-J, m_{11} Figure 140. Plot III-J, m_9

Figure 141. Plot IV-J, m_9

Figure 142. Plot III-J, m_{12}

Figure 143. Plot IV-J, m_{12}

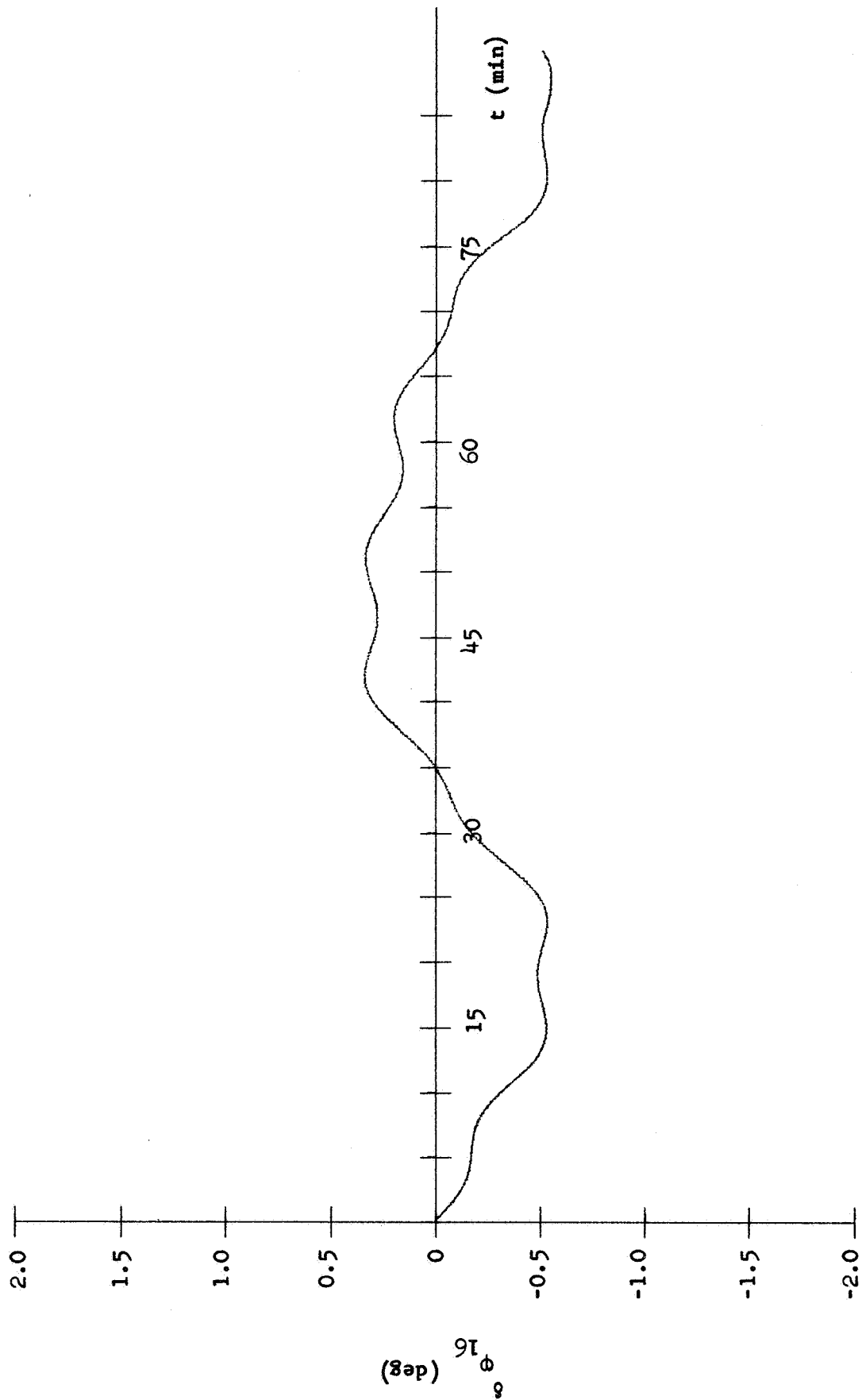


Figure 144. Plot III-J, m_{16}

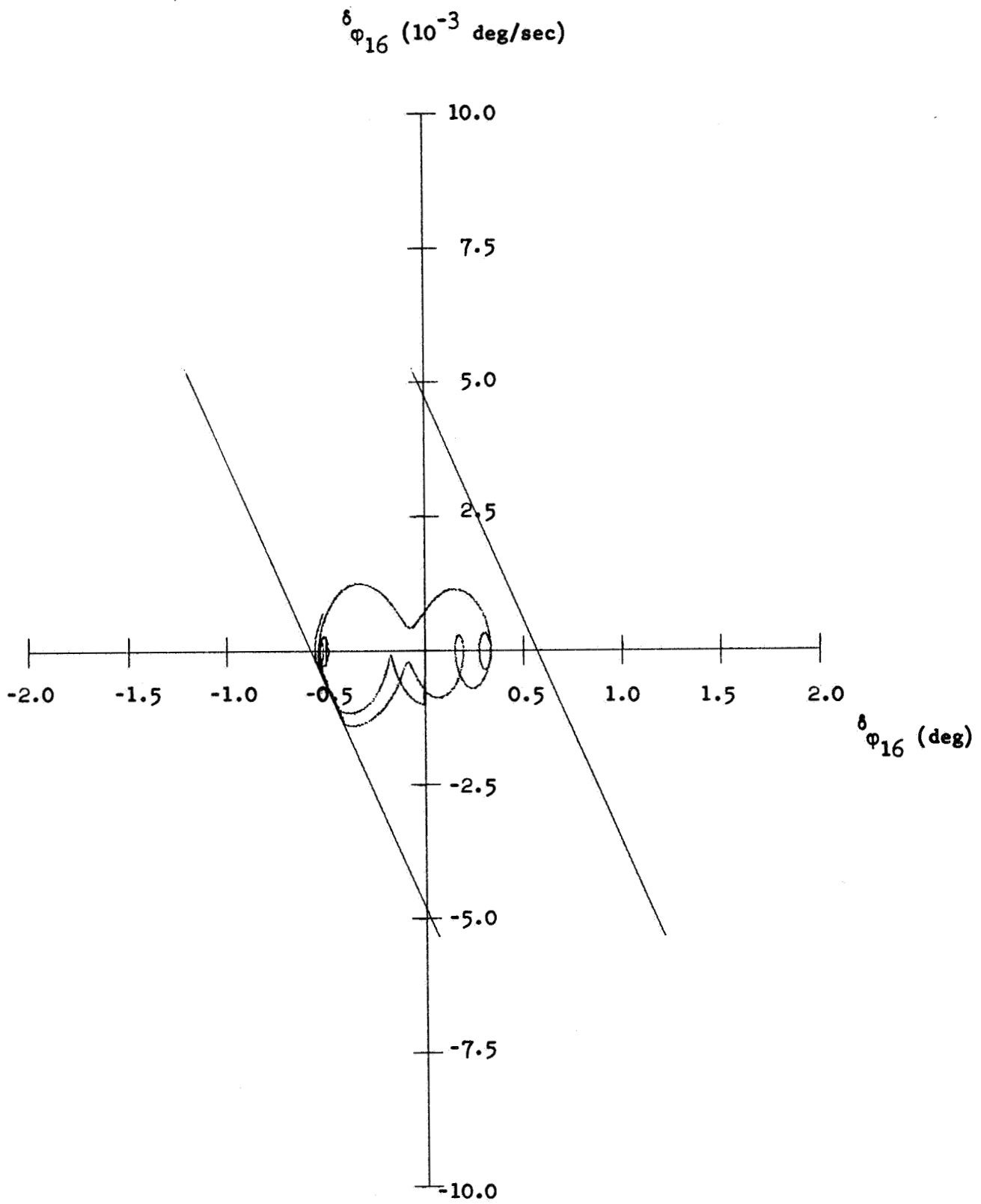
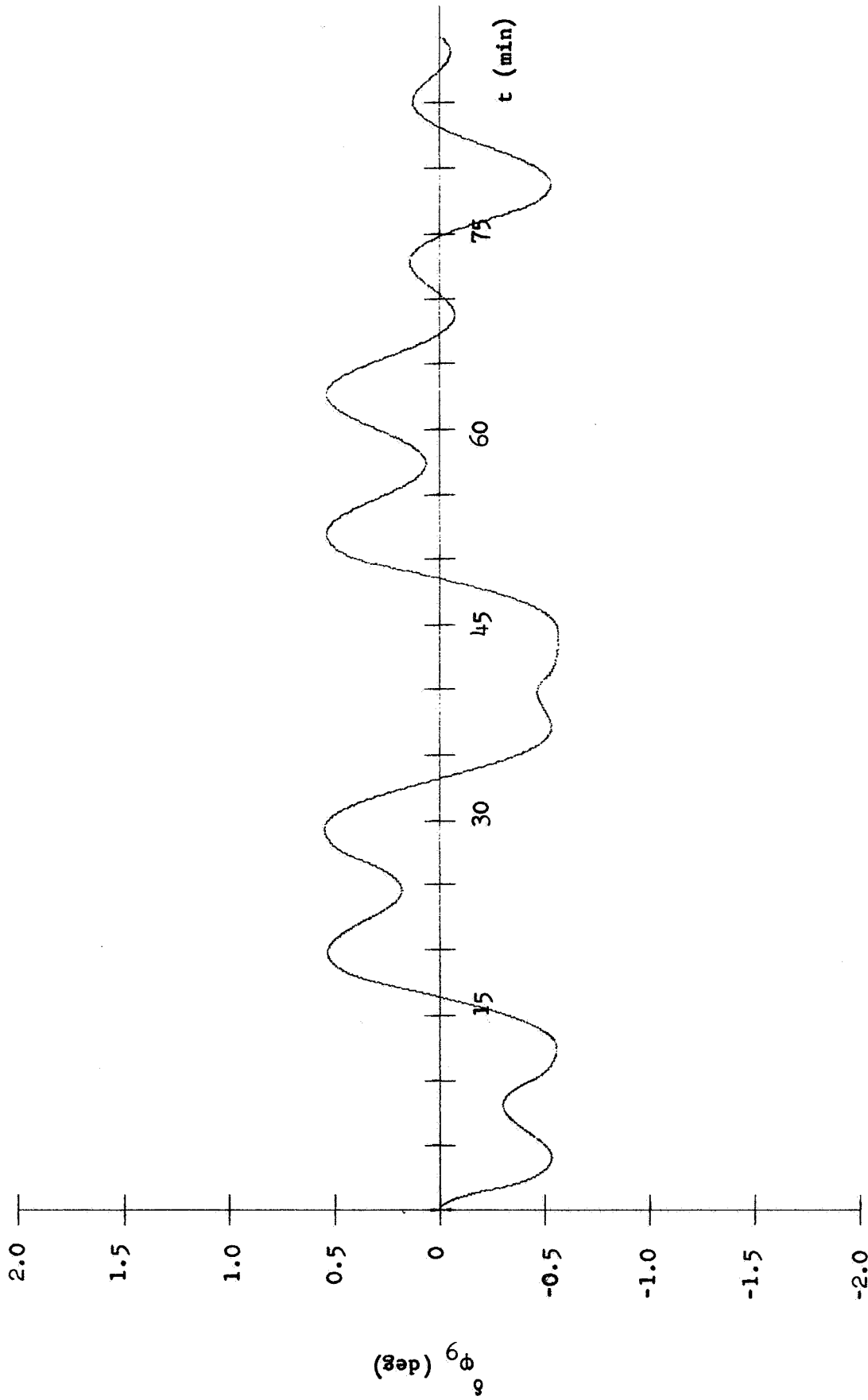
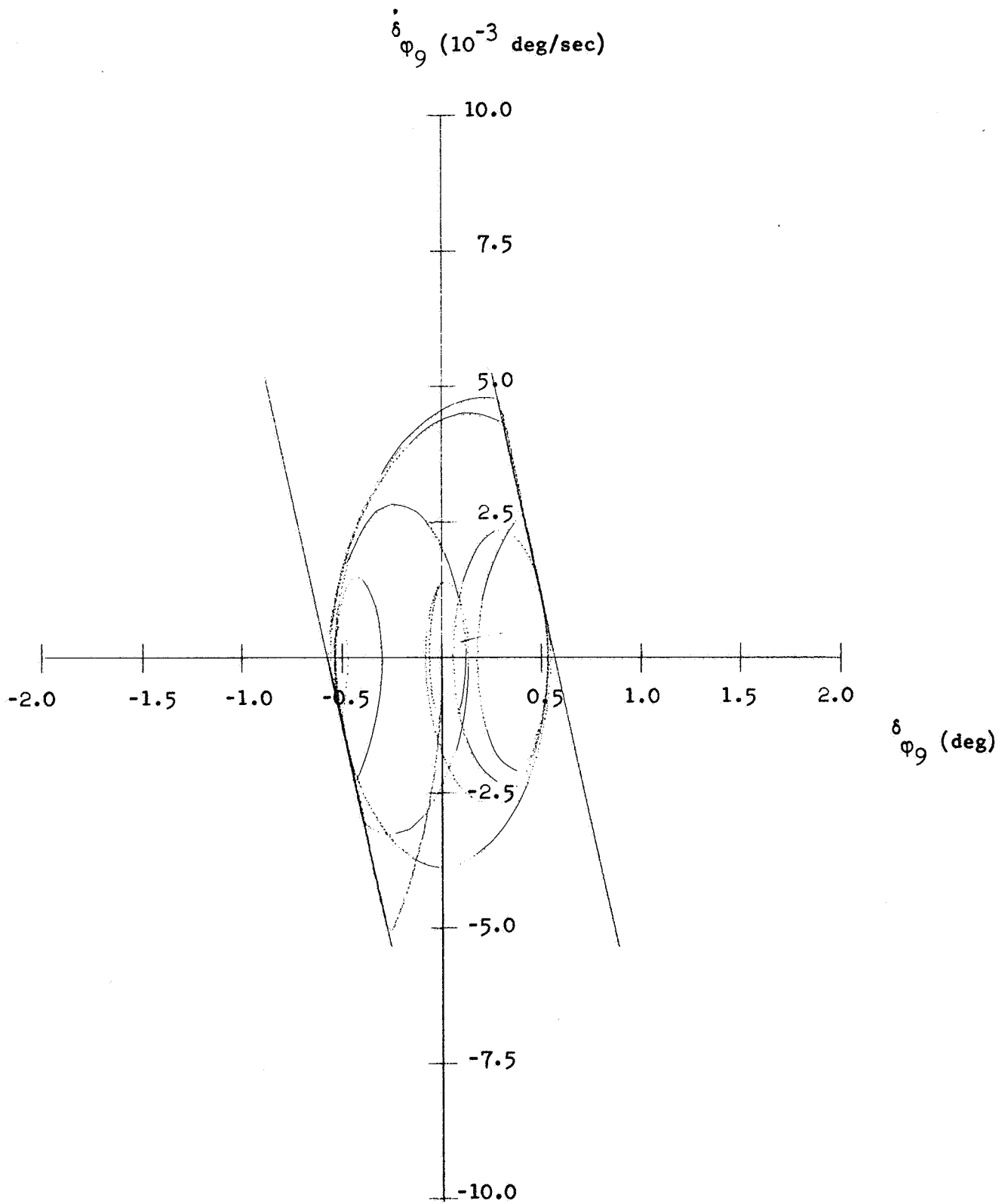
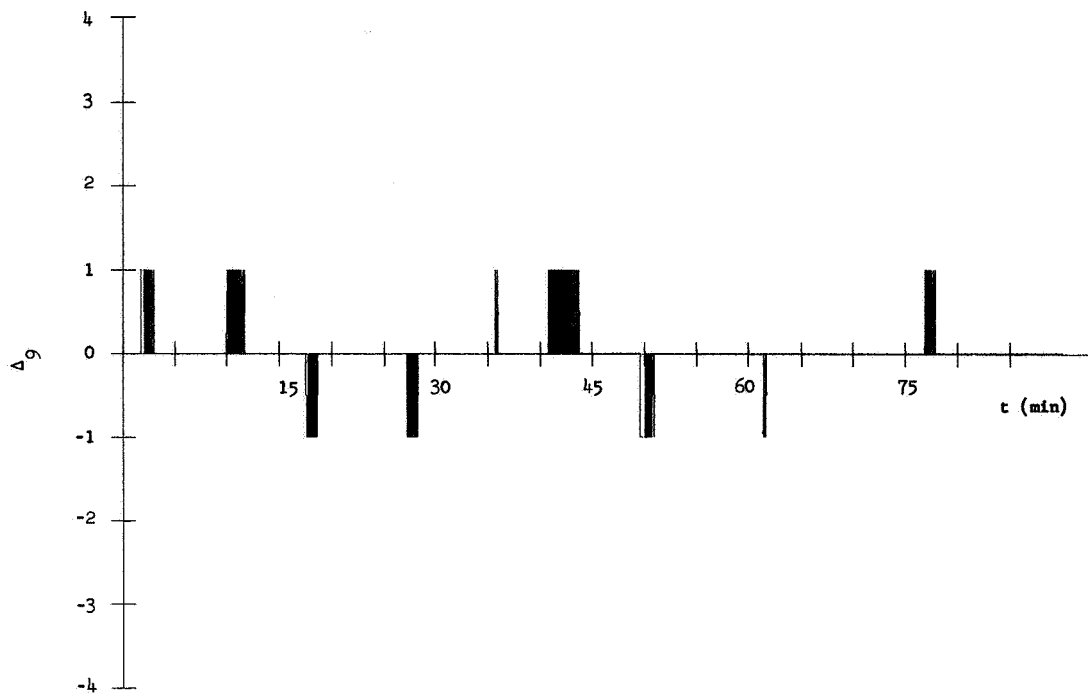
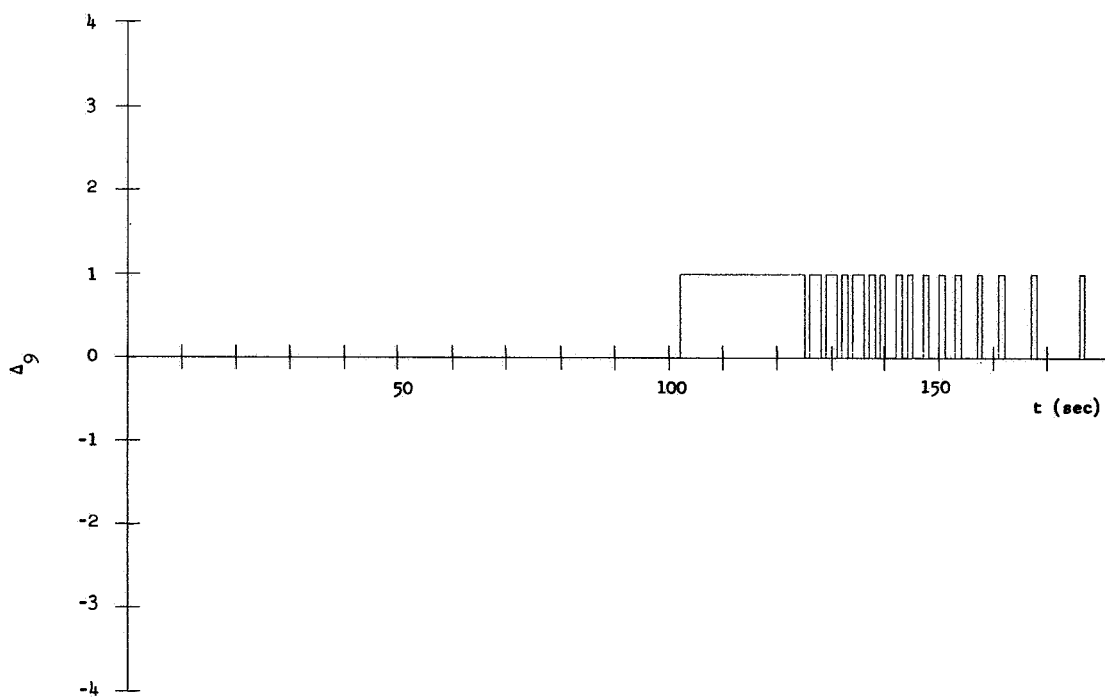


Figure 145. Plot IV-J, m_{16}

Figure 146. Plot ϕ_g , m

Figure 147. Plot IV-L, m_9

Figure 148. Plot V-L, m_g Figure 149. Plot VI-L, m_g

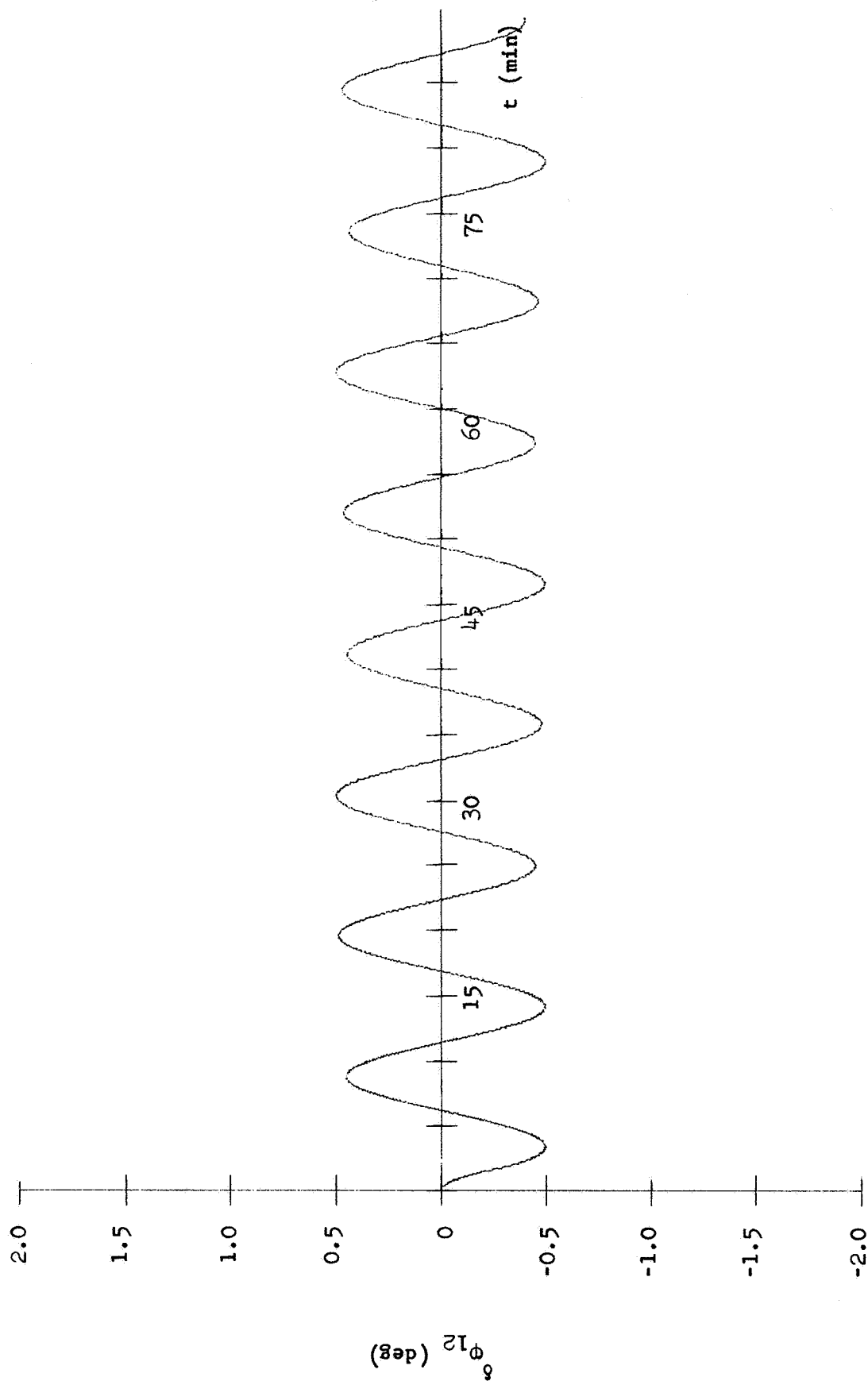


Figure 150. Plot III-L, m_{12}

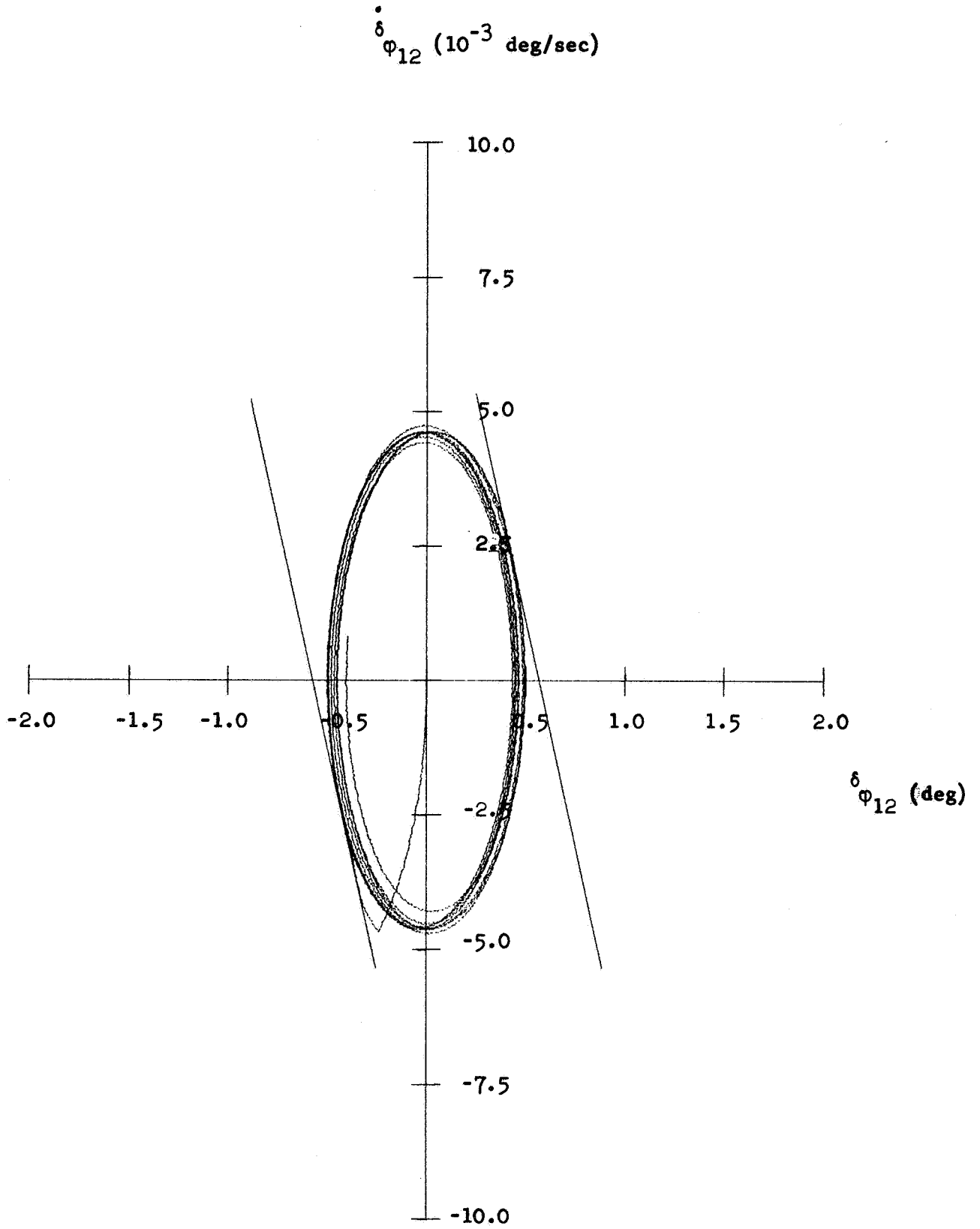
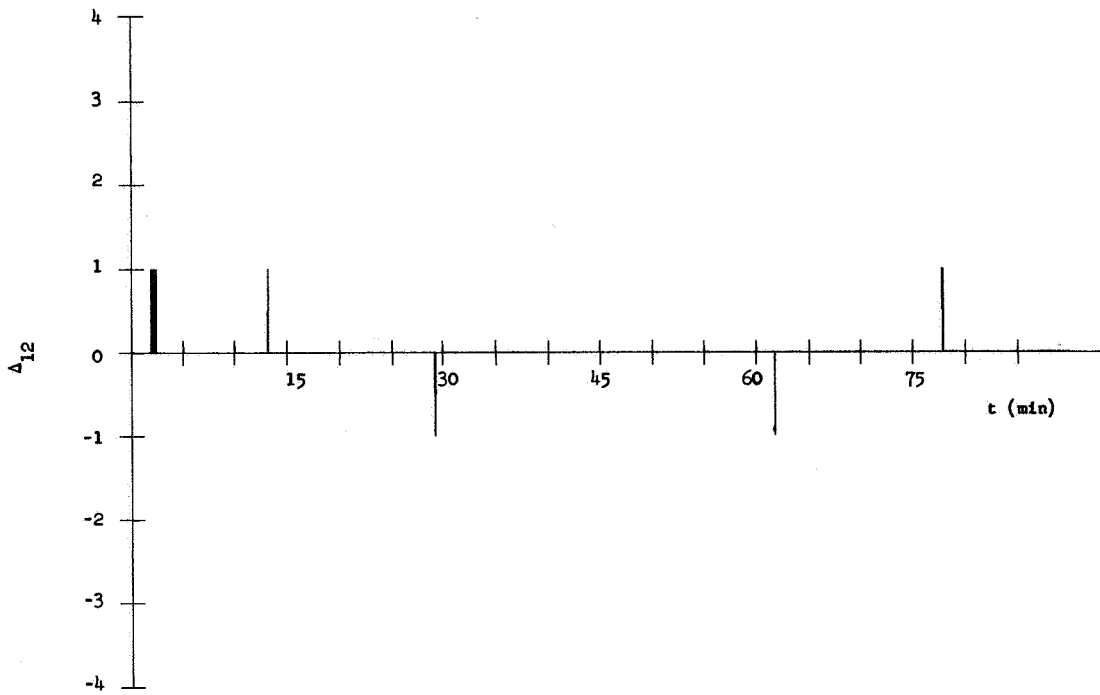
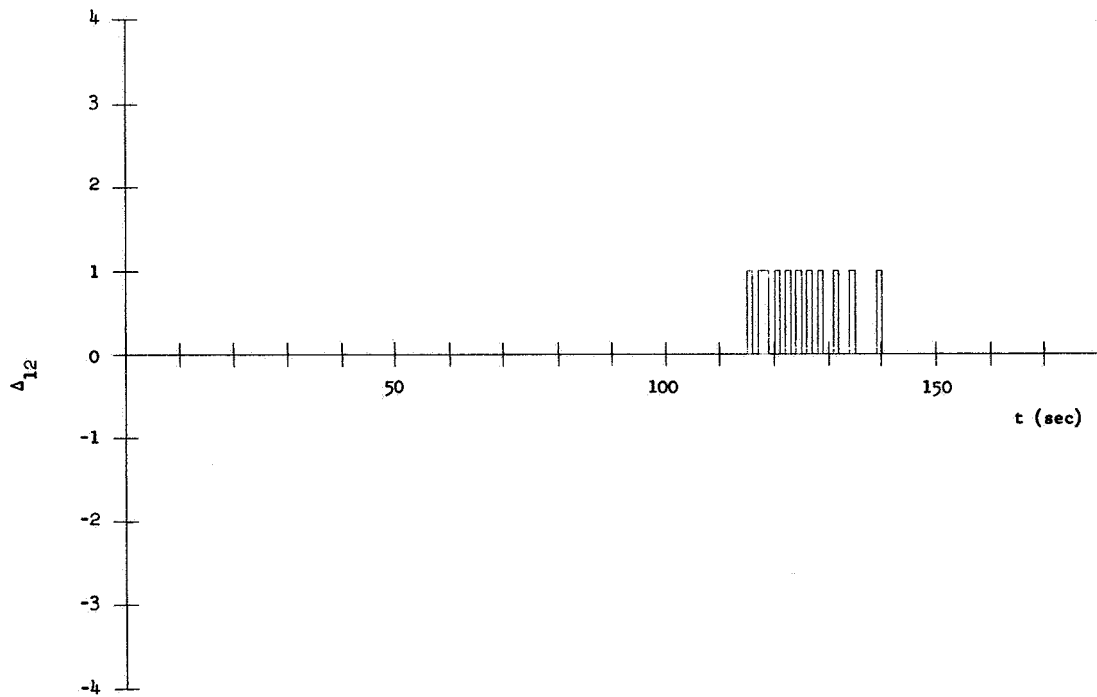


Figure 151. Plot IV-L, m_{12}

Figure 152. Plot V-L, m_{12} Figure 153. Plot VI-L, m_{12}

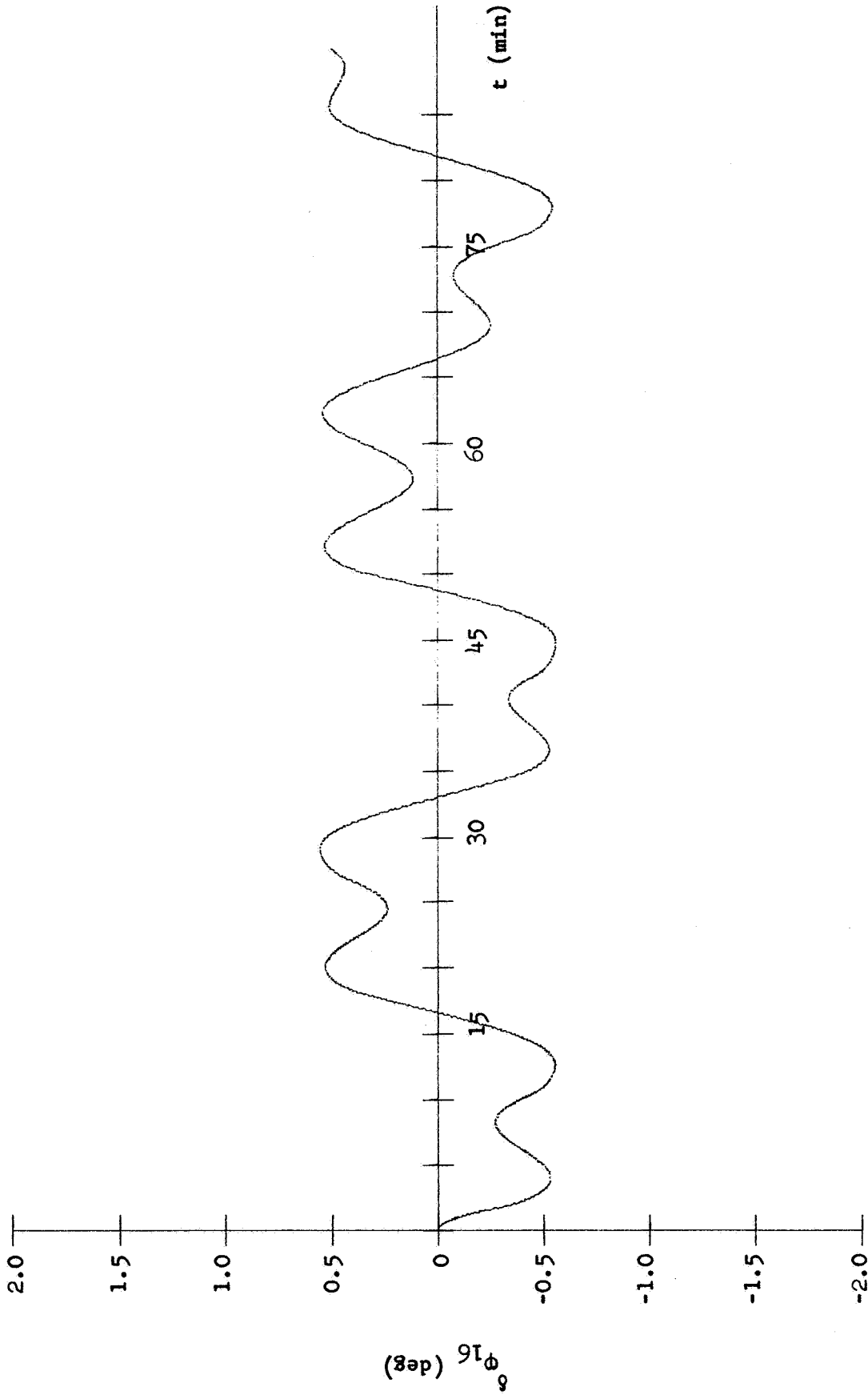


Figure 154. Plot III-L, m_{16}

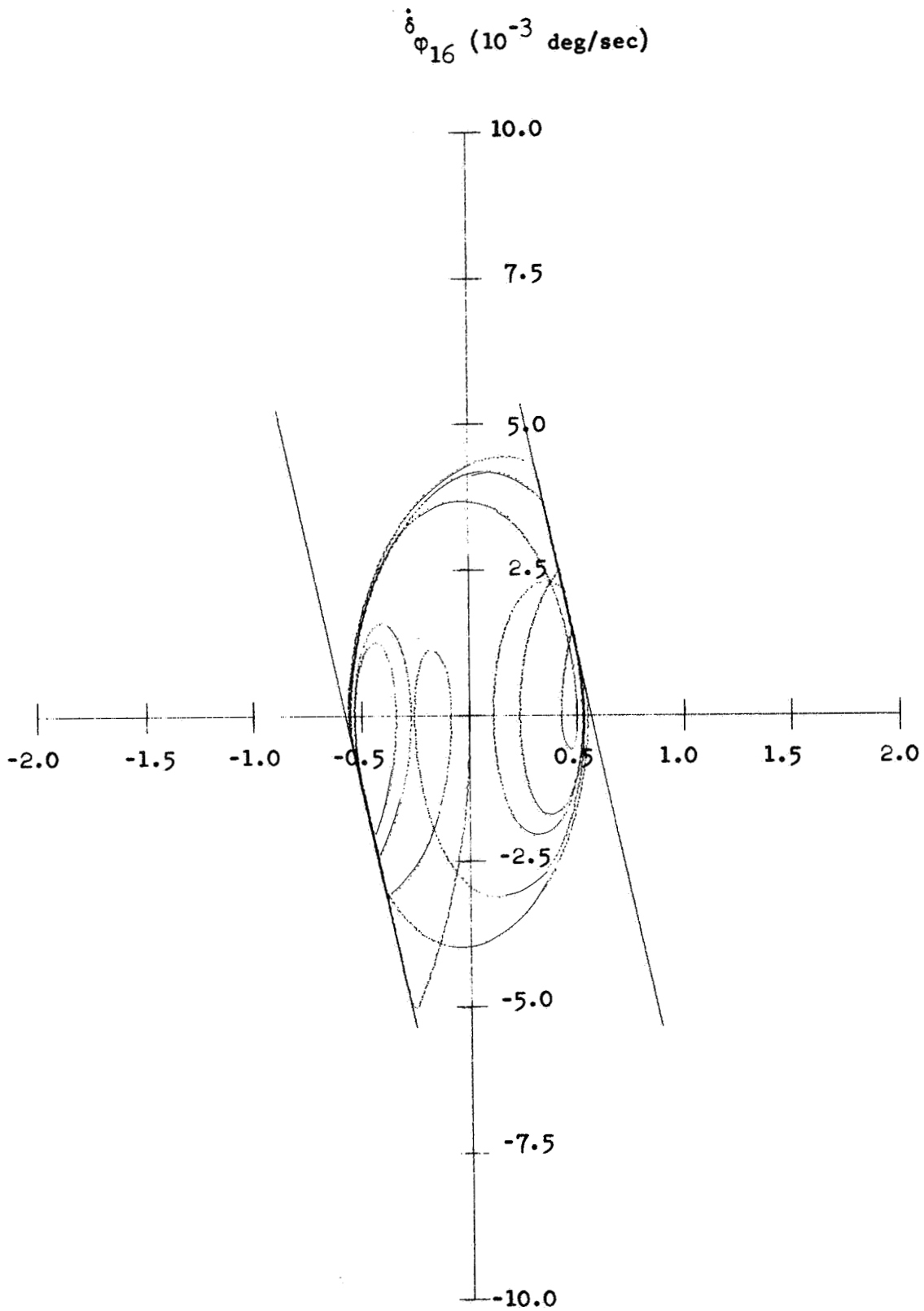
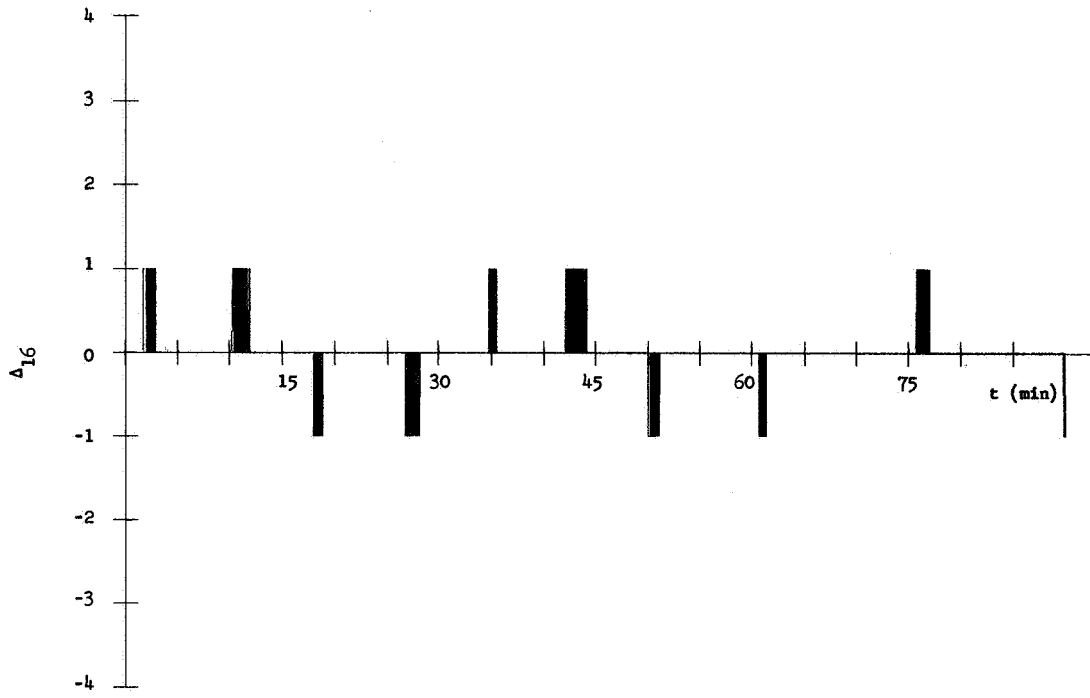
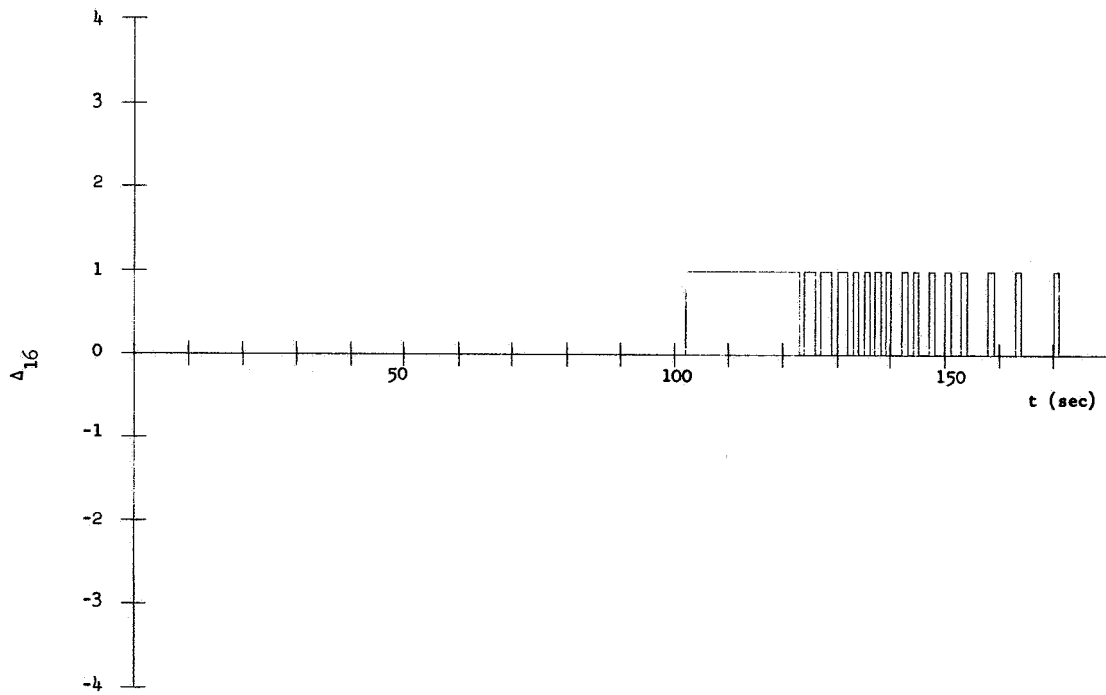
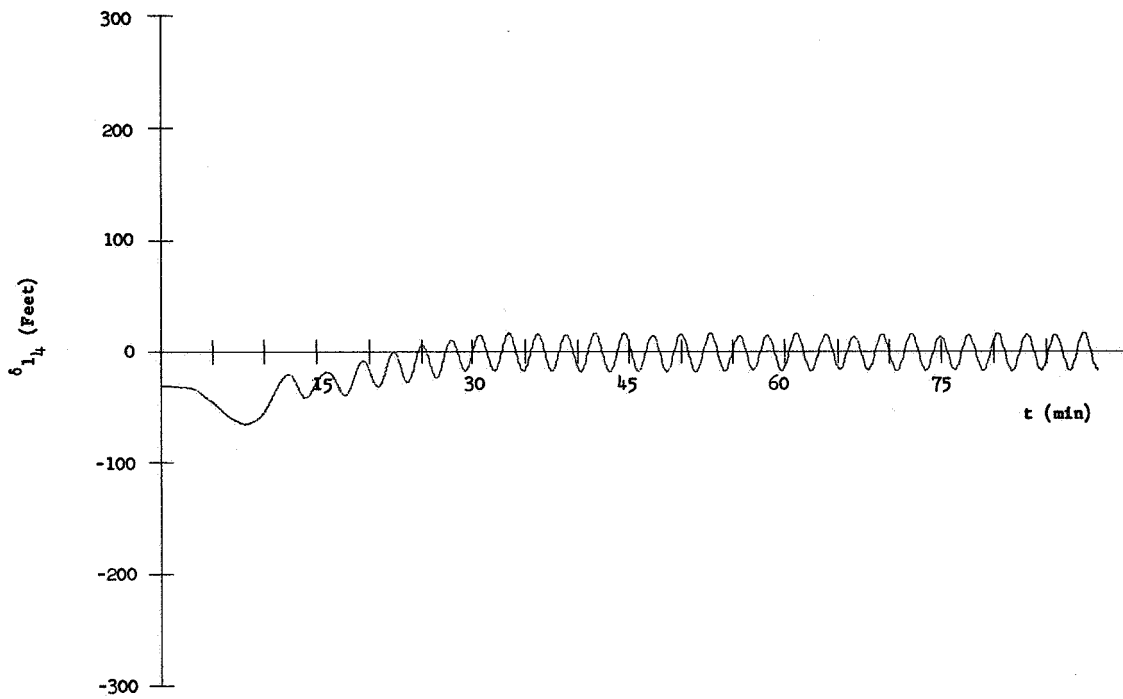
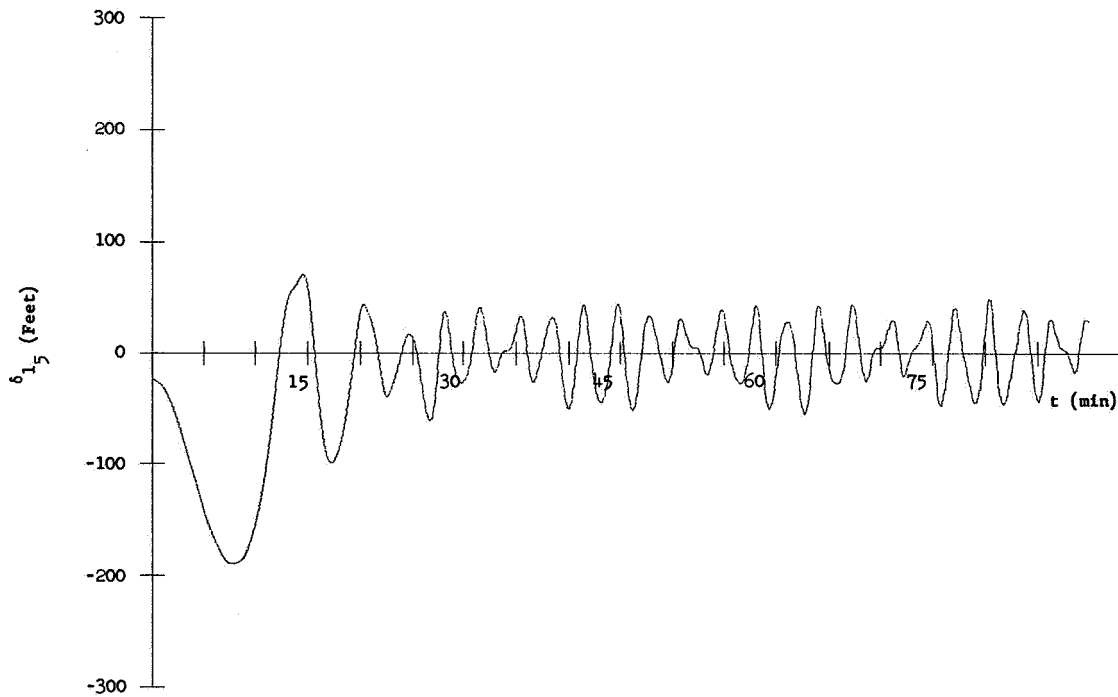


Figure 155. Plot IV-L, m_{16}

Figure 156. Plot V-L, m_{16} Figure 157. Plot VI-L, m_{16}

Figure 158. Plot I-M, m_4 Figure 159. Plot I-M, m_5

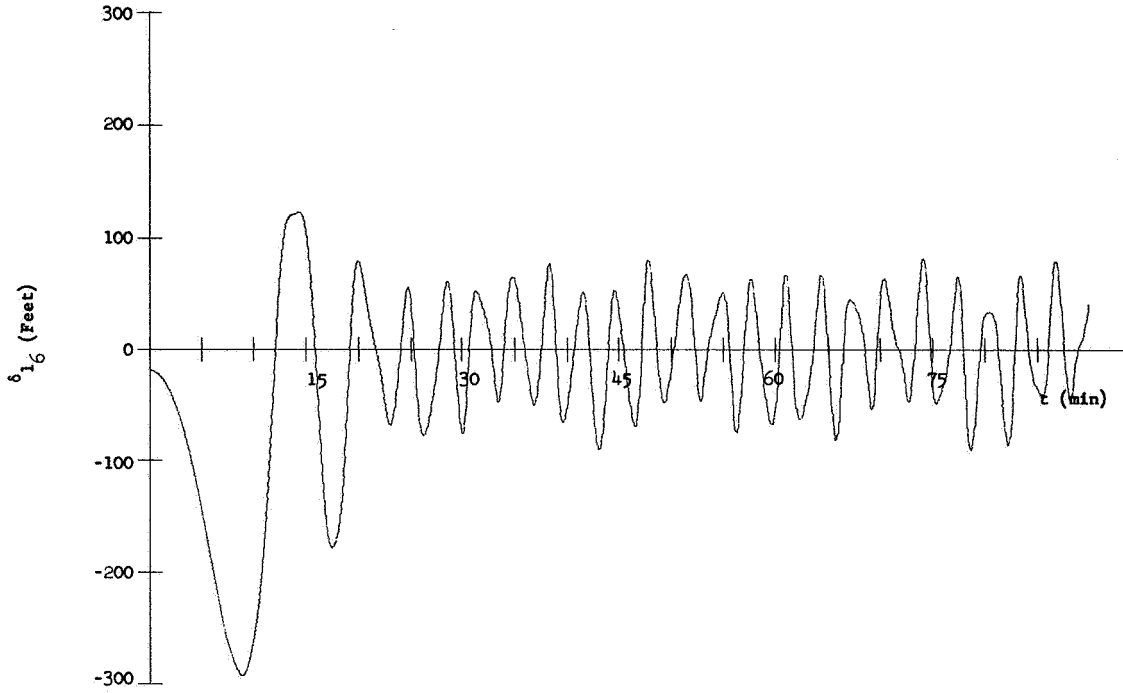


Figure 160. Plot I-M, m_6

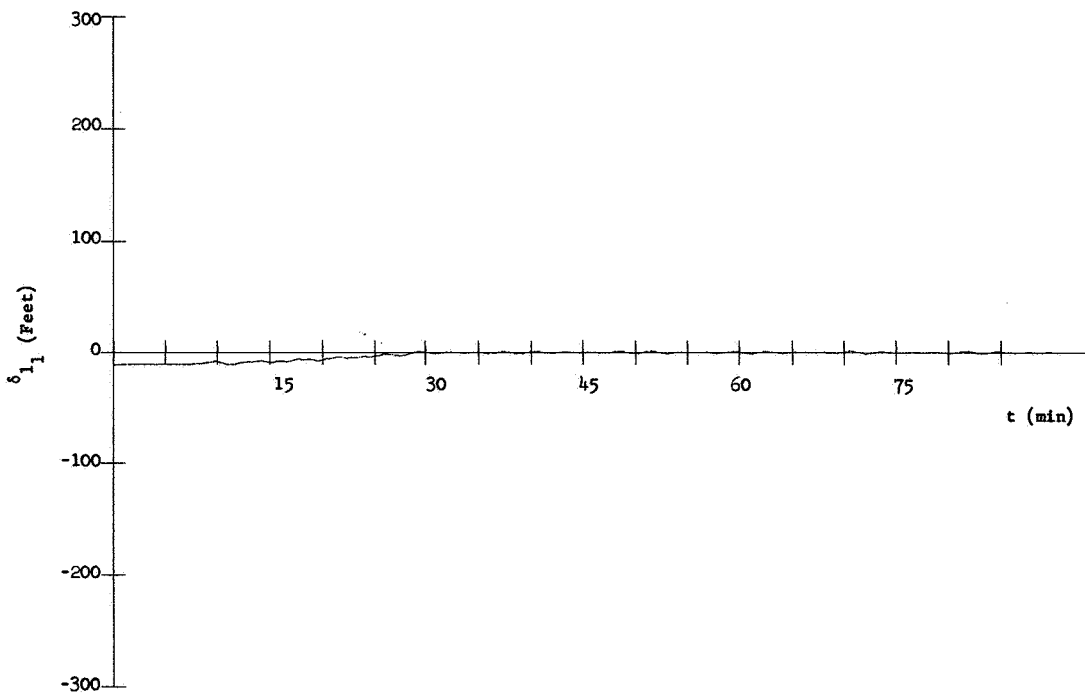
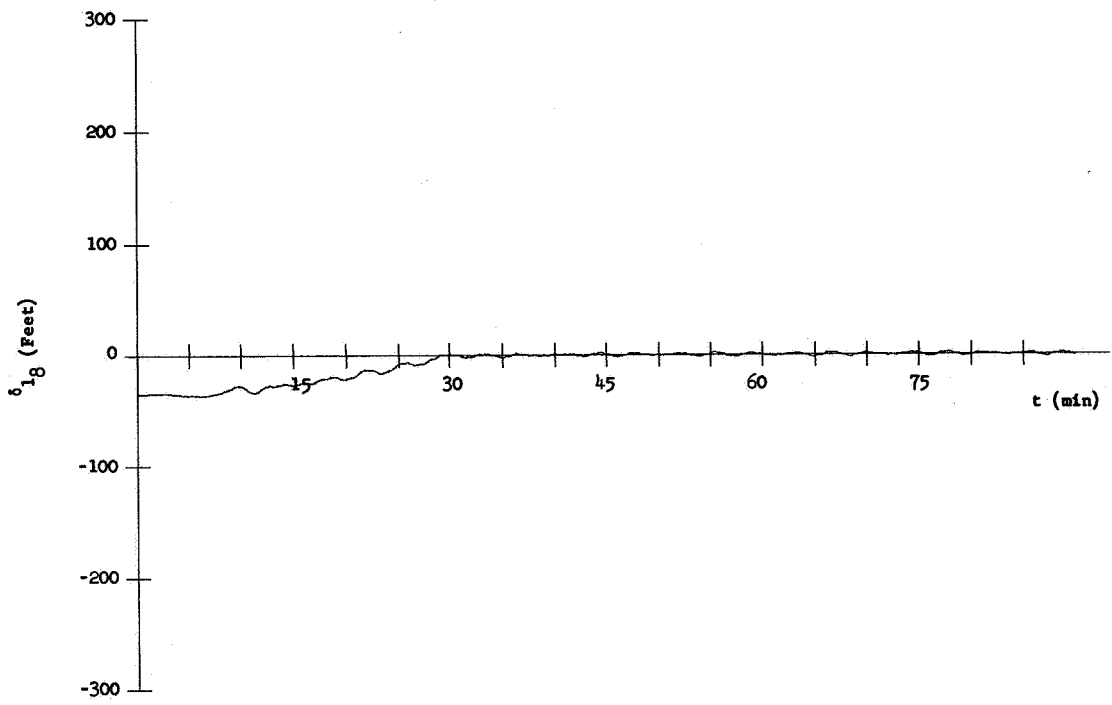
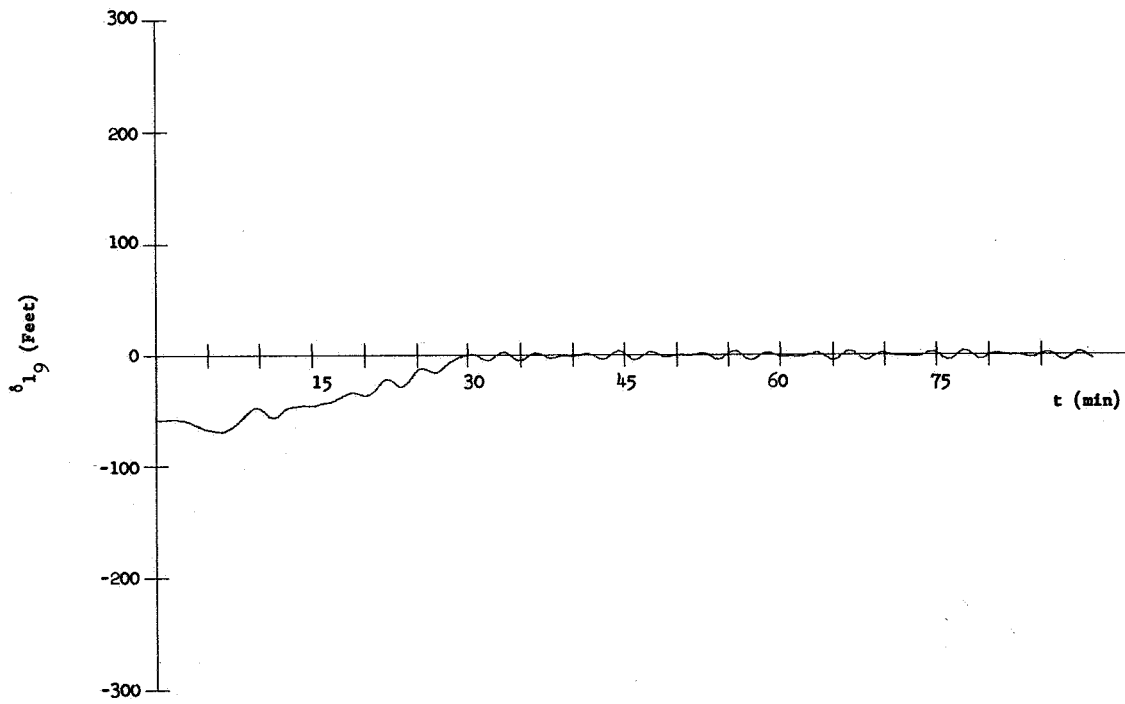
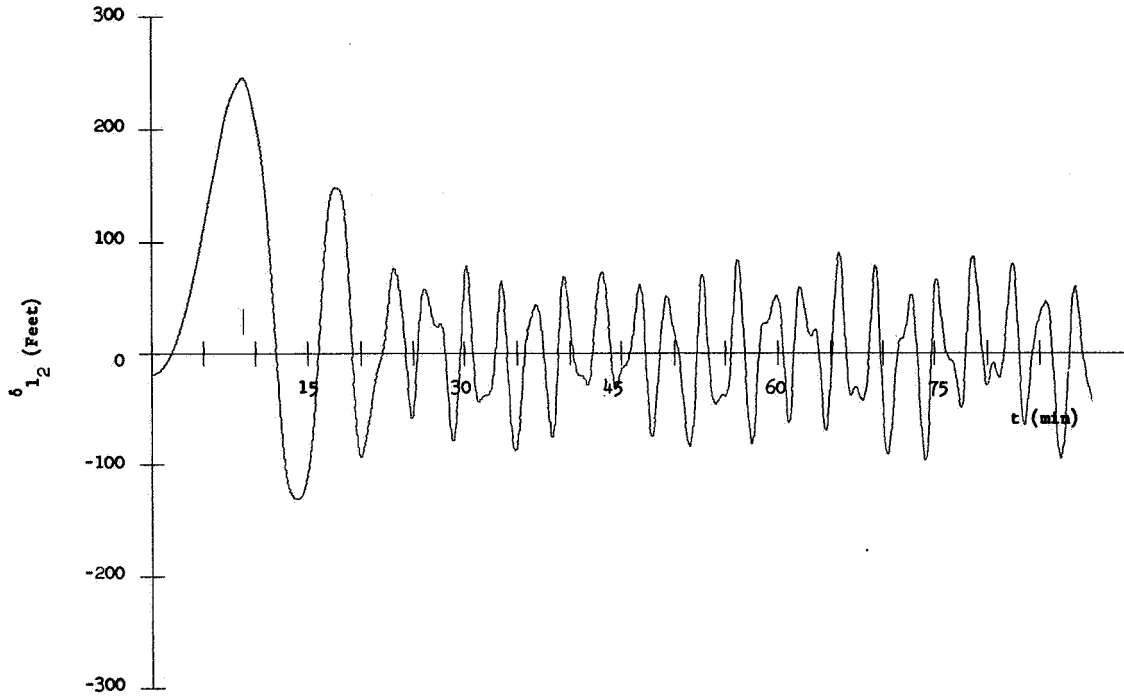
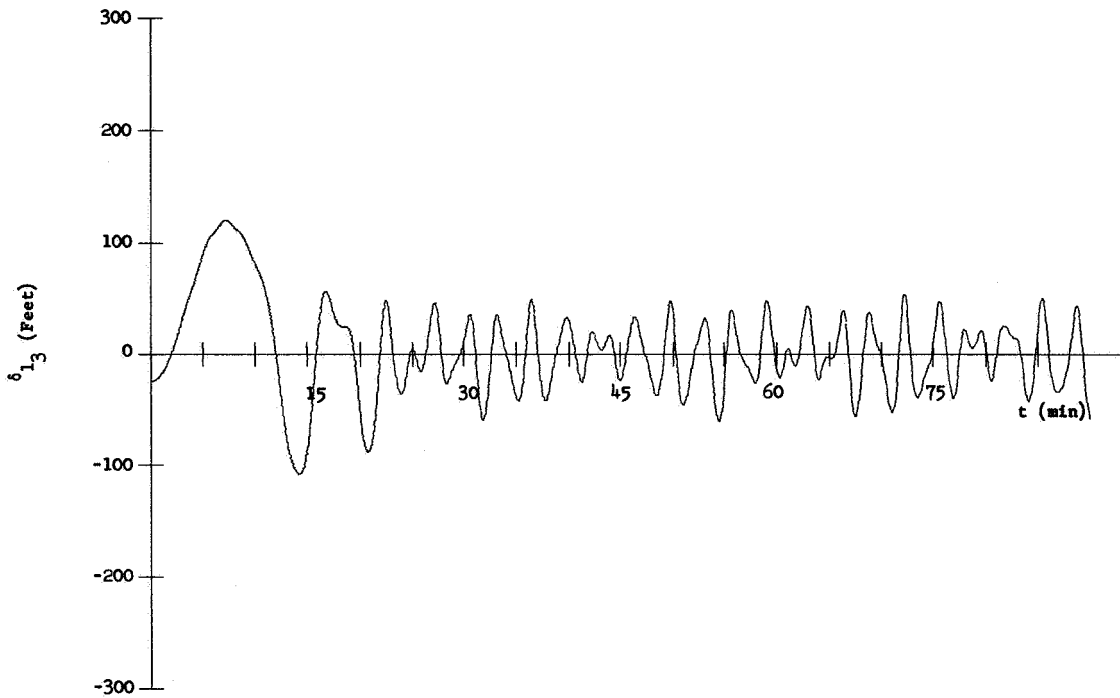
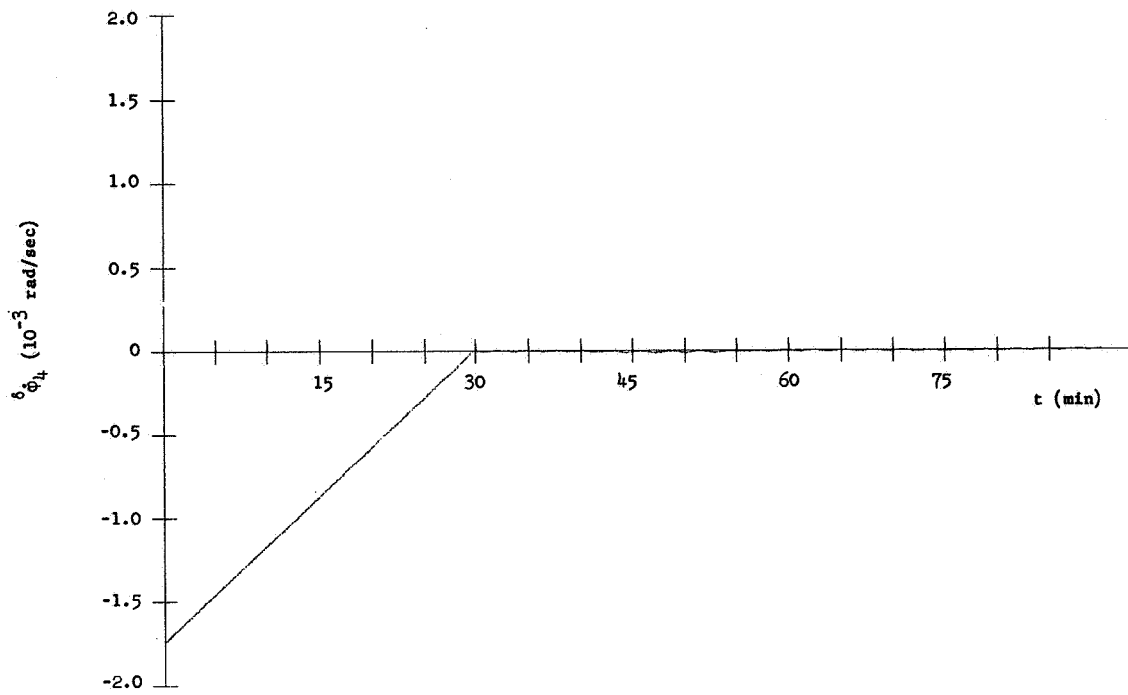
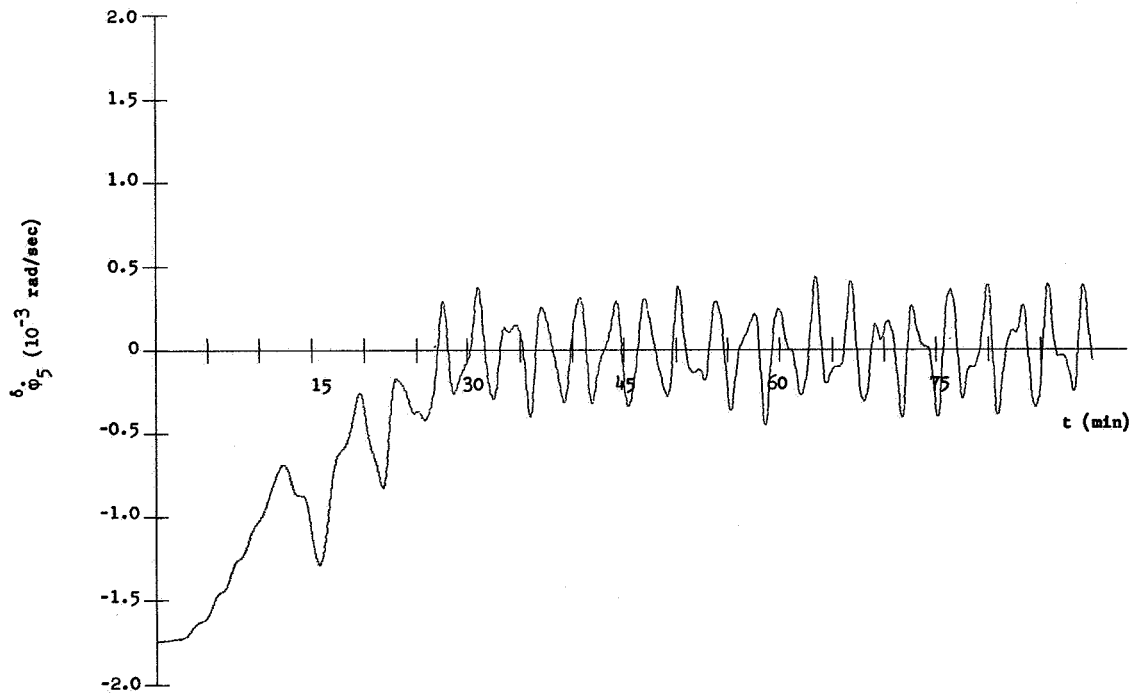
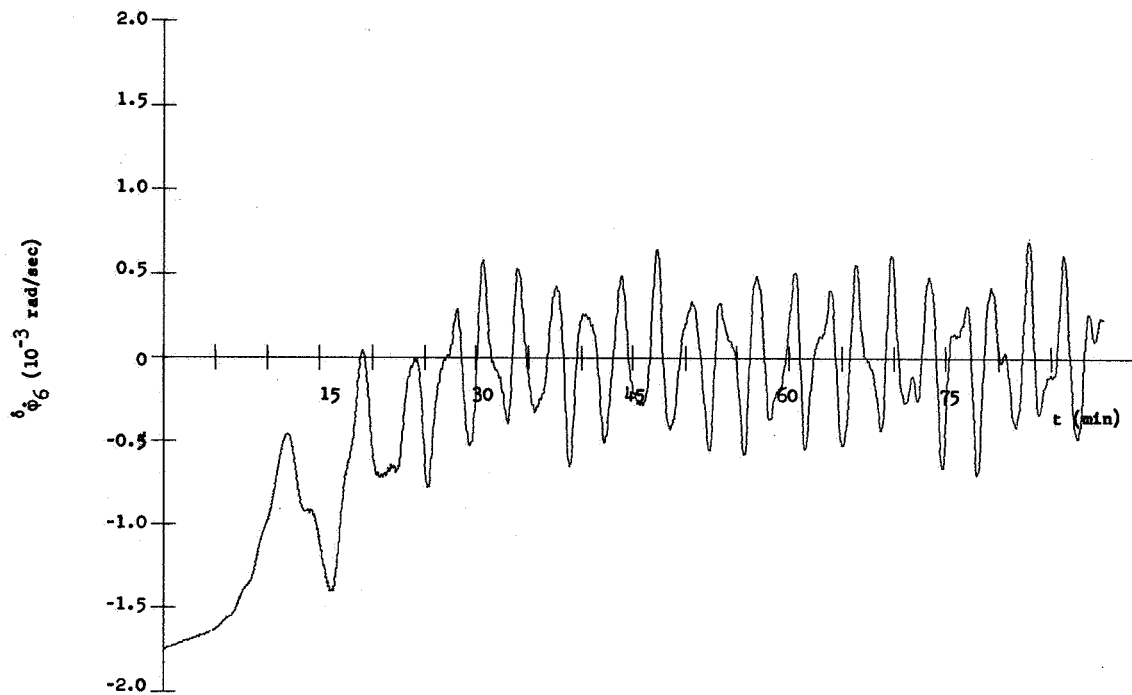
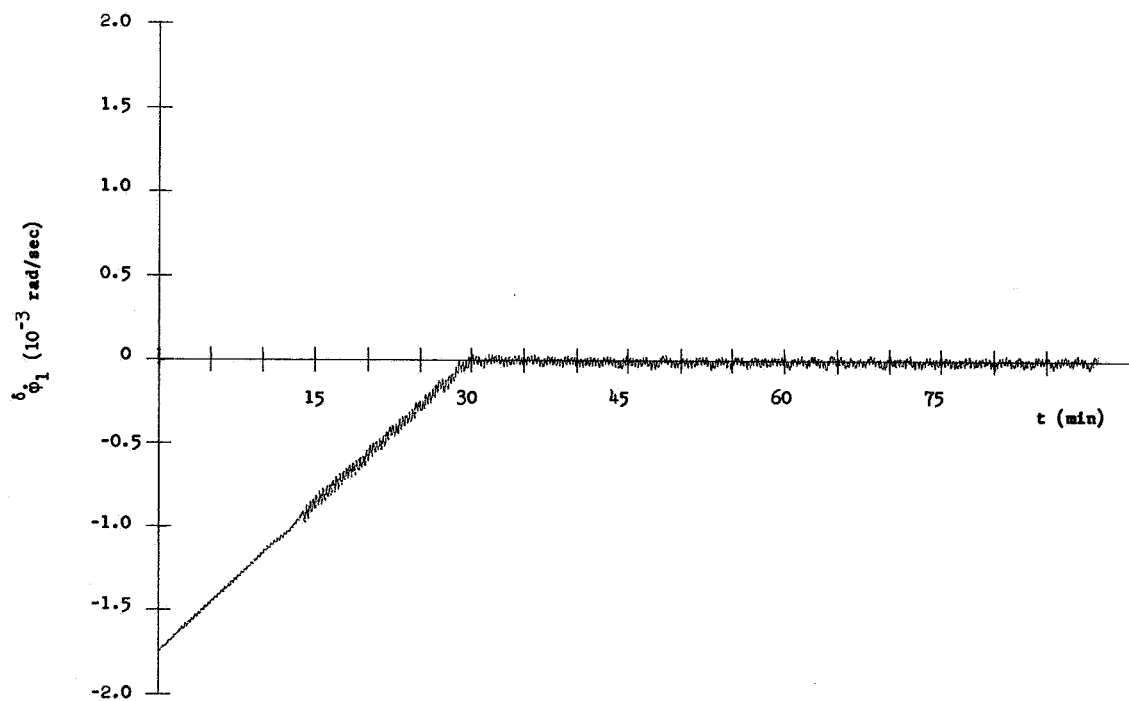


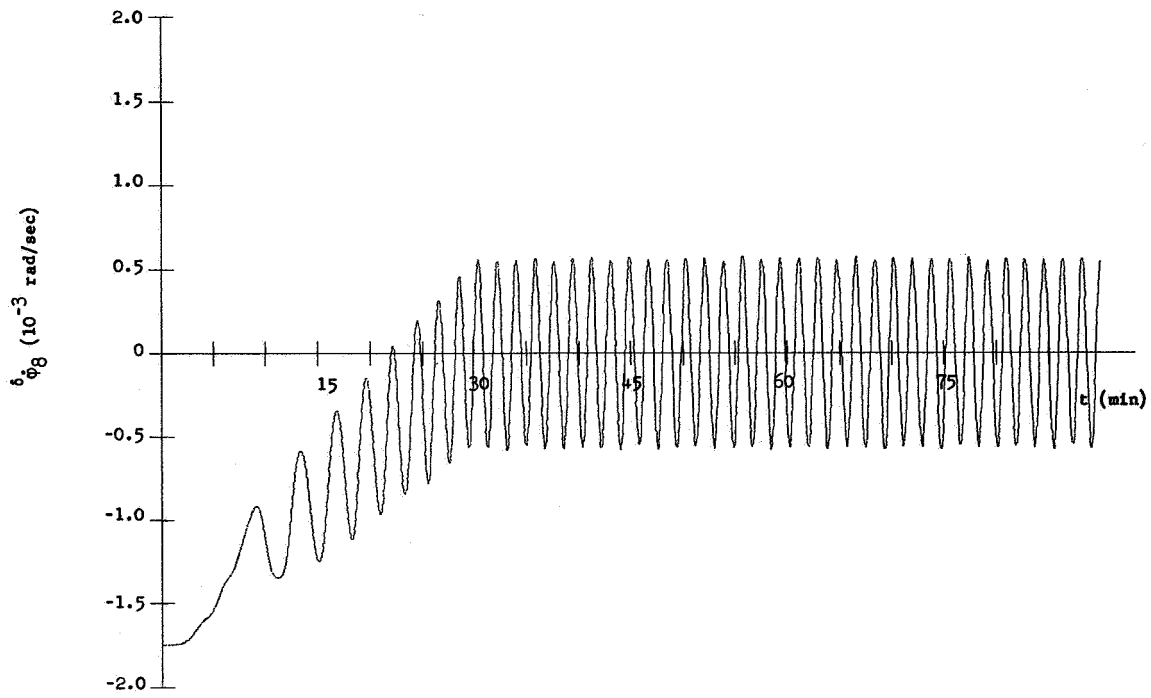
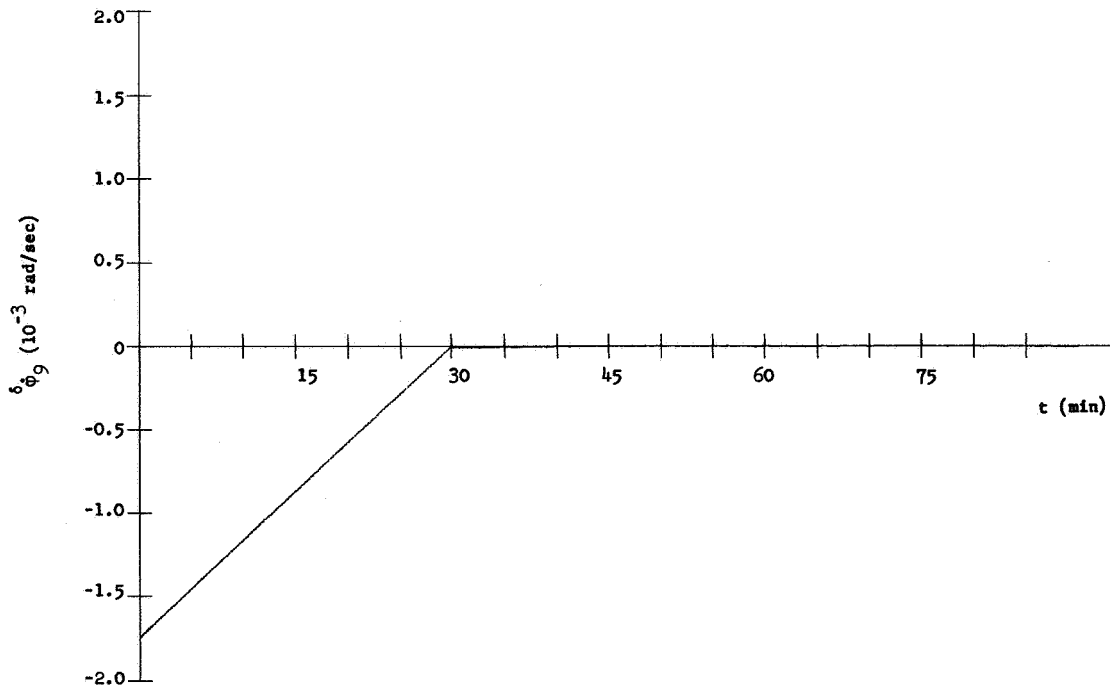
Figure 161. Plot I-M, m_1

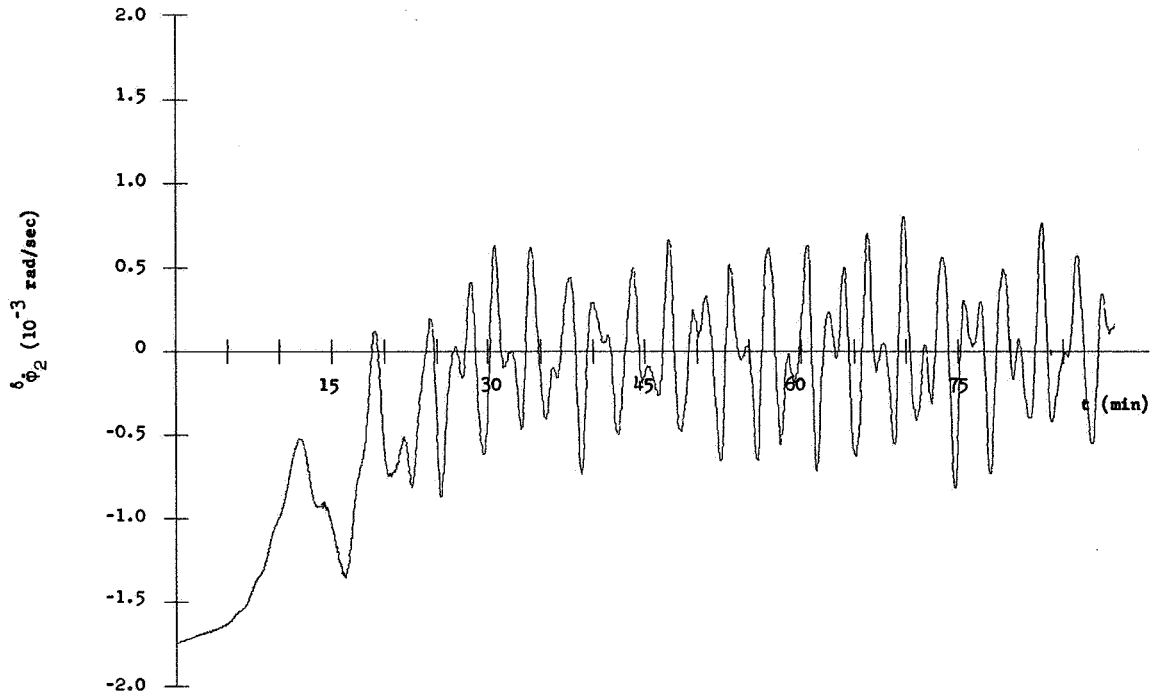
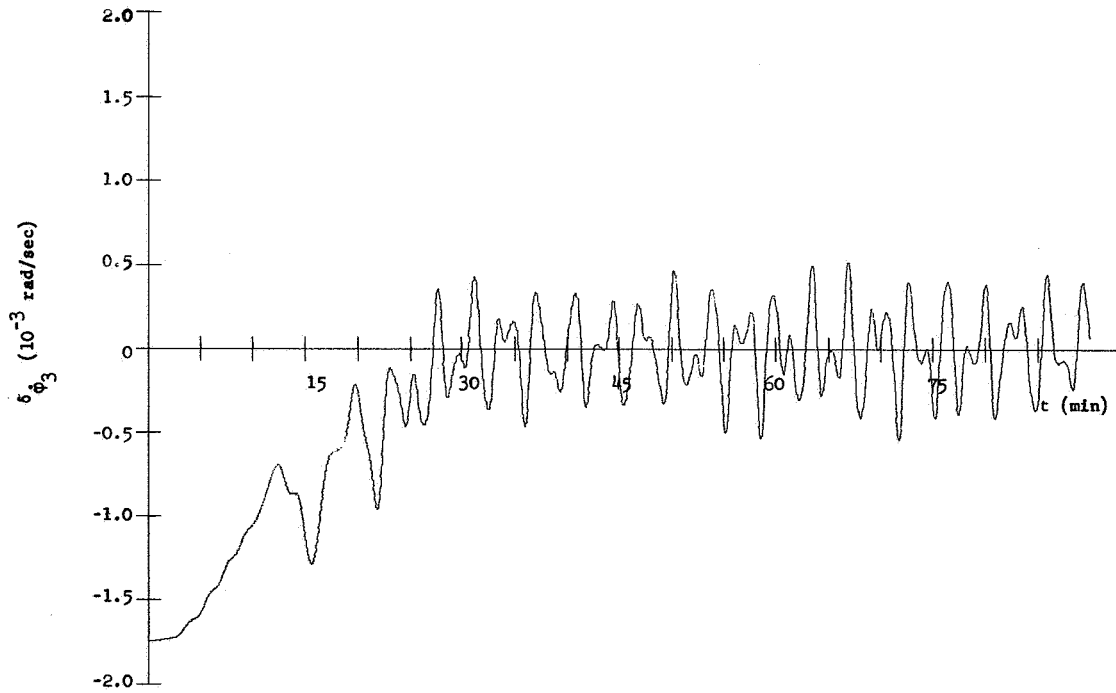
Figure 162. Plot I-M, m_8 Figure 163. Plot I-M, m_9

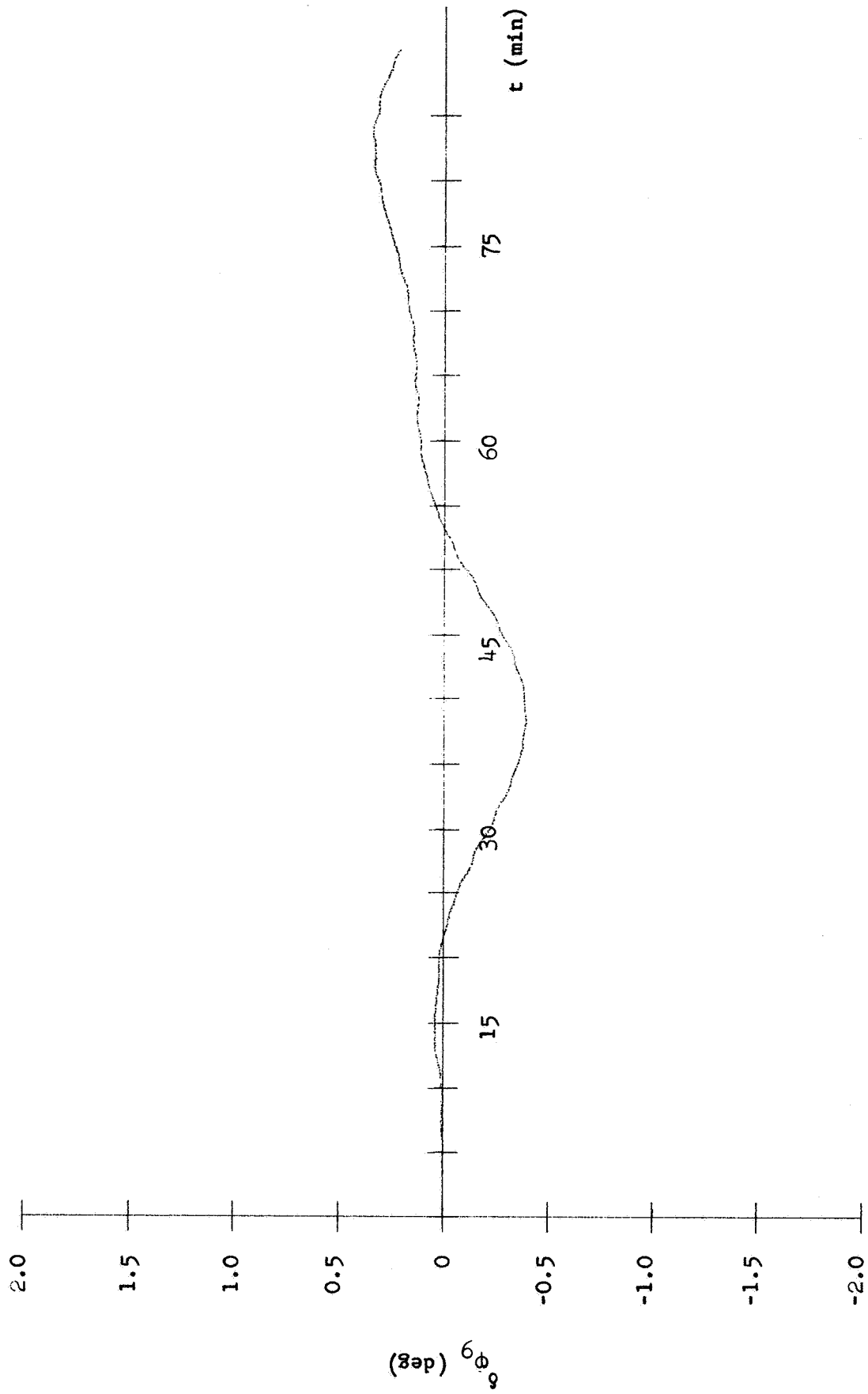
Figure 164. Plot I-M, m_2 Figure 165. Plot I-M, m_3

Figure 166. Plot II-M, m_4 Figure 167. Plot II-M, m_5

Figure 168. Plot II-M, m_6 Figure 169. Plot II-M, m_1

Figure 170. Plot II-M, m_8 Figure 171. Plot II-M, m_9

Figure 172. Plot II-M, n_2 Figure 173. Plot II-M, n_3

Figure 174. Plot III-M, m_9

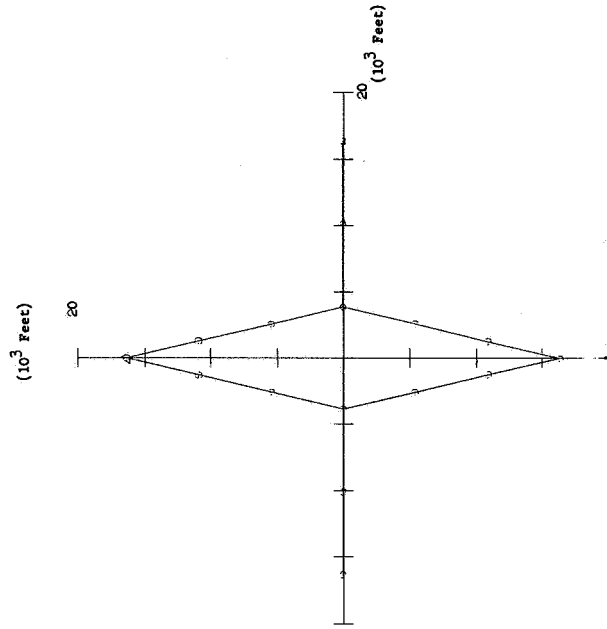


Figure 176. Structure diagram, $t = 0 \text{ sec}$, Case M

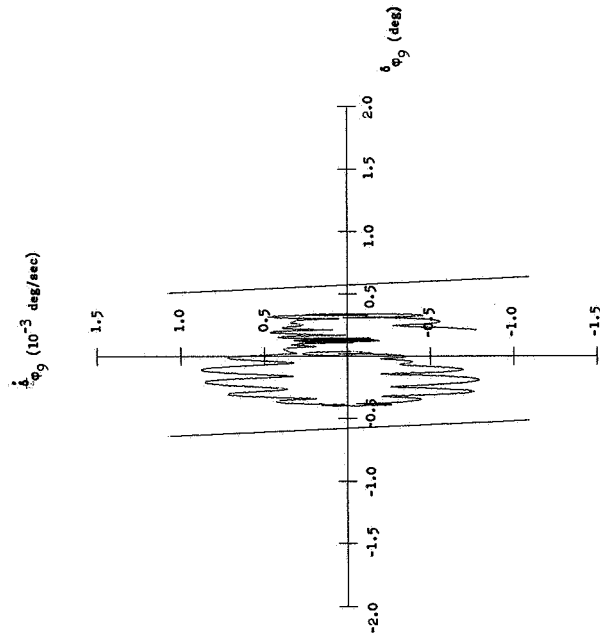


Figure 175. Plot IV-M, w_9

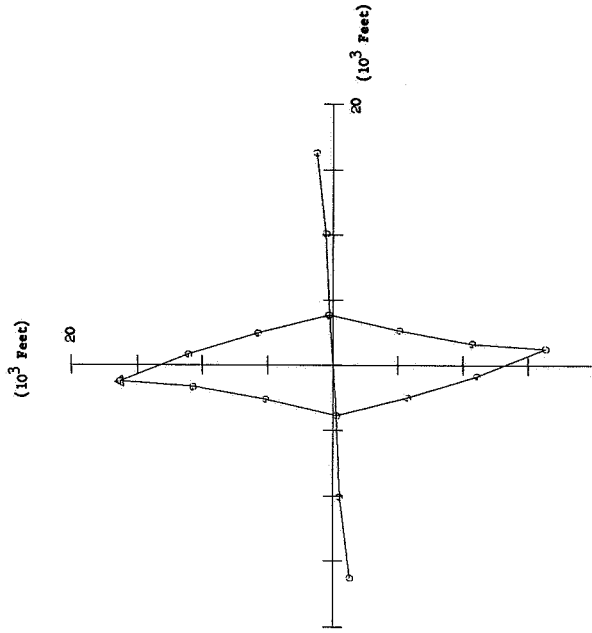


Figure 176. Structure diagram, $t = 400$ sec, Case II

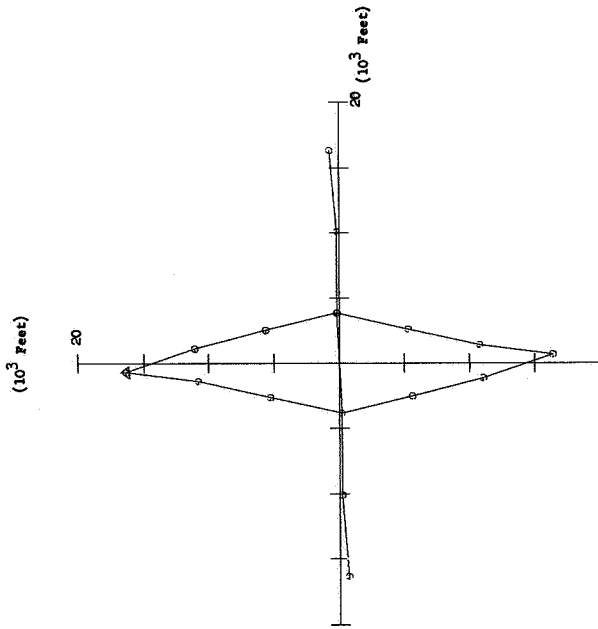


Figure 177. Structure diagram, $t = 300$ sec, Case II

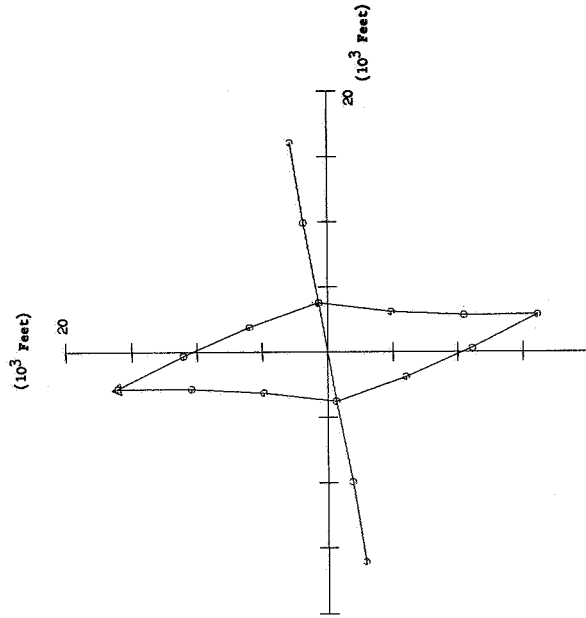


Figure 180. Structure diagram, $t = 500$ sec, Case M

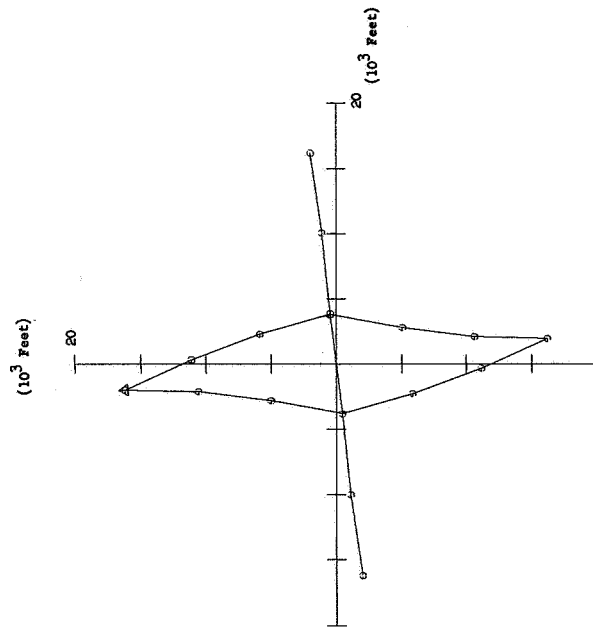


Figure 179. Structure diagram, $t = 600$ sec, Case M

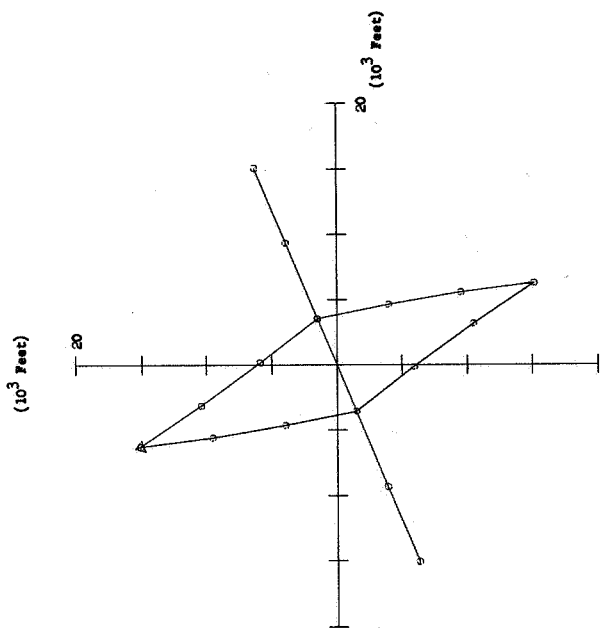


Figure 182. Structure diagram, $t = 500 \text{ sec}$, Case M

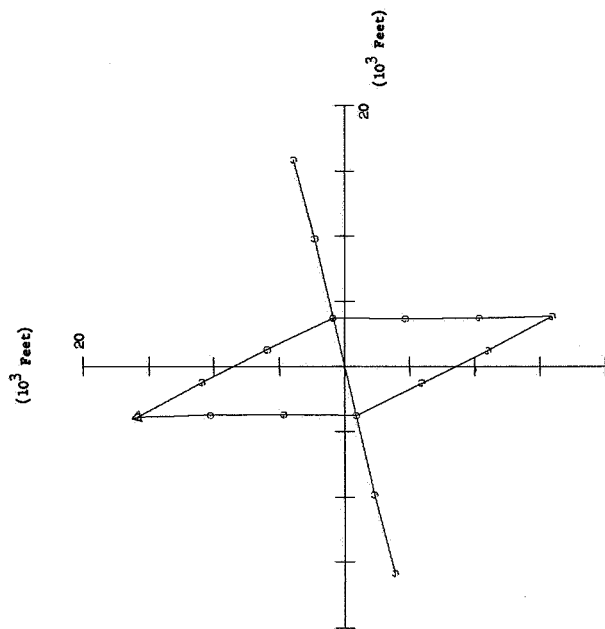


Figure 181. Structure diagram, $t = 700 \text{ sec}$, Case M

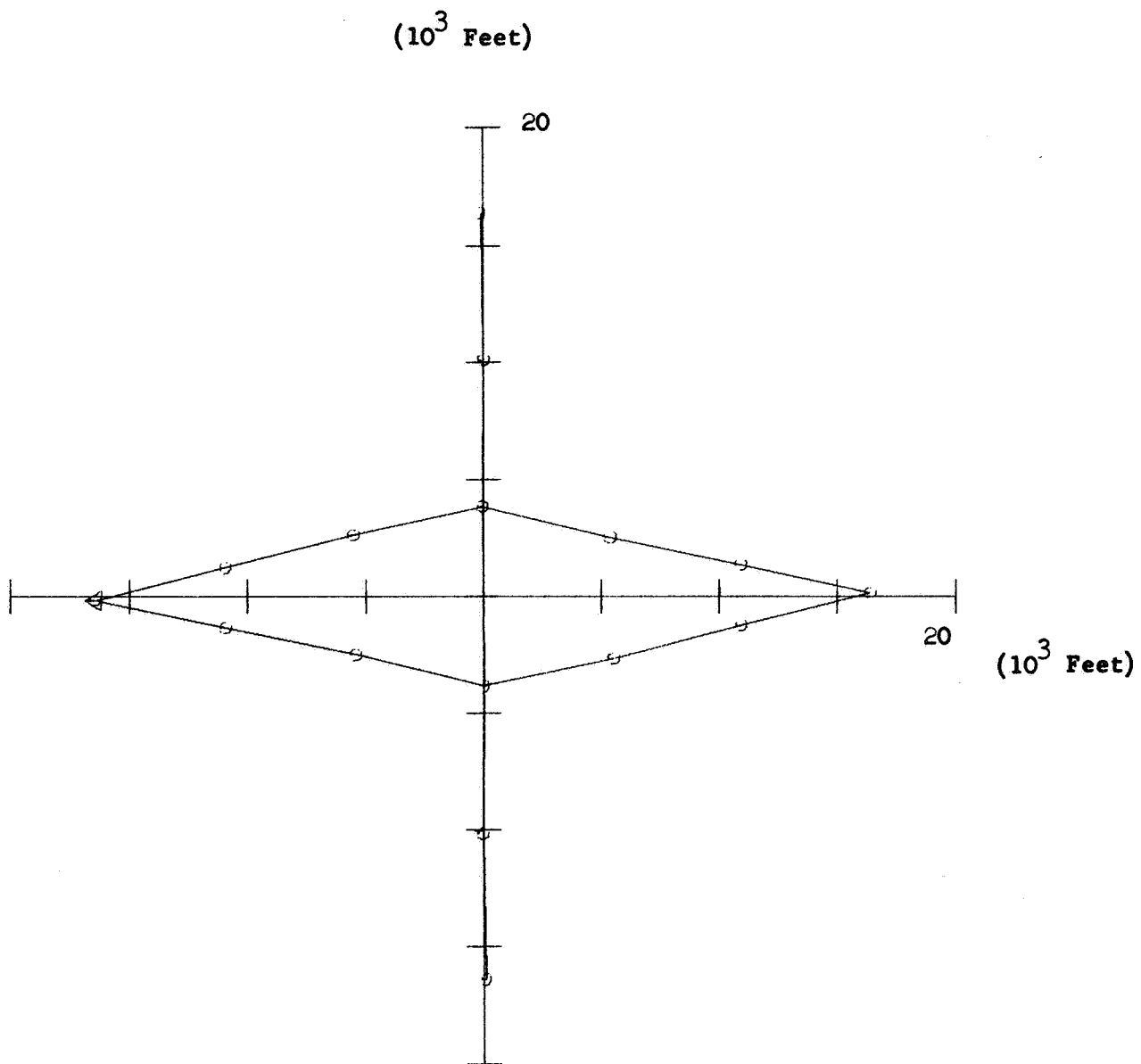


Figure 183. Structure diagram, $t = 1800$ sec, Case M